



UNIwersytet
Przyrodniczy
we Wrocławiu

WYDZIAŁ BIOTECHNOLOGII I NAUK O ŻYWNOSCI

KATEDRA CHEMII ŻYWNOSCI I BIOKATALIZY

Joanna Gach

**Aktywność biologiczna ftalidów i ich metabolitów pochodzenia
mikrobiologicznego**

Biological activity of phthalides and its microbial derivatives

Promotor: **prof. dr hab. Teresa Olejniczak**

Promotor pomocniczy: **dr Stefano Serra**

Wrocław 2023

Badania prowadzone w ramach projektu pn. „UPWR 2.0: międzynarodowy i interdyscyplinarny program rozwoju Uniwersytetu Przyrodniczego we Wrocławiu”, współfinansowanego ze środków Europejskiego Funduszu Społecznego w ramach Działania 3.5. Kompleksowe programy szkół wyższych Osi III Szkolnictwo wyższe dla gospodarki i rozwoju Programu Operacyjnego Wiedza Edukacja Rozwój oraz budżetu państwa na podstawie umowy o dofinansowanie nr POWR.03.05.00-00-Z062/18 z dnia 4 czerwca 2019 r. oraz „Innowacyjny doktorat” N070/0013/20 – „Badanie potencjału laktonów jako nowych naturalnych środków przedłużających trwałość żywności”

Dziękuję Promotor pracy,

Pani Profesor dr hab. Teresie Olejniczak za opiekę merytoryczną, cierpliwość i rady jakie otrzymywałam podczas realizacji badań.

Chciałam również wyrazić wdzięczność wobec Promotora pomocniczego, dr. Stefano Serry za opiekę podczas stażu naukowego we Włoszech, życzliwość i okazaną pomoc.

Dziękuję pracownikom i doktorantom Katedry Chemii Żywności i Biokatalizy za wsparcie oraz wiele cennych dyskusji naukowych. Szczególnie jestem wdzięczna dr. hab. inż. Filipowi Boratyńskiemu, prof. UPWr, za wszelką pomoc.

Słowa podziękowania kieruję również do pracowników Consiglio Nazionale delle Ricerche i zespołu Profesor Marii Elisabetty Brenny z Politecnico di Milano za miłe przyjęcie mnie, dobre rady i atmosferę pracy.

Nie sposób nie wymienić również Rodziców i ich udzielonego wsparcia oraz przyjaciół, w szczególności Moniki, Pauliny, Gosi, Kasi, Łukasza, Moniki, Kuby, Sylwii i Jessici, którzy wspierali mnie na tym etapie życia.

SPIS TREŚCI

SPIS TREŚCI.....	5
PUBLIKACJE WCHODZĄCE W SKŁAD ROZPRAWY DOKTORSKIEJ.....	6
STRESZCZENIE W JĘZYKU POLSKIM	7
STRESZCZENIE W JĘZYKU ANGIELSKIM.....	9
WPROWADZENIE.....	11
CEL PRACY I HIPOTEZY	15
MATERIAŁY I METODY	16
Biokatalizatory	16
Substraty do badań.....	16
Biotransformacje	17
Aktywność przeciwdrobnoustrojowa	18
Badania wpływu 3- <i>n</i> -butylidenoftalidu na wybrane fragmenty przemian metabolicznych drożdży.....	19
Efekt synergistyczny.....	19
Aktywność inhibująca monoaminooksydazę A (MAO-A) (aktywność przeciwdepresyjna).....	19
Badania wybranych parametrów farmakokinetycznych	19
WYNIKI I DYSKUSJA.....	21
Biotransformacje	23
Aktywność biologiczna.....	30
<i>Aktywność fungistatyczna</i>	30
<i>Mechanizm efektu fungistatycznego</i>	34
<i>Aktywność ftalidów jako inhibitorów monoaminooksydazy A (MAO-A)</i>	38
Predykcje wybranych parametrów farmakokinetycznych.....	39
PODSUMOWANIE I WNIOSKI	42
LITERATURA.....	44
OŚWIADCZENIA O WKŁADZIE W PUBLIKACJE	50
PUBLIKACJE.....	53
DOROBEK NAUKOWY	54
Publikacje.....	54
Patenty	54
Zgłoszenia patentowe.....	55
Monografie.....	55
Wystąpienia konferencyjne	55
Udział w projektach badawczych	57
Staże zagraniczne	57

PUBLIKACJE WCHODZĄCE W SKŁAD ROZPRAWY
DOKTORSKIEJ

PUBLIKACJA I (P1)

Gach, J.; Olejniczak, T.; Krężel, P.; Boratyński, F. Microbial Synthesis and Evaluation of Fungistatic Activity of 3-Butyl-3-Hydroxyphthalide, the Mammalian Metabolite of 3-*n*-Butylidenephthalide. *IJMS* **2021**, *22*, 7600.

(IF = 6,208, 140 pkt MEIN)

PUBLIKACJA II (P2)

Gach, J.; Grzelczyk, J.; Strzała, T.; Boratyński, F.; Olejniczak, T. Microbial Metabolites of 3-*n*-Butylphthalide as Monoamine Oxidase A Inhibitors. *IJMS* **2023**, *24*, 10605.

(IF = 5,6, 140 pkt MEIN)

PUBLIKACJA III (P3)

Gach, J.; Olejniczak, T.; Pannek, J.; Boratyński, F. Fungistatic Effect of Phthalide Lactones on *Rhodotorula mucilaginosa*. *Molecules* **2023**, *28*, 5423.

(IF = 4,927, 140 pkt. MEIN)

STRESZCZENIE W JĘZYKU POLSKIM

Ftalidy to bioaktywne laktony, kształtujące zapach roślin selerowatych. Działanie farmakologiczne jednego ze związków z tej grupy, 3-*n*-butyloftalidu, obejmuje właściwości neuroprotektoryjne, znajdujące zastosowanie w terapii chorych po udarze niedokrwiennym mózgu. Oprócz tego w literaturze występują wzmianki o działaniu przeciwdepresyjnym tego ftalidu. Inną aktywnością, ważną w obliczu rosnącej oporności mikroorganizmów na leki, jest zdolność do inhibicji wzrostu mikroorganizmów.

Mimo wielu doniesień literaturowych na temat bioaktywności ftalidów, działanie ich metabolitów pozostaje niezbadane. Otrzymanie tych pochodnych w warunkach *in vivo* jest trudne do realizacji, z uwagi na ich relatywnie małą zawartość. Rozwiązaniem, zapewniającym otrzymanie związków w ilościach umożliwiających przeprowadzenie testów biologicznych, jest użycie całych komórek grzybów strzępkowych jako biokatalizatorów w transformacjach ftalidów.

W badaniach opisanych w niniejszej rozprawie, wykorzystałam mikroorganizmy do otrzymania związków o strukturach identycznych jak metabolity 3-*n*-butylidenoftalidu oraz 3-*n*-butyloftalidu. Zastosowanie grzybów *Absidia cylindrospora* AM336, *Aspergillus candidus* AM386, *Chaetomium indicum* AM158 skutkowało otrzymaniem 3-*n*-butylo-3-hydroksyftalidu, metabolitu 3-*n*-butylidenoftalidu powstającego w organizmie szczurów. Prawdopodobny mechanizm tej biotransformacji opierał się na przyłączeniu cząsteczki wody z użyciem hydratazy. Użycie *Penicillium dierckxii* AM32, *Penicillium* sp. AM91, *Botrytis cinerea* AM235, *Botrytis* sp. KKP3292 do przekształceń 3-*n*-butyloftalidu umożliwiło uzyskanie metabolitów powstających u człowieka - 3-*n*-butylo-10-hydroksyftalidu, 3-*n*-butylo-11-hydroksyftalidu i kwasu 3-*n*-butyloftalid-11-owego.

Oba ftalidy, 3-*n*-butylidenoftalid jak i jego nasycony analog, 3-*n*-butyloftalid, okazały się skutecznymi inhibitorami wzrostu *Candida albicans*, co ważne, w tym szczepu klinicznego opornego na działanie flukonazolu. Tymczasem bardziej polarny metabolit 3-*n*-butylidenoftalidu, 3-*n*-butylo-3-hydroksyftalid, wykazał znikomą inhibicję wzrostu drożdży z rodzaju *Candida*. Doszło więc do procesu detoksykacji na drodze biotransformacji. Co ciekawe, zablokowanie grupy hydroksylowej nie zmieniło znacząco aktywności fungistatycznej.

Zarówno 3-*n*-butyloftalid jak i jego metabolity wykazały wysoką skuteczność jako inhibitory monoaminoooksydazy A (MAO-A), enzymu powodującego degradację prekursora serotoniny. Metabolit ftalidu, 3-*n*-butylo-11-hydroksyftalid, wykazał najwyższą aktywność inhibującą. Tym razem, podczas metabolizmu doszło do procesu bioaktywacji, co jest częstym zjawiskiem w przypadku I fazy biotransformacji. Ftalidy mają szansę stać się alternatywą dla komercyjnie dostępnych inhibitorów MAO-A w leczeniu depresji. Badania *in silico* wykazały większą toksyczność metabolitów niż prekursora, wciąż jednak nie przekraczała ona 2 g/kg masy ciała szczura. Konieczne są dalsze testy laboratoryjne by potwierdzić dane z predykcji komputerowych.

W pracy przebadalam również siedem laktonów ftalidowych wobec drożdży *Rhodotorula mucilaginosa* IHEM18459, powodujących zarówno zakażenia grzybicze, jak i będących przyczyną mikrobiologicznego psucia się żywności. Sześć związków charakteryzowało się dobrym działaniem fungistatycznym, w przeciwieństwie do flukonazolu, wobec którego drożdże wykazały oporność. Najsilniejszym fungistatykiem okazał się 3-*n*-butylidenoftalid z wartością IC₅₀ równą 13 µg/mL. Wykonałam dalsze eksperymenty z użyciem tego ftalidu. Wykazały one, że ilość suchej biomasy drożdży malała wraz ze wzrostem stężenia związku dodawanego do hodowli, ergosterol pozostawał na poziomie porównywalnym z próbą kontrolną, zwiększały się proporcje nienasyconych kwasów tłuszczowych, wzrosła zawartość reaktywnych form tlenu oraz zmienił się profil karotenoidów w próbkach poddanych działaniu związku.

Analizując wyniki można stwierdzić fakt istnienia innego mechanizmu efektu fungistatycznego ftalidu, niż ten, występujący w przypadku flukonazolu. Świadczą o tym: wzrost stresu oksydacyjnego, indukcja produkcji bezbarwnego prekursora karotenoidów o działaniu przeciwzapalnym, a także fakt wykazania efektu synergistycznego wraz z flukonazolem. Przypuszczalnie, 3-*n*-butylidenoftalid oprócz wpływu na zawartość reaktywnych form tlenu, zahamował wpływ fungistatyku z komórki.

STRESZCZENIE W JEZYKU ANGIELSKIM

Phthalides are bioactive lactones that affects the aroma of celery plants. The pharmacological effects of one of the compounds of this group, 3-*n*-butylphthalide, include neuroprotective properties, which find application in the treatment of patients after ischemic stroke. In addition, there are reports on the antidepressant effect of this phthalide in the literature. Another activity, important in the face of increasing drug resistance of microorganisms, is the inhibition of microbial growth.

Despite many literature reports on the bioactivity of phthalides, the effects of their metabolites remain unexplored. Preparation of these derivatives *in vivo* is difficult to carry out, due to their relatively low content. An approach that ensures the compounds are obtained in quantities sufficient for biological assays involves the use of whole cells of filamentous fungi as the biocatalysts in phthalide transformations.

In the research described in this dissertation, I used microorganisms to obtain compounds with structures identical to the metabolites of 3-*n*-butylidene-phthalide and 3-*n*-butylphthalide. The use of the fungi *Absidia cylindrospora* AM336, *Aspergillus candidus* AM386, and *Chaetomium indicum* AM158 resulted in the production of 3-*n*-butyl-3-hydroxyphthalide, a metabolite of 3-*n*-butylphthalide formed in the rat organism. The probable mechanism of this biotransformation was based on the water molecule addition using hydratase. The use of *Penicillium dierckxii* AM32, *Penicillium* sp. AM91, *Botrytis cinerea* AM235, *Botrytis* sp. KKP3292 to transform 3-*n*-butylphthalide allowed the production of metabolites formed in human - 3-*n*-butyl-10-hydroxyphthalide, 3-*n*-butyl-11-hydroxyphthalide and 3-*n*-butylphthalide-11-oic acid.

Both phthalides, 3-*n*-butylidene-phthalide as well as its saturated analog, 3-*n*-butylphthalide, proved to be effective inhibitors of *Candida albicans* growth, notably, including the fluconazole-resistant clinical strain. Meanwhile, the polar metabolite of 3-*n*-butylidene-phthalide, 3-*n*-butyl-3-hydroxyphthalide, showed negligible inhibition of *Candida* yeast growth. Thus, a detoxification process occurred. Interestingly, blocking the hydroxyl group did not significantly change the fungistatic activity.

Both 3-*n*-butylphthalide and its metabolites showed high efficacy as an inhibitor of monoamine oxidase A (MAO-A), the enzyme that causes degradation of the precursor of the serotonin. The metabolite of phthalide, 3-*n*-butyl-11-hydroxyphthalide showed the highest inhibitory activity. This time, a bioactivation process occurred during the metabolism, which is

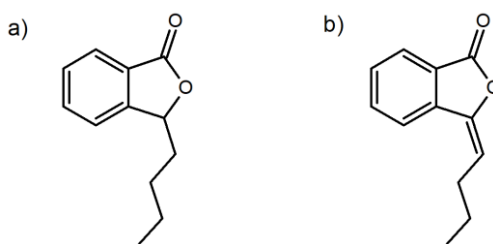
a common phenomenon for phase I biotransformation. Phthalides have the potential to become an alternative to commercially available MAO-A inhibitors in the treatment of depression. *In silico* studies showed greater toxicity of the metabolites than of the precursor, but it still did not exceed 2 g/kg of rat body weight. Further laboratory tests are required to confirm the computer prediction data.

In this work, I also tested seven phthalide lactones against the yeast *Rhodotorula mucilaginosa* IHEM18459, causing fungal infections and being the reason for microbial spoilage of food. The six compounds showed good fungistatic activity, in contrast to fluconazole, towards which the yeasts showed resistance. The most potent fungistatic was 3-*n*-butylidenephthalide with an IC₅₀ value of 13 µg/mL. Further experiments were carried out using this phthalide. These demonstrated that the amount of dry yeast biomass decreased as the concentration of the compound increased, ergosterol remained at a level comparable with the control sample, the proportion of unsaturated fatty acids increased, as well as the content of reactive oxygen species, and the profile of carotenoids in the samples treated with the compound changed.

Analyzing the results, it is possible to conclude that there is a different mechanism of the fungistatic effect of phthalide than that occurring with fluconazole. This is evidenced by the increase in oxidative stress, the induction of the production of a colorless carotenoid precursor with anti-inflammatory activity, as well as the fact that a synergistic effect was demonstrated in conjunction with fluconazole. Presumably, 3-*n*-butylidenephthalide, in addition to its effect on the content of reactive oxygen species, inhibited the efflux of fungistatic from the cell.

WPROWADZENIE

Ftalidy należą do kluczowych bioaktywnych związków występujących w roślinach z rodziny selerowatych, kształtując ich charakterystyczny zapach [1-4]. Jednym z najczęściej wspominanych przez badaczy laktonów ftalidowych jest 3-*n*-butyloftalid. Związek ten, wraz z jego nienasyconym odpowiednikiem, 3-*n*-butylidenoftalidem został zatwierdzony jako środek aromatyzujący żywność przez Europejski Urząd ds. Bezpieczeństwa Żywności (EFSA) [5-6] (Rysunek 1).



Rysunek 1. Wzory strukturalne: a) 3-*n*-butyloftalidu, b) 3-*n*-butylidenoftalidu

Szeroko badane są właściwości farmakologiczne 3-*n*-butyloftalidu, szczególnie w obliczu faktu jego stosowania jako leku w Chinach, od 2002 roku jako środka poprawiającego kondycję chorych po udarze niedokrwiennym mózgu [7-10]. W literaturze można napotkać doniesienia o inhibicji apoptozy neuronów, poprawie mózgowego przepływu krwi, wystąpieniu działania przeciwzapalnego w modelach choroby Alzheimera, Parkinsona, stwardnienia rozsianego, stwardnienia zanikowego bocznego, urazowego uszkodzenia mózgu [7; 11].

Na uwagę zasługują doniesienia o przeciwdepresyjnej aktywności 3-*n*-butyloftalidu [12]. Depresja jest złożonym zaburzeniem, którego etiologia i patofizjologia nie zostały do końca poznane [13]. Wśród dostępnych metod jej leczenia można wymienić selektywne inhibitory zwrotnego wychwyty serotoniny, a także noradrenaliny, trójcykliczne leki przeciwdepresyjne, a także inhibitory monoaminoooksydaz (MAO). MAO odpowiadają za deaminację neurotransmiterów. Istnieją dwie izoformy tych enzymów – A i B [14-15]. MAO-A odpowiada za deaminację 5-hydrokсыtryptofanu [16]. Większość dostępnych na rynku inhibitorów wymaga zachowania pewnych restrykcji dietetycznych podczas leczenia, z uwagi na ryzyko nadmiernej akumulacji tyraminy, co może doprowadzić do zespołu serotoninowego [17]. Stąd istnieje konieczność poszukiwania nowych alternatyw dla komercyjnych inhibitorów MAO.

Badania na szczurach przeprowadzone przez Chen i wsp. ujawniły właściwości przeciwdepresyjne 3-*n*-butyloftalidu, wskazując na jego działanie zarówno na drodze serotonergicznej, jak i poprzez wpływ na neurotroficzny czynnik pochodzenia mózgowego i enzymu mTOR [12]. Brakuje jednak informacji na temat aktywności metabolitów tego ftalidu.

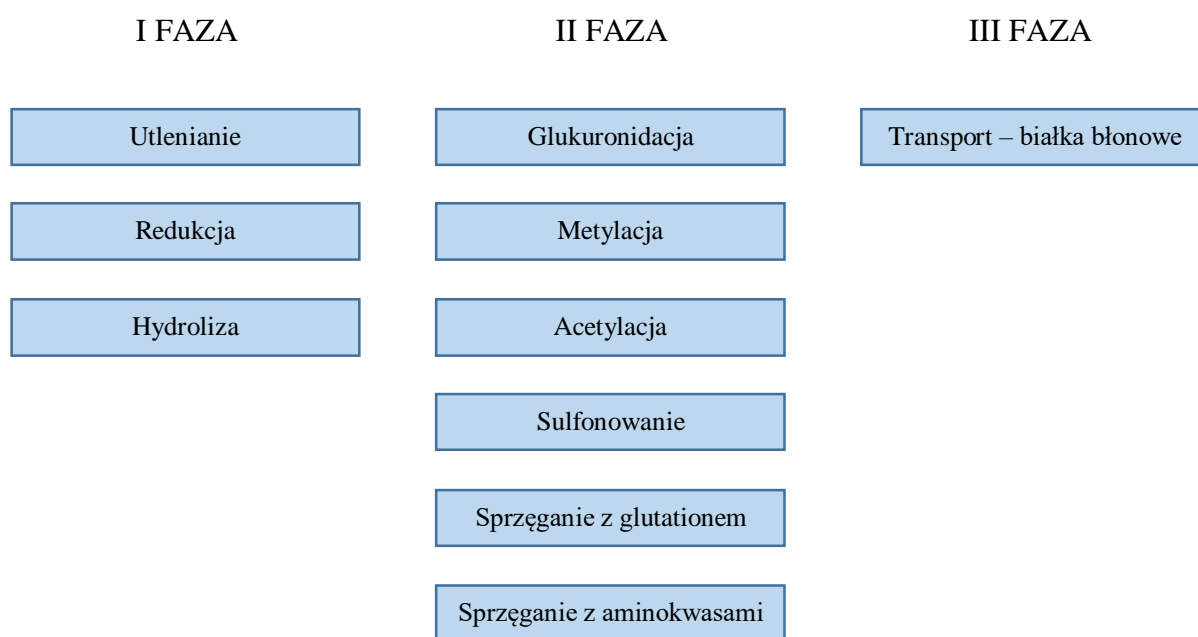
Ftalidy są także znane z właściwości fungistatycznych. Według literatury wykazywały one aktywność wobec *Botrytis cinerea*, *Fusarium oxysporum*, grzybom z rodzaju *Trichophyton* oraz *Colletotrichum*, a także drożdżom z rodzaju *Candida* [18-21]. Obecnie coraz poważniejszy problem stanowi oporność mikroorganizmów na powszechnie stosowane fungistatyki. Przykładowo, drożdże *Candida auris* zostały wymienione na liście Centrum Zapobiegania i Kontroli Chorób jako patogen o szczególnym zagrożeniu opornością na antybiotyki [22]. Azole, powszechnie stosowane w infekcjach grzybiczych, działają blokując biosyntezę ergosterolu poprzez wpływ na 14- α -demetylazę lanosterolu (Erg11p). W efekcie przemian powstaje inny, toksyczny dla komórek sterol [23-24]. Mechanizmy oporności wobec azoli obejmują: zmniejszenie powinowactwa fungistatyku, nadekspresję docelowego miejsca działania, zwiększone wydalanie leku przez nadekspresję białkowych pomp wyrzutu leków [22,25]. W obliczu powyższego, poszukiwanie nowych fungistatyków jest jednym z wiodących trendów badawczych.

W literaturze brak jest doniesień na temat aktywności biologicznej laktonów ftalidowych wobec drożdży *Rhodotorula mucilaginosa*, mikroorganizmu izolowanego szczególnie z produktów nabiałowych [26-27]. Drożdże te mogą również prowadzić do grzybic skóry oraz, w mniejszym stopniu, do infekcji rogówki, zakażeń krwi, zapaleń otrzewnej u osób z obniżoną odpornością [28-30].

Ciekawym zagadnieniem w temacie aktywności przeciwdrobnoustrojowej jest zjawisko synergii – pojawiające się, gdy połączenie dwóch lub większej ilości związków powoduje zwiększenie ich właściwości inhibicyjnych porównując z sumarycznym efektem działania pojedynczo stosowanych leków [31]. Efekt synergistyczny został zaobserwowany przez Gong i wsp. [32] oraz potwierdzony w badaniach naszego zespołu [33] podczas testów 3-*n*-butyloftalidu oraz flukonazolu wobec *Candida albicans*.

Wykorzystanie bioaktywnych związków w przemyśle, szczególnie farmaceutycznym, powinno zostać poprzedzone badaniami na temat ich metabolizmu. Pełni on kluczową rolę w określeniu farmakokinetyki, farmakodynamiki i profilu bezpieczeństwa potencjalnych leków [34]. Biotransformacje ksenobiotyku zwykle prowadzą do powstania bardziej polarnych

pochodnych, by łatwiej można było je wydaląć z organizmu [35]. Z reguły proces ten można podzielić na trzy etapy (Rysunek 2). Reakcje I fazy biotransformacji polegają na wprowadzeniu polarnej grupy funkcyjnej poprzez utlenienie, redukcję lub hydrolizę, w procesach tych biorą udział katalizatory takie jak enzymy cytochromu P450, monooksygenazy flawinowe, esterazy i amidazy. W niektórych przypadkach wytworzony metabolit może wykazywać wyższą aktywność niż jego prekursor. Faza II obejmuje reakcje sprzężenia i zwykle metabolity wytworzone na jej drodze nie wykazują aktywności farmakologicznej. Po zakończeniu tego etapu można wyszczególnić III fazę metabolizmu, podczas której metabolity są wydalane z komórek [35-37].



Rysunek 2. Główne fazy metabolizmu ksenobiotyków (na podstawie Phang-Lyn i Llerena [36])

Standardowe metody badania metabolizmu leków bazują na użyciu testów: *in vitro*, poprzez inkubację z mikrosomami wątrobowymi, a także *in vivo* na zwierzętach. Jednakże, z uwagi na małe stężenia związków w matrycy, detekcja, a tym bardziej izolacja metabolitów jest znacznie utrudniona [38]. Zastosowanie w tych celach biotransformacji z wykorzystaniem całych komórek grzybów strzępkowych jest ciekawym rozwiązaniem, z uwagi na możliwość uzyskania metabolitów w dużej ilości przy małym nakładzie ekonomicznym [37].

Biotransformacje z użyciem grzybów umożliwiają otrzymanie związków z wysoką regio- i stereoselektywnością poprzez redukcję, utlenianie, epoksydację, uwodornienie, hydrolizę, aminację, acylację, glikozylację, przyłączenie cząsteczki wody, metylację,

hydroksylację, dzięki obecności cytochromu P450 [39-41]. Mikroorganizmy te posiadają enzymy umożliwiające przekształcenie ksenobiotyków, co umożliwia w pewnym stopniu naśladowanie metabolizmu ssaczego [39].

Badania nad ftalidami i ich metabolitami powinny obejmować nie tylko oznaczenie ich struktury, czy też zbadanie ich aktywności, ale i ocenę parametrów związanych z adsorpcją, dystrybucją, metabolizmem, wydalaniem i toksycznością (ADMET) [42]. Ma to duże znaczenie w obliczu tego, że blisko 90% przypadków zaprzestania dalszych badań nad potencjalnymi lekami wystąpiło z powodu nieprawidłowych właściwości farmakokinetycznych [43]. Obecnie coraz większą uwagę w predycji tych parametrów zyskują narzędzia bioinformatyczne. Zaletami wykorzystania systemów *in silico* jest możliwość eliminacji kosztów, czasu, nakładów pracy, ponadto, w obliczu kwestii etycznych, oznaczają się większą akceptacją niż badania na zwierzętach [42].

Jednym z parametrów związanych z ADMET jest lipofilowość, określana jako powinowactwo związku do środowiska niepolarnego [44]. Lipofilowość wpływa na transport związku przez błony biologiczne. Ponadto determinuje zdolność cząsteczek do wiązania się z białkami osocza i receptorami w miejscu jego działania [45], stąd, w literaturze podejmowane były próby powiązania lipofilowości z aktywnością biologiczną [46-47].

W eksperymentach, zawartych w niniejszej pracy, użyłam całych komórek grzybów strzępkowych w celu otrzymania takich samych metabolitów jak te, powstające *in vivo* u ssaków. Zbadałam aktywność biologiczną zarówno prekursora – 3-*n*-butylidenoftalidu, produktu, jak i podobnych strukturalnie związków, na przykładzie aktywności przeciwdrobnoustrojowej wobec *Candida albicans*. Oprócz tego przebadałam w sumie siedem ftalidów wobec drożdży *Rhodotorula mucilaginosa*, porównując ich aktywność do fungistatyku flukonazolu. Najsilniej działający 3-*n*-butylidenoftalid testowałam dodatkowo innymi metodami, w tym używając matryc spożywczych w celu odwzorowania środowiska wzrostu drożdży. Oprócz tego zbadałam zjawisko synergii ftalidu oraz jego wpływ na zawartość estrów metylowych kwasów tłuszczowych, ergosterolu, profil karotenoidów, w celu zaproponowania mechanizmu działania. Inną testowaną właściwością była aktywność przeciwdepresyjna 3-*n*-butyloftalidu oraz jego metabolitów. We wszystkich przypadkach dokonałam również predycji wybranych parametrów ADMET, sprawdzając zależność między polarnością, lipofilowością a aktywnością biologiczną.

CEL PRACY I HIPOTEZY

Celem niniejszej pracy było:

- mikrobiologiczne przekształcenie syntetycznych laktonów ftalidowych o strukturach identycznych jak występujące w roślinach *Apiaceae* do pochodnych, będących metabolitami 3-*n*-butyloftalidu lub 3-*n*-butylidenoftalidu, powstających w organizmie człowieka lub szczura,
- zbadanie aktywności przeciwdrobnoustrojowej ftalidów wobec *Rhodotorula mucilaginosa* oraz *Candida albicans*, wraz z zaproponowaniem mechanizmu ich działania,
- testy metabolitów otrzymanych w biotransformacji pod kątem właściwości przeciwdepresyjnych.

Hipotezy badawcze:

- Transformacje grzybami strzępkowymi laktonów ftalidowych do struktur identycznych jak metabolity powstające w organizmie ssaków dowiodą podobieństwa między aktywnością enzymów cytochromu P450 w organizmie ludzkim i w badanych mikroorganizmach.
- Związki o wyższej lipofilowości będą wykazywać silniejsze działanie fungistatyczne.
- Pochodne 3-*n*-butyloftalidu będą wykazywać aktywność wobec monoaminoooksydazy A (MAO-A).

MATERIAŁY I METODY

Biokatalizatory

W badaniach użyłam następujących biokatalizatorów pochodzących z kolekcji Katedry Chemii Żywności i Biokatalizy Uniwersytetu Przyrodniczego we Wrocławiu (AM), Kolekcji Kultur Drobnosutrojów Przemysłowych Instytutu Biotechnologii Przemysłu Rolno-Spożywczego (KKP), Polskiej Kolekcji Mikroorganizmów (PCM):

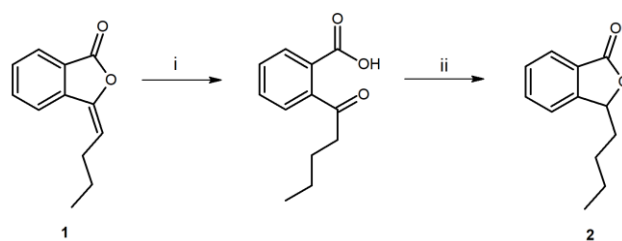
Bakterie: *Bacillus lentus* PCM450, *B. sphaericus* PCM485, *B. stearothermophilus* PCM2104, *Dietzia maris* PCM2292, *Dietzia sp.* DSM44016, *Gordonia bronchialis* PCM2167, *Gordonia sputi* PCM2144, *Rhodococcus equi* PCM559, *R. rhodochrous* PCM909, *R. ruber* PCM2166, *Streptomyces griseus subsp. griseus* PCM2331.

Drożdże: *Candida viswanathi* AM120, *Rhodotorula glutinis* AM242, *R. mucilaginosa* AM44, *R. rubra* AM4, *R. rubra* AM82, *Saccharomyces cerevisiae* AM464, *Yarrowia lipolytica* AM71, *Yarrowia lipolytica* AM72.

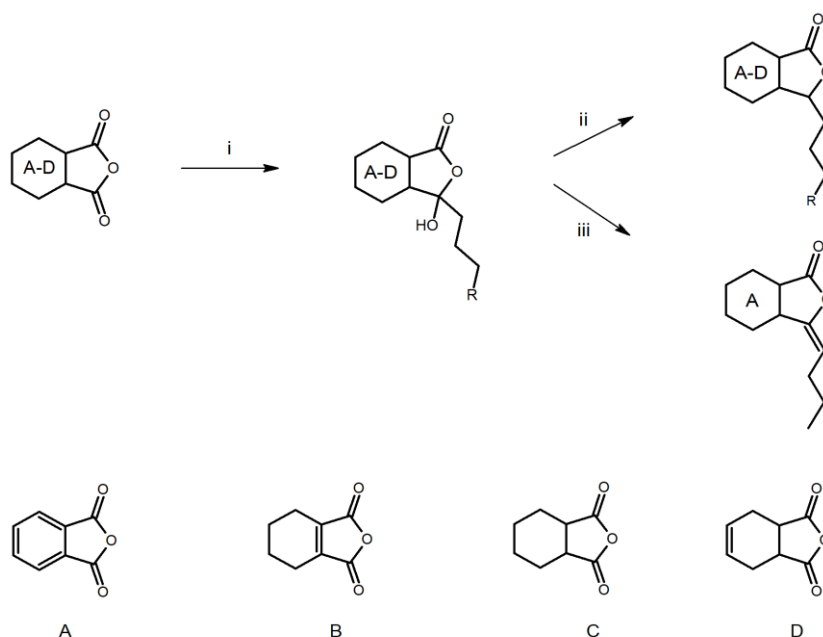
Grzyby strzępkowe: *Absidia cylindrospora* AM336, *Acremoniella atra* AM29, *Aphanocladium album* AM417, *Ascospaera apis* AM496, *Aspergillus candidus* AM386, *A. flavus* KKP686, *A. flavus* KKP689, *A. niger* KKP423, *A. niger* KKP424, *A. niger* KKP45, *Beauveria bassiana* AM278, *Botrytis cinerea* AM235, *Botrytis sp.* KKP3292, *Chaetomium indicum* AM158, *Cunninghamella japonica* AM472, *Fusarium culmorum* AM7, *F. culmorum* AM9, *Fusarium culmorum* AM9, *Fusicoccum amygdali* AM258, *Mortierella isabellina* AM212, *Mucor hiemalis* AM450, *M. spinosus* AM398, *Papularia rosea* AM17, *Penicillium chrysogenum* AM112, *P. dierckxii* AM32, *Penicillium sp.* AM91, *Phanerochaete chrysosporium* KKP784, *Poria placenta* AM38, *Pycnidiella resinae* AM50, *Sclerophoma pythiopila* AM55, *Trichoderma lignorum* KKP786, *Verticillium sp.* AM424.

Substraty do badań

3-*n*-Butylidenoftalid (**1**) do badań biotransformacji (*P1*) oraz 3-*n*-propylidenoftalid (**8**) (*P3*) zakupiono w firmie Sigma-Aldrich. Pozostałe laktony zostały zsyntetyzowane przez zespół badawczy prof. Teresy Olejniczak, a syntezy chemiczne były częścią rozprawy doktorskiej dr. Jakuba Pannka. Poniżej przedstawiono schematy syntez: 3-*n*-butyloftalidu (**2**) do badań zawartych w publikacji *P2* (Rysunek 3) oraz ftalidów **1-2** i **9-12** do eksperymentów opisanych w publikacji *P3* (Rysunek 4).



Rysunek 3. Synteza 3-*n*-butyloftalidu (2) poprzez hydrolizę 3-*n*-butylydenoftalidu (1)
(i-KOH w MeOH, HCl, ekstrakcja, filtracja, ii-THF, NaBH₄, HCl)



Rysunek 4. Synteza ftalidów 1-2 i 9-12. R = H lub Me; i-Et₂O, Mg, *n*-C₄H₉Br lub C₃H₇Br, CdCl₂;
ii-THF, NaBH₄; iii-toluen, TsOH

Biotransformacje

W celu wyboru biokatalizatorów zdolnych do efektywnego przekształcenia substratów - 3-*n*-butyloftalidu i 3-*n*-butylydenoftalidu, przeprowadzono biotransformacje w skali przesiewowej (20 mg związku rozpuszczonego w 0,5 mL acetonu) w kolbach Erlenmeyera o pojemności 300 mL, prowadząc hodowlę wstrząsaną. Do hodowli użyto podłoża Sabouraud o składzie: glukoza 3%, pepton 1%, woda destylowana.

W celu izolacji powstałych produktów przeprowadzono biotransformacje w zwiększonej skali. Zastosowano dwie metody – pierwsza objęła biotransformacje w kolbach o pojemności 2L, druga natomiast zakładała użycie bioreaktora New Brunswick Scientific BioFlo III o pojemności 3L. Postęp biotransformacji kontrolowano wykorzystując: chromatografię cienkwarstwową (TLC), wysokosprawną chromatografię cieczową z detektorem fotodiodowym (HPLC-DAD; aparat HPLC-Dionex UltiMate 3000), a także chromatografię

gazową z detektorem płomieniowo-jonizacyjnym (GC-FID; aparat Agilent Technologies 8860). Hodowle ekstrahowano octanem etylu.

Produkty biotransformacji oczyszczano, używając chromatografii cienkowarstwowej w odwróconym układzie faz (RP-TLC) oraz chromatografii kolumnowej z użyciem silikażelu stosując elucję gradientową. Struktury wyizolowanych związków oznaczono metodą spektroskopii magnetycznego rezonansu jądrowego ^1H , ^{13}C , a także technik dwuwymiarowych: COSY, HSQC, HMBC. Do ich potwierdzenia użyto też chromatografii cieczowej z tandemową spektrometrią mas z jonizacją elektrospray (LC-HR-MS/MS; aparat RSLC UltiMate 3000 ze spektrometrem mas maXis Impact-Q-TOF).

Aktywność przeciwdrobnoustrojowa

Do badań użyto następujących szczepów: *Candida albicans* ATCC 90028 z kolekcji American Type Culture Collection (ATCC), klinicznych izolatów *Candida albicans* 636/20, *Candida albicans* 595/20 and *Candida albicans* 38 z Uniwersytetu Medycznego we Wrocławiu (P1), a także *Rhodotorula mucilaginosa* IHEM 18459 z Belgian Coordinated Collections of Microorganisms (BCCM) (P3).

Aktywność fungistatyczną laktonów oraz ich metabolitów wobec 4 szczepów *Candida albicans* zbadano za pomocą techniki mikrorozcieńczeń w podłożu płynnym. Wobec izolatu *Rhodotorula mucilaginosa* natomiast, oprócz powyższej, dla 3-*n*-butylidenoftalidu wykorzystano także pomiar suchej biomasy i metodę płytkową z preinkubacją zarówno w podłożu klasycznym, jak i w matrycach spożywczych.

Metoda mikrorozcieńczeń: Podłoża wykorzystane do badań obejmowały YPG (*Candida albicans*) oraz dostępne komercyjnie podłoże RPMI 1640 buforowane MOPS (*Rhodotorula mucilaginosa*). Skład podłoża YPG: 2% glukozy, 2% bactopectonu, 1% ekstraktu drożdżowego, woda detylowana, pH 6,5. Skorzystano ze zmodyfikowanej metody opracowanej przez CLSI [48].

Metoda pomiaru suchej biomasy: Wpływ dodatku 3-*n*-butylidenoftalidu na zawartość suchej masy zbadano, inkubując mikroorganizm wraz ze związkiem. Przeprowadzono dwa eksperymenty z użyciem inokulum 0,5% i 10%. Uzyskane próbki biomasy przemyto i zliofilizowano do stałej masy.

Metoda płytkowa: Do hodowli wykorzystano zarówno podłoże Sabouraud, jak i matryce spożywcze – trzy rodzaje jogurtów. Po 48-godzinnej inkubacji, dokonano serii rozcieńczeń każdej próbki, następnie uzyskane zawiesiny przeniesiono i rozprowadzono na podłożu stałym Sabourauda. Po kolejnej 48-godzinnej inkubacji oznaczono liczbę kolonii.

Badania wpływu 3-*n*-butylidenoftalidu na wybrane fragmenty przemian metabolicznych drożdży

W celu zbadania mechanizmu działania 3-*n*-butylidenoftalidu, przetestowano wpływ związku na: zawartość i profil kwasów tłuszczowych, zawartość ergosterolu, zawartość reaktywnych form tlenu, profil karotenoidów drożdży *Rhodotorula mucilaginosa*. Kwasy tłuszczowe oznaczono metodą GC-FID, po saponifikacji i derywatywacji do estrów metylowych. Zawartość ergosterolu wyznaczono metodą spektrofotometryczną używając aparatu Cintra 101 firmy GBC Scientific [49], zaś poziom reaktywnych form tlenu – metodą fluorymetryczną z użyciem dioctanu 2,7-dichlorofluoresceiny (H₂DCFDA) (czytnik płytek Synergy H1 microplate reader firmy BioTek Instruments).

Profil karotenoidów oraz zawartość β -karotenu zbadano po uprzedniej lizie komórek i ekstrakcji, wykorzystując HPLC-DAD oraz HPLC z wysokorozdzielczą spektrometrią mas z jonizacją chemiczną pod ciśnieniem atmosferycznym (HPLC-HR-APCI-MS; aparat RSLC UltiMate 3000 ze spektrometrem APCI-Q-TOF, maXis impact).

Efekt synergistyczny

3-*n*-Butylidenoftalid przetestowano pod kątem możliwego efektu synergistycznego z flukonazolem. W tym celu użyto metody szachownicy, opisanej w literaturze [33,50].

Aktywność inhibująca monoaminooksydazę A (MAO-A) (aktywność przeciwdepresyjna)

Do zbadania aktywności inhibującej 3-*n*-butyloftalidu oraz jego metabolitów wykorzystano izotermiczną metodę kalorymetryczną, rejestrując ciepło wydzielane w wyniku interakcji między związkami: 3-*n*-butyloftalidem i jego metabolitami, a enzymem [51]. Do przetworzenia wyników użyto oprogramowania MicroCal PEAQ-ITC.

Badania wybranych parametrów farmakokinetycznych

W celu wyznaczenia parametrów związanych z farmakokinetyką związków: lipofilowości, rozpuszczalności, użyto narzędzi bioinformatycznych: SwissADME (<http://www.swissadme.ch/index.php>), Way2Drug (<http://www.way2drug.com/gusar/acutoxpredict.html> (dostęp 25 marca 2023)).

Lipofilowość została także wyznaczona z użyciem metody chromatograficznej HPLC-DAD, po wyznaczeniu współczynnika retencji i wykreśleniu zależności między

logarytmem tego parametru, a procentową zawartością rozpuszczalnika organicznego w eluencie [52].

WYNIKI I DYSKUSJA

W skład rozprawy doktorskiej wchodzi trzy publikacje o tematyce biotransformacji ftalidów i bioaktywności związków prekursorowych oraz ich metabolitów (Rysunek 5).

Pierwsza publikacja (P1) dotyczy biotransformacji 3-*n*-butylidenoftalidu (1) do 3-*n*-butylo-3-hydroksyftalidu (3) – związku powstającego jako metabolit powyższego ftalidu w organizmie szczurów. Dodatkowo, zbadalam lipofilowość i aktywność fungistatyczną powyższych związków, wraz z jego analogami, 3-*n*-butyloftalidem (2) oraz 3-*n*-butylo-3-metoksyftalidem (7).

W publikacji drugiej (P2) opisałam otrzymywanie produktów mikrobiologicznych przekształceń 3-*n*-butyloftalidu (2). Powstałe produkty - 3-*n*-butylo-10-hydroksyftalid (4), 3-*n*-butylo-11-hydroksyftalid (5) i kwas 3-*n*-butyloftalid-11-owy (6) zostały następnie zbadane pod kątem aktywności inhibującej enzym monoaminooksydazę A. Testy bioaktywności wykonano we współpracy z dr Joanną Grzelczyk z Politechniki Łódzkiej. Dokonałam również predykcji wybranych parametrów farmakokinetycznych.

Publikacja trzecia (P3) dotyczyła badań nad efektem fungistatycznym laktonów ftalidowych wobec *Rhodotorula mucilaginosa*. Przetestowałam siedem laktonów, 3-*n*-butylidenoftalid (1), 3-*n*-butyloftalid (2), 3-*n*-propylidenoftalid (8), 3-*n*-propyloftalid (9), 3-*n*-butylo-4,5,6,7-tetrahydroftalid (10), 3-*n*-butylo-heksahydroftalid (11) i 3-*n*-butylo-3a,4,7,7a-tetrahydroftalid (12), pod kątem aktywności fungistatycznej za pomocą metody mikrorozcieńczeń w podłożu płynnym. Następnie, sprawdziłam wpływ najbardziej aktywnego laktonu, 3-*n*-butylidenoftalidu (1) na wybrane fragmenty przemian metabolicznych drożdży, by sprawdzić mechanizm działania związku.

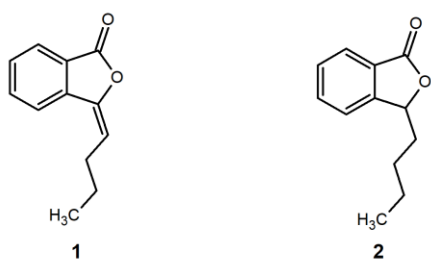
Niniejsza rozprawa, w celu zapewnienia ciągłości tematyki, jak i optymalnej dyskusji wyników została podzielona na następujące zagadnienia:

I Biotransformacje (P1-P3)

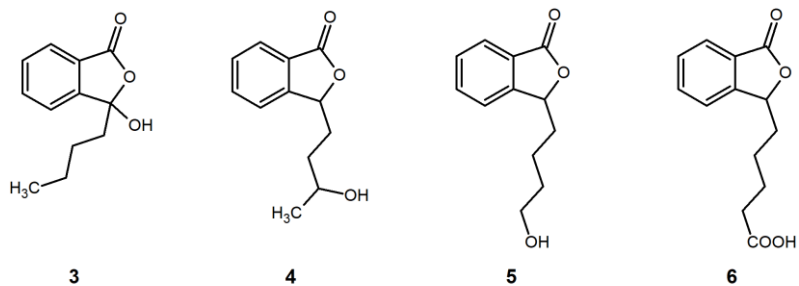
II Aktywność biologiczna, w tym przeciwdrobnoustrojowa, wraz z mechanizmem działania (P1, P3) oraz aktywność antydepresyjna (P2)

III Predykcje wybranych parametrów farmakokinetycznych (P1-P3)

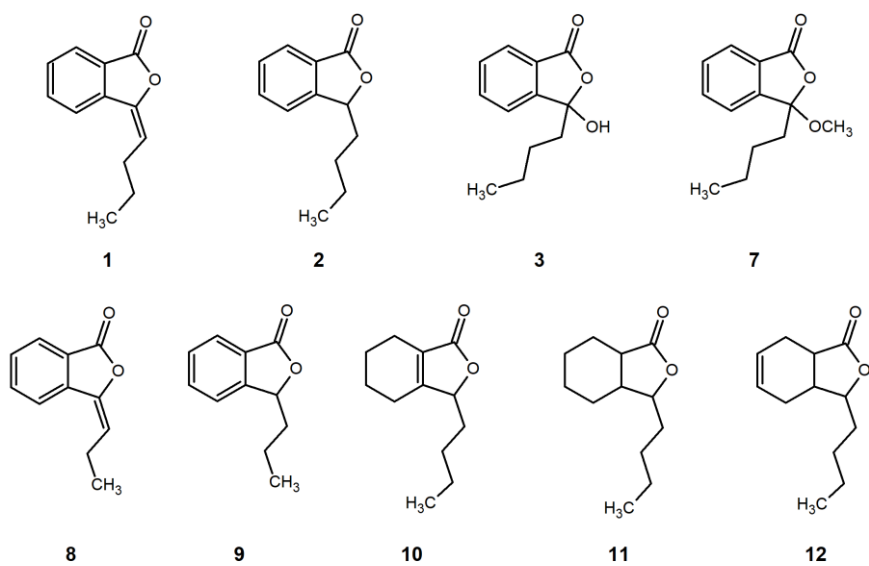
Substraty użyte do biotransformacji



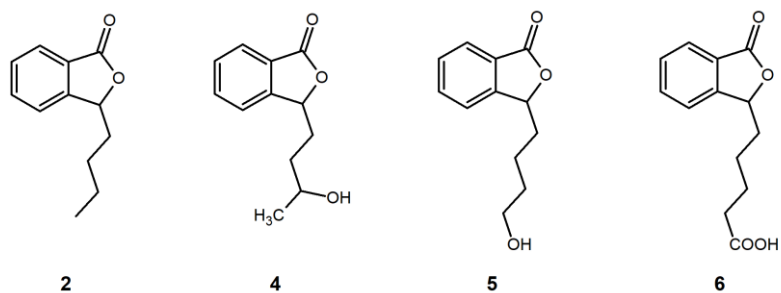
Produkty biotransformacji



Związki do badań aktywności fungistatycznej



Związki do badań inhibicji monoaminoksydazy MAO-A

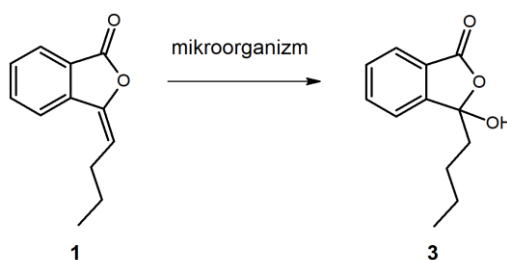


Rysunek 5. Wzory strukturalne związków wykorzystanych w pracy

Biotransformacje

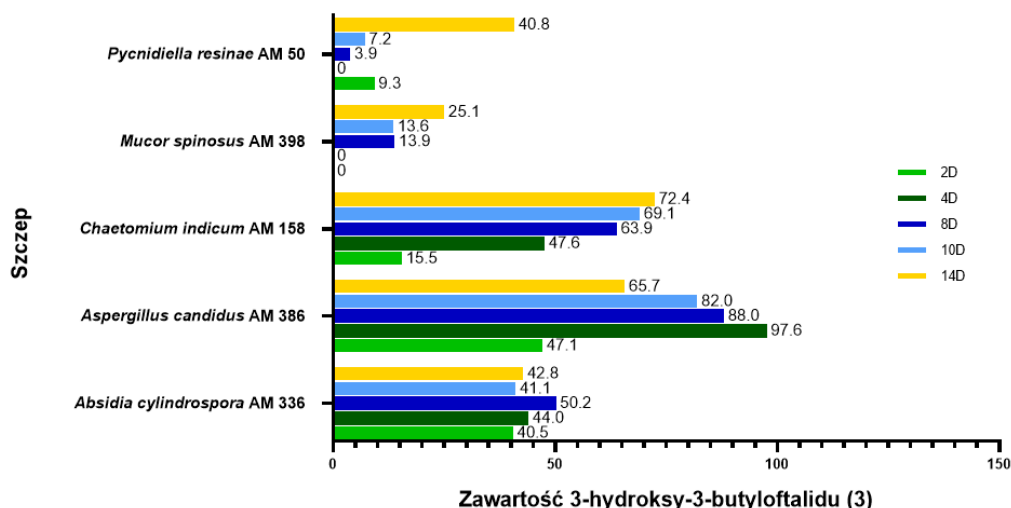
Biotransformacje za pomocą całych komórek grzybów przeprowadziłam w celu izolacji metabolitów ssaczyc – w przypadku 3-*n*-butylidenoftalidu (**1**) była to główna pochodna powstająca w organizmach szczurów, natomiast nasycony analog – 3-*n*-butyloftalid (**2**) przekształcany był do głównych metabolitów identyfikowanych w organizmie człowieka po podaniu prekursora. Skoncentrowałam się na produktach I fazy reakcji metabolicznych.

Zdolność do przekształceń 3-*n*-butylidenoftalidu (**1**) do 3-*n*-butylo-3-hydroksyftalidu (**3**) (Rysunek 6) przetestowałam w skali przesiewowej używając wybranych przedstawicieli bakterii, drożdży jak i grzybów strzępkowych. Niestety, zastosowanie bakterii i drożdży nie przyczyniło się do uzyskania wysokiej konwersji substratu, stąd w badaniach skoncentrowałam się na użyciu jako biokatalizatorów grzybów strzępkowych. Wyniki dla 5 z nich, gdzie stwierdzono powstanie produktu z zawartością powyżej 20%, zostały przedstawione na Rysunku 7.



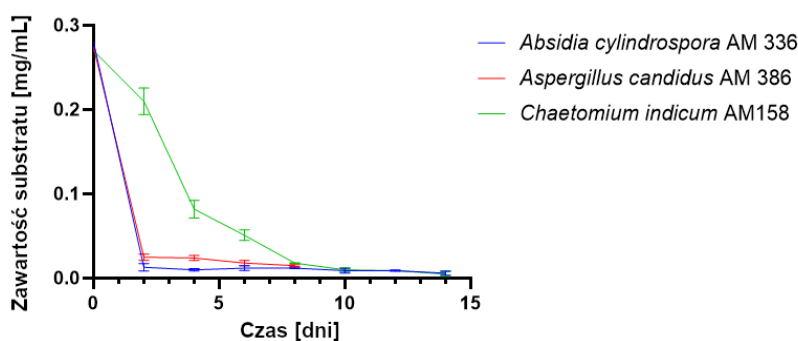
Rysunek 6. Biotransformacje 3-*n*-butylidenoftalidu (**1**) do 3-*n*-butylo-3-hydroksyftalidu (**3**)

Najskuteczniejszymi biokatalizatorami okazały się grzyby *Absidia cylindrospora* AM336, *Aspergillus candidus* AM386, *Chaetomium indicum* AM158. Według analiz HPLC, największą zawartość procentową produktu (**3**) charakteryzował się octanowy ekstrakt *A. candidus* - 97,61% związku po 4 dniach biotransformacji. Podczas kontynuacji procesu widoczny był jednak spadek udziału produktu z grupą hydroksylową, co świadczy o dalszych przekształceniach produktu do innego metabolitu. Pozostałe mikroorganizmy wytwarzały związek z wydajnością pomiędzy 25-72%, biorąc pod uwagę 14 dzień biotransformacji.



Rysunek 7. Procentowa zawartość 3-*n*-butylo-3-hydroksyfalitydu (**3**) w ekstraktach z biotransformacji w czasie

W celu wydzielenia produktu zdecydowałam się na przeprowadzenie biotransformacji w zwiększonej skali z użyciem trzech wyżej wymienionych najefektywniej biotransformujących szczepów grzybów strzępkowych, by sprawdzić wydajność izolowaną procesu, zależną od ilości metabolitów. Użyte stężenie substratu było zbliżone do poprzednio stosowanego w skali przesiewowej (~0.3 g/L).

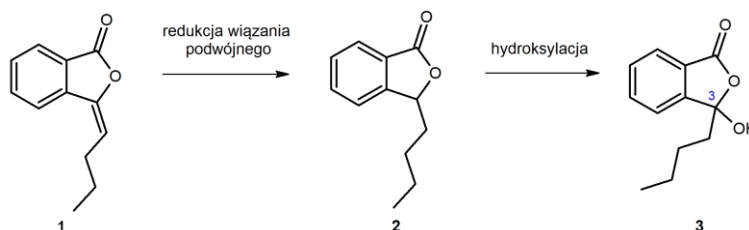


Rysunek 8. Zawartość 3-*n*-butylidenoftalidu (**1**) w próbkach pobranych podczas biotransformacji

Analizując wykres zawartości substratu (**1**) w ekstraktach prób pobranych w czasie i analizowanych za pomocą chromatografii gazowej, można zauważyć zanik 3-*n*-butylidenoftalidu (**1**) przy zastosowaniu wszystkich trzech mikroorganizmów (Rysunek 8). Biotransformacja katalizowana całymi komórkami *Chaetomium indicum* AM 158 miała wolniejszy przebieg. Biorąc pod uwagę spadek zawartości związku **3** w trakcie biotransformacji z użyciem *Aspergillus candidus* AM386 w trakcie badań przesiewowych, proces przerwano po 8 dniach. Pozostałe biotransformacje zakończono po 14 dniach.

Produkt wyizolowałam z użyciem chromatografii cienkowarstwowej w odwróconym układzie faz. Pozwoliło to na eliminację zjawiska silnego powinowactwa grupy hydroksylowej do fazy stacjonarnej, która wystąpiła przy próbie oczyszczania związku w normalnym układzie faz, co skutkowało „ogonowaniem” związku na płytce TLC. Wydajność izolowana procesu wyniosła od 29,2% w przypadku użycia *A. cylindrospora* AM336, do 45,4% przy zastosowaniu *Aspergillus candidus* AM386. Strukturę związku potwierdziłam za pomocą technik ^1H NMR, ^{13}C NMR oraz widm korelacyjnych, a masę jego jonu molekularnego 221 ($M + 1$) wyznaczyłam za pomocą chromatografii gazowej z detektorem masowym, po derywatacji w metoksy pochodną **7**.

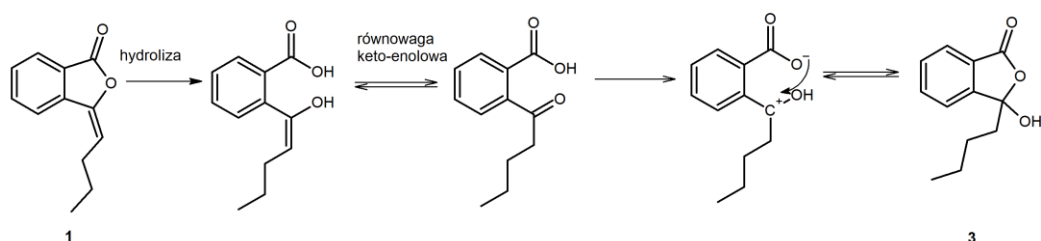
Analizując przebieg biotransformacji, pierwszym możliwym mechanizmem jest redukcja wiązania podwójnego w łańcuchu bocznym 3-*n*-butylidenoftalidu (**1**), a następnie hydroksylacja do nasyconego odpowiednika związku (Rysunek 9).



Rysunek 9. Proponowany mechanizm biotransformacji 3-*n*-butylidenoftalidu (**1**) do 3-*n*-butylo-3-hydroksyftalidu (**3**) poprzez 3-*n*-butyloftalid (**2**) jako produkt przejściowy

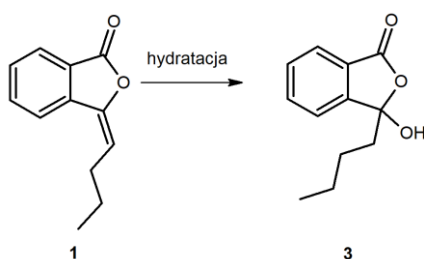
W celu sprawdzenia powyższego mechanizmu, poddałam biotransformacji 3-*n*-butyloftalid (**2**) z użyciem tych samych mikroorganizmów, co w przypadku biotransformacji w zwiększonej skali. Ekstrakty poddałam analizie ^{13}C NMR. Nie stwierdziłam jednak obecności sygnału charakterystycznego dla atomu węgla C-3 produktu **3** ($\delta = 107,9$ ppm).

Kolejnym koniecznym do rozważenia mechanizmem mogła być hydroliza 3-*n*-butylidenoftalidu z wystąpieniem tautomerii keto-enolowej, a następnie zamknięcie pierścienia laktonowego. Jednakże przeprowadzone badania produktu **3** potwierdziły jego zdolność do skręcania płaszczyzny światła spolaryzowanego. Tymczasem omawiany przypadek wiąże się z dużym prawdopodobieństwem otrzymania racematu, z uwagi na to, że płaski karbokation może zostać zaatakowany z dwóch stron płaszczyzny (Rysunek 10).



Rysunek 10. Proponowany mechanizm biotransformacji 3-*n*-butylidenoftalidu (**1**) do 3-*n*-butylo-3-hydroksyftalidu (**3**) poprzez hydrolizę, a następnie zamknięcie pierścienia laktonowego

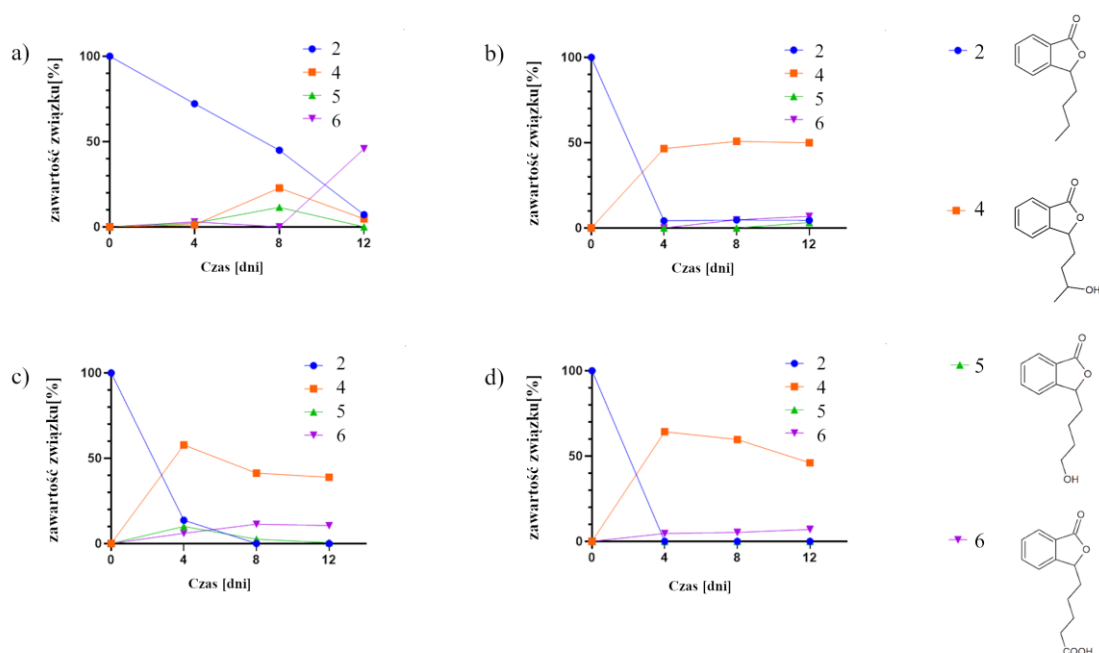
Za najbardziej prawdopodobny mechanizm uznano więc addycję cząsteczki wody do wiązania podwójnego 3-*n*-butyloftalidu (Rysunek 11). Mechanizm ten zgodny jest z propozycją literaturową [53].



Rysunek 11. Proponowany mechanizm biotransformacji 3-*n*-butylidenoftalidu (**1**) do 3-*n*-butylo-3-hydroksyftalidu (**3**) poprzez przyłączenie cząsteczki wody

Przedstawiona powyżej metoda otrzymywania 3-*n*-butylo-3-hydroksyftalidu (**3**) została opisana w formie trzech zgłoszeń patentowych, z czego dwa (P.437711 i P.437712) znajdują się pod ochroną patentową.

Przekształcenia 3-*n*-butyloftalidu (**2**) przeprowadziłam dokonując najpierw badań przesiewowych na 37 grzybach strzępkowych, z czego 12 nie biotransformowało substratu. Do dalszych badań wyselekcjonowałam cztery szczepy: *Penicillium dierckxii* AM32, *Penicillium* sp. AM91, *Botrytis cinerea* AM235, *Botrytis* sp. KKP3292 (Rysunek 12).



Rysunek 12. Biotransformacje 3-*n*-butyloftalidu (**2**) za pomocą: a) *Penicillium dierckxii* AM32, b) *Penicillium* sp. AM91, c) *Botrytis cinerea* AM235, d) *Botrytis* sp. KKP3292

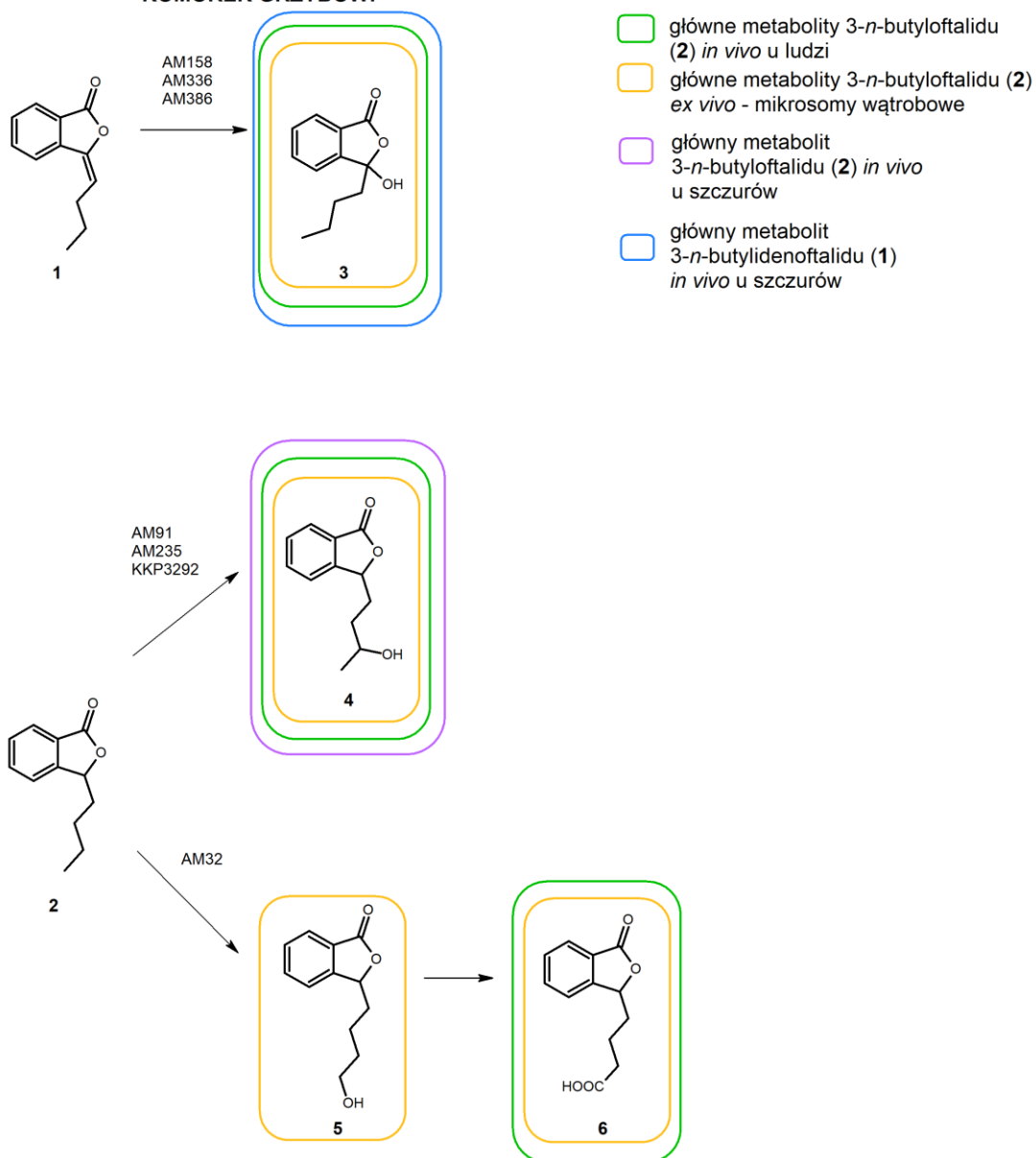
W większości przypadków, biotransformacje 3-*n*-butyloftalidu (**2**) doprowadziły do powstania w przeważającej mierze 3-*n*-butylo-10-hydroksybutyloftalidu (**4**) jako mieszaniny dwóch diastereoizomerów w stosunku 2,5:1. Związek ten jest głównym krążącym metabolitem w organizmie człowieka po przyjęciu 3-*n*-butyloftalidu (**2**) [54], ponadto stwierdzono jego obecność w osoczu i mikrosomach wątroby szczura [53,55] (Rysunek 13). Powstawał on w przypadku użycia wszystkich biokatalizatorów, jednakże można zauważyć tendencję spadkową zawartości tego produktu podczas procesu. Co ciekawe, doniesienia literaturowe nie wskazują na powstanie tego związku na drodze metabolizmu w formie dwóch diastereoizomerów, jednak ich obecność została potwierdzona w ekstrakcie *Ligusticum chuanxiong* [56].

Ponadto stwierdzono powstanie pochodnej z grupą hydroksylową w pozycji C-11 (**5**) w przypadku zastosowania *Penicillium dierckxii* AM32, *Penicillium* sp. AM91, *Botrytis cinerea* AM235. W dwóch przypadkach można zaobserwować zanik związku **5** w czasie na rzecz pojawienia się związku **6**. Sugeruje to, że 3-*n*-butylo-11-hydroksyftalid (**5**) jest produktem przejściowym, utlenianym następnie do kwasu 3-*n*-butyloftalid-11-owego (**6**), co znajduje swoje potwierdzenie w literaturze. Obecność związku **5** stwierdzono dokonując inkubacji 3-*n*-butyloftalidu (**2**) wraz z ludzkimi mezosomami wątrobowymi (HLM), jednakże głównymi produktami biotransformacji był 3-*n*-butylo-10-hydroksyftalid (**4**) oraz 3-*n*-butylo-3-hydroksyftalid (**3**) wyizolowany przeze mnie podczas biotransformacji

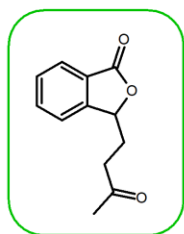
3-*n*-butylidenoftalidu (**1**). Co warte podkreślenia, kwas 3-*n*-butyloftalid-11-owy (**6**), będący jednym z głównych ludzkich metabolitów 3-*n*-butyloftalidu (**2**) *in vivo*, powstawał jedynie w niewielkiej ilości podczas inkubacji z HLM. Jego otrzymanie z 3-*n*-butylo-11-hydroksyftalidu (**5**) było możliwe, stosując frakcje cytozolu wątroby bogate w dehydrogenazę alkoholową lub aldehydową wraz z suplementacją NADPH [54]. Użyte przeze mnie biokatalizatory, szczególnie *Penicillium dierckxii* AM32 dostarczyły obu tych produktów w ilościach umożliwiającą przeprowadzenie badań biologicznych.

METABOLITY OTRZYMANE ZA POMOCĄ CAŁYCH KOMÓREK GRZYBÓW:

Legenda:



NIEOTRZYMANY METABOLIT



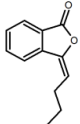
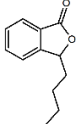
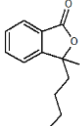
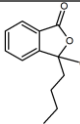
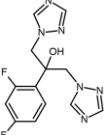
Rysunek 13. Główne metabolity 3-*n*-butylidenoftalidu (1) oraz 3-*n*-butyloftalidu (2) otrzymane za pomocą biotransformacji z użyciem całych komórek grzybów strzępkowych z zaznaczeniem ich wytworzenia *in vivo* w organizmie człowieka lub szczura, lub *ex vivo*; opracowanie na podstawie badań własnych Yan i wsp. 2012 [53] oraz Diao i wsp. [54,57-58]

Aktywność biologiczna

Aktywność fungistatyczna

Z uwagi na to, że wiele farmakologicznie czynnych związków powstaje na drodze reakcji pierwszej fazy biotransformacji [35], zasadne jest zbadanie bioaktywności metabolitów ftalidów. W tym celu, dla 3-*n*-butylidenoftalidu (**1**) oraz jego metabolitu **3** i pochodnych przeprowadziłam test aktywności inhibującej wzrost *Candida albicans*, wliczając w to zarówno szczepy kliniczne 636/20, 595/20, 38, jak i szczep referencyjny ATTC 90028 (*PI*) (Tabela 1).

Tabela 1. Wartości stężeń związków powodujących zahamowanie wzrostu szczepów *C. albicans* o połowę (IC₅₀) [µg/mL]

Związek	<i>C. albicans</i> 636/20	<i>C. albicans</i> 595/20	<i>C. albicans</i> 38	<i>C. albicans</i> ATTC 90028
1 	88	<50	<50	110
2 	123	<50	87	89
3 	203	>250*	250	>250*
7 	244	115	>250*	>250*
Flukonazol 	>250*	0.89	0.44	4.5

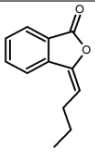
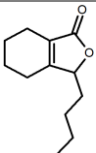
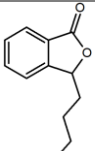
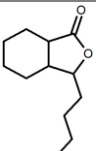
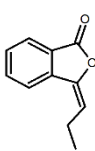
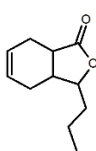
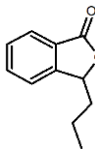
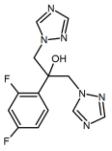
*związek nieaktywny przy najwyższym testowanym stężeniu 250 µg/mL

Najskuteczniejszym inhibitorem wzrostu *Candida* był 3-*n*-butylidenoftalid (**1**), zdolny do zahamowania wzrostu drożdży o połowę poniżej stężenia 50 µg/mL, w przypadku szczepów klinicznych 595/20 oraz 38. Związek ten był również skuteczny w hamowaniu wzrostu szczepu klinicznego 636/20, wobec którego flukonazol, powszechnie stosowany fungistatyk, nie był aktywny nawet przy najwyższym z testowanych stężeń, 250 µg/mL. Wysoką aktywnością inhibującą odznaczał się także 3-*n*-butyloftalid (**2**). Tymczasem metabolit 3-*n*-butylidenoftalidu

(1), 3-*n*-butylo-3-hydroksyftalid (3), wykazywał niską aktywność jedynie wobec szczepu klinicznego 636/20, opornego na flukonazol. W pozostałych przypadkach nie hamował wzrostu innych szczepów *C. albicans*. W pracy przetestowałam także pochodną metoksyłową, 3-*n*-butylo-3-hydroksyftalid (3), jednak wprowadzenie tej grupy funkcyjnej w pozycji C-3, zwiększyło bioaktywność jedynie wobec jednego szczepu klinicznego z IC₅₀ równym 115 µg/mL.

Biorąc pod uwagę obiecujące wyniki odnośnie wykazywanej aktywności fungistatycznej ftalidów, szczególnie w przypadku szczepu opornego na flukonazol, postanowiłam przeprowadzić kolejne eksperymenty. W tym celu, zbadalam aktywność 7 związków wobec drożdży *Rhodotorula mucilaginosa* IHEM 18459, z których 6 zostało zsyntetyzowanych. W pierwszej kolejności, jako metody przesiewowej, użyłam techniki mikrorozcieńczeń w podłożu płynnym z inkubacją prowadzoną w dwóch różnych temperaturach (P2) (Tabela 2).

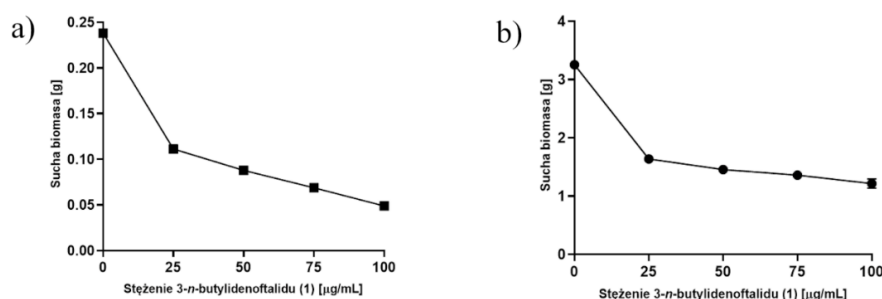
Tabela 2. Wartości stężeń związków powodujących zahamowanie wzrostu *Rhodotorula mucilaginosa* o połowę IC₅₀ [µg/mL]

Związek	IC ₅₀ [µg/mL] 25°C	IC ₅₀ [µg/mL] 30°C	Związek	IC ₅₀ [µg/mL] 25°C	IC ₅₀ [µg/mL] 30°C
1 	13	13	10 	65	66
2 	20	23	11 	42	43
8 	38	32	12 	54	57
9 	130	109	Flukonazol 	199	207

Sześć testowanych związków wykazało aktywność inhibującą wzrost drożdży *Rhodotorula* przy stężeniach 13-66 µg/mL. Najbardziej aktywny, podobnie jak w przypadku inhibicji drożdży *Candida* okazał się 3-*n*-butylidenoftalid (1). Nieznacznie mniej skuteczny był jego

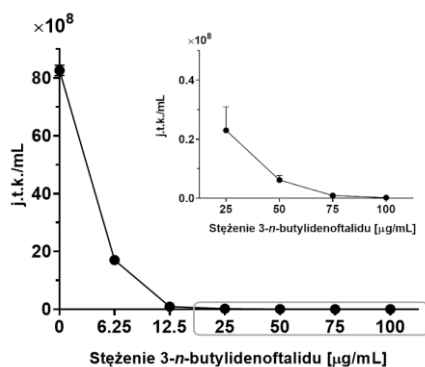
nasycony odpowiednik (2). Flukonazol wykazał słabą aktywność wobec testowanego szczepu *Rhodotorula*, co zgodne jest z doniesieniami literaturowymi o często występującej oporności tych drożdży na związki azolowe [59]. Ponadto sugeruje to, że związki ftalidowe mogą podlegać innemu mechanizmowi działania niż fungistatyki azolowe.

Dalsze eksperymenty obejmowały sprawdzenie wpływu najskuteczniejszego z testowanych fungistyków na biomasę drożdży (Rysunek 14). W testach użyto dwóch dawek inokulum – 0,5 i 10%. 3-*n*-Butylidenoftalid (1), dodawany do hodowli drożdży, w obu przypadkach przyczynił się do zmniejszenia zawartości suchej biomasy już przy najniższym z testowanych stężeń. Dla porównania, flukonazol przyczynił się jedynie do niewielkiego zahamowania biomasy – o blisko 0,03 g mniej niż w przypadku kontroli.



Rysunek 14. Sucha biomasa [g] w zależności od stężenia związku 1 użytego do hodowli wraz z a) 0,5% obj., b) 10% obj. inokulum

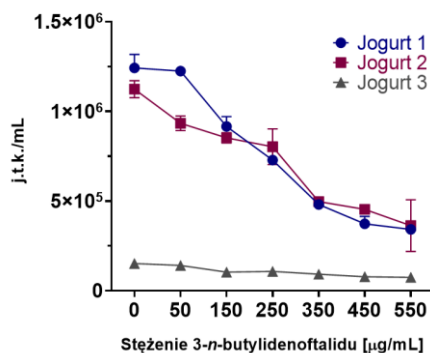
Inna użyta przeze mnie metoda obejmowała oszacowanie ogólnej liczby drożdży w próbkach kontrolnych oraz poddanych działaniu związku 1. Do tego celu wykorzystałam zarówno podłoże płynne Sabouraud (Rysunek 15), jak i matryce spożywcze (Rysunek 16), by zbadać możliwe zastosowanie ftalidu jako środka konserwującego żywność. W przypadku zastosowania klasycznej pożywki można zauważyć znaczne zahamowanie liczby kolonii już przy najniższym z testowanych stężeń ftalidu 1 (z $8,26 \times 10^9$ j.t.k./mL na $1,7 \times 10^9$ j.t.k./mL). Dla porównania, flukonazol, testowany przy 50 µL spowodował spadek liczby drożdży do $5,87 \times 10^9$ j.t.k.



Rysunek 15. Ogólna liczba drożdży *R. mucilaginosa* IHEM 18459 w zależności od dodatku 3-*n*-butyliidenoftalidu (**1**) w podłożu Sabouraud (j.t.k./mL – jednostki tworzące kolonie w 1 mL rozcieńczalnika)

Biorąc pod uwagę obiecujące wyniki aktywności fungistatycznej, przeprowadziłam próbę z wykorzystaniem matryc spożywczych do wzrostu mikroorganizmów, które stanowiły trzy komercyjnie dostępne jogurty, z czego 1 i 2 to jogurty gęste, natomiast 3 to jogurt pitny. Ważnym składnikiem tego typu przetworów mlecznych są bakterie kwasu mlekowego, które same w sobie wykazują działanie fungistatyczne [60-61]. Zależało mi, by zachować oryginalne właściwości organoleptyczne produktów, stąd też ich sterylizacja w celu ich eliminacji, przed zaszczerpieniem inokulum *R. mucilaginosa* nie była możliwa. Rozwiązaniem tego problemu było ujęcie w eksperymencie próby kontrolnej, z dodatkiem rozpuszczalnika związku. Ponieważ podczas początkowych testów, z użyciem stężeń 3-*n*-butyliidenoftalidu (**1**) do 50 µg/mL, nie zauważyłam zahamowania wzrostu *R. mucilaginosa*, zdecydowałam się na sprawdzenie ftalidu **1** w zakresach stężeń 50-550 µg/mL.

Do zahamowania wzrostu drożdży hodowanych w matrycach spożywczych niezbędne było zwiększenie dawki 3-*n*-butyliidenoftalidu (**1**). Zmniejszenie liczby kolonii o połowę w przypadku gęstych jogurtów nastąpiło przy użyciu fungistatyku w zakresie stężeń 220-250 µg/mL, natomiast jogurtu płynnego – 450-550 µg/mL. Tak dużą różnicę między aktywnościami w klasycznych pożywkach płynnych, a w matrycach spożywczych można tłumaczyć nierównomiernym rozprowadzeniem fungistatyku w produkcie. Problem ten został już wspomniany w literaturze omawiając kwestię stabilności i dystrybucji naturalnych związków przeciwdrobnoustrojowych [62].

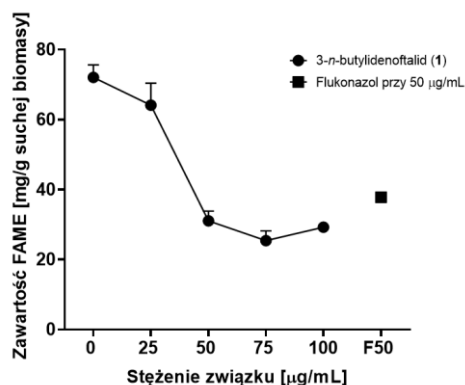


Rysunek 16. Ogólna liczba drożdży *R. mucilaginosa* IHEM 18459 w zależności od dodatku 3-*n*-butylidenoftalidu (**1**) w matrycach spożywczych

Mechanizm efektu fungistatycznego

Szukając wyjaśnienia aktywności fungistatycznej laktonów również wobec szczepów opornych na flukonazol, postanowiłam sprawdzić wpływ 3-*n*-butylidenoftalidu (**1**) na takie elementy jak: biosynteza ergosterolu, profil i skład kwasów tłuszczowych komórek drożdży oraz ilościowy i jakościowy skład karotenoidów.

Drożdże *Rhodotorula mucilaginosa* uważane są za mikroorganizmy olejodajne [63-64]. Lipidy stanowią integralną część błon komórkowych, kształtując ich właściwości fizyczne i regulując działanie białek błonowych [65]. Badając zawartość kwasów tłuszczowych po derywatywacji w estry metylowe i analizie chromatograficznej, można zauważyć ich ilościowe i jakościowe zmiany w próbkach wraz z dodatkiem fungistatyków (Rysunek 17).



Rysunek 17. Zawartość FAME w suchej biomasy drożdży *R. mucilaginosa* IHEM 18459 w zależności od stężenia 3-*n*-butylidenoftalidu (**1**), a także flukonazolu

Zawartość FAME w próbce kontrolnej wynosiła 75,65 mg/g suchej biomasy *R. mucilaginosa* IHEM 18459. Maksymalna zawartość według Knot i wsp. w komórkach drożdży szczepu IPL32 wyniosła 97,23 mg/g suchej biomasy [63]. Należy jednak pamiętać,

że wartość ta zależy od natlenienia, składu podłoża i czasu hodowli [66]. W próbach widoczny jest znaczny spadek FAME przy dodatku 3-*n*-butylidenoftalidu (**1**) od stężenia 50 µg/mL o blisko 57%. Flukonazol, testowany przy takiej samej zawartości, w podobnym, choć mniejszym stopniu przyczynił się do zmniejszenia zawartości estrów kwasów tłuszczowych. Oceniając skład ilościowy próbki kontrolnej można zauważyć, że zdecydowaną większość w komórkach drożdży stanowiły jednonienasycone kwasy tłuszczowe (79,5%), z czego przeważał kwas oleinowy (blisko 77%). Następne w kolejności były kwasy: palmitynowy, lignocerynowy, stearynowy oraz linolowy. Zawartość innych wykrytych kwasów tłuszczowych nie przekroczyła 1%.

W Tabeli 3. przedstawiono procentowy udział poszczególnych estrów kwasów tłuszczowych w próbkach. Próbka kontrolna zawierała blisko 19% estrów nasyconych kwasów tłuszczowych, jednak nieco większy ich udział został odnotowany dla próbki z dodatkiem 25 µg/mL 3-*n*-butylidenoftalidu (**1**). Zastosowanie większych stężeń ftalidu **1** skutkowało odwróceniem tej tendencji – zanotowano znaczny wzrost udziału nienasyconych kwasów tłuszczowych (z 81% w przypadku próbki kontrolnej do 86% w przy dodatku 100 µg/mL związku). Wraz ze wzrostem nienasylenia, zwiększał się procent wielonienasyconych kwasów tłuszczowych. Również flukonazol wpłynął na większą zawartość nienasyconych kwasów tłuszczowych. Fakt wpływu azoli na zmiany w procesie desaturacji kwasów tłuszczowych znajduje potwierdzenie w literaturze [67].

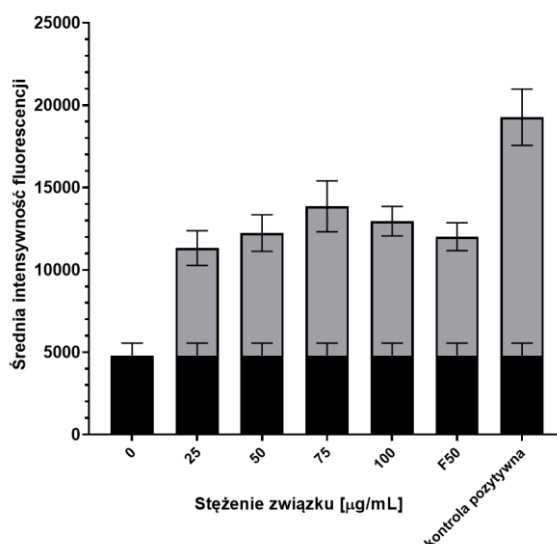
Tabela 3. Wpływ związków na profil estrów kwasów tłuszczowych przy dodatku 3-*n*-butylidenoftalidu (**1**) w stężeniach 25-100 µg/mL oraz flukonazolu (F) przy 50 µg/mL

Stężenie związku [µg/mL]	Nasycone [%]	Nienasycone [%]	Nienasycone, z podziałem na:	
			Jednonienasycone [%]	Wielonienasycone [%]
0	19,02 ± 0,08	80,98 ± 0,08	98,16 ± 0,14	1,84 ± 0,14
25	20,31 ± 0,05	79,69 ± 0,05	95,06 ± 0,02	4,94 ± 0,02
50	16,77 ± 0,01	83,23 ± 0,01	95,74 ± 0,02	4,26 ± 0,02
75	16,54 ± 0,04	83,46 ± 0,04	96,43 ± 0,09	3,57 ± 0,09
100	14,12 ± 0,18	85,88 ± 0,18	95,82 ± 0,05	4,18 ± 0,05
F50	15,27 ± 0,14	84,73 ± 0,14	98,00 ± 0,12	2,00 ± 0,12

Wzrost proporcji nienasyconych kwasów tłuszczowych sugeruje zwiększenie płynności błon komórkowych. Możliwym wytłumaczeniem tego efektu jest wpływ na ekspresję genów kodujących desaturazy kwasów tłuszczowych.

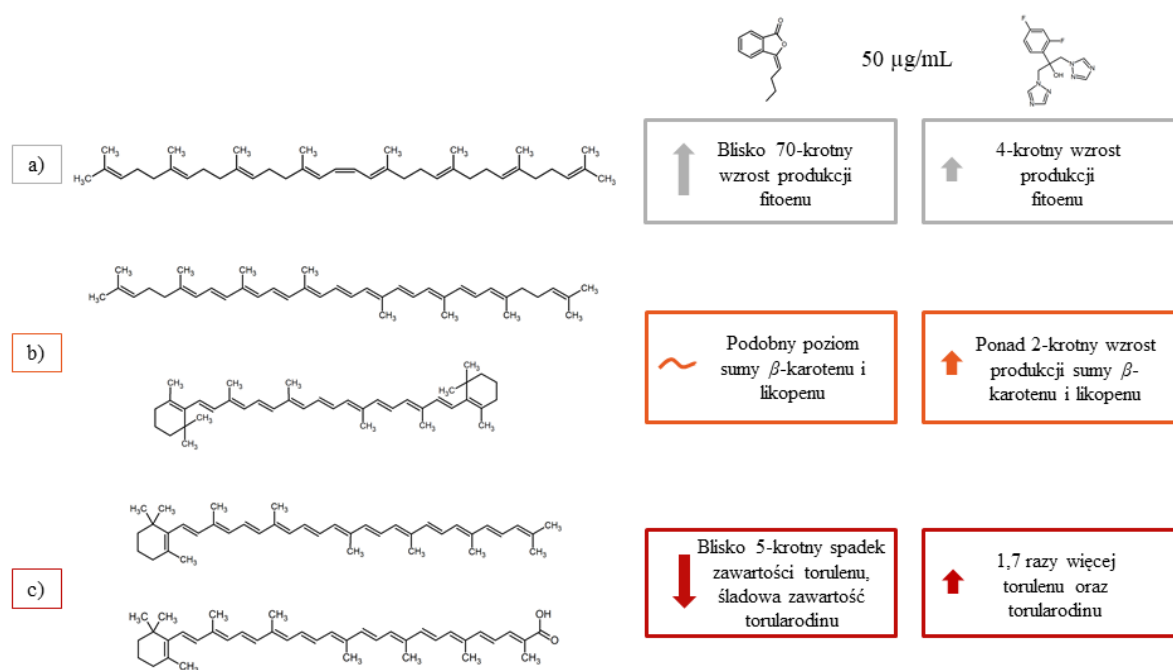
Wpływ na zawartość ergosterolu poprzez obniżenie aktywności 14-*a*-demetylasy lanosterolu jest znanym mechanizmem działania związków azolowych [23,68-69]. By sprawdzić mechanizm fungistatycznego działania ftalidów, przeprowadziłam eksperyment z użyciem metody spektrofotometrycznej. Badania te dowiodły, że zarówno 3-*n*-butylidenoftalid, jak i flukonazol nie wpływają znacząco na zawartość ergosterolu w suchej biomase drożdży. Pewien spadek widoczny był w przypadku zastosowania stężenia ftalidu (**1**) równego 100 µg/mL, jednakże fakt wykazywanej aktywności również przy mniejszych jego stężeniach świadczy o istnieniu innego mechanizmu bioaktywności.

Z uwagi na proponowany w literaturze mechanizm, bazujący na wytworzeniu reaktywnych form tlenu (ROS) [32], dokonałam pomiaru ich zawartości z wykorzystaniem metody adhezyjnej na płytkach mikrotitracyjnych z detekcją fluorymetryczną. Badania te dowiodły, że w przypadku inkubacji komórek z 3-*n*-butylidenoftalidem następuje wzrost zawartości ROS o blisko 50%, w stosunku do poziomu fizjologicznego (Rysunek 18). Co ciekawe, flukonazol testowany w stężeniu 50 µg/mL również przyczynił się do podwyższenia miernika poziomu stresu oksydacyjnego komórek.



Rysunek 18. Poziom reaktywnych form tlenu (ROS) w odpowiedzi na dodatek związków: 3-*n*-butylidenoftalidu (**1**) testowanego w stężeniach 25-100 µg/mL, flukonazolu przy stężeniu 50 µg/mL; czarny kolor oznacza fizjologiczny poziom stresu oksydacyjnego w komórkach

Potwierdzeniem wpływu 3-*n*-butylidenoftalidu (**1**) na wywołanie stresu oksydacyjnego jest również eksperyment polegający na ilościowej analizie porównawczej karotenoidów w próbkach poddanych działaniu ftalidu **1**. Pierwszym etapem tych badań było opracowanie metody umożliwiającej ekstrakcję karotenoidów z biomasy drożdży. Z uwagi na to, że barwniki te znajdują się w ciałach lipidowych komórek, istotna jest odpowiednia metoda ich dezintegracji przed ekstrakcją [70]. Rozwiązanie z inkubacją biomasy wraz z dodatkiem DMSO w 50°C i ekstrakcja acetonem, nie było skuteczne, gdyż barwniki pozostawały w komórkach. Najbardziej efektywne okazało się użycie lizy za pomocą ultradźwięków, połączonej z 2-krotną serią wirowania oraz ekstrakcji za pomocą DMSO oraz roztworu Folcha. Uzyskane ekstrakty zostały poddane analizie LC-HR-MS.



Rysunek 19. Wyniki ilościowej analizy porównawczej karotenoidów za pomocą LC-HR-MS z jonizacją chemiczną pod ciśnieniem atmosferycznym (APCI); a) fitoenu, b) β -karotenu i likopenu, c) torulenu i torularodiny

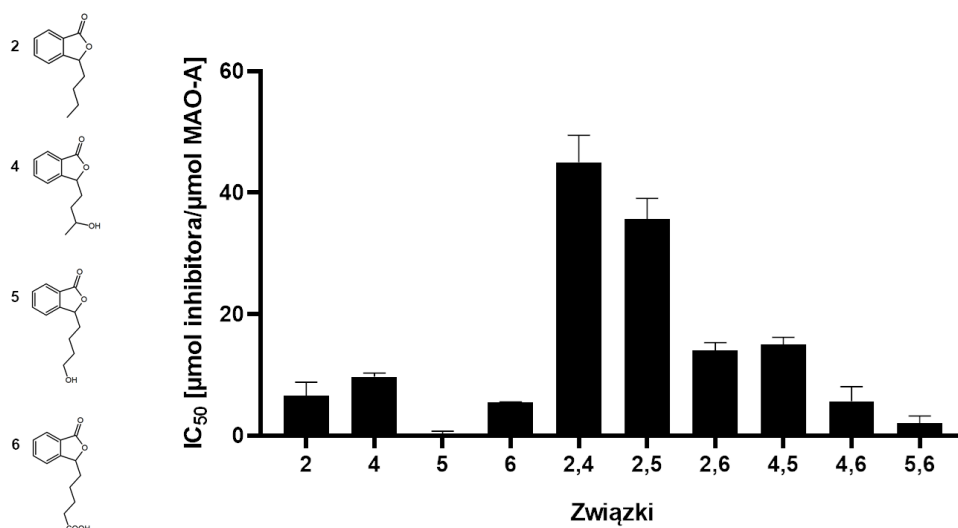
Uzyskane wyniki obrazują zmiany w produkcji karotenoidów spowodowane użyciem fungistatyków. W przypadku 3-*n*-butylidenoftalidu, dochodzi do depigmentacji komórek (Rysunek 19). Widoczny jest 70-krotny wzrost produkcji fitoenu będącego bezbarwnym prekursorem barwnych karotenoidów, przy stężeniu 50 µg/mL 3-*n*-butylidenoftalidu (**1**). Akumulacja tego karotenoidu świadczy o wpływie ftalidu **1** na enzym syntazę fitoenu. Takie samo zjawisko zostało zaobserwowane w przypadku fungicydu difenyloaminy [71]. Dodatkowo, można zauważyć spadek produkcji barwników typowych dla drożdży z rodzaju

Rhodotorula – torulenu i torularodinu [70-71]. Powiązanie między wpływem na profil karotenoidów drożdży a czynnikami wywołującymi stres oksydacyjny zostało opisane w literaturze [72]. Przepuszczalnie więc, nadprodukcja fitoenu o właściwościach przeciwzapalnych i antyoksydacyjnych [73], wiąże się z mechanizmem obronnym przeciwko wolnym rodnikom wytwarzanym w komórkach. Co ciekawe, odwrotne zjawisko można zaobserwować w przypadku flukonazolu – jego zastosowanie zwiększyło co prawda produkcję fitoenu, ale w dużo mniejszym stopniu, jedynie 4-krotnie, zanotowano także zwiększenie produkcji barwnych związków: β -karotenu, torulenu i torularodinu.

Gong i wsp. w swoich badaniach dotyczących wpływu 3-*n*-butyloftalidu (**2**) na zahamowanie wzrostu *Candida albicans*, wysnuł tezę o mechanizmie efektu synergistycznego związku z flukonazolem. Ftalid miał za zadanie ułatwić wniknięcie fungistatyku do komórki i uniemożliwić jego wydalenie przez regulację pomp wyrzutu leków. W efekcie udało się wyeliminować oporność drożdży z rodzaju *Candida* na azol [32]. Aby sprawdzić, czy możliwe będzie zmniejszenie stężenia flukonazolu, niezbędnego do zahamowania *R. mucilagnosa*, przeprowadziłam badanie efektu synergistycznego. Jego wyniki wskazały, że możliwe jest uzyskanie 90-procentowego zahamowania wzrostu drożdży łącząc 4 $\mu\text{g/mL}$ ftalidu **1** i 32 $\mu\text{g/ml}$ flukonazolu, podczas gdy związki używane oddzielnie do uzyskania takiego samego efektu wymagałyby odpowiednio stężeń 32 i 256 $\mu\text{g/mL}$. Potwierdza to wystąpienie zjawiska synergii w aktywności fungistatycznej 3-*n*-butylidenoftalidu (**1**) oraz flukonazolu.

Aktywność ftalidów jako inhibitorów monoaminoooksydazy A (MAO-A)

Istnieje sporo odniesień literaturowych odnośnie farmakologicznego działania 3-*n*-butyloftalidu (**2**) m. in. na układ nerwowy. Badano także działanie antydepresyjne związku [12,74]. Metabolity ftalidu **2** nie zostały jednak w tym kontekście opisane, stąd testy inhibicji MAO-A, enzymu powodującego deaminację neurotransmiterów [17], przeprowadzone we współpracy z Politechniką Łódzką.



Rysunek 20. Wartości IC₅₀ dla 3-*n*-butyloftalidu (**2**) oraz jego metabolitów (**4-6**)

Przedstawione wyniki badań (Rysunek 20) dowodzą, że wszystkie związki są zdolne do redukcji deaminacji 5-hydroksytryptofanu, prekursora serotoniny [Maffei 2020]. Najskuteczniejszy okazał się 3-*n*-butylo-11-hydroksyftalid (**5**), z dawką niezbędną do zahamowania aktywności MAO-A o połowę przy 1,3 µmol/µmol enzymu. Równie efektywne okazało się połączenie związków **5** i **6** z IC₅₀ wynoszącym 2 µmol/µmol enzymu. Co ciekawe, zaobserwowano również antagonistyczny efekt podania równomolowej mieszaniny 3-*n*-butyloftalidu (**2**) i każdego z metabolitów.

Podsumowując, uzyskane w procesie biotransformacji związki mogą stanowić alternatywę dla komercyjnie dostępnych inhibitorów monoaminooksydazy, z których wiele z nich przyczynia się do wystąpienia skutków ubocznych.

Przybliżone wybranych parametrów farmakokinetycznych

Właściwości absorpcji, dystrybucji, metabolizmu, wydalania i toksyczności (ADMET) są kluczowe dla wykorzystania bioaktywnych związków w przemyśle farmaceutycznym [76]. Korzystając z narzędzie bioinformatycznych SwissADME oraz Way2Drug, dokonałam profilowania wybranych parametrów farmakokinetycznych, w tym lipofilowości i toksyczności. Pierwszy z parametrów potwierdziłam dodatkowo, używając techniki chromatograficznej.

Parametr lipofilowości określa takie właściwości związku jak jego przenikalność przez błony biologiczne oraz rozpuszczalność [77]. Zgodnie z teorią, optymalna wartość logP powinna oscylować w granicach 1-3 [44]. Laktony **1** i **2** wykazywały wyższą wartość tego parametru niż ich metabolity (Tabela 4).

Tabela 4. Podsumowanie lipofilowości [$\log P_{o/w}$], aktywności biologicznej i toksyczności LC_{50} [mg/kg] wobec szczurów, wyznaczonych *in silico*, dla związków **1-12**

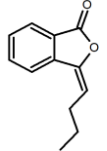
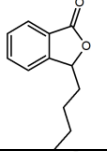
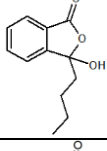
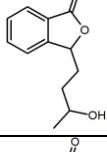
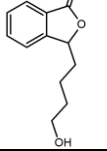
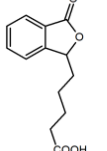
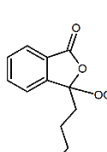
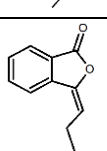
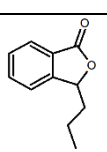
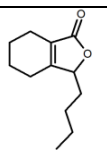
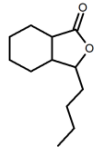
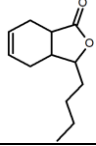
Związek	Lipofilowość [$\log P_{o/w}$]	Aktywność biologiczna	Toksyczność LC_{50} [mg/kg]
1 	2,93-3,38	Przeciwdrobnoustrojowa	1865
2 	2,81-3,00	Przeciwdrobnoustrojowa, aktywność jako inhibitor MAO-A	4872
3 	2,09	Brak lub niska aktywność przeciwdrobnoustrojowa	2601
4 	1,92	Aktywność jako inhibitor MAO-A	4582
5 	1,94	Aktywność jako inhibitor MAO-A	3896
6 	1,60	Wysoka aktywność jako inhibitor MAO-A	2065
7 	2,86	Brak lub niska aktywność przeciwdrobnoustrojowa	2142
8 	2,78	Przeciwdrobnoustrojowa	1895
9 	2,44	Niska aktywność przeciwdrobnoustrojowa	4061
10 	2,93	Przeciwdrobnoustrojowa	5184

Tabela 4. (cd.) Podsumowanie lipofilowości [$\log P_{o/w}$], aktywności biologicznej i toksyczności LC_{50} [mg/kg] wobec szczurów, wyznaczonych *in silico*, dla związków **1-12**

Związek	Lipofilowość [$\log P_{o/w}$]	Aktywność biologiczna	Toksyczność LC_{50} [mg/kg]
11 	2,96	Przeciwdrobnoustrojowa	4702
12 	2,93	Przeciwdrobnoustrojowa	4186

3-*n*-butylidenoftalid (**1**) okazał się być skutecznym inhibitorem wzrostu mikroorganizmów. Jego metabolit zaś, polarny 3-*n*-butylo-3-hydroksyftalid (**3**) charakteryzował się niską aktywnością przeciwdrobnoustrojową lub nawet jej brakiem. W połączeniu z informacją na temat jego niższej toksyczności niż prekursora, zanik aktywności świadczy o procesie detoksykacji ksenobiotyku. Co interesujące, wprowadzenie grupy metoksyłowej do 3-*n*-butylo-3-metoksyftalidu (**7**), związku o wyższej lipofilowości, nie zwiększyło znacząco bioaktywności, stąd wniosek, że nie ma prostej zależności między lipofilowością a aktywnością biologiczną. Należy jednak przeanalizować wpływ struktury a szczególnie zawady przestrzennej, którą może stanowić grupa metoksyłowa przy trzecim atomie węgla laktonu.

Odwrotny do detoksykacji proces widoczny jest w przypadku metabolitów 3-*n*-butyloftalidu (**2**) – związków **4-6**. Można zaobserwować, że, wskutek biotransformacji, nie zanikły właściwości inhibujące enzym MAO-A, a wręcz uległy one zwiększeniu. We wszystkich przypadkach wiązało się to także z przewidywanym wzrostem toksyczności związków. Konieczne są więc badania laboratoryjne, by ocenić bezpieczeństwo metabolitów.

PODSUMOWANIE I WNIOSKI

1. Biotransformacje ftalidów za pomocą grzybów strzępkowych stanowią skuteczne narzędzie do otrzymania związków, wytwarzanych w procesach *in vivo* w małych ilościach.

- Wykorzystując całe komórki mikroorganizmów otrzymałam metabolity biologicznie czynnych ftalidów: 3-*n*-butylidenoftalidu oraz 3-*n*-butyloftalidu, powstające u ssaków w I fazie reakcji metabolicznych.
- 3-*n*-Butylo-3-hydroksyftalid to główna pochodna powstająca w organizmie szczura po przyjęciu 3-*n*-butylidenoftalidu, do otrzymania której użyłam szczepów: *Aspergillus candidus* AM386, *Absidia cylindrospora* AM336 i *Chaetomium indicum* AM158.
- 3-*n*-Butylo-10-hydroksyftalid i kwas 3-*n*-butyloftalid-11-owy to dominujące metabolity wytwarzane w organizmie człowieka po podaniu 3-*n*-butyloftalidu. Wyizolowałam także produkt przejściowy, 3-*n*-butylo-11-hydroksyftalid. Biokatalizatorami, które wykorzystywałam w tych celach były szczepy: *Penicillium* sp. AM91, *P. dierckxii* AM32, *Botrytis* sp. KKP3292, *B. cinerea* AM235.
- Nie udało się otrzymać metabolitu 3-*n*-butyloftalidu, powstającego u ludzi, z grupą ketonową w pozycji C-10.

2. Uzyskane za pomocą biotransformacji metabolity mogą posłużyć do badań aktywności biologicznej.

- Zarówno 3-*n*-butylidenoftalid jak i 3-*n*-butyloftalid skutecznie hamowały wzrost *Candida albicans*, w tym szczepu klinicznego opornego na działanie flukonazolu. Jednak polarny metabolit 3-*n*-butylidenoftalidu, 3-*n*-butylo-3-hydroksyftalid, okazał się nieskutecznym inhibitorem wzrostu drożdży z rodzaju *Candida*.
- Podczas biotransformacji prekursora dochodzi do procesu detoksykacji do nieaktywnej biologicznie pochodnej. Potwierdzeniem jest spadek toksyczności hydroksy-metabolitu względem 3-*n*-butylidenoftalidu w badaniach *in silico*.
- Metabolity 3-*n*-butyloftalidu wykazały wysoką skuteczność jako inhibitory monoaminooksydazy A, potencjalnie mogą więc stać się alternatywą dla stosowanych dotychczas inhibitorów MAO wykazujących skutki uboczne.

- Podczas biotransformacji 3-*n*-butyloftalidu doszło do bioaktywacji – uzyskane metabolity mają silniejsze właściwości przeciwdepresyjne niż prekursor. Według predykcji bioinformatycznych są jednak także bardziej od niego toksyczne. W tym świetle konieczna jest ewaluacja ich toksyczności w badaniach laboratoryjnych.
- 3. Nie ma prostej zależności między wyższą lipofilowością a silniejszą aktywnością biologiczną.**
- Wprowadzenie grupy metoksyłowej o większej lipofilowości nie zwiększyło aktywności fungistatycznej w porównaniu do 3-*n*-butylo-3-hydroksyftalidu.
- 4. Laktony ftalidowe wykazują aktywność fungistatyczną wobec *Rhodotorula mucilaginosa* IHEM18459.**
- Przebadalam 7 laktonów, z czego 6 wykazywało wysoką aktywność inhibującą wzrost drożdży. Flukonazol tymczasem wykazał słabą aktywność, co świadczy o oporności tego szczepu na związki azolowe.
- 5. Największą skutecznością jako fungistatyk przeciwko drożdżom *Rhodotorula* wykazał się 3-*n*-butylidenoftalid, z wartością IC₅₀ równą 13 µg/mL.**
- Wraz ze wzrostem stężenia tego ftalidu dodawanego do hodowli drożdży: malała zawartość suchej biomasy, zwiększał się udział nienasyconych kwasów tłuszczowych, zawartość ergosterolu w komórkach drożdży pozostawała na podobnym poziomie, zmieniał się profil karotenoidów, rosła zawartość reaktywnych form tlenu (ROS).
 - Mechanizm działania ftalidów jest inny niż dla związków azolowych, bazujących na zahamowaniu biosyntezy ergosterolu – polega na indukcji ROS. Świadczy o tym również fakt wpływu 3-*n*-butylidenoftalidu na nadprodukcję fitoenu, prekursora barwnych karotenoidów, co przypuszczalnie jest mechanizmem obronnym drożdży przeciwko ROS.
 - Stwierdziłam efekt synergistyczny 3-*n*-butylidenoftalidu i flukonazolu – co doprowadziło do zmniejszenia dawki flukonazolu koniecznej do zahamowania wzrostu *Rhodotorula*.
 - W celu sprawdzenia możliwości wykorzystania ftalidu jako środka konserwującego żywność przeprowadziłam badania używając matryc spożywczych. Ftalid wykazał niższą aktywność, niż z użyciem standardowych testów *in vitro*, co związane jest najprawdopodobniej z nierównomierną dystrybucją fungistatyku w produkcie.

LITERATURA

1. Miran, M.; Monsef Esfahani, H.R.; Jung, J.H.; Aliahmadi, A.; Skropeta, D.; Abbas-Mohammadi, M.; Ebrahimi, S.; Moridi Farimani, M. Characterization and Antibacterial Activity of Phthalides from the Roots of the Medicinal Herb *Levisticum Officinale* W.D.J. Koch. *IJPR* **2020**, *19*.
2. Renzetti, A.; Fukumoto, K. Synthesis of Phthalides and α,β -Butenolides by Transition Metal-Catalyzed Activation of C—H Bonds. *Molecules* **2019**, *24*, 824.
3. Turner, L.; Lignou, S.; Gawthrop, F.; Wagstaff, C. Investigating the Factors That Influence the Aroma Profile of *Apium Graveolens*: A Review. *Food Chemistry* **2021a**, *345*, 128673.
4. Turner, L.; Wagstaff, C.; Gawthrop, F.; Lignou, S. Consumer Acceptability and Sensory Profile of Three New Celery (*Apium Graveolens*) Hybrids and Their Parental Genotypes. *IJMS* **2021b**, *22*, 13561.
5. Rozporządzenie Parlamentu Europejskiego i Rady (WE) Nr 1334/2008 z dnia 16 grudnia 2008 r. w sprawie środków aromatyzujących i niektórych składników żywności o właściwościach aromatyzujących do użycia w oraz na środkach spożywczych oraz zmieniające rozporządzenie Rady (EWG) nr 1601/91, rozporządzenia (WE) nr 2232/96 oraz (WE) nr 110/2008 oraz dyrektywę 2000/13/WE (**2008**).
6. Rozporządzenie Wykonawcze Komisji (UE) nr 872/2012 w sprawie przyjęcia wykazu substancji aromatycznych przewidzianego rozporządzeniem Parlamentu Europejskiego i Rady (WE) nr 2232/96 (**2012**).
7. Luo, R.; Wangqin, R.; Zhu, L.; Bi, W. Neuroprotective Mechanisms of 3-*n*-butylphthalide in Neurodegenerative Diseases (Review). *Biom Rep* **2019**, *11*, 235-240.
8. Lv, J.; Zhao, D.; Zhao, G.; Xie, Z. Efficacy and Safety of Butylphthalide in Secondary Prevention of Stroke: Study Protocol for a Multicenter, Real World Trial Based on Internet. *BMC Neurol* **2022**, *22*, 305.
9. Wang, W.; Cha, X.-X.; Reiner, J.; Gao, Y.; Qiao, H.-L.; Shen, J.-X.; Chang, J.-B. Synthesis and Biological Activity of N-Butylphthalide Derivatives. *European Journal of Medicinal Chemistry* **2010**, *45*, 1941–1946.
10. Yang, L.-C.; Li, J.; Xu, S.-F.; Cai, J.; Lei, H.; Liu, D.-M.; Zhang, M.; Rong, X.-F.; Cui, D.-D.; Wang, L.; et al. L-3-*n*-Butylphthalide Promotes Neurogenesis and Neuroplasticity in Cerebral Ischemic Rats. *CNS Neurosci Ther* **2015**, *21*, 733–741.
11. Zhou, Q.; Han, C.; Xia, Y.; Wan, F.; Yin, S.; Li, Y.; Kou, L.; Chi, X.; Hu, J.; Sun, Y.; et al. Efficacy and Safety of 3-*n*-butylphthalide for the Treatment of Cognitive Impairment: A Systematic Review and Meta-analysis. *CNS Neurosci Ther* **2022**, *28*, 1706–1717.
12. Chen, C.; Ma, H.; Fu, Z. Antidepressant-like Effect of 3-*n*-Butylphthalide in Rats Exposed to Chronic Unpredictable Mild Stress: Modulation of Brain-Derived Neurotrophic Factor Level and MTOR Activation in Cortex. *Neurochem. Res.* **2021**, *46*, 3075–3084.
13. Kaltenboeck, A.; Harmer, C. The Neuroscience of Depressive Disorders: A Brief Review of the Past and Some Considerations about the Future. *Brain and Neuroscience Advances* **2018**, *2*, 1-6.

14. Merce, A.P.; Ionică, L.N.; Bîină, A.M.; Popescu, S.; Lighezan, R.; Petrescu, L.; Borza, C.; Sturza, A.; Muntean, D.M.; Crețu, O.M. Monoamine Oxidase Is a Source of Cardiac Oxidative Stress in Obese Rats: The Beneficial Role of Metformin. *Mol. Cell. Biochem.* **2023**, *478*, 59–67.
15. Muellers, S.N.; Tararina, M.A.; Kuzmanovic, U.; Galagan, J.E.; Allen, K.N. Structural Insights into the Substrate Range of a Bacterial Monoamine Oxidase. *Biochemistry* **2023**, *62*, 851–862.
16. Syu, G.-D.; Sutandy, F.X.R.; Chen, K.; Cheng, Y.; Chen, C.-S.; Shih, J.C. Autoantibody Profiling of Monoamine Oxidase A Knockout Mice, an Autism Spectrum Disorder Model. *Brain Behav. Immun.* **2023**, *107*, 193–200.
17. Finberg, J.P.M.; Rabey, J.M. Inhibitors of MAO-A and MAO-B in Psychiatry and Neurology. *Front. Pharmacol.* **2016**, *7*, 340.
18. Meepagala, K.M.; Sturtz, G.; Wedge, D.E.; Schrader, K.K.; Duke, S.O. Phytotoxic and Antifungal Compounds from Two Apiaceae Species, *Lomatium Californicum* and *Ligusticum Hultenii*, Rich Sources of Z-Ligustilide and Apiol, Respectively. *J Chem Ecol* **2005**, *31*, 1567–1578.
19. Momin, R.A.; Nair, M.G. Mosquitocidal, Nematicidal, and Antifungal Compounds from *Apium Graveolens* L. Seeds. *J. Agric. Food Chem.* **2001**, *49*, 142–145.
20. Wedge, D.E.; Klun, J.A.; Tabanca, N.; Demirci, B.; Ozek, T.; Baser, K.H.C.; Liu, Z.; Zhang, S.; Cantrell, C.L.; Zhang, J. Bioactivity-Guided Fractionation and GC/MS Fingerprinting of *Angelica Sinensis* and *Angelica Archangelica* Root Components for Antifungal and Mosquito Deterrent Activity. *J. Agric. Food Chem.* **2009**, *57*, 464–470.
21. Sim, Y.; Shin, S. Combinatorial Anti-Trichophyton Effects of Ligusticum Chuanxiong Essential Oil Components with Antibiotics. *Arch. Pharm. Res.* **2008**, *31*, 497–502.
22. Fisher, M.C.; Alastruey-Izquierdo, A.; Berman, J.; Bicanic, T.; Bignell, E.M.; Bowyer, P.; Bromley, M.; Brüggemann, R.; Garber, G.; Cornely, O.A.; et al. Tackling the Emerging Threat of Antifungal Resistance to Human Health. *Nat Rev Microbiol* **2022**, *20*, 557–571.
23. Bhattacharya, S.; Sae-Tia, S.; Fries, B.C. Candidiasis and Mechanisms of Antifungal Resistance. *Antibiotics* **2020**, *9*, 312.
24. Delattin, N.; Cammue, B.P.; Thevissen, K. Reactive Oxygen Species-Inducing Antifungal Agents and Their Activity against Fungal Biofilms. *Future Med. Chem.* **2014**, *6*, 77–90.
25. Arastehfar, A.; Gabaldón, T.; Garcia-Rubio, R.; Jenks, J.D.; Hoenigl, M.; Salzer, H.J.F.; Ilkit, M.; Lass-Flörl, C.; Perlin, D.S. Drug-Resistant Fungi: An Emerging Challenge Threatening Our Limited Antifungal Armamentarium. *Antibiotics* **2020**, *9*, 877.
26. Fleet, G.H. Yeasts in fruit and fruit products. In *Yeasts in Food. Beneficial and Detrimental Aspects*; Boekhout, T., Robert, V., Eds.; CRC Press Woodhead Publishing: Cambridge, UK, **2003**, *28*, 219–316.
27. Geronikou, A.; Srimahaeak, T.; Rantsiou, K.; Triantafyllidis, G.; Larsen, N.; Jespersen, L. Occurrence of Yeasts in White-Brined Cheeses: Methodologies for Identification, Spoilage Potential and Good Manufacturing Practices. *Front. Microbiol.* **2020**, *11*, 582778.

28. Ge, G.; Li, D.; Mei, H.; Lu, G.; Zheng, H.; Liu, W.; Shi, D. Different Toenail Onychomycosis Due to *Rhodotorula Mucilaginosa* and *Candida Parapsilosis* in an Immunocompetent Young Adult. *Medical Mycology Case Reports* **2019**, *24*, 69–71.
29. Ioannou, P.; Vamvoukaki, R.; Samonis, G. *Rhodotorula* Species Infections in Humans: A Systematic Review. *Mycoses* **2019**, *62*, 90–100.
30. Uludag Altun, H.; Meral, T.; Turk Aribas, E.; Gorpelioglu, C.; Karabicak, N. A Case of Onychomycosis Caused by *Rhodotorula Glutinis*. *Case Reports in Dermatological Medicine* **2014**, *2014*, 1–4.
31. Tallarida, R.J. Quantitative Methods for Assessing Drug Synergism. *Genes & Cancer* **2011**, *2*, 1003–1008.
32. Gong, Y.; Liu, W.; Huang, X.; Hao, L.; Li, Y.; Sun, S. Antifungal Activity and Potential Mechanism of N-Butylphthalide Alone and in Combination with Fluconazole Against *Candida albicans*. *Front. Microbiol.* **2019**, *10*, 1461.
33. Krężel, P.; Olejniczak, T.; Tołoczko, A.; Gach, J.; Weselski, M.; Bronisz, R. Synergic Effect of Phthalide Lactones and Fluconazole and Its New Analogues as a Factor Limiting the Use of Azole Drugs against Candidiasis. *Antibiotics* **2022**, *11*, 1500.
34. Zhang, Z.; Tang, W. Drug Metabolism in Drug Discovery and Development. *Acta Pharmaceutica Sinica B* **2018**, *8*, 721–732.
35. Kebamo, S.; Tesema, S. The Role of Biotransformation in Drug Discovery and Development. *J Drug Metab Toxicol* **2015**, *06*.
36. Phang-Lyn S, Llerena VA. Biochemistry, Biotransformation. In: StatPearls. *StatPearls Publishing, Treasure Island (FL)* **2022**.
37. Shanu-Wilson, J.; Evans, L.; Wrigley, S.; Steele, J.; Atherton, J.; Boer, J. Biotransformation: Impact and Application of Metabolism in Drug Discovery. *ACS Med. Chem. Lett.* **2020**, *11*, 2087–2107.
38. Duan, F.; Xu, W.; Liu, J.; Jia, Z.; Chen, K.; Chen, Y.; Wang, M.; Ma, K.; Dong, J.; Chen, L.; et al. Preparing the Key Metabolite of Z -Ligustilide in Vivo by a Specific Electrochemical Reaction. *J. Sep. Sci.* **2018**, *41*, 2799–2807.
39. Hüttel, W.; Hoffmeister, D. Fungal Biotransformations in Pharmaceutical Sciences. In *Industrial Applications*; Hofrichter, M., Ed.; Springer: Berlin/Heidelberg, Germany, **2011**; pp. 293–317.
40. Kelly, S.L.; Kelly, D.E. Microbial Cytochromes P450: Biodiversity and Biotechnology. Where Do Cytochromes P450 Come from, What Do They Do and What Can They Do for Us? *Philos. Trans. R. Soc. B: Biol. Sci.* **2013**, *368*, 20120476.
41. Lu, W.; Feng, J.; Chen, X.; Bao, Y.-J.; Wang, Y.; Wu, Q.; Ma, Y.; Zhu, D. Distinct Regioselectivity of Fungal P450 Enzymes for Steroidal Hydroxylation. *Appl. Environ. Microbiol.* **2019**, *85*, e01182-19.

42. Zadorozhnii, P.V.; Kiselev, V.V.; Kharchenko, A.V. In Silico ADME Profiling of Salubrinal and Its Analogues. *Future Pharmacology* **2022**, *2*, 160–197.
43. Dulsat, J.; López-Nieto, B.; Estrada-Tejedor, R.; Borrell, J.I. Evaluation of Free Online ADMET Tools for Academic or Small Biotech Environments. *Molecules* **2023**, *28*, 776.
44. Chmiel, T.; Mieszkowska, A.; Kempieńska-Kupczyk, D.; Kot-Wasik, A.; Namieśnik, J.; Mazerska, Z. The Impact of Lipophilicity on Environmental Processes, Drug Delivery and Bioavailability of Food Components. *Microchem. J.* **2019**, *146*, 393–406.
45. Morak-Młodawska, B.; Jeleń, M.; Martula, E.; Korlacki, R. Study of Lipophilicity and ADME Properties of 1,9-Diazaphenothiazines with Anticancer Action. *IJMS* **2023**, *24*, 6970.
46. Benkova, M.; Soukup, O.; Prchal, L.; Šleha, R.; Eleršek, T.; Novak, M.; Sepčić, K.; Gunde-Cimerman, N.; Dolezal, R.; Bostik, V.; et al. Synthesis, Antimicrobial Effect and Lipophilicity-Activity Dependence of Three Series of Dichained N -Alkylammonium Salts. *ChemistrySelect* **2019**, 12076 – 12084.
47. Tamaian, R.; Moț, A.; Silaghi-Dumitrescu, R.; Ionuț, I.; Stana, A.; Oniga, O.; Nastasă, C.; Benedec, D.; Tiperciuc, B. Study of the Relationships between the Structure, Lipophilicity and Biological Activity of Some Thiazolyl-Carbonyl-Thiosemicarbazides and Thiazolyl-Azoles. *Molecules* **2015**, *20*, 22188–2220.
48. CLSI, Reference Reference Method for Broth Dilution Antifungal Susceptibility Testing of Yeasts, Approved Standard, 2nd ed., NCCLS document M27-A2. CLSI, 940 West Valley Road, Suite 1400, Wayne, Pennsylvania 19087-1898, USA, **2002**.
49. Arthington-Skaggs, B.A.; Lee-Yang, W.; Ciblak, M.A.; Frade, J.P.; Brandt, M.E.; Hajjeh, R.A.; Harrison, L.H.; Sofair, A.N.; Warnock, and D.W. Comparison of Visual and Spectrophotometric Methods of Broth Microdilution MIC End Point Determination and Evaluation of a Sterol Quantitation Method for In Vitro Susceptibility Testing of Fluconazole and Itraconazole against Trailing and Nontrailing *Candida* Isolates. *Antimicrob Agents Chemother* **2002**, *46*, 2477–2481.
50. Pillai, S.K., Moellering, R.C. and Eliopoulos, G.M. Antimicrobial Combinations. In *Antibiotics in Laboratory Medicine*, Lorian, V., Ed.; Lippincott Williams & Wilkins, Philadelphia, USA, **2005**, 365-440.
51. Grzelczyk, J.; Budryn, G.; Peña-García, J.; Sz wajgier, D.; Gałazka-Czarnecka, I.; Oracz, J.; Pérez-Sánchez, H. Evaluation of the Inhibition of Monoamine Oxidase A by Bioactive Coffee Compounds Protecting Serotonin Degradation. *Food Chemistry* **2021**, *348*, 129108.
52. Sima, I.A.; Kot-Wasik, A.; Wasik, A.; Namieśnik, J.; Sârbu, C. Assessment of Lipophilicity Indices Derived from Retention Behavior of Antioxidant Compounds in RP-HPLC. *Molecules* **2017**, *22*, 550.
53. Yan, R.; Ling Ko, N.; Ma, B.; Kau Tam, Y.; Lin, G. Metabolic Conversion from Co-Existing Ingredient Leading to Significant Systemic Exposure of Z-Butylidenephthalide, a Minor Ingredient in Chuanxiong Rhizoma in Rats. *CDM* **2012**, *13*, 524–534.

54. Diao, X.; Deng, P.; Xie, C.; Li, X.; Zhong, D.; Zhang, Y.; Chen, X. Metabolism and Pharmacokinetics of 3- *n* -Butylphthalide (NBP) in Humans: The Role of Cytochrome P450s and Alcohol Dehydrogenase in Biotransformation. *Drug Metab. Dispos.* **2013a**, *41*, 430–444.
55. Lin, L.; Lin, L.; Lin, T.; Wu, Y. Simultaneous Determination of 3-*n*-butylphthalide and Its Metabolite 10-hydroxy-butylphthalide in Rat Plasma Using Liquid Chromatography–Tandem Mass Spectrometry and Application to a Pharmacokinetic Study. *Biomed. Chromatogr.* **2021**, *35*, e5184.
56. Zhang, X.; Feng, Z.; Yang, Y.; Jiang, J.; Zhang, P. Bioactive Butylphthalide Derivatives from *Ligusticum Chuanxiong*. *Bioorganic Chem.* **2019**, *84*, 505–510.
57. Diao, X.; Ma, Z.; Wang, H.; Zhong, D.; Zhang, Y.; Jin, J.; Fan, Y.; Chen, X. Simultaneous Quantitation of 3-*n*-Butylphthalide (NBP) and Its Four Major Metabolites in Human Plasma by LC–MS/MS Using Deuterated Internal Standards. *Journal of Pharmaceutical and Biomedical Analysis* **2013b**, *78–79*, 19–26.
58. Diao, X.; Zhong, K.; Li, X.; Zhong, D.; Chen, X. Isomer-Selective Distribution of 3-*n*-Butylphthalide (NBP) Hydroxylated Metabolites, 3-Hydroxy-NBP and 10-Hydroxy-NBP, across the Rat Blood-Brain Barrier. *Acta Pharmacol Sin* **2015**, *36*, 1520–1527.
59. Diekema, D.J.; Petroelje, B.; Messer, S.A.; Hollis, R.J.; Pfaller, M.A. Activities of Available and Investigational Antifungal Agents against *Rhodotorula* Species. *J Clin Microbiol* **2005**, *43*, 476–478.
60. Afzali, S.; Edalatian Dovom, M.R.; Habibi Najafi, M.B.; Mazaheri Tehrani, M. Determination of the Anti-Yeast Activity of Lactobacillus Spp. Isolated from Traditional Iranian Cheeses in Vitro and in Yogurt Drink (Doogh). *Sci. Rep.* **2020**, *10*, 6291.
61. Mishra, B.; Mishra, A.K.; Kumar, S.; Mandal, S.K.; Nsv, L.; Kumar, V.; Baek, K.-H.; Mohanta, Y.K. Antifungal Metabolites as Food Bio-Preservative: Innovation, Outlook, and Challenges. *Metabolites* **2021**, *12*, 12.
62. Blanco-Padilla, A.; Soto, K.M.; Hernández Iturriaga, M.; Mendoza, S. Food Antimicrobials Nanocarriers. *Sci. World J.* **2014**, *2014*, 837215.
63. Khot, M.; Ghosh, D. Lipids of *Rhodotorula mucilaginosa* IIPL32 with Biodiesel Potential: Oil Yield, Fatty Acid Profile, Fuel Properties. *J. Basic Microbiol.* **2017**, *57*, 345–352.
64. Patel, A.; Pruthi, V.; Pruthi, P.A. Synchronized Nutrient Stress Conditions Trigger the Diversion of CDP-DG Pathway of Phospholipids Synthesis towards de Novo TAG Synthesis in Oleaginous Yeast Escalating Biodiesel Production. *Energy* **2017**, *139*, 962–974.
65. Singh, P. Budding Yeast: An Ideal Backdrop for In Vivo Lipid Biochemistry. *Front. Cell Dev. Biol.* **2017**, *4*.
66. Dasgupta, D.; Sharma, T.; Bhatt, A.; Bandhu, S.; Ghosh, D. Cultivation of Oleaginous Yeast *Rhodotorula mucilaginosa* IIPL32 in Split Column Airlift Reactor and Its Influence on Fuel Properties. *Biocatal. Agric. Biotechnol.* **2017**, *10*, 308–316.
67. Sorgo, A.G.; Heilmann, C.J.; Dekker, H.L.; Bekker, M.; Brul, S.; de Koster, C.G.; de Koning, L.J.; Klis, F.M. Effects of Fluconazole on the Secretome, the Wall Proteome, and Wall Integrity of the Clinical Fungus *Candida albicans*. *Eukaryot. Cell* **2011**, *10*, 1071–1081.

68. Warrilow, A.G.S.; Price, C.L.; Parker, J.E.; Rolley, N.J.; Smyrniotis, C.J.; Hughes, D.D.; Thoss, V.; Nes, W.D.; Kelly, D.E.; Holman, T.R.; et al. Azole Antifungal Sensitivity of Sterol 14 α -Demethylase (CYP51) and CYP5218 from *Malassezia Globosa*. *Sci Rep* **2016**, *6*, 27690.
69. Han, G.; Liu, N.; Li, C.; Tu, J.; Li, Z.; Sheng, C. Discovery of Novel Fungal Lanosterol 14 α -Demethylase (CYP51)/Histone Deacetylase Dual Inhibitors to Treat Azole-Resistant Candidiasis. *J. Med. Chem.* **2020**, *63*, 5341–5359.
70. Kot, A.M.; Błazejak, S.; Kurcz, A.; Gientka, I.; Kieliszek, M. *Rhodotorula Glutinis*—Potential Source of Lipids, Carotenoids, and Enzymes for Use in Industries. *Appl. Microbiol. Biotechnol.* **2016**, *100*, 6103–6117.
71. Moliné, M.; Libkind, D.; van Broock, M. Production of Torularhodin, Torulene, and *b*-Carotene by *Rhodotorula* Yeasts. In *Microbial Carotenoids from Fungi*; Barredo, J.-L., Ed.; Methods in Molecular Biology; Humana Press: Totowa, NJ, USA, **2012**; Volume 898, pp. 275–283.
72. Irazusta, V.; Nieto-Peñalver, C.G.; Cabral, M.E.; Amoroso, M.J.; de Figueroa, L.I.C. Relationship among Carotenoid Production, Copper Bioremediation and Oxidative Stress in *Rhodotorula mucilaginosa* RCL-11. *Process Biochem.* **2013**, *48*, 803–809.
73. Xu, Y.; Harvey, P.J. Mitosis Inhibitors Induce Massive Accumulation of Phytoene in the Microalga *Dunaliella Salina*. *Marine Drugs* **2021**, *19*, 595.
74. Geng, C.; Hao, G.; Yi, Q.; Guo, Y.; Chen, D.; Han, W.; Zhang, J.; Yang, M.; Jiang, P. The Impact of D1-3-n-Butylphthalide on the Lipidomics of the Hippocampus in a Rat Model of Lipopolysaccharide-Induced Depression. *Prostaglandins Other Lipid Mediat.* **2020**, *150*, 106464.
75. Maffei, M.E. 5-Hydroxytryptophan (5-HTP): Natural Occurrence, Analysis, Biosynthesis, Biotechnology, Physiology and Toxicology. *IJMS* **2020**, *22*, 181.
76. Guan L, Yang H, Cai Y, Sun L, Di P, Li W, Liu G, Tang Y. ADMET-score - a comprehensive scoring function for evaluation of chemical drug-likeness. *Medchemcomm.* **2018**, *10*, 148-157.
77. Miller, R.R.; Madeira, M.; Wood, H.B.; Geissler, W.M.; Raab, C.E.; Martin, I.J. Integrating the Impact of Lipophilicity on Potency and Pharmacokinetic Parameters Enables the Use of Diverse Chemical Space during Small Molecule Drug Optimization. *J. Med. Chem.* **2020**, *63*, 12156–12170.

OŚWIADCZENIA O WKŁADZIE W PUBLIKACJE

Publikacja 1

Gach, J.; Olejniczak, T.; Krężel, P.; Boratyński, F. Microbial Synthesis and Evaluation of Fungistatic Activity of 3-Butyl-3-Hydroxyphthalide, the Mammalian Metabolite of 3-*n*-Butylidenephthalide. *IJMS* **2021**, *22*, 7600.

Załącznik nr 3 do Trybu postępowania w sprawie nadania stopnia naukowego doktora

Joanna Gach

imię i nazwisko

Wrocław, 21.08.2023

miejsowość i data

Katedra Chemii Żywności i Biokatalizy,
Uniwersytet Przyrodniczy we Wrocławiu, ul. C.K. Norwida 25, 50-375 Wrocław
afiliacja

OŚWIADCZENIE

Oświadczam, że w pracy: Gach J., Olejniczak T., Krężel P., Boratyński F. 2021, Microbial Synthesis and Evaluation of Fungistatic Activity of 3-Butyl-3-hydroxyphthalide, the Mammalian Metabolite of 3-*n*-Butylidenephthalide, International Journal of Molecular Sciences, 22, 7600; mój udział polegał na wykonaniu biotransformacji 3-*n*-butylidenoftalidu, ekstrakcji, przygotowaniu prób i analizie za pomocą wysokosprawnej chromatografii cieczowej z detektorem DAD, a także chromatografii gazowej z detektorem FID, oczyszczeniu chromatograficznym, przygotowaniu prób i analizie widm magnetycznego rezonansu jądrowego, chromatograficznym wyznaczeniu lipofilowości, dokonaniu analiz *in silico*, przetworzeniu danych i analizie eksperymentu aktywności fungistatycznej, wizualizacji danych i napisaniu manuskryptu.

21.08.23 Gach.....

data i podpis

Potwierdzam treść oświadczenia.

21.08.2023 Olejniczak.....
data i podpis promotora

Publikacja 2

Gach, J.; Grzelczyk, J.; Strzała, T.; Boratyński, F.; Olejniczak, T. Microbial Metabolites of 3-*n*-Butylphthalide as Monoamine Oxidase A Inhibitors. *IJMS* **2023**, *24*, 10605.

Załącznik nr 3 do Trybu postępowania w sprawie nadania stopnia naukowego doktora

Joanna Gach
imię i nazwisko

Wrocław, 21.08.2023
miejscowość i data

Katedra Chemii Żywności i Biokatalizy,
Uniwersytet Przyrodniczy we Wrocławiu, ul. C.K. Norwida 25, 50-375 Wrocław
afiliacja

OŚWIADCZENIE

Oświadczam, że w pracy: Gach J., Grzelczyk J., Strzała T., Boratyński F., Olejniczak T., 2023, Microbial Metabolites of 3-*n*-butylphthalide as Monoamine Oxidase A Inhibitors, International Journal of Molecular Sciences, 24, 10605, mój udział polegał na opracowaniu koncepcji badań, wykonaniu biotransformacji 3-*n*-butyloftalidu, ekstrakcji, przygotowaniu prób i analizie za pomocą wysokosprawnej chromatografii cieczowej z detektorem DAD, przygotowaniu prób i analizie widm magnetycznego rezonansu jądrowego, analizie otrzymanych wyników LC/ESI-MS/MS, przygotowaniu schematów 1-5 oraz tabeli 1, napisaniu manuskryptu z wyłączeniem sekcji 2.2. Inhibition of MAO-A Activity, 2.4. Molecular Species Identification i części dyskusji dotyczącej aktywności MAO-A i metodyki dotyczącej powyższych punktów.

21.08.23 Gach
data i podpis

Potwierdzam treść oświadczenia.

21.08.2023 Olejniczak
data i podpis promotora

Publikacja 3

Gach, J.; Olejniczak, T.; Pannek, J.; Boratyński, F. Fungistatic Effect of Phthalide Lactones on *Rhodotorula mucilaginosa*. *Molecules* **2023**, *28*, 5423.

Załącznik nr 3 do Trybu postępowania w sprawie nadania stopnia naukowego doktora

Joanna Gach

imię i nazwisko

Wrocław, 21.08.2023

miejsowość i data

Katedra Chemii Żywności i Biokatalizy,
Uniwersytet Przyrodniczy we Wrocławiu, ul. C.K. Norwida 25, 50-375 Wrocław
afiliacja

OŚWIADCZENIE

Oświadczam, że w pracy: Gach J., Olejniczak T., Pannek J., Boratyński F. 2023, Fungistatic Effect of Phthalide Lactones on *Rhodotorula mucilaginosa*. *Molecules*, 28, 5423; mój udział polegał na wykonaniu eksperymentów odnośnie aktywności fungistatycznej, dokonania analiz *in silico*, badania wpływu laktonu na zawartość ergosterolu, wolnych rodników oraz ekstrakcji karotenoidów z biomasy, analiz HPLC-DAD i przygotowania prób do analiz karotenoidów LC/HRMS, analiz zawartości i profilu estrów metylowych kwasów tłuszczowych, interpretacji i wizualizacji danych (Schematy 3-13; Tabele 1-4) i napisaniu manuskryptu z wyłączeniem wstępu, wprowadzenia do dyskusji wyników, fragmentu 2.6. „Synergistic Effect of 3-*n*-Butylidene-phthalide and Fluconazole”.

21.08.23 Gach

data i podpis

Potwierdzam treść oświadczenia.

21.08.2023 Olejniczak

data i podpis promotora

PUBLIKACJE



Article

Microbial Synthesis and Evaluation of Fungistatic Activity of 3-Butyl-3-hydroxyphthalide, the Mammalian Metabolite of 3-*n*-Butylidenephthalide

Joanna Gach * , Teresa Olejniczak * , Piotr Krężel and Filip Boratyński

Department of Chemistry, Wrocław University of Environmental and Life Sciences, Norwida 25, 50-375 Wrocław, Poland; piotr.krezel@outlook.com (P.K.); filip.boratynski@upwr.edu.pl (F.B.)

* Correspondence: joanna.gach@upwr.edu.pl (J.G.); teresa.olejniczak@upwr.edu.pl (T.O.)

Abstract: Phthalides are bioactive compounds that naturally occur in the family Apiaceae. Considering their potentially versatile applications, it is desirable to determine their physical properties, activity and metabolic pathways. This study aimed to examine the utility of whole-cell biocatalysts for obtaining 3-butyl-3-hydroxyphthalide, which is the metabolite formulated during mammalian metabolism of 3-*n*-butylidenephthalide. We performed transformations using 10 strains of fungi, five of which efficiently produced 3-butyl-3-hydroxyphthalide. The product yield, determined by high-performance liquid chromatography, reached 97.6% when *Aspergillus candidus* AM 386 was used as the biocatalyst. Increasing the scale of the process resulted in isolation yields of 29–45% after purification via reversed-phase thin layer chromatography, depending on the strain of the microorganism used. We proposed different mechanisms for product formation; however, hydration of 3-*n*-butylidenephthalide seems to be the most probable. Additionally, all phthalides were tested against clinical strains of *Candida albicans* using the microdilution method. Two phthalides showed a minimum inhibitory concentration, required to inhibit the growth of 50% of organisms, below 50 µg/mL. The 3-*n*-butylidenephthalide metabolite was generally inactive, and this feature in combination with its low lipophilicity suggests its involvement in the detoxification pathway. The log *P* value of tested compounds was in the range of 2.09–3.38.

Keywords: biotransformations; Apiaceae; bioactivity; phthalides; lipophilicity; lactones; antifungal activity



Citation: Gach, J.; Olejniczak, T.; Krężel, P.; Boratyński, F. Microbial Synthesis and Evaluation of Fungistatic Activity of 3-Butyl-3-hydroxyphthalide, the Mammalian Metabolite of 3-*n*-Butylidenephthalide. *Int. J. Mol. Sci.* **2021**, *22*, 7600. <https://doi.org/10.3390/ijms22147600>

Academic Editor: Barbora Szotáková

Received: 21 May 2021

Accepted: 13 July 2021

Published: 15 July 2021

Publisher's Note: MDPI stays neutral with regard to jurisdictional claims in published maps and institutional affiliations.



Copyright: © 2021 by the authors. Licensee MDPI, Basel, Switzerland. This article is an open access article distributed under the terms and conditions of the Creative Commons Attribution (CC BY) license (<https://creativecommons.org/licenses/by/4.0/>).

1. Introduction

Phthalides are a group of bioactive secondary metabolites that are found mainly in plants from the family Apiaceae, such as *Angelica acutiloba*, *Angelica sinensis*, *Apium graveolens*, *Cnidium officinale*, *Levisticum officinale* and *Ligusticum porteri* [1–6]. These compounds have been widely tested for their pharmacological properties [7–11]. 3-*n*-butylphthalide has been authorized for treating brain ischemia in China [7]. Moreover, the analog of this compound, 3-*n*-butylidenephthalide, showed a positive effect on the cardiovascular system, inhibiting angiogenesis in vitro, ex vivo and in vivo in animal models [8]. Furthermore, 3-*n*-butylidenephthalide also exhibited neuroprotective activity by reducing secreted proinflammatory molecules in rat brain glial cells, thus increasing the lifespan of mice with amyotrophic lateral sclerosis [9,10]. A study also reported its antihyperglycemic activity in an animal model [11].

Phthalides have also been examined as potential fungistatic agents. 3-*n*-butylidenephthalide appeared to be more active against dermatophytes than the antifungals itraconazole and ketoconazole [12]. Significantly, similarly structured 3-*n*-butylphthalide inhibited the growth of four clinical strains of *Candida albicans*, while the reference drug, fluconazole, was inactive at much higher concentrations [13]. *Candida* species are one of the most common causes of fungal infections worldwide. Even though these microorganisms are ubiquitous

in humans, they can establish mucus membrane infections in cases of microbiome disturbances or even severe systemic candidiasis in immunocompromised patients [14–16]. The development of novel antifungals is necessitated by the rising resistance of *Candida* yeasts to antifungals, such as azoles, and drawbacks of these compounds, such as toxicity and possible drug-drug interactions [17–20]. Notably, approximately 80% of antifungal agents are not investigated owing to their adverse effects [20]. The possible pharmacological application of phthalides warrants the assessment of their metabolic pathways. It is crucial to evaluate the toxicity and bioavailability of novel treatments at the earliest possible stage in order to avoid problems during subsequent phases. For instance, compounds may undergo bioactivation to reactive hepatotoxic derivatives [21]. Thus, the products of phthalide metabolism must be studied extensively. The small amounts of drug metabolites tested in vivo may pose an issue with their detection [22]; therefore, the in vitro preparation of metabolites may allow for easier determination of their structure and facilitate further investigations. Microbial whole-cell transformation is a viable system utilized for this purpose; it enables the metabolite to be obtained in high quantities and at a feasible cost [23].

Fungi-mediated biotransformations allow production of compounds with high regio- and stereoselectivity through reduction, oxidation, epoxidation, hydrogenation, hydrolysis, amination, acylation, glucosylation, epoxidation, hydration, methylation and hydroxylation by cytochrome P450 enzymes, especially regarding steroid conversion [24–26]. Moreover, the valuable characteristic of a fungi-based approach is the complexity of their metabolic abilities, allowing for xenobiotic degradation that is partially reminiscent of mammalian metabolism [26].

Diao et al. reported that hydroxylation of 3-*n*-butylphthalide, a saturated analogue of 3-*n*-butylidenephthalide, was the main metabolic route in humans, and that this hydroxylation occurred on the side chain instead of the relatively stable benzene ring. Similarly, use of this substrate in the culture of *Cunninghamella blakesleana* ATCC9244 also yielded hydroxylated compounds, including hydroxy-3-butylphthalide [27]. Furthermore, Yan et al. reported the formation of this product during the metabolism of 3-*n*-butylidenephthalide in rats [28]. Nevertheless, 3-*n*-butylidenephthalide has not previously been transformed using microbial whole cells.

Lipophilicity, defined as the affinity of a compound towards nonpolar phase, is also significant for potential drug evaluation [29]. The log *P* parameter is linked to the absorption, distribution, metabolism and excretion processes [30,31]. It has been shown that lipophilicity that is too high is associated with undesirable properties, such as accumulation of the compound in the adipose tissue [32]. According to Lipinski's rule of five, the log *P* value should not exceed 5 [33].

Research on phthalides and their metabolites should focus not only on determining their structure, but also on assessing their physical properties, activity and metabolic pathways by analyzing structural analogs. Therefore, our primary aim was to determine whether the fungi transform 3-*n*-butylidenephthalide to 3-butyl-3-hydroxyphthalide: the identical compound that is formed in small quantities during rat metabolism, precluding its isolation. Efficient synthesis of this metabolite using microorganisms would be an attractive alternative approach in comparison to chemical synthesis.

Moreover, we aimed to elucidate the mechanisms of the biotransformation process. Considering the possible pharmacological applications of this research, we also assessed the lipophilicity of the substrate and its metabolite and compared their inhibitory potential against four *Candida albicans* strains.

2. Results and Discussion

Screening biotransformations involving fungal strains were performed to select the most effective biocatalysts for producing 3-butyl-3-hydroxyphthalide (**2**). This approach allowed the resulting microorganisms to be used in scale-up processes to isolate the metabolite and confirm its structure by nuclear magnetic resonance (NMR) spectroscopy

(Figures S1–S16, Supplementary Materials). Next, we evaluated the lipophilicity of compounds using reversed-phase high-performance liquid chromatography (RP-HPLC) and tested their antimicrobial properties against selected *Candida* yeasts. We also aimed to establish whether a metabolite with a different polarity also exhibits bioactive potential or is suggestive of xenobiotic detoxification.

2.1. Biotransformations of 3-*n*-Butylidenephthalide (1)

To obtain 3-butyl-3-hydroxyphthalide (2) from 3-*n*-butylidenephthalide (1), whole cells of fungi were used (Figure 1).

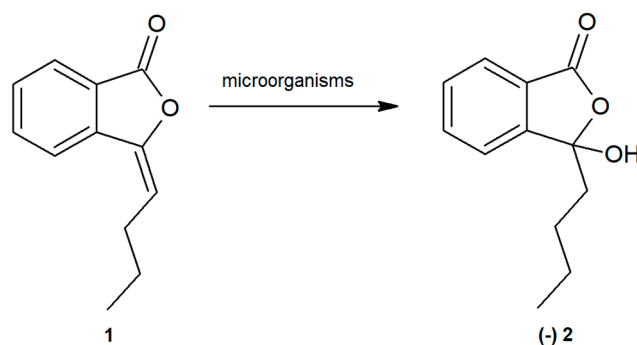


Figure 1. Biotransformation of 3-*n*-butylidenephthalide (1) to (-)-3-butyl-3-hydroxyphthalide (2) using whole fungal cells.

Initially, screening-scale biotransformation of 3-*n*-butylidenephthalide (1) was conducted using 10 fungal strains, which were analyzed for their catalytic potential. These strains included *Absidia cylindrospora* AM 336, *Ascospaera apis* AM 496, *Aspergillus candidus* AM 386, *Chaetomium indicum* AM 158, *Fusarium culmorum* AM 9, *Fusicoccum amygdali* AM 258, *Laetisporus sulphurens* AM 515, *Mucor spinosus* AM 398, *Penicillium chrysogenum* AM 112 and *Pycnidiella resinae* AM 50 (data not shown). Of these, the five strains that exhibited the most efficient product (2) formation were *Aspergillus candidus* AM 386, *Absidia cylindrospora* AM 336, *Mucor spinosus* AM 398, *Chaetomium indicum* AM 158 and *Pycnidiella resinae* AM 50. These five strains were chosen for further screening.

Biotransformation of 3-*n*-butylidenephthalide (1) as a mixture of (*E*) and (*Z*) isomers (9:1) at a concentration of 0.27 mg/mL was carried out for 14 days at 25 °C with shaking culture in Sabouraud medium. Samples were taken every 2 days, extracted with ethyl acetate and analyzed via thin layer chromatography (TLC) and HPLC (Figures S14–16, Supplementary Materials).

The highest product (2) yield of 97.61% was obtained using *A. candidus* AM 386 on day 4, as determined by HPLC (Figure 2). However, in contrast to that in other strains, *A. candidus* AM 386 further metabolized compound (2) to unidentified derivatives. The other tested microorganisms, *A. cylindrospora* AM 336, *M. spinosus* AM 398, *C. indicum* AM 158 and *P. resinae* AM 50, produced yields between 25.13% and 72.40% by day 14. We also focused on the pH of the cultures over the course of the biotransformations (Figure 3). In cultures with *M. spinosus* AM 398 and *P. resinae* AM 50, the conditions were slightly acidic (pH 5–6), whereas the *A. cylindrospora* AM 336 and *C. indicum* AM 158 strains subtly alkalinized the culture (pH 7.4–8.5). In the *A. candidus* AM 386 culture, the pH was in the range of 5.5–5.0 in the first few days but subsequently increased to 8.5. The sudden change in pH value presumably occurred due to the change in nutrient availability. During culture growth, depletion of the carbon source causes stress for the microbial cells, resulting in extracellular release of ammonia [34]. The stability of the compounds under extreme pH conditions were examined using a mixture of substrates and products.

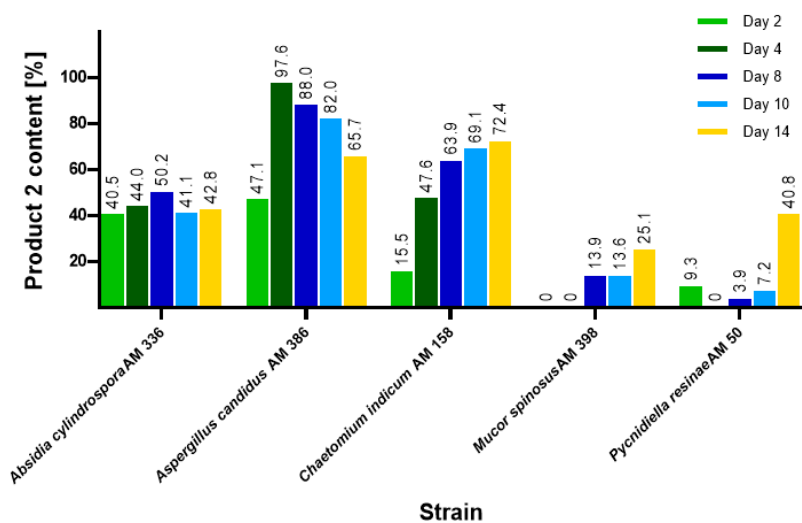


Figure 2. Content of product (2) during the screening-scale biotransformations of 3-*n*-butylidene-phthalide (1) determined using a high-performance liquid chromatography-diode array detector.

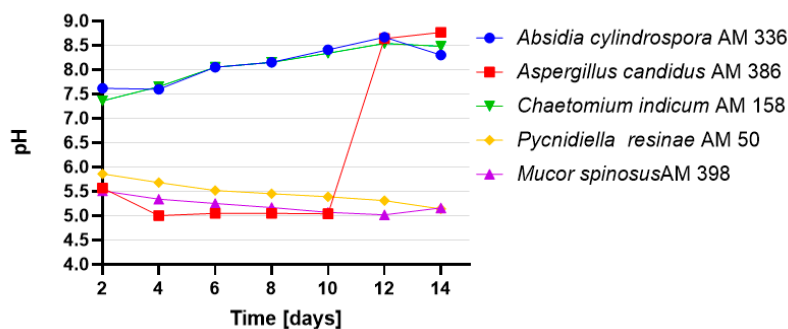


Figure 3. pH values of cultures during the screening-scale transformations of 3-*n*-butylidene-phthalide (1).

In order to confirm the structure of compound (2) and determine its mechanism of action, we scaled up the biotransformation with the following strains: *A. candidus* AM 386, *A. cylindrospora* AM 336 and *C. indicum* AM 158. We decided to use three strains on a preparative scale instead of focusing on only one of them, as the isolation yields of product (2) might have been diversified. This issue may result from different metabolite concentrations in particular strains, which are not visible during screening-scale transformation while the biotransformation is monitored by HPLC. We also sought to determine the stereoselectivity of the process for particular strains. Biotransformations were performed in 2000-mL shaken flasks with 3-*n*-butylidene-phthalide (1) at a concentration of 150 mg/500 mL at 25 °C. The products were analyzed using gas chromatography (GC), HPLC and RP-TLC. All three microorganisms sufficiently transformed 3-*n*-butylidene-phthalide (1) (Figure 4). The conversion of the substrate was slower in *C. indicum* AM 158, which is consistent with the results of the small-scale experiments. The biotransformations continued until day 14 with the exception of *A. candidus* AM 386, which was only continued to day 8 because of an observed decrease in product yield.

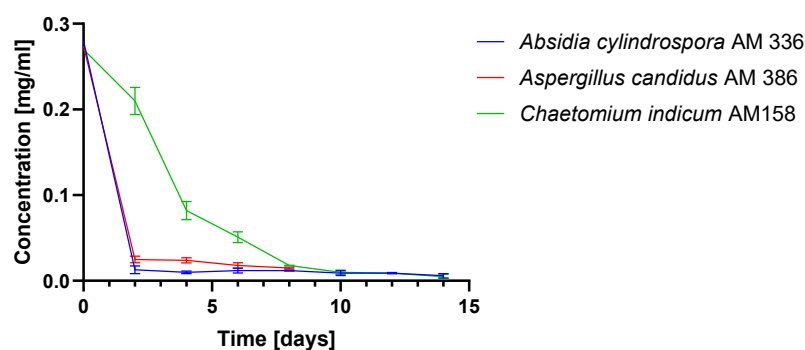


Figure 4. Change in 3-*n*-butylidene-phthalide (1) concentration during scale-up biotransformation determined by gas chromatography.

The pH of the culture media was in the range of 7–8.25 when using fungi from the genera *Chaetomium* and *Absidia*. Meanwhile, the pH of cultures of fungi from the genus *Aspergillus* was acidic and remained stable at pH 5 during biotransformation. Monitoring the pH value allowed us to determine whether it was necessary to acidify the samples to extract the product from the organic phase. The biotransformation mixtures were extracted by ethyl acetate and purified on RP-TLC plates (Figure S12, Supplementary Materials).

Using NMR spectra, we confirmed that the main isolated product of the biotransformation was (-)-3-butyl-3-hydroxyphthalide (2). The assignment of aromatic signals of 3-butyl-3-hydroxyphthalide (2) in the range of $\delta = 7.56$ – 7.81 ppm was mainly allowed by Correlation Spectroscopy (COSY) (coupling of H-5 with H-6 and H-4 protons). This was also facilitated via Nuclear Multiple Bond Coherence (HMBC) spectrum coupling of C-13 with protons H-5 and H-7 without correlation with H-4, as well as a coupling of C-12 with H-4 and H-6 without correlation with H-7 (Figure 5). The presence of a hydroxyl group was confirmed by the broad signal in the range of $\delta = 3.70$ – 4.50 ppm (Figure S3, Supplementary Materials). The characteristic signal for the proton H-8 in the substrate structure at $\delta = 5.64$ was absent in the spectra of this derivative. The signal for the carbon atom with the hydroxyl group (C-3) in the 3-butyl-3-hydroxyphthalide (2) spectrum was shifted upfield ($\delta = 107.9$) when compared to that of the unsubstituted carbon atom ($\delta = 145.9$) in the precursor compound (1) (Figure S4, Supplementary Materials).

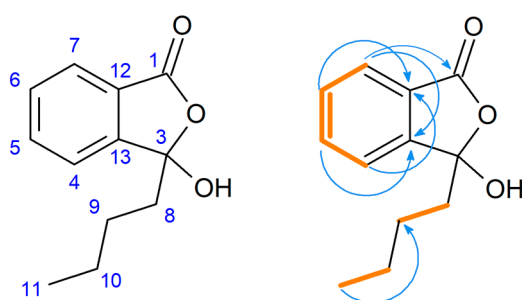


Figure 5. Pivotal Correlation Spectroscopy (orange bolded) and Nuclear Multiple Bond Coherence (arrows) correlations of 3-butyl-3-hydroxyphthalide (2).

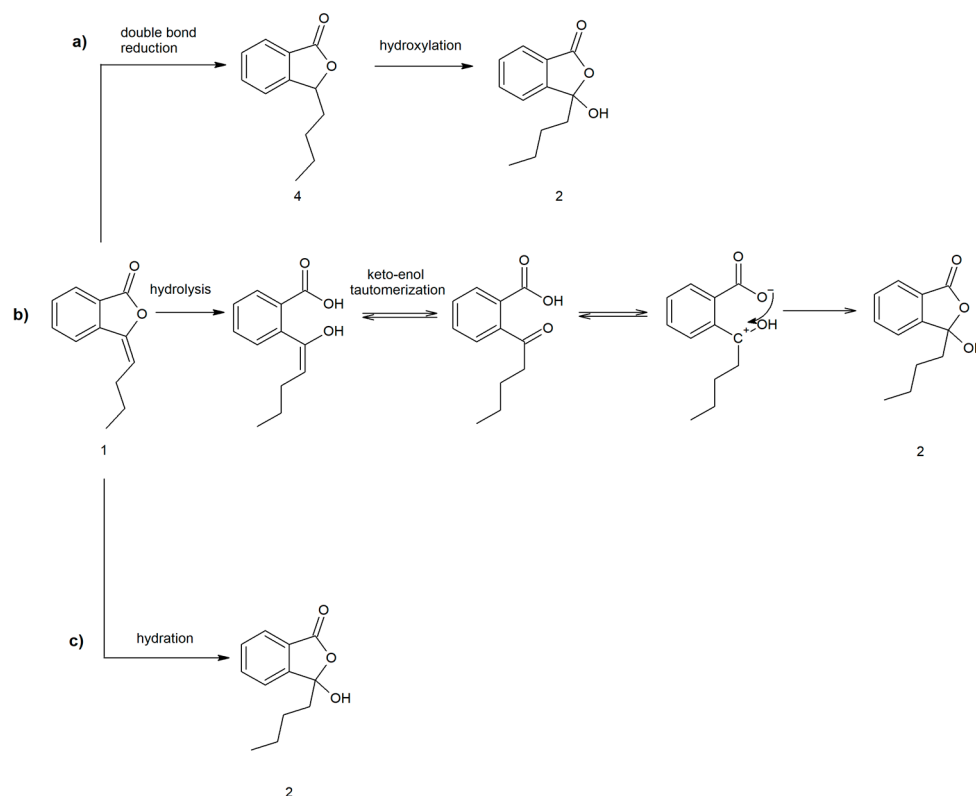
Overall, the yield of the product (2) in the biotransformation mixture at the end of the process was in the range 57–82% depending on the strain used, as determined by HPLC. The yield after isolation was approximately 29–45% (Table 1). The specific rotations $[\alpha]_{589}^{25}$ of product (2) isolated from particular strains were as follows: -2.4 ($c = 1.0$, CHCl_3) for *A. cylindrospora* AM 336; -0.5 ($c = 1.0$, CHCl_3) for *A. candidus* AM 386; and -3.6 ($c = 1.0$, CHCl_3) for *C. indicum* AM 158.

Table 1. Product (2) content in the biotransformation mixtures at the end of the processes both before and after isolation.

Strain	Time of the Process [Days]	3-Butyl-3-hydroxyphthalide (2)	
		(Based on HPLC) [%]	(Isolation Yield) [%]
<i>Chaetomium indicum</i> AM 158	14	69.8	36.6
<i>Absidia cylindrospora</i> AM 336	14	57.0	29.2
<i>Aspergillus candidus</i> AM 386	8	82.2	45.4

2.2. Proposed Pathways for 3-Butyl-3-hydroxyphthalide (2) Formation

Hydroxylation frequently occurs via cytochrome P450 enzymes involved in xenobiotic metabolism [35]. To examine the possibility of 3-butyl-3-hydroxyphthalide (2) formation through hydroxylation of the saturated analog (4) of 3-*n*-butylidenephthalide (1) (Figure 6), we also performed biotransformations of 3-*n*-butylphthalide (4) using the three previously used microorganisms.

**Figure 6.** Proposed mechanism of 3-butyl-3-hydroxyphthalide (2) formation via (a) the intermediary product 3-*n*-butylphthalide (4); (b) hydrolysis of 3-*n*-butylidenephthalide (1) and (c) hydration of 3-*n*-butylidenephthalide (1).

However, our experiments showed that 3-*n*-butylphthalide (4) was not converted to product (2). We used ^{13}C NMR as a diagnostic tool to analyze the biotransformation mixture. Spectra of the biotransformation mixtures showed a lack of the characteristic signal for the C-3 carbon in 3-butyl-3-hydroxyphthalide (2) at $\delta = 107.9$ ppm (Figure S13, Supplementary Materials). Additionally, the saturated analog (4) of 3-*n*-butylidenephthalide (1) was not observed during the biotransformations. Therefore, the possibility of the conversion of

the compound (1) through the reduction of a double bond followed by hydroxylation was rejected.

Another proposed mechanism involves the microbial hydrolysis of 3-*n*-butylidenephthalide (1), keto-enol tautomerism and the closing of the lactone moiety (Figure 6). Aldol-lactonizations may be selectively conducted by enzymes [36]; however, in the proposed mechanism, the molecule with a positive charge on C-3 carbon is formed (sp^2 hybridization). Such flat carbocation is attacked by all sides of the plane, and thus, obtaining of a racemate is probable. Therefore, as we obtained an optically active product, we excluded this mechanism as a possibility.

The most probable pathway included hydration, which is the addition of water to a double bond in the C-3 position (Figure 6). The hydration route was also proposed by Yan et al. when they investigated the conversion pathway of ligustilide in rat plasma, as well as in later research concerning the metabolism of 3-*n*-butylidenephthalide (1). The researchers proposed the aromatization of ligustilide to 3-*n*-butylidenephthalide (1), with a further addition of water to obtain 3-butyl-3-hydroxyphthalide (2) [28,37]. Hydratases reportedly have certain advantages over synthetic catalyst-mediated enantioselective hydration, as the latter often requires harsh environmental conditions [38].

Unfortunately, to the best of our knowledge, there is no available data on phthalide hydratases. In order to exclude acid-catalyzed hydration as a possible mechanism, compound (1) was additionally dissolved in a water and organic solvent mixture (35:65) in the presence of HCl (pH = 1). Compound (2) was not observed during HPLC analysis of the sample.

Interestingly, Li et al. observed the further methylation of product (2) in rat bile as a metabolite of a Chinese herbal formula containing phthalides, including 3-*n*-butylidenephthalide (1) [39]. Even though 3-butyl-3-methoxyphthalide (3) (Figure 7) was not observed during biotransformations in the cultures of fungal strains, we chemically synthesized this compound. We conducted hydrolysis and a reaction with boron trifluoride of the biotransformation mixture from *A. candidus* AM 386. We then examined whether the incorporation of a methoxy group affects the bioactivity. The substitution of the hydroxyl group in 3-butyl-3-methoxyphthalide (3) was evidenced by the presence of a three-proton singlet at 3.04 ppm (H-3a) (Figure S8, Supplementary Materials).

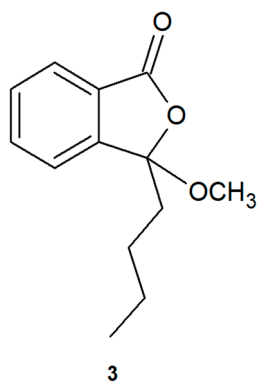


Figure 7. Product (3-butyl-3-methoxyphthalide) (3) of the esterification of the biotransformation mixture of *Aspergillus candidus* AM 386.

2.3. Influence of Lipophilicity and Fungistatic Activity

Xenobiotics are usually converted to more polar metabolites so that they are easily excreted from the organism. The converted compounds may exhibit pharmacological activity or become inactive [21]. We planned to determine whether there is a dependent relationship between the polarity of the metabolite (2) of 3-*n*-butylidenephthalide (1) and its bioactivity. In order to achieve this, we evaluated the pharmacodynamic parameters and fungistatic properties of these compounds.

To assess the lipophilicity of phthalides and their metabolites, the chromatographic partition coefficient ($\log k_w$) and hydrophobicity index (φ_0) values were determined using RP-HPLC based on retention parameters. The partition coefficient ($\log P$) values were calculated using theoretical methods proposed at ALOGPS 2.1.

RP-HPLC is a useful method for preliminary research into drug lipophilicity due to the small amount of compound required [40]. The method is based on the evaluation of the retention factor (k). It has been previously stated that there is a linear correlation between the $\log k$ value and the volume fraction of organic solvent [41]. This dependence, involving the $\log k$ values of five compounds, is presented in Figure 8.

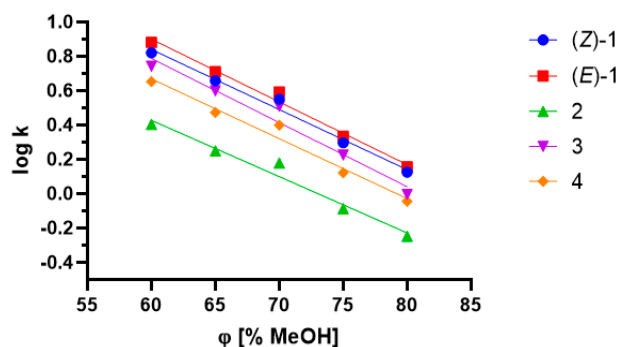


Figure 8. $\log k$ and methanol volume fraction dependence for 3-*n*-butylidene-phthalide (1); 3-butyl-3-hydroxyphthalide (2); 3-butyl-3-methoxyphthalide (3); and 3-*n*-butylphthalide (4).

The chromatographic lipophilicity parameters are presented in Table 2. Overall, high coefficient values of determination (≥ 0.9633) were obtained for all the examined compounds. The highest $\log k_w$ value was achieved for 3-*n*-butylidene-phthalide (1) at -3.094 for isomer (*E*). The metabolite of the abovementioned compound, 3-butyl-3-hydroxyphthalide (2), had a notably higher polarity ($\log k_w = 2.397$). This result confirmed the introduction of a new polar group into the compound, which is typical for phase 1 reactions [21]. Introduction of a methyl group into the structure of 3-butyl-3-methoxyphthalide (3) resulted in increased hydrophobicity ($\varphi_0 = 81.200$) in comparison to (2) ($\varphi_0 = 73.079$). The lack of a double bond in the side chain of 3-*n*-butylphthalide (4) resulted in a higher polarity ($\log k_w = 2.7623$) compared with that of compound (1). The $\log P$ values according to ALOGPS 2.1 did not exceed 3.38 for the abovementioned compounds.

Table 2. Chromatographic partition coefficient ($\log k_w$) and hydrophobicity index (φ_0) for substrate (1) and products of its conversion (3-butyl-3-hydroxyphthalide (2), 3-butyl-3-methoxyphthalide (3) and 3-*n*-butylphthalide (4)) along with the calculated partition coefficient.

Compound	$\log k_w$ **	Standard Error for the Slope	Standard Error for the Intercept	Coefficient of Determination	φ_0 **	$\log P$ (Calculated)
(Z)-1	2.9422	0.0025	0.1747	0.9851	84.063	3.38
*(E)-1 *	3.094	0.0024	0.1673	0.9875	84.536	3.38
2	2.397	0.0032	0.2256	0.9721	73.079	2.09
3	3.029	0.0042	0.2958	0.9633	81.200	2.86
4	2.7623	0.0032	0.2256	0.9752	79.149	3.00

* The separation of (*Z*) and (*E*) isomers are shown on the chromatogram (Figure S14, Supplementary Materials);

** The r value, indicating the correlation between measured $\log k_w$ and calculated $\log P$ values, is 0.8675.

It has been previously stated that 90% of compounds that reach phase 2 clinical trials do not exceed a $\log P$ value of 5 [33]. Studies conducted by Tamaian et al. (2015) on thiazolyl-carbonyl-thiosemicarbazides and thiazolyl-azoles emphasized the importance of optimum hydrophilic-lipophilic balance. These studies showed that the highest bioactivity was observed for the compounds that had medium values for the lipophilicity parameters [42].

Log P values that are too high may result in poorer drug solubility. For instance, the widely used fungistatic ketoconazole with a log P value of 3.73 reportedly belongs to class II of the Biopharmaceutics Classification System, suggesting that the compound has high permeability and low solubility [43,44]. Conversely, another antimycotic fluconazole has a log P value of 0.5 [45]. In theory, such low lipophilicity should be connected with lower membrane permeability [46].

Considering the bioactive potential of phthalides, including 3-*n*-butylidenephthalide (1) and 3-*n*-butylphthalide (4) [7–11,47,48], we determined the antimicrobial potential of these compounds. Moreover, we also tested whether their derivatives (3-butyl-3-hydroxyphthalide (2) and 3-butyl-3-methoxyphthalide (3)) show similar inhibitory properties against selected strains of *C. albicans*. We were particularly interested in whether metabolite (2), with the hydroxyl group in the C-3 position, and its methoxy analogue (3) would also inhibit microorganism growth and whether their lipophilicity influences their activity.

Phthalides from Apiaceae plants, such as 3-*n*-butyl-4,5-dihydrophthalide and sedanolide, have been previously tested against *Candida* yeasts. These phthalides were mostly found to be capable of completely inhibiting these yeasts at a concentration of 100 µg/mL [47,48]. 3-*n*-Butylphthalide (4) showed fungistatic properties against clinical isolates of *Candida albicans* with an MIC₈₀ of 128 µg/mL [13]. However, 3-*n*-butylidenephthalide (1) has not been previously studied against this microorganism.

Overall, we observed that phthalides (1) and (4) were active against all tested *Candida* strains and had MIC₅₀ values ranging from below the smallest tested concentration (23 µg/mL) to 123 µg/mL (Table 3). In two cases, the activity of unsaturated lactone (1) was higher than that of its analog, which did not have the double bond in its side chain (4).

Table 3. Minimal inhibitory concentration (MIC₅₀) [µg/mL] for substrate (1), the product of its conversion: 3-butyl-3-hydroxyphthalide (2), its derivatives 3-butyl-3-methoxyphthalide (3) and 3-*n*-butylphthalide (4) when compared with that of fluconazole.

Compound	<i>C. albicans</i> 636/20	<i>C. albicans</i> 595/20	<i>C. albicans</i> 38	<i>C. albicans</i> ATTC 90028
1	88	<50	<50	110
2	203	>250 ¹	250	>250 ¹
3	244	115	>250 ¹	>250 ¹
4	123	<50	87	89
Fluconazole	>250 ¹	0.89	0.44	4.50

¹ Compounds inactive at the highest tested concentration (250 µg/mL).

3-*n*-Butylidenephthalide (1) efficiently inhibited the growth of the *C. albicans* clinical isolates 595/20 and 38, with an MIC₅₀ below 50 µg/mL. It also inhibited strain 636/20, showing an MIC₅₀ value of 88 µg/mL. By contrast, strain 636/20 was not inhibited by the fluconazole at the highest concentration used (250 µg/mL). This phthalide was slightly less active against *C. albicans* ATTC 90028 and had an MIC₅₀ of 110 µg/mL. 3-*n*-Butylphthalide (4) was also significantly active against the clinical isolate *C. albicans* 595/20, showing an MIC₅₀ below 50 µg/mL. These inhibitory activities of phthalides (1) and (4) might correlate with their high lipophilicity, and thereby with their sufficient membrane permeability.

It appeared that (-)-3-butyl-3-hydroxyphthalide (2) was slightly active only in the case of strains 636/20 and 38, with MIC₅₀ values of 203 and 250 µg/mL, respectively. The compound did not influence the growth of other strains. The lack of activity of 3-butyl-3-hydroxyphthalide (2) suggests that 3-*n*-butylidenephthalide (1) is subjected to an inactivation pathway during its conversion. The lack of activity of (2) corresponds with significantly lower log k_w values, which may indicate that the permeability of the compound is too low. Introduction of the methoxy group in the C-3 position resulted in enhanced activity toward strain 595/20 (MIC₅₀ = 115 µg/mL) compared with that of the metabolite, but it did not improve its fungistatic activity toward strain 636/20

(MIC₅₀ = 244 µg/mL). However, the lipophilicity of (2) had a value close to that displayed by 3-*n*-butylidene-phthalide (1). These results suggest that lipophilicity is not the main determinant of the antifungal activity of phthalides. In the case of 3-butyl-3-methoxyphthalide (3), its molecular structure and the occurrence of spatial hindrance may also influence its decreased activity.

Structure-activity dependences for phthalides have been previously proposed. Considering the dependence between the structure and fungistatic activity, available data focuses on preliminary structure-activity tests of more complex 3-substituted phthalides against selected phytopathogens. It has been stated that -OH and -NH₂ groups incorporated in the benzene ring may increase the antifungal activity of phthalides due to the formation of a hydrogen bond with the active site of the pathogen enzyme [49]. In fact, the lack of the activity of the tested compounds (2) and (3) may be explained by the -OH and -OCH₃ groups at the C-3 position. Xiao et al. showed the linkage between the structure of marine fungal phthalide derivatives and peroxisome proliferator-activated receptor gamma (PPAR-γ) binding and activation properties. This study also showed that the occurrence of an -OH group in the benzene ring has a positive effect on higher bioactivity; conversely, the presence of a double side chain at C-3 in phthalides resulted in lower binding and activation properties compared to compounds with a single chain [50].

3. Materials and Methods

3.1. Compounds

The substrate for the biotransformations—3-*n*-butylidene-phthalide (1) was purchased from Sigma-Aldrich (St. Louis, MO, USA) as the mixture of (*E*) and (*Z*) isomers, at the ratio of 9:1 according to the ¹H NMR and HPLC (wavelength 274 nm).

3-butyl-3-methoxyphthalide (3) was obtained through 24 h alkaline hydrolysis of a mixture of products (80 mg) obtained in the biotransformation catalyzed by *A. candidus* AM 386. The biotransformation was conducted using 3 mL 0.5M KOH in MeOH, and esterification was carried out using 4 mL 20% BF₃ in methanol. After 1 h, the mixture was briefly filtered using silica gel to remove BF₃. The mixture was then eluted by diethyl ether. Crude product was concentrated in a rotary evaporator and purified using silica gel and a hexane:ethyl acetate 19:1 (*v/v*) eluent. The yield of 3-butyl-3-methoxyphthalide (3) was 41.52 mg (51.9%).

3-*n*-Butylphthalide (4) was synthesized as follows: *n*-butyllithium in hexane (*n*-BuLi; Sigma-Aldrich, St. Louis, MO, USA) was added dropwise to the phthalic anhydride dissolved in tetrahydrofuran (7.4 g, 0.05 mol) at -78 °C (isopropanol/CO₂ (s)). The molar ratio of the anhydride to *n*-BuLi was 3:1. The reaction was run for 20 min and then quenched with 10% hydrochloric acid, extracted with diethyl ether, washed with water and dried with MgSO₄. The solvent was then evaporated. The crude extract was dissolved in 30 mL THF and NaBH₄ (1.13 g, 0.03 mol; Sigma-Aldrich, St. Louis, MO, USA) was added. The reaction was stopped by adding 10% hydrochloric acid. THF was evaporated and the mixture was extracted with diethyl ether and washed with water. The organic layer was dried with MgSO₄ and collected. After concentration, the crude product was purified by column chromatography using petroleum ether:acetone 3:1 (*v/v*) as eluent. The yield of 3-*n*-butylphthalide (4) was 2.12 g (67%). The progress of the reactions was monitored by analytical TLC and GC. The structures of the compounds (3,4) were confirmed by NMR spectroscopy.

3.2. Microorganisms

The following strains were used in the biotransformations: *Mucor spinosus* AM 398, *Absidia cylindrospora* AM 336, *Pycnidium resinae* AM 50, *Penicillium chrysogenum* AM 112, *Chaetomium indicum* AM 158, *Fusarium culmorum* AM 9, *Aspergillus candidus* AM 386, *Laetisporus sulphurens* AM 515, *Fusicoccum amygdali* AM 258 and *Ascosphaera apis* AM 496. These were all obtained from the Department of Chemistry collection at the Wrocław Uni-

versity of Environmental and Life Sciences. These strains were maintained on Sabouraud or Czapek agar slants at 4 °C.

Fungistatic activity was detected against *Candida albicans* ATCC 90028 from American Type Culture Collection, and its clinical isolates *Candida albicans* 636/20, *Candida albicans* 595/20 and *Candida albicans* 38 were obtained from Wrocław Medical University, Poland.

3.3. Biotransformations

The biotransformations were conducted in 300 mL Erlenmeyer flasks. Each strain was inoculated using the sterile Sabouraud medium (75 mL), which consisted of 30 g glucose (Chempur, Piekary Śląskie, Poland), 10 g bactopectone (Biocorp, Warszawa, Poland) and 1 L distilled water (pH 6.88). After 5 days of incubation at 25 °C on a rotary shaker, 3-*n*-butylideneephthalide (**1**) was added (20 mg dissolved in 0.5 mL of acetone) and samples were collected every 2 days to measure pH values. Product yield was determined on days 2, 4, 6, 8 and 14. The samples were acidified to pH 5 using hydrochloric acid (if necessary) and extracted using ethyl acetate. The samples were then dried using MgSO₄ and subjected to evaporation at 25 °C. Next, the samples were dissolved in methanol, filtered using a 0.45 µm PTFE filter and analyzed by HPLC.

Three microorganisms were chosen for the scale-up process: *A. cylindrospora* AM 336, *C. indicum* AM 158 and *A. candidus* AM 386. The preparative biotransformations were conducted in 2000 mL Erlenmeyer flasks using 500 mL of a sterile Sabouraud medium and precultivated inoculum, which constituted 10% of the medium volume. After 5 days of incubation at 25 °C on a rotary shaker, 3-*n*-butylideneephthalide (**1**) was added (150 mg dissolved in 1 mL acetone) to the culture. The samples were collected every 2 days and the pH values were measured. The samples were prepared as previously described (except for the evaporation step) and subjected to GC analysis in ethyl acetate. Product mixtures were collected on day 8 of the process for *A. candidus* AM 386 and on day 14 for *C. indicum* AM 158 and *A. cylindrospora* AM 336. The collected samples were acidified with 10% hydrochloric acid, extracted twice using ethyl acetate and analyzed by RP-TLC.

The product was purified using 250 µm thick TLC Silica gel 60 RP-18 F254s plates (Merck, Darmstadt, Germany) with 70% MeCN and 30% H₂O acidified by 1% HCOOH eluent. After separation, the plates were visualized using a UV lamp at 254 and 365 nm. The product was scraped off and extracted with ethyl acetate, after which the organic layer was collected, dried with MgSO₄ and evaporated by the rotary evaporator. The structures of the compounds were determined by NMR.

3.4. Analysis

TLC analysis was performed on glass plates covered with silica gel 60 F254 (Merck) and developed using hexane:acetone 2:1 (*v/v*) eluent. After elucidation, the plates were visualized by a solution of 1% Ce(SO₄)₂ and 2% phosphoromolybdic acid in 10% H₂SO₄.

HPLC analysis was performed using a Dionex UltiMate 3000 instrument equipped with a diode array detector (Thermo Fisher Scientific, Waltham, MA, USA) with a Phenomenex Luna[®] 5 µm C18 100 Å, 250 × 4.6 mm column (Phenomenex, Torrance, CA, USA). The mobile phase was composed of water acidified with 5% formic acid (A) and methanol (B). Gradient elution conditions were as follows: 0–10 min, 35% A/65% B; 10–20 min, 30% A/70% B; 21–30 min, 0% A, 100% B; 31–35 min, 65% A/35% B; and 35–45 min, 35% A, 65% B. To observe the product, the following parameters were selected: flow rate, 1.0 mL/min; injection volume, 8 µL; column incubation temperature, 30 °C; and detection wavelength, 274 nm.

GC analysis (FID, H₂ as carrier gas) was performed on an Agilent Technologies 7890 N GC System (Santa Clara, CA, USA) using a Cyclosil-B column (30 m × 0.25 mm × 0.25 µm, Agilent Technologies). The temperature program was 120 °C, 200 °C (8 °C/min), and 240 °C (10 °C/min).

Molecular weights of compounds were assessed using GC-MS on a Saturn 2000 MS Varian Chrompack CP-3800 (Walnut Creek, CA, USA).

The optical rotation of 3-butyl-3-hydroxyphthalide (**2**) was measured using JASCO P-2000-Na digital polarimeter (ABL & E-JASCO, Kraków, Poland) in chloroform. The specific rotations $[\alpha]_{589}^{25}$ of product (**2**) isolated from particular strains were as follows: -2.4 ($c = 1.0$, CHCl_3) for *A. cylindrospora* AM 336; -0.5 ($c = 1.0$, CHCl_3) for *A. candidus* AM 386; and -3.6 ($c = 1.0$, CHCl_3) for *C. indicum* AM 158.

NMR spectra (^1H NMR, ^{13}C NMR) of compounds (**1**), (**3,4**) were recorded on a Bruker Avance DRX-500 spectrometer (Bruker, Billerica, MA, USA) in CDCl_3 . 3-butyl-3-hydroxyphthalide (**2**) (^1H NMR, ^{13}C NMR, COSY, HSQC, HMBC) was measured on JNM-ECZS 400 MHz NMR spectrometer (JEOL USA, Peabody, MA, USA). The spectral data are presented below as well as in the attached Supplementary Materials.

3-*n*-butylidene-phthalide (**1**).

^1H NMR (500 MHz), δ (ppm): 0.98 (t, 3H, $J = 7.40$, H-11), 1.54 (m, 2H, H-10), 2.45 (q, 2H, $J_1 = 15.00$, $J_2 = 7.50$, H-9), 5.63 (t, 1H, $J = 7.80$, H-8), 7.49 (t, 1H, $J = 7.30$, H-5), 7.64 (m, 2H, H-4), 7.66 (m, 2H, H-6), 7.88 (d, 1H, $J = 7.70$, H-7).

^{13}C NMR (151 MHz), δ (ppm): 13.9 (C-11), 22.6 (C-10), 28.0 (C-9), 109.6 (C-8), 119.8 (C-4), 124.6 (C-12), 125.4 (C-7), 129.5 (C-6), 134.3 (C-5), 139.7 (C-3), 145.9 (C-13), 167.3 (C-1).

GC-EIMS 189 (M + 1).

3-butyl-3-hydroxyphthalide (**2**).

^1H NMR: (400 MHz), δ (ppm): 0.85 (t, 3H, H-11, $J = 7.22$ Hz), 1.14 (m, 1H, one of H-9), 1.31 (m, 2H, H-10), 1.38 (m, 1H, one of H-9), 2.07 (ddd, 1H, one of H-8, $J_1 = 14.0$, $J_2 = 11.8$, $J_3 = 4.5$ Hz), 2.20 (m, 1H, one of H-8) 7.56 (m, 2H, H-4, H-6), 7.70 (t, 1H, H-5, $J = 7.48$ Hz), 7.81 (d, 1H, H-7, $J = 7.52$ Hz).

^{13}C NMR (101 MHz), δ (ppm): 13.9 (C-11), 22.6 (C-10), 25.5 (C-9), 38.7 (C-8), 107.9 (C-3), 122.4 (C-4), 125.6 (C-7), 126.9 (C-12), 130.7 (C-6), 134.8 (C-5), 149.0 (C-13), 168.9 (C-1).

3-butyl-3-hydroxyphthalide (**2**) due to the low volatility was assessed at the GC-EIMS after esterification as 3-butyl-3-methoxyphthalide (**3**)-GC-EIMS 221 (M + 1).

3-butyl-3-methoxyphthalide (**3**).

^1H NMR: (500 MHz), δ (ppm): 0.83 (t, 3H, H-11, $J = 7.3$), 1.12 (m, 1H, one of H-10), 1.28 (m, 2H, H-9), 1.39 (m, 1H, one of H-10), 2.01 (ddd, 1H, one of H-8, $J_1 = 4.58$, $J_2 = 11.74$, $J_3 = 14.05$), 2.16 (ddd, 1H, one of H-8, $J_1 = 4.72$, $J_2 = 11.85$, $J_3 = 14.04$) 3.04 (s, 3H, H-3a), 7.47 (d, 1H, H-4, $J = 7.6$), 7.59 (td, 1H, H-6, $J_1 = 0.82$, $J_2 = 7.55$, $J_3 = 7.53$), 7.71 (td, 1H, H-5, $J_1 = 0.99$, $J_2 = 7.50$, $J_3 = 7.50$), 7.88 (d, 1H, H-7, $J = 7.65$).

^{13}C NMR (151 MHz), δ (ppm): 13.9 (C-11), 22.7 (C-10), 25.3 (C-9), 38.3 (C-8), 51.2 (C-3a), 111.1 (C-3), 122.6 (C-4), 125.6 (C-7), 128.2 (C-12), 130.7 (C-6), 134.6 (C-5), 146.8 (C-13), 168.5 (C-1).

GC-EIMS 221 (M + 1).

3-*n*-butylphthalide (**4**).

^1H NMR (500 MHz), δ (ppm): 0.91 (t, 3H, $J = 7.2$, H-11), 1.39 (m, 2H, H-10), 1.48 (m, 2H, H-9), 1.76 (m, 1H, one of H-8), 2.04 (m, 1H, one of H-8), 5.47 (dd, 1H, $J_1 = 7.9$, $J_2 = 3.7$, H-3), 7.44 (d, 1H, $J = 7.7$, CH-4), 7.52 (t, 1H, $J = 7.5$, H-6), 7.66 (t, 1H, $J = 7.5$, H-5), 7.89 (d, 1H, $J = 7.7$, H-7).

^{13}C NMR (151 MHz), δ (ppm): 14.0 (C-11), 22.6 (C-10), 27.0 (C-9), 34.6 (C-8), 81.6 (C-3), 121.8 (C-4), 125.8 (C-7), 126.3 (C-12) 129.1 (C-6), 134.1 (C-5), 150.3 (C-13), 170.8 (C-1).

GC-EIMS 191 (M + 1).

3.5. Lipophilicity

The concentration of tested compounds (**1–4**) was 0.1 mg/mL. Dead time (t_0) was measured by injecting 1% aqueous NaNO_3 solution. The injection volume was 10 μL , the temperature was 35 °C and the flow rate was 1.5 mL/min. The retention time (t_R) of the samples was also assessed by RP-HPLC in triplicate using the abovementioned column and isocratic elution. The eluents consisted of methanol and water, both of which were acidified by 1% formic acid *v/v* at 60–80% of the organic phase. The retention factor (k) was calculated according to the following equation: $k = (t_R - t_0)/t_0$. A graph

of $\log k$ as a function of the volume fraction of organic solvent was plotted. The value of the chromatographic lipophilicity index, $\log k_w$ ($\log k$ value with 0% methanol in the mobile phase), was determined by extrapolating this correlation. The chromatographic hydrophobicity index φ_0 was also assessed as the volume fraction of methanol that yields a $\log k$ value of 0 [31]. Theoretical $\log P$ (partition coefficient) values were calculated with the use of ALOGPS 2.1. Pearson's correlation coefficients between the $\log P$ and $\log k_w$ were determined using GraphPad Prism, and differences with $p < 0.05$ were considered statistically significant.

3.6. Fungistatic Activity

Compounds (1–4) were tested against four *Candida albicans* strains (*C. albicans* ATCC 90028 and its clinical isolates *C. albicans* 636/20, *C. albicans* 595/20 and *C. albicans* 38) using the broth microdilution technique. The medium used for the tests was YPD, consisting of 20 g glucose (Chempur, Piekary Śląskie, Poland), 20 g bactopectone (Biocorp, Warszawa, Poland), 10 g yeast extract (BTL, Łódź, Poland) and 1 L distilled water; the pH was adjusted to 6.5. The solutions of the compounds were prepared in dimethyl sulfoxide (DMSO) and diluted in YPD to obtain final concentrations in the range of 50–250 $\mu\text{g}/\text{mL}$. Fluconazole was tested at the range of 0.064–64 $\mu\text{g}/\text{mL}$ with the exception of the resistant strain 636/20, which was additionally tested in the range of 50–250 $\mu\text{g}/\text{mL}$. Next, 100 μL of each solution was pipetted into wells of a 96-well microtiter plate. The inoculum was standardized to 0.5 McFarland standard and then diluted to obtain the final suspension with a cell density of 0.5×10^3 to 2.5×10^3 CFU/mL. The inoculum size used was 100 μL . The positive control comprised DMSO added in the same concentration as the tested compounds in the inoculum, while the negative control was DMSO diluted in the broth without the addition of inoculum. All samples were tested at least in triplicate. The microtiter plates were incubated at 35 °C for 24 h in a Biosan PST-60 HL ThermoShaker (Riga, Latvia) at 1000 rpm. The fungistatic activity of the compounds was assessed by measuring the absorbance at a wavelength of 595 nm (Epoch, BioTek, Winooski, VT, USA) to determine the MIC₅₀ value (i.e., the concentration of a compound required to inhibit the growth of 50% of microorganisms).

4. Conclusions

In this study, we confirmed the utility of microbially catalyzed biotransformation for obtaining the mammalian metabolite (2) of bioactive 3-*n*-butylidenephthalide (1). We show that microbiological transformations can efficiently produce the target compound and can be used to better understand phthalide lactone metabolism. Overall, 10 fungal strains were tested, five of which efficiently produced hydroxy-3-butylphthalide (2). We proposed three mechanisms by which 3-*n*-butylidenephthalide (1) conversion may occur. Even though hydroxylation remains popular in xenobiotic metabolism, we excluded this pathway based on ¹³C NMR spectra and suggested the hydration pathway as the most probable mechanism. Valuable contributions of this research include the analysis of the lipophilicity and fungistatic activity of both phthalides (1) and (4) and the metabolite (2). Antifungal assays revealed the potential of both 3-*n*-butylidenephthalide (1) and 3-*n*-butylphthalide (4) against clinical isolates of *C. albicans*, with an MIC₅₀ value below 50 $\mu\text{g}/\text{mL}$. We did not observe the influence of a double bond-containing side chain on the activity of compounds (1) and (4). We noticed weak or even a lack of inhibitory properties for metabolite (2), which has lower lipophilicity and presumably lower permeability than compounds (1) and (4). We did not observe a straightforward correlation between lipophilicity and fungistatic activity. Apart from the lipophilicity, the spatial structure of compounds is the factor that influences their biological activity. The presence of –OH groups in compound (2) or –OCH₃ groups in compound (3) causes the decrease of antifungal activity compared to that of 3-*n*-butylphthalide (4). Compound (1), which has a double bond in its structure, shows similar polarity to 3-butyl-3-methoxyphthalide (3); however, this compound had high

biological activity. Considering the possible applications for phthalides, there is a necessity for further research, particularly regarding the biological activity of their metabolites.

Supplementary Materials: The following are available online at <https://www.mdpi.com/article/10.3390/ijms22147600/s1>.

Author Contributions: Conceptualization, J.G. and T.O.; methodology, J.G., T.O., F.B.; formal analysis, J.G., T.O.; investigation, J.G., P.K.; resources, J.G., T.O., F.B.; writing—original draft preparation, J.G., T.O.; writing—review and editing, F.B., P.K.; visualization, J.G.; supervision, T.O.; funding acquisition, J.G. All authors have read and agreed to the published version of the manuscript.

Funding: This research and APC was funded by the project “UPWR 2.0: international and interdisciplinary program of development of Wrocław University of Environmental and Life Sciences”, co-financed by the European Social Fund under the Operational Program Knowledge Education Development, under contract No. POWR.03.05.00-00-Z062/18 of 4 June 2019.

Institutional Review Board Statement: Not applicable.

Informed Consent Statement: Not applicable.

Data Availability Statement: The data presented in this study are available on request from the corresponding author.

Conflicts of Interest: The authors declare no conflict of interest.

References

- Chen, H.-C.; Tsai, Y.-J.; Lin, L.-Y.; Wu, C.-S.; Tai, S.-P.; Chen, Y.-C.; Chiang, H.-M. Volatile Compounds from Roots, Stems and Leaves of *Angelica Acutiloba* Growing in Taiwan. *Nat. Prod. Commun.* **2014**, *9*, 583–586. [CrossRef]
- Chen, W.-R.; Yu, Y.; Zulfajri, M.; Lin, P.-C.; Wang, C.C. Phthalide Derivatives from *Angelica Sinensis* Decrease Hemoglobin Oxygen Affinity: A New Allosteric-Modulating Mechanism and Potential Use as 2,3-BPG Functional Substitutes. *Sci. Rep.* **2017**, *7*, 5504. [CrossRef]
- Baananou, S.; Piras, A.; Marongiu, B.; Dessì, M.A.; Falconieri, D.; Porcedda, S.; Rosa, A.; Boughattas, N.A. Antiulcerogenic Activity of *Apium Graveolens* Seeds Oils Isolated by Supercritical CO₂. *Afr. J. Pharm. Pharmacol.* **2012**, *6*, 752–762. [CrossRef]
- Chae, S.-H.; Kim, S.-I.; Yeon, S.-H.; Lee, S.-W.; Ahn, Y.-J. Adulticidal Activity of Phthalides Identified in *Cnidium Officinale* Rhizome to B- and Q-Biotypes of *Bemisia Tabaci*. *J. Agric. Food Chem.* **2011**, *59*, 8193–8198. [CrossRef] [PubMed]
- Spréa, R.M.; Fernandes, Â.; Finimundy, T.C.; Pereira, C.; Alves, M.J.; Calhelha, R.C.; Canan, C.; Barros, L.; Amaral, J.S.; Ferreira, I.C.F.R. Lovage (*Levisticum Officinale* W.D.J. Koch) Roots: A Source of Bioactive Compounds towards a Circular Economy. *Resources* **2020**, *9*, 81. [CrossRef]
- León, A.; Toscano, R.A.; Tortoriello, J.; Delgado, G. Phthalides and Other Constituents from *Ligusticum Porteri*; Sedative and Spasmolytic Activities of Some Natural Products and Derivatives. *Nat. Prod. Res.* **2011**, *25*, 1234–1242. [CrossRef]
- Jia, J.; Wei, C.; Liang, J.; Zhou, A.; Zuo, X.; Song, H.; Wu, L.; Chen, X.; Chen, S.; Zhang, J.; et al. The Effects of DL-3-n-Butylphthalide in Patients with Vascular Cognitive Impairment without Dementia Caused by Subcortical Ischemic Small Vessel Disease: A Multicentre, Randomized, Double-Blind, Placebo-Controlled Trial. *Alzheimer's Dement.* **2016**, *12*, 89–99. [CrossRef] [PubMed]
- Yeh, J.-C.; Cindrova-Davies, T.; Belleri, M.; Morbidelli, L.; Miller, N.; Cho, C.-W.C.; Chan, K.; Wang, Y.-T.; Luo, G.-A.; Ziche, M.; et al. The Natural Compound N-Butylidenephthalide Derived from the Volatile Oil of *Radix Angelica Sinensis* Inhibits Angiogenesis In Vitro and In Vivo. *Angiogenesis* **2011**, *14*, 187–197. [CrossRef] [PubMed]
- Zhou, Q.-M.; Zhang, J.-J.; Li, S.; Chen, S.; Le, W.-D. N-Butylidenephthalide Treatment Prolongs Life Span and Attenuates Motor Neuron Loss in SOD1^{G93A} Mouse Model of Amyotrophic Lateral Sclerosis. *CNS Neurosci. Ther.* **2017**, *23*, 375–385. [CrossRef] [PubMed]
- Nam, K.N.; Kim, K.-P.; Cho, K.-H.; Jung, W.-S.; Park, J.-M.; Cho, S.-Y.; Park, S.-K.; Park, T.-H.; Kim, Y.-S.; Lee, E.H. Prevention of Inflammation-Mediated Neurotoxicity by Butylidenephthalide and Its Role in Microglial Activation: BP Inhibits Microglial Inflammatory Response. *Cell Biochem. Funct.* **2013**, *31*, 707–712. [CrossRef]
- Brindis, F.; Rodríguez, R.; Bye, R.; González-Andrade, M.; Mata, R. (Z)-3-Butylidenephthalide from *Ligusticum porteri*, an α -Glucosidase Inhibitor. *J. Nat. Prod.* **2011**, *74*, 314–320. [CrossRef]
- Sim, Y.; Shin, S. Combinatorial Anti-Trichophyton Effects of *Ligusticum Chuanxiong* Essential Oil Components with Antibiotics. *Arch. Pharm. Res.* **2008**, *31*, 497–502. [CrossRef] [PubMed]
- Gong, Y.; Liu, W.; Huang, X.; Hao, L.; Li, Y.; Sun, S. Antifungal Activity and Potential Mechanism of N-Butylphthalide Alone and in Combination With Fluconazole Against *Candida Albicans*. *Front. Microbiol.* **2019**, *10*, 1461. [CrossRef] [PubMed]
- Aguiar, F.L.L.D.; Santos, N.C.; de Paula Cavalcante, C.S.; Andreu, D.; Baptista, G.R.; Gonçalves, S. Antibiofilm Activity on *Candida Albicans* and Mechanism of Action on Biomembrane Models of the Antimicrobial Peptide Ctn [15–34]. *Int. J. Mol. Sci.* **2020**, *21*, 8339. [CrossRef] [PubMed]

15. Bhattacharya, S.; Sae-Tia, S.; Fries, B.C. Candidiasis and Mechanisms of Antifungal Resistance. *Antibiotics* **2020**, *9*, 312. [[CrossRef](#)] [[PubMed](#)]
16. Singh, A.; Verma, R.; Murari, A.; Agrawal, A. Oral Candidiasis: An Overview. *J. Oral Maxillofac. Pathol.* **2014**, *18*, 81. [[CrossRef](#)]
17. Spettel, K.; Barousch, W.; Makristathis, A.; Zeller, I.; Nehr, M.; Selitsch, B.; Lackner, M.; Rath, P.-M.; Steinmann, J.; Willinger, B. Analysis of Antifungal Resistance Genes in *Candida Albicans* and *Candida Glabrata* Using next Generation Sequencing. *PLoS ONE* **2019**, *14*, e0210397. [[CrossRef](#)]
18. Yassin, M.T.; Mostafa, A.A.; Al-Askar, A.A.; Bdeer, R. In Vitro Antifungal Resistance Profile of Candida Strains Isolated from Saudi Women Suffering from Vulvovaginitis. *Eur. J. Med. Res.* **2020**, *25*, 1. [[CrossRef](#)] [[PubMed](#)]
19. Bühler, T.; Medinger, M.; Bouitbir, J.; Krähenbühl, S.; Leuppi-Taegtmeyer, A. Hepatotoxicity Due to Azole Antimycotic Agents in a HLA B * 35:02-Positive Patient. *Front. Pharmacol.* **2019**, *10*, 645. [[CrossRef](#)]
20. Van Daele, R.; Spriet, I.; Wauters, J.; Maertens, J.; Mercier, T.; Van Hecke, S.; Brüggemann, R. Antifungal Drugs: What Brings the Future? *Med Mycol.* **2019**, *57*, S328–S343. [[CrossRef](#)]
21. Kebamo, S.; Tesema, S. The Role of Biotransformation in Drug Discovery and Development. *J. Drug Metab. Toxicol.* **2015**, *6*. [[CrossRef](#)]
22. Duan, F.; Xu, W.; Liu, J.; Jia, Z.; Chen, K.; Chen, Y.; Wang, M.; Ma, K.; Dong, J.; Chen, L.; et al. Preparing the Key Metabolite of Z-Ligustilide in Vivo by a Specific Electrochemical Reaction. *J. Sep. Sci.* **2018**, *41*, 2799–2807. [[CrossRef](#)] [[PubMed](#)]
23. Shanu-Wilson, J.; Evans, L.; Wrigley, S.; Steele, J.; Atherton, J.; Boer, J. Biotransformation: Impact and Application of Metabolism in Drug Discovery. *ACS Med. Chem. Lett.* **2020**, *11*, 2087–2107. [[CrossRef](#)] [[PubMed](#)]
24. Kelly, S.L.; Kelly, D.E. Microbial Cytochromes P450: Biodiversity and Biotechnology. Where Do Cytochromes P450 Come from, What Do They Do and What Can They Do for Us? *Philos. Trans. R. Soc. B: Biol. Sci.* **2013**, *368*, 20120476. [[CrossRef](#)] [[PubMed](#)]
25. Lu, W.; Feng, J.; Chen, X.; Bao, Y.-J.; Wang, Y.; Wu, Q.; Ma, Y.; Zhu, D. Distinct Regioselectivity of Fungal P450 Enzymes for Steroidal Hydroxylation. *Appl. Environ. Microbiol.* **2019**, *85*, e01182-19. [[CrossRef](#)] [[PubMed](#)]
26. Hüttel, W.; Hoffmeister, D. Fungal Biotransformations in Pharmaceutical Sciences. In *Industrial Applications*; Hofrichter, M., Ed.; Springer: Berlin/Heidelberg, Germany, 2011; pp. 293–317.
27. Diao, X.; Deng, P.; Xie, C.; Li, X.; Zhong, D.; Zhang, Y.; Chen, X. Metabolism and Pharmacokinetics of 3-*n*-Butylphthalide (NBP) in Humans: The Role of Cytochrome P450s and Alcohol Dehydrogenase in Biotransformation. *Drug Metab. Dispos.* **2013**, *41*, 430–444. [[CrossRef](#)]
28. Yan, R.; Ko, N.L.; Ma, B.; Tam, Y.K.; Lin, G. Metabolic Conversion from Co-Existing Ingredient Leading to Significant Systemic Exposure of Z-Butylidenephthalide, a Minor Ingredient in Chuanxiong Rhizoma in Rats. *Curr. Drug Metab.* **2012**, *13*, 524–534. [[CrossRef](#)]
29. Nycz-Empel, A.; Bober, K.; Wyszomirski, M.; Kisiel, E.; Zięba, A. The Application of CA and PCA to the Evaluation of Lipophilicity and Physicochemical Properties of Tetracyclic Diazaphenothiazine Derivatives. *J. Anal. Methods Chem.* **2019**, *2019*, 8131235. [[CrossRef](#)]
30. Ciura, K.; Fedorowicz, J.; Andrić, F.; Greber, K.E.; Gurgielewicz, A.; Sawicki, W.; Sączewski, J. Lipophilicity Determination of Quaternary (Fluoro)Quinolones by Chromatographic and Theoretical Approaches. *Int. J. Mol. Sci.* **2019**, *20*, 5288. [[CrossRef](#)]
31. Klose, M.; Theiner, S.; Varbanov, H.; Hofer, D.; Pichler, V.; Galanski, M.; Meier-Menches, S.; Keppler, B. Development and Validation of Liquid Chromatography-Based Methods to Assess the Lipophilicity of Cytotoxic Platinum (IV) Complexes. *Inorganics* **2018**, *6*, 130. [[CrossRef](#)]
32. Chmiel, T.; Mieszkowska, A.; Kempnińska-Kupczyk, D.; Kot-Wasik, A.; Namieśnik, J.; Mazerska, Z. The Impact of Lipophilicity on Environmental Processes, Drug Delivery and Bioavailability of Food Components. *Microchem. J.* **2019**, *146*, 393–406. [[CrossRef](#)]
33. Lipinski, C.A. Lead- and Drug-like Compounds: The Rule-of-Five Revolution. *Drug Discov. Today Technol.* **2004**, *1*, 337–341. [[CrossRef](#)]
34. Fernandes, T.R.; Segorbe, D.; Prusky, D.; Di Pietro, A. How Alkalinization Drives Fungal Pathogenicity. *PLoS Pathog.* **2017**, *13*, e1006621. [[CrossRef](#)]
35. Zöllner, A.; Buchheit, D.; Meyer, M.R.; Maurer, H.H.; Peters, F.T.; Bureik, M. Production of Human Phase 1 and 2 Metabolites by Whole-Cell Biotransformation with Recombinant Microbes. *Bioanalysis* **2010**, *2*, 1277–1290. [[CrossRef](#)] [[PubMed](#)]
36. Lin, C.-I.; McCarty, R.M.; Liu, H. The Enzymology of Organic Transformations: A Survey of Name Reactions in Biological Systems. *Angew. Chem. Int. Ed.* **2017**, *56*, 3446–3489. [[CrossRef](#)] [[PubMed](#)]
37. Yan, R.; Ko, N.L.; Li, S.-L.; Tam, Y.K.; Lin, G. Pharmacokinetics and Metabolism of Ligustilide, a Major Bioactive Component in Rhizoma Chuanxiong, in the Rat. *Drug Metab. Dispos.* **2008**, *36*, 400–408. [[CrossRef](#)] [[PubMed](#)]
38. Engleder, M.; Pichler, H. On the Current Role of Hydratases in Biocatalysis. *Appl. Microbiol. Biotechnol.* **2018**, *102*, 5841–5858. [[CrossRef](#)]
39. Li, C.-Y.; Qi, L.-W.; Li, P. Correlative Analysis of Metabolite Profiling of Danggui Buxue Tang in Rat Biological Fluids by Rapid Resolution LC-TOF/MS. *J. Pharm. Biomed. Anal.* **2011**, *55*, 146–160. [[CrossRef](#)]
40. Zheng, B.; West, L.M. Estimating The Lipophilicity Of Natural Products Using A Polymeric Reversed Phase Hplc Method. *J. Liq. Chromatogr. Relat. Technol.* **2009**, *33*, 118–132. [[CrossRef](#)]
41. Sima, I.A.; Kot-Wasik, A.; Wasik, A.; Namieśnik, J.; Sârbu, C. Assessment of Lipophilicity Indices Derived from Retention Behavior of Antioxidant Compounds in RP-HPLC. *Molecules* **2017**, *22*, 550. [[CrossRef](#)] [[PubMed](#)]

42. Tamaian, R.; Moț, A.; Silaghi-Dumitrescu, R.; Ionuț, I.; Stana, A.; Oniga, O.; Nastasă, C.; Benedec, D.; Tipericiuc, B. Study of the Relationships between the Structure, Lipophilicity and Biological Activity of Some Thiazolyl-Carbonyl-Thiosemicarbazides and Thiazolyl-Azoles. *Molecules* **2015**, *20*, 22188–22201. [[CrossRef](#)]
43. Ghazal, H.S.; Dyas, A.M.; Ford, J.L.; Hutcheon, G.A. The Impact of Food Components on the Intrinsic Dissolution Rate of Ketoconazole. *Drug Dev. Ind. Pharm.* **2015**, *41*, 1647–1654. [[CrossRef](#)] [[PubMed](#)]
44. Tsume, Y.; Mudie, D.M.; Langguth, P.; Amidon, G.E.; Amidon, G.L. The Biopharmaceutics Classification System: Subclasses for in Vivo Predictive Dissolution (IPD) Methodology and IVIVC. *Eur. J. Pharm. Sci.* **2014**, *57*, 152–163. [[CrossRef](#)] [[PubMed](#)]
45. Corrêa, J.C.R.; Salgado, H.R.N. Review of Fluconazole Properties and Analytical Methods for Its Determination. *Crit. Rev. Anal. Chem.* **2011**, *41*, 124–132. [[CrossRef](#)]
46. Bennion, B.J.; Be, N.A.; McNerney, M.W.; Lao, V.; Carlson, E.M.; Valdez, C.A.; Malfatti, M.A.; Enright, H.A.; Nguyen, T.H.; Lightstone, F.C.; et al. Predicting a Drug's Membrane Permeability: A Computational Model Validated With in Vitro Permeability Assay Data. *J. Phys. Chem. B* **2017**, *121*, 5228–5237. [[CrossRef](#)] [[PubMed](#)]
47. Momin, R.A.; Nair, M.G. Mosquitocidal, Nematicidal, and Antifungal Compounds from *Apium Graveolens* L. Seeds. *J. Agric. Food Chem.* **2001**, *49*, 142–145. [[CrossRef](#)]
48. Pannek, J.; Gach, J.; Boratyński, F.; Olejniczak, T. Antimicrobial Activity of Extracts and Phthalides Occurring in Apiaceae Plants: Antimicrobial Activity of Phthalides. *Phytother. Res.* **2018**, *32*, 1459–1487. [[CrossRef](#)]
49. Fan, L.; Luo, B.; Luo, Z.; Zhang, L.; Fan, J.; Xue, W.; Tang, L.; Li, Y. Synthesis and Antifungal Activities of 3-Substituted Phthalide Derivatives. *Z. Für Nat. B* **2019**, *74*, 811–818. [[CrossRef](#)]
50. Xiao, B.; Yin, J.; Park, M.; Liu, J.; Li, J.L.; Kim, E.L.; Hong, J.; Chung, H.Y.; Jung, J.H. Design and Synthesis of Marine Fungal Phthalide Derivatives as PPAR- γ Agonists. *Bioorganic Med. Chem.* **2012**, *20*, 4954–4961. [[CrossRef](#)]

Microbial Synthesis and Evaluation of Fungistatic Activity of 3-Butyl-3-hydroxyphthalide, the Mammalian Metabolite of 3-*n*-Butylidenephthalide

Joanna Gach *, Teresa Olejniczak *, Piotr Krężel and Filip Boratyński

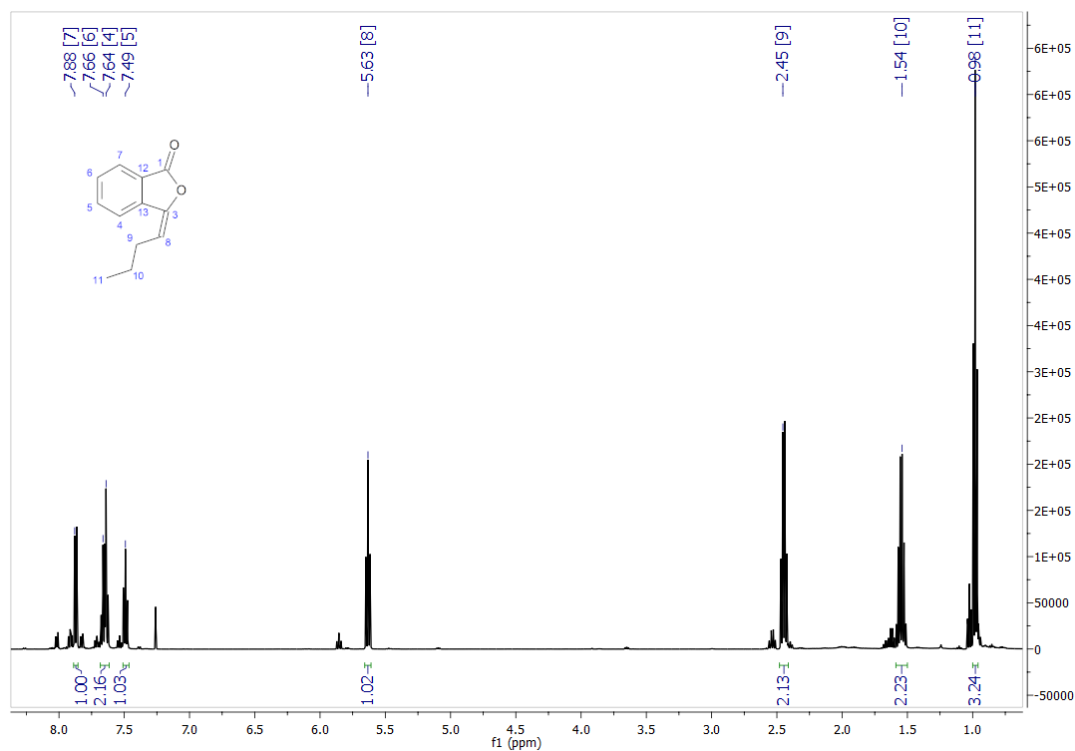


Figure S1. ¹H NMR spectrum of 3-*n*-butylidenephthalide (1).

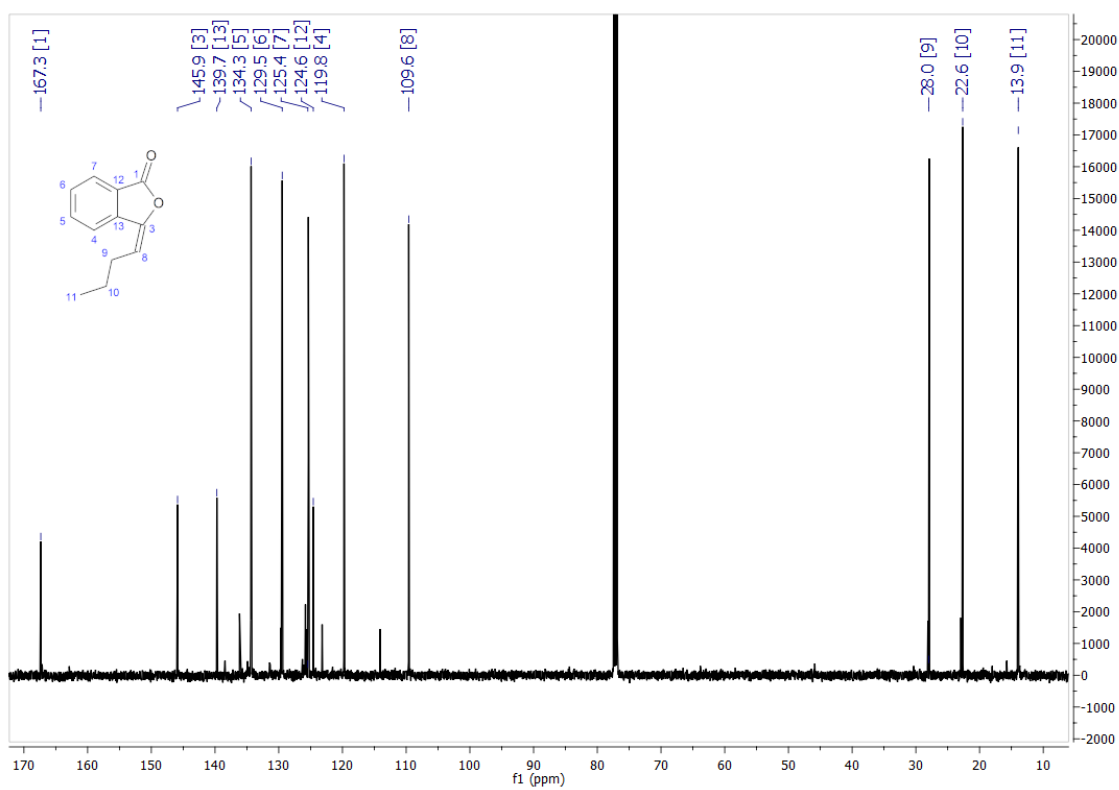


Figure S2. ¹³C NMR spectrum of 3-*n*-butylideneephthalide (1).

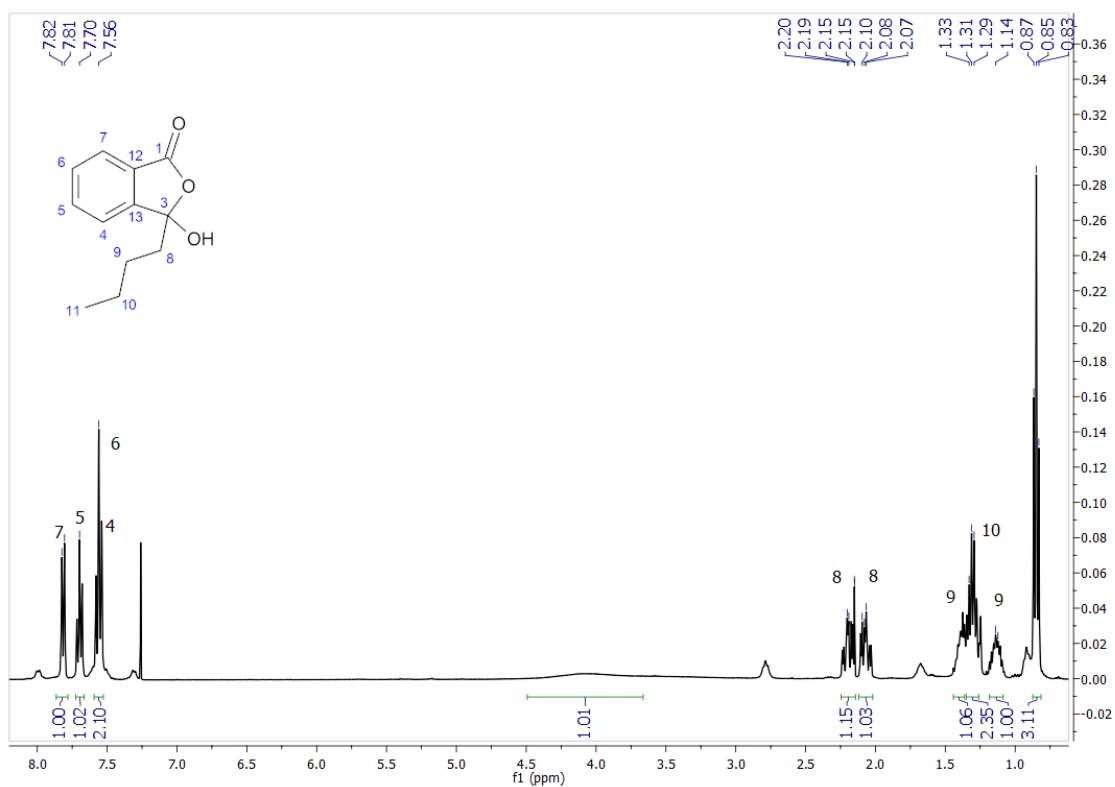


Figure S3. ¹H NMR spectrum of 3-butyl-3-hydroxyphthalide (2).

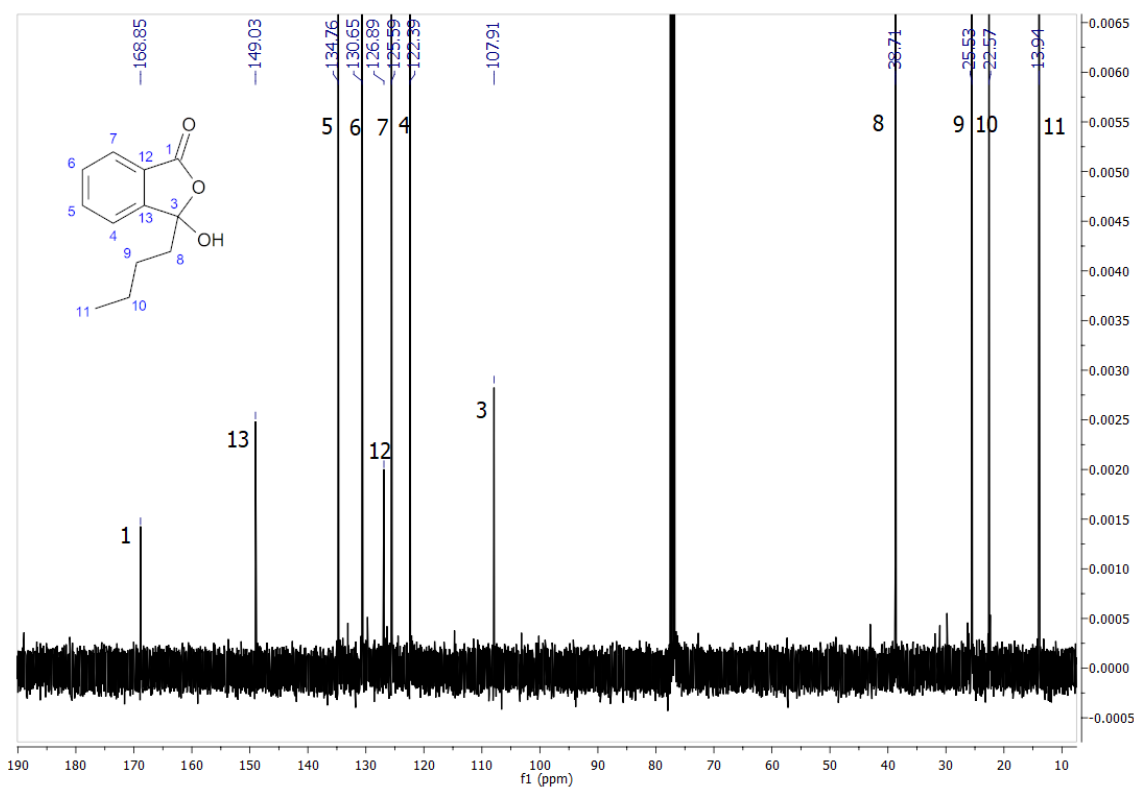


Figure S4. ^{13}C NMR spectrum of 3-butyl-3-hydroxyphthalide (2).

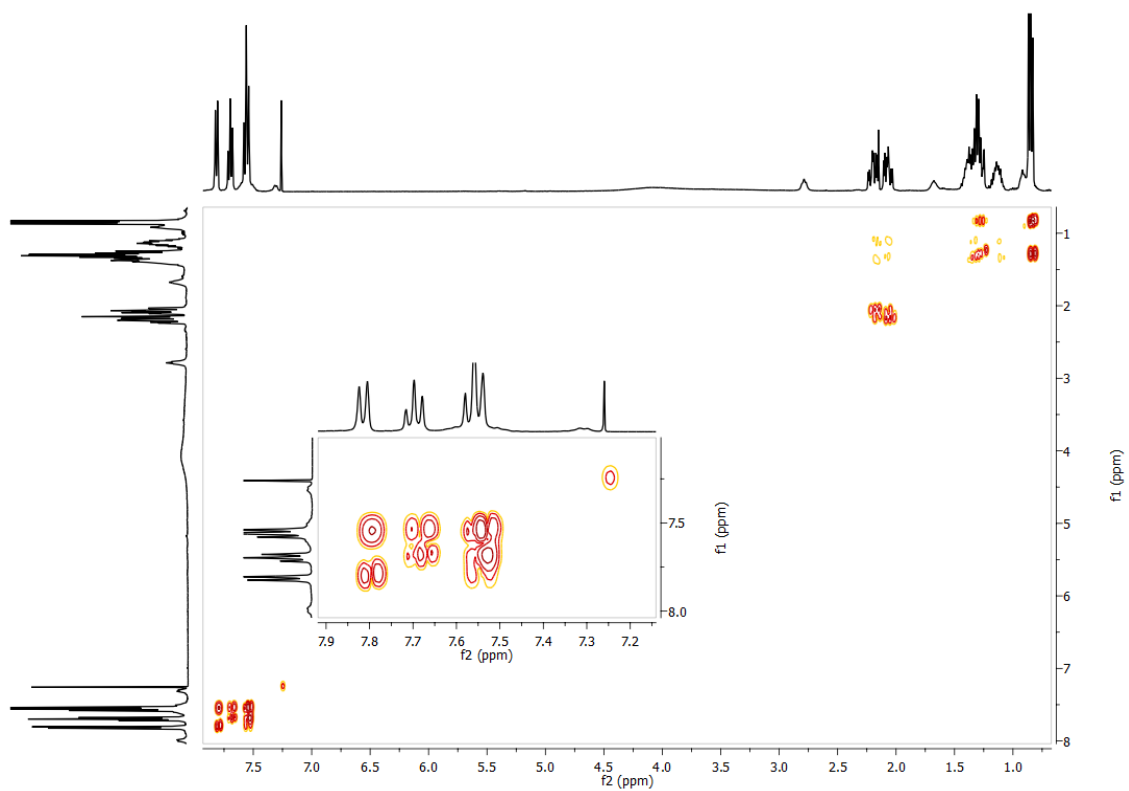


Figure S5. COSY spectrum of 3-butyl-3-hydroxyphthalide (2).

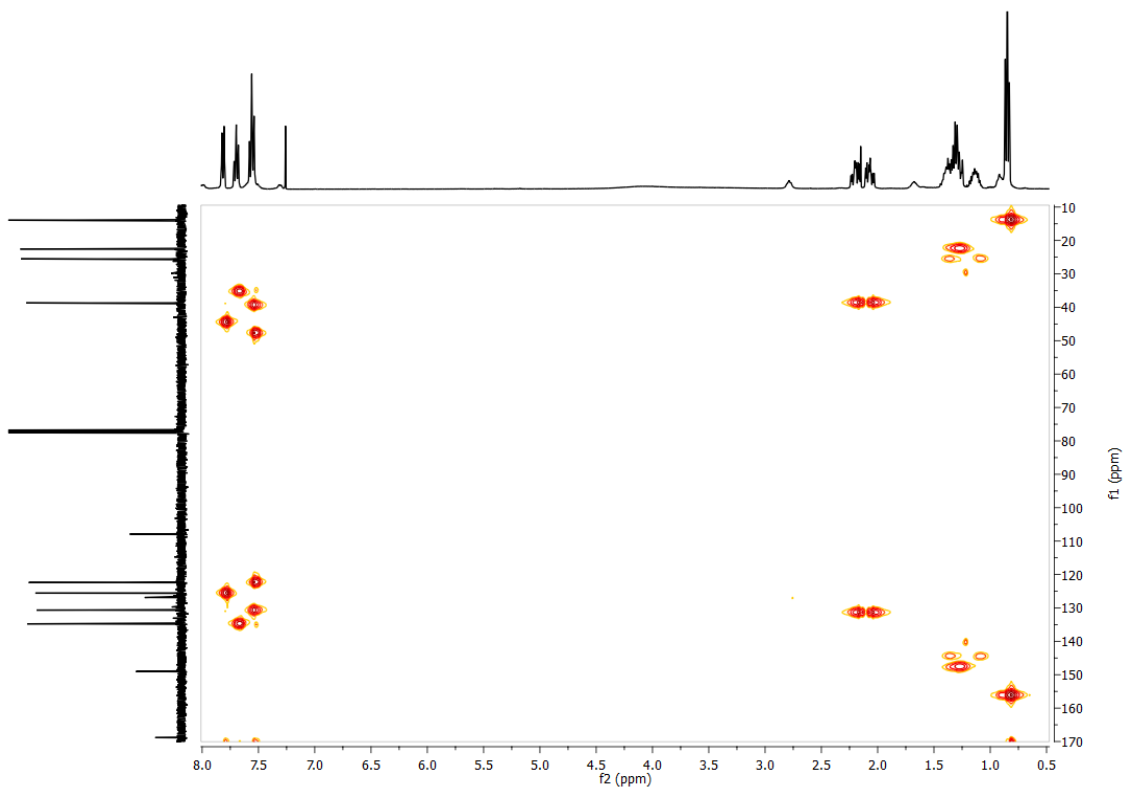


Figure S6. HSQC spectrum of 3-butyl-3-hydroxyphthalide (2).

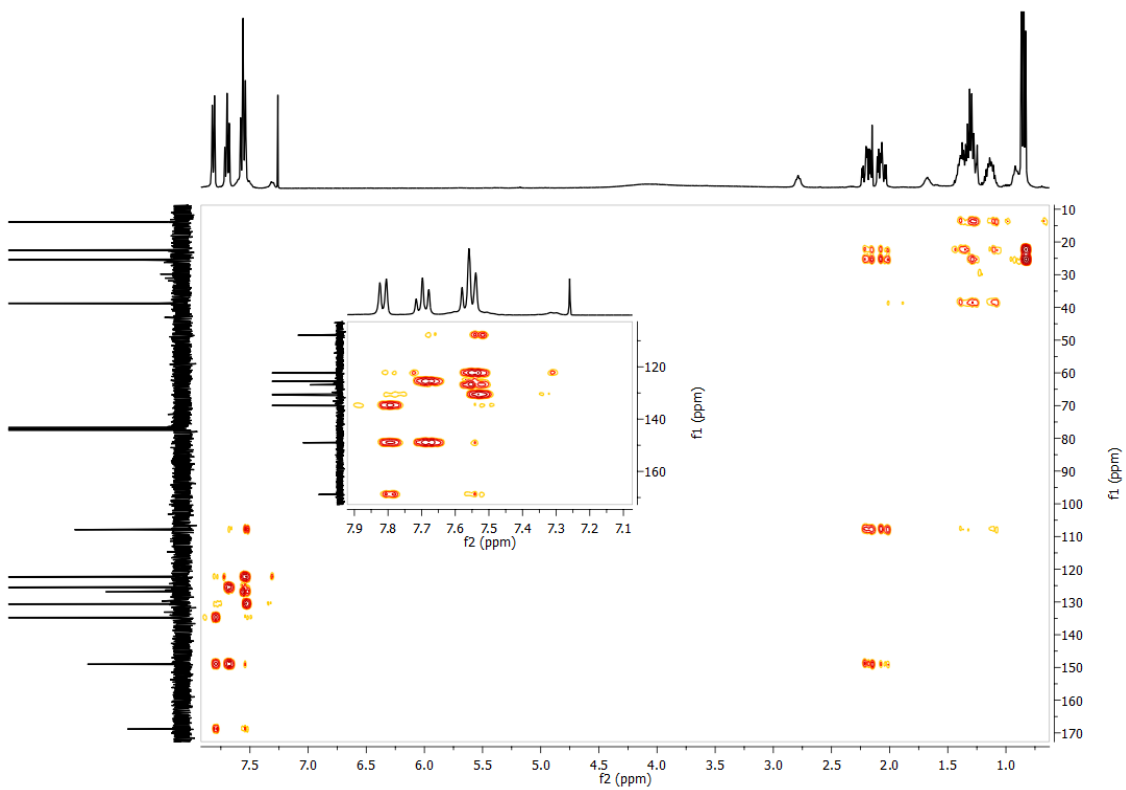


Figure S7. HMBC spectrum of 3-butyl-3-hydroxyphthalide (2).

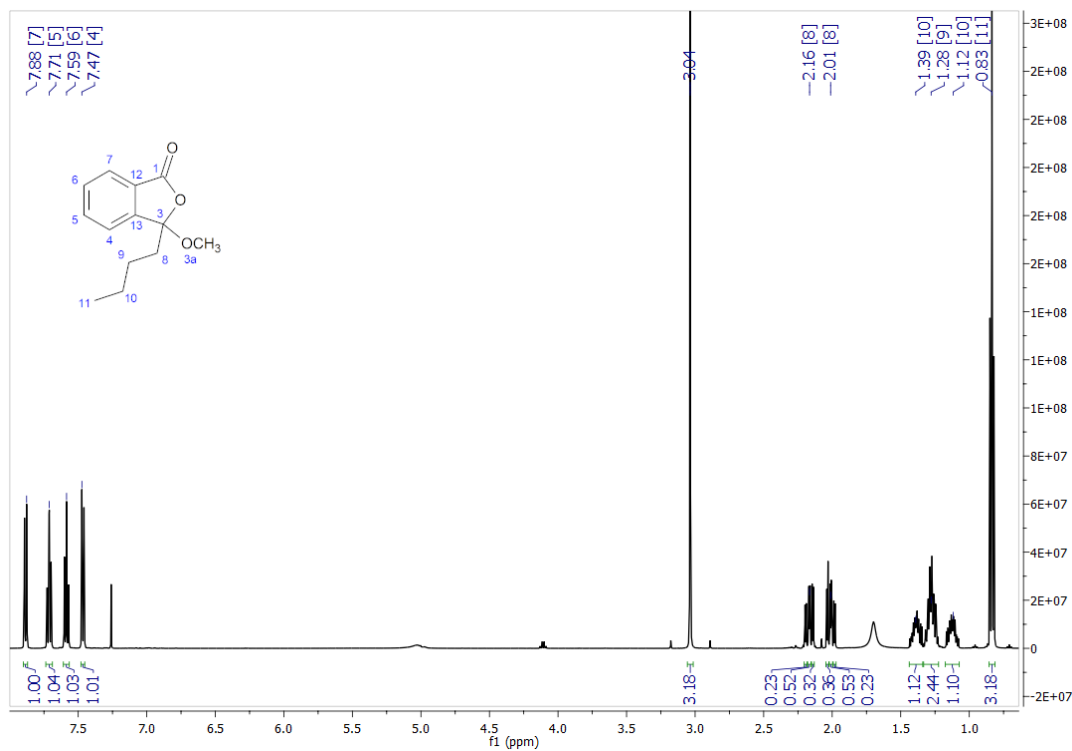


Figure S8. ¹H NMR spectrum of 3-butyl-3-methoxyphthalide (3).

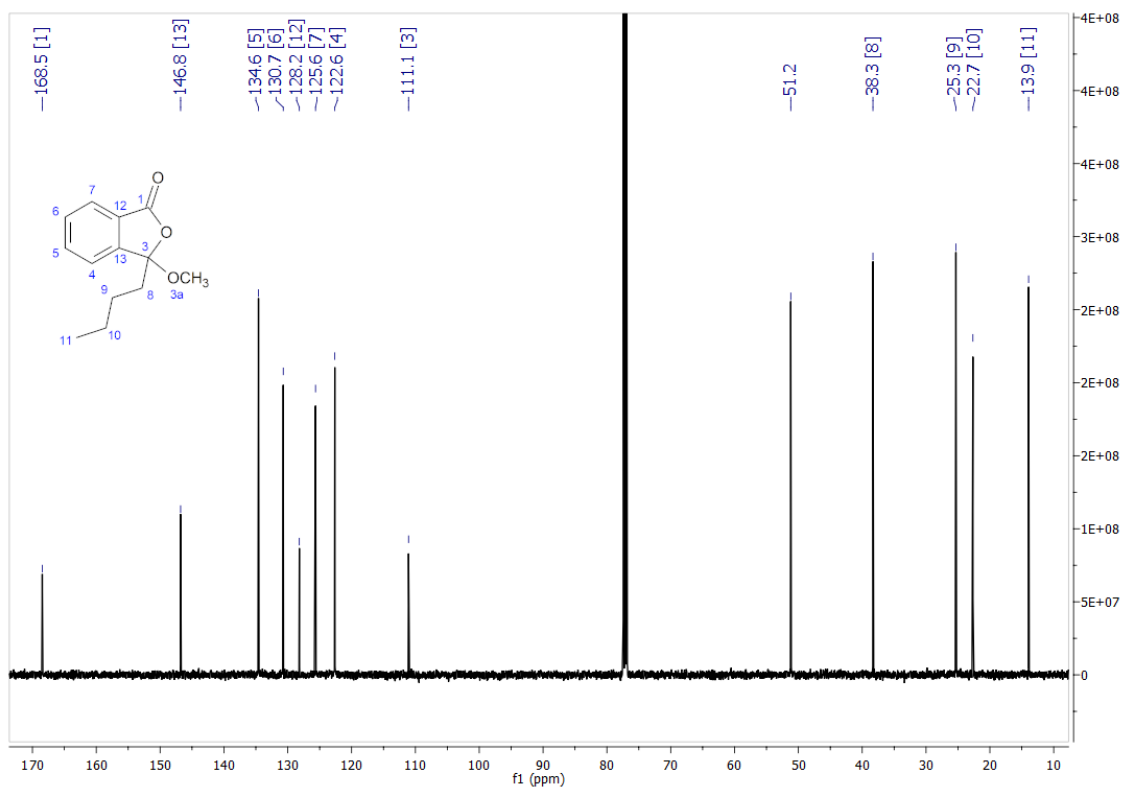


Figure S9. ¹³C NMR spectrum of 3-butyl-3-methoxyphthalide (3).

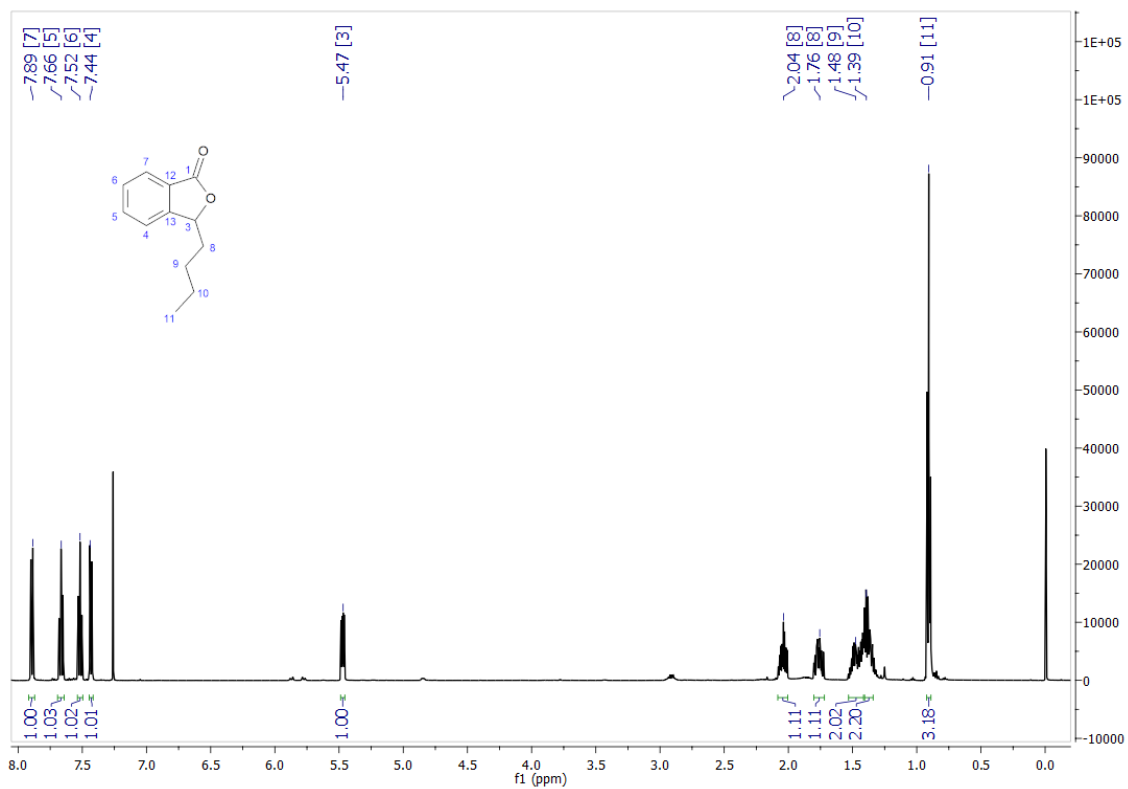


Figure S10. ¹H NMR spectrum of 3-*n*-butylphthalide (4).

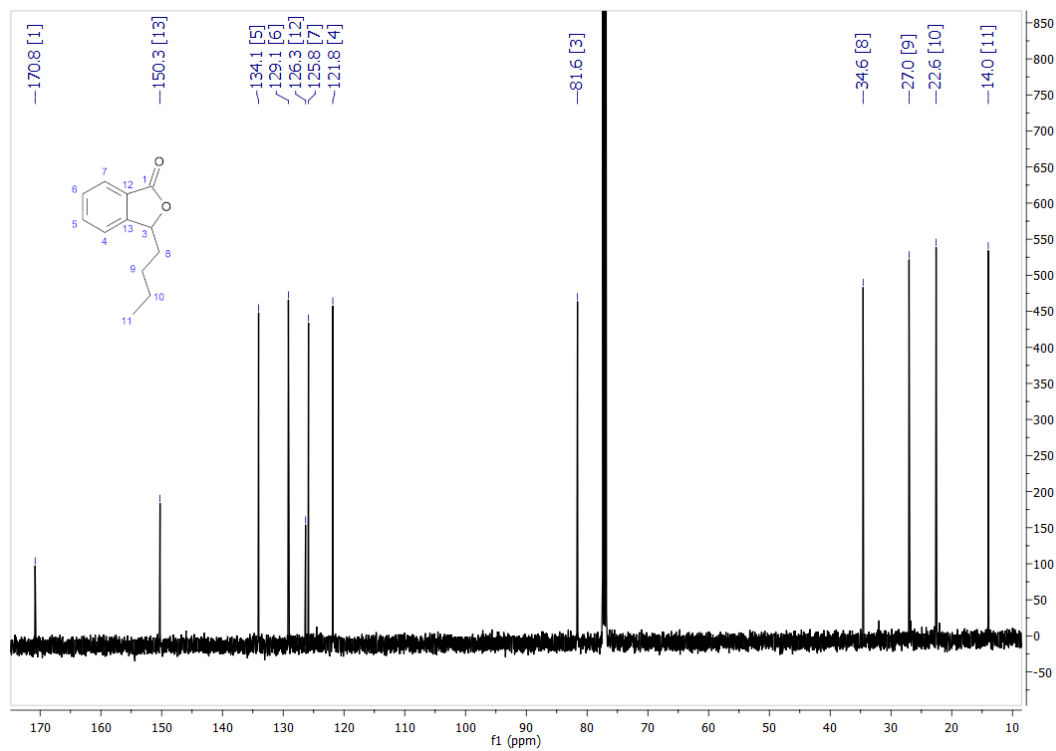


Figure S11. ¹³C NMR spectrum of 3-*n*-butylphthalide (4).

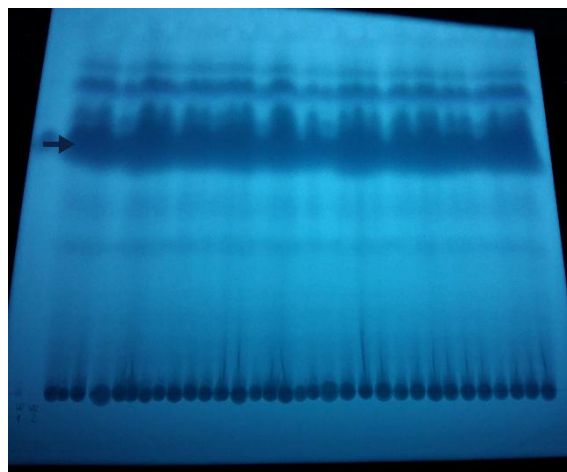


Figure S12. Purification of the product formed during biotransformation on reversed-phase thin layer chromatography plate. The product is indicated by an arrow.

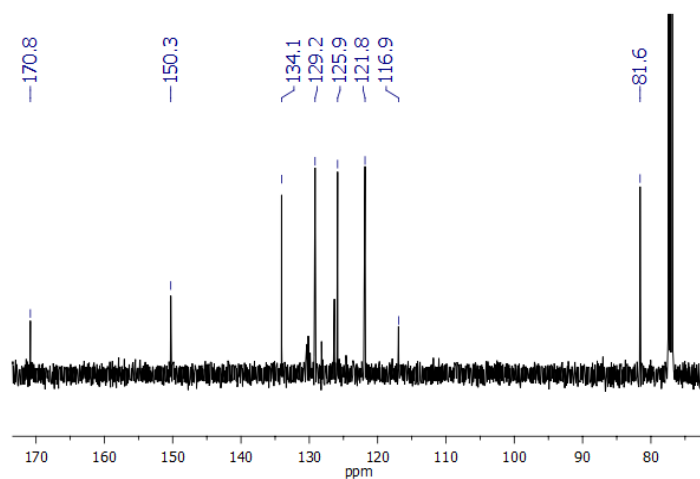


Figure S13. Fragment of the ^{13}C NMR spectrum of the *Chaetomium indicum* AM 158 biotransformation mixture.

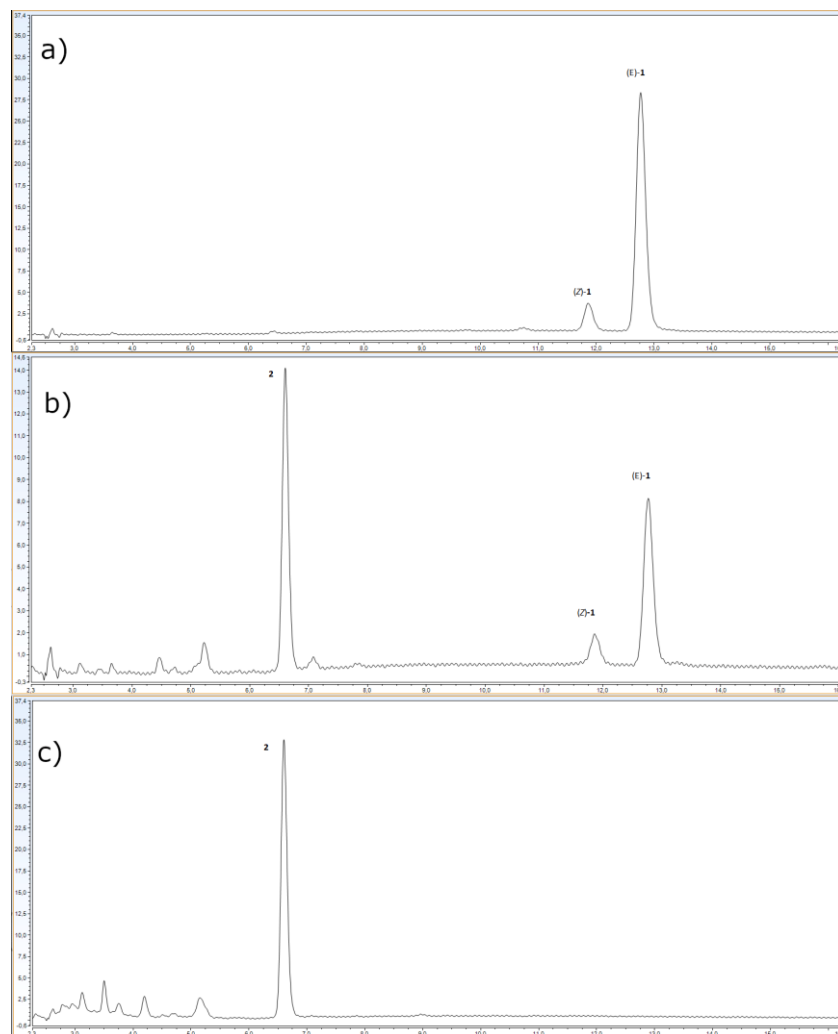


Figure S14. Chromatograms of 3-*n*-butylideneephthalide (1) – (*Z*) and (*E*) isomers (a) and the biotransformation mixtures of *Aspergillus candidus* AM 386 on days 2 (b) and 14 of the process (c).

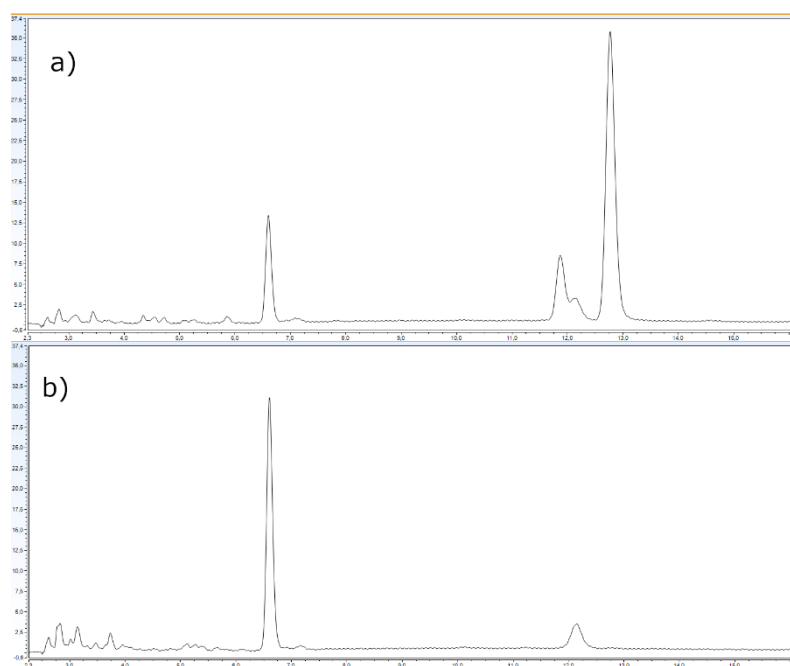


Figure S15. Chromatograms of the biotransformation mixtures of *Chaetomium indicum* AM 158 on days 2 (a) and 14 of the process (b).

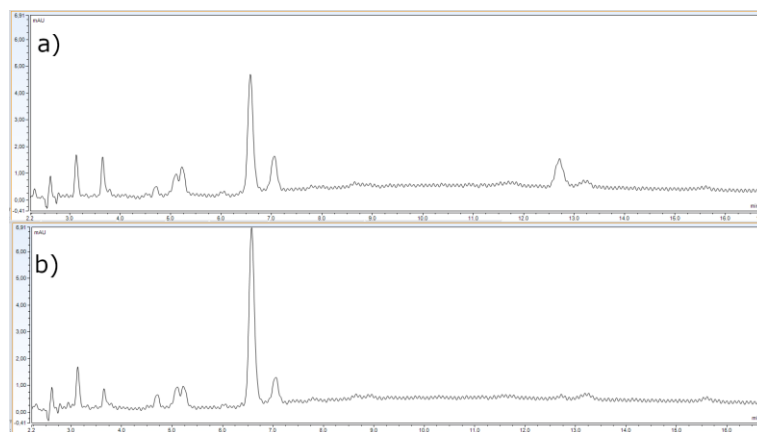


Figure S16. Chromatograms of the biotransformation mixtures of *Absidia cylindrospora* AM 336 on days 2 (a) and 14 of the process (b).



Article

Microbial Metabolites of 3-*n*-butylphthalide as Monoamine Oxidase A Inhibitors

Joanna Gach ^{1,*} , Joanna Grzelczyk ² , Tomasz Strzała ³, Filip Boratyński ¹ and Teresa Olejniczak ^{1,*}

¹ Department of Food Chemistry and Biocatalysis, Wrocław University of Environmental and Life Sciences, Norwida 25, 50-375 Wrocław, Poland; filip.boratynski@upwr.edu.pl

² Institute of Food Technology and Analysis, Faculty of Biotechnology and Food Sciences, Lodz University of Technology, Stefanowskiego 2/22, 90-924 Łódź, Poland; joanna.grzelczyk@p.lodz.pl

³ Department of Genetics, Wrocław University of Environmental and Life Sciences, Koźuchowska 7, 51-631 Wrocław, Poland; tomasz.strzala@upwr.edu.pl

* Correspondence: joanna.gach@upwr.edu.pl (J.G.); teresa.olejniczak@upwr.edu.pl (T.O.)

Abstract: Novel compounds with antidepressant activity via monoamine oxidase inhibition are being sought. Among these, derivatives of 3-*n*-butylphthalide, a neuroprotective lactone from *Apiaceae* plants, may be prominent candidates. This study aimed to obtain the oxidation products of 3-*n*-butylphthalide and screen them regarding their activity against the monoamine oxidase A (MAO-A) isoform. Such activity of these compounds has not been previously tested. To obtain the metabolites, we used fungi as biocatalysts because of their high oxidative capacity. Overall, 37 strains were used, among which *Penicillium* and *Botrytis* spp. were the most efficient, leading to the obtaining of three main products: 3-*n*-butyl-10-hydroxyphthalide, 3-*n*-butylphthalide-11-oic acid, and 3-*n*-butyl-11-hydroxyphthalide, with a total yield of 0.38–0.82 g per g of the substrate, depending on the biocatalyst used. The precursor–3-*n*-butylphthalide and abovementioned metabolites inhibited the MAO-A enzyme; the most active was the carboxylic acid derivative of the lactone with inhibitory constant (K_i) < 0.001 $\mu\text{mol/L}$. The *in silico* prediction of the drug-likeness of the metabolites matches the assumptions of Lipinski, Ghose, Veber, Egan, and Muegge. All the compounds are within the optimal range for the lipophilicity value, which is connected to adequate permeability and solubility.

Keywords: 3-*n*-butylphthalide; monoamine oxidase A inhibitor; biotransformation; serotonin; fungal strains



Citation: Gach, J.; Grzelczyk, J.; Strzała, T.; Boratyński, F.; Olejniczak, T. Microbial Metabolites of 3-*n*-butylphthalide as Monoamine Oxidase A Inhibitors. *Int. J. Mol. Sci.* **2023**, *24*, 10605. <https://doi.org/10.3390/ijms241310605>

Academic Editor: István Zupkó

Received: 24 May 2023

Revised: 21 June 2023

Accepted: 22 June 2023

Published: 25 June 2023



Copyright: © 2023 by the authors. Licensee MDPI, Basel, Switzerland. This article is an open access article distributed under the terms and conditions of the Creative Commons Attribution (CC BY) license (<https://creativecommons.org/licenses/by/4.0/>).

1. Introduction

Depression is a disease with many faces that affects people of all ages. There are several hypotheses regarding its etiology [1]. The most described and valid theory in the literature is the monoamine hypothesis, which assumes that depression is caused by the dysfunction of serotonergic (5-HT) and noradrenergic pathways [2]. In addition to reduced levels of 5-HT, dopamine, and norepinephrine in various areas of the brain (e.g., hippocampus, amygdala), there may be a genetic mutation of the 5-HT transporter and the amino oxidase (MAO) enzyme, which is associated with gene polymorphism and passed from mother to child [2,3]. This disease can affect people with dementia and those on the autistic spectrum or with bipolar diseases [1–5]. Monoamine oxidase belongs to the family of flavoenzymes located in the mitochondrial membrane [6]. There are two isoforms, MAO-A and MAO-B, which differ in affinity to the substrate and susceptibility to inhibition [7]. Generally, the enzymes are responsible for the deamination of neurotransmitters [6,8]. MAO-A is the main enzyme that deaminates 5-HT in the brain, affecting behavioral disorders [9]. Almost all MAO-A inhibitors on the market act irreversibly and require dietary restrictions to avoid tyramine accumulation, leading to serotonin toxicity syndrome [7]. The only reversible commercially available drug that regulates MAO is moclobemide [7,10]. Therefore, there is

a necessity for novel, non-toxic compounds that would regulate the level of serotonin in the human body.

The compound 3-*n*-butylphthalide is a biologically active lactone found in plants from the celery family [11,12]. Originally an ingredient in traditional Chinese medicine, it was accepted in China as a drug for cerebral ischemic stroke that improves the neurological function of the patients [13–15]. The compound restores microcirculation and protects the mitochondria. It shows vasodilatory, antiplatelet, and anti-inflammatory activity [15–17]. The antidepressant properties of 3-*n*-butylphthalide have also been studied [18]. The available literature outlines the positive effect of 3-*n*-butylphthalide in lipopolysaccharide (LPS)-induced depression [19] among chronic-stressed rats by the alteration of the serotonergic system, BDNF-ERK-mTOR signaling [18], and other mechanisms [20].

According to the research conducted by Diao et al. [21], the lactone in the human body is rapidly metabolized to 23 compounds, and mainly hydroxyderivatives and glucosidation products are observed. Although 3-*n*-butylphthalide has been widely tested regarding its biological activity, information on the monoamine oxidase A (MAO-A)-inhibiting properties of its metabolites is lacking. Moreover, other biological activities of these phthalide metabolites remain undiscovered, as obtaining them in sufficient amounts for research often poses a challenge. Biotransformation using whole fungal cells may provide a solution to this issue. Filamentous fungi feature many CYP isoenzymes and are, therefore, particularly known for their oxidative capacity. As a result, these biocatalysts lead to the formation of aliphatic and aromatic hydroxy derivatives [22]. Fungal-mediated biotransformations have been exploited by Diao et al. [21] for 3-*n*-butylphthalide and by us for its derivative with an unsaturated bond in the side chain [23].

Thus, this study aimed to obtain human metabolites of 3-*n*-butylphthalide through biotransformation by whole cells of filamentous fungi. After obtaining the oxidation products, we tested them in terms of their MAO-A enzyme-inhibiting properties. In addition, selected pharmacokinetic parameters were investigated using bioinformatics tools to assess the suitability of the compounds as potential antidepressant drugs.

2. Results

2.1. Chemical Synthesis of 3-*n*-butylphthalide (1) and Biotransformations

The first step of the research was the synthesis and purification of substrate 1, obtained in a two-step process (Figure 1).

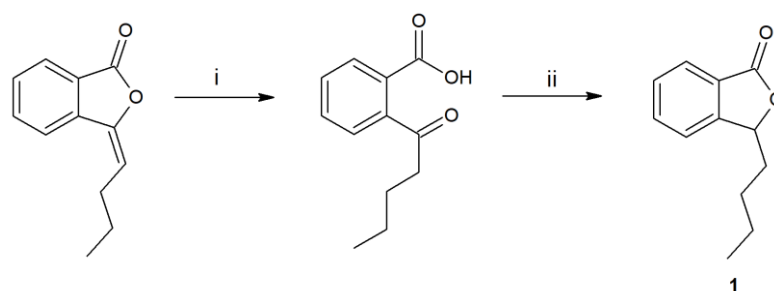


Figure 1. Synthesis of 3-*n*-butylphthalide (1) by the hydrolysis of 3-*n*-butylidene-2-phthalide to ketoacid (i-KOH in MeOH), its reduction by borohydride, and acidification (ii-THF, NaBH₄, HCl).

After obtaining the 3-*n*-butylphthalide (1), the screening of whole fungal cells was carried out. We searched for biocatalysts capable of efficiently converting 3-*n*-butylphthalide (1) to oxidation products. During the biotransformation processes, we collected samples 4, 8, and 12 days after adding the substrate. After extraction with ethyl acetate, we performed high-performance liquid chromatography-diode array detector (HPLC-DAD) analyses.

Overall, we tested 37 fungal strains, and 12 (*Fusarium culmorum* AM7, *Sclerophoma pythiopila* AM55, *Spicaria fusispora* AM136, *Beauveria bassiana* AM278, *Pleurotus ostreatus* AM482, *Aspergillus niger* strains KKP45, KKP423, KKP424, *Aspergillus flavus* KKP686, KKP689, *Phanerochaete chrysosporium* KKP784, and *Trichoderma lignorum* KKP786) did not

transform the substrate. In the other biotransformation processes, we observed products formed from 3-*n*-butylphthalide (**1**) (Figure 2).

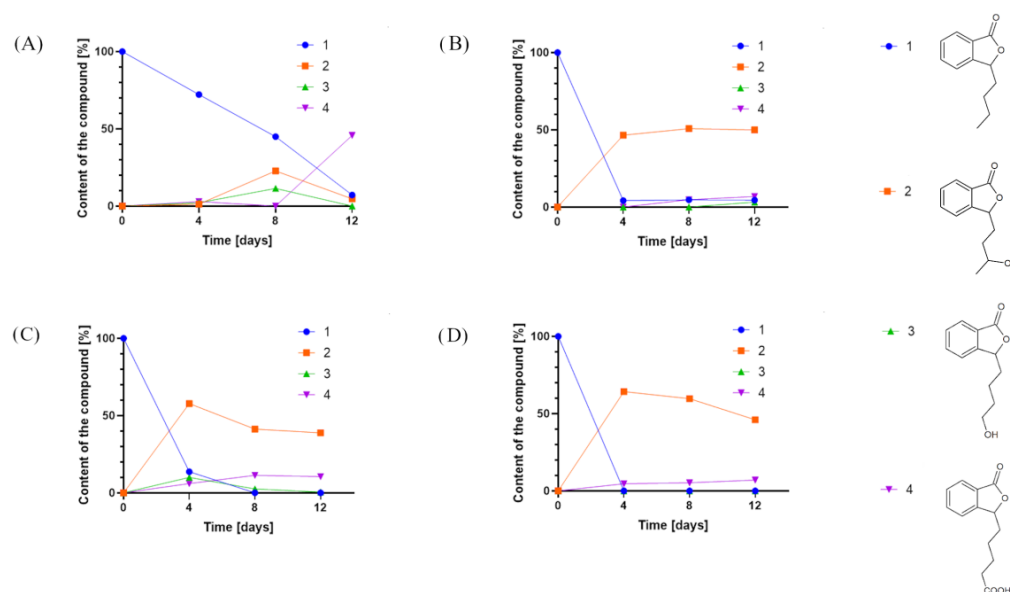


Figure 2. Product content of 3-*n*-butylphthalide (**1**) biotransformations catalyzed by (A) *Penicillium dierckxii* AM32, (B) *Penicillium* sp. AM91, (C) *Botrytis cinerea* AM235, and (D) *Botrytis* sp. KKP3292, determined by an HPLC-DAD at a wavelength of 274 nm.

In most cases, the application of whole cells of fungi resulted in product **2** as the predominant product. Interestingly, during the biotransformations catalyzed by *Penicillium dierckxii* AM32, *Botrytis* sp. KKP3292, and *Botrytis cinerea* AM235, we observed a decrease in content during the biotransformation. Product **3** was observed using *Penicillium dierckxii* AM32, *Penicillium* sp. AM91, and *Botrytis cinerea* AM235. An almost total conversion of the starting substrate (**1**) was noted using both *Botrytis* strains as the catalysts.

We conducted the upscale processes to determine the structure of products **2–4**. The biotransformations with biocatalysts AM91 and AM235 were conducted in the bioreactor at a concentration of substrate (**1**) equaling 0.4 g/L, while that with AM32 was conducted in a 2 L flask. After extraction with ethyl acetate and evaporation, the mixtures were purified by column chromatography on silica gel using gradient elution, gradually increasing the concentration of polar solvents. The structures of compounds **2–4** were determined based on nuclear magnetic resonance (NMR) spectroscopy and confirmed by high-resolution electrospray ionization mass spectrometry (HRMS). Figure 3 shows the LC/ESI-MS/MS chromatograms, while Table 1 presents information about the quasi-molecular ions, the proposed elemental formula, and fragment ions of compounds **1–4**, both from the experiments and from the literature. The NMR spectra for compounds **1–4** are presented in the Supplementary Materials (Figures S1–S8).

The ^1H NMR spectra of compound **2** revealed duplicated peaks in the area of 1.40–5.60 ppm corresponding to protons in the side chain of the lactone, which suggested the presence of two diastereoisomers. The characteristic signal of substrate **1** for proton H-3 ($\delta = 5.47$ ppm) was present, excluding the possibility of hydroxylation at the C-3 position, the predominant direction of biotransformation of 3-*n*-butylidenophthalide found in our previous study [23]. Correlation spectroscopy (COSY) revealed the coupling of H-5 with H-6 and H-7, and H-6 with H-7 in the aromatic region (Figure 4). Other key couplings between the protons in the side chain were H-8 with H-3 and H-9 and H-10 with H-11. The most characteristic signal of the carbon spectrum was a downfield shift of C-10 carbon in relation to the substrate (22.6 ppm) corresponding signal. Instead, signals appeared at $\delta = 81.18$ and $\delta = 81.68$ ppm (two signals of the isomers).

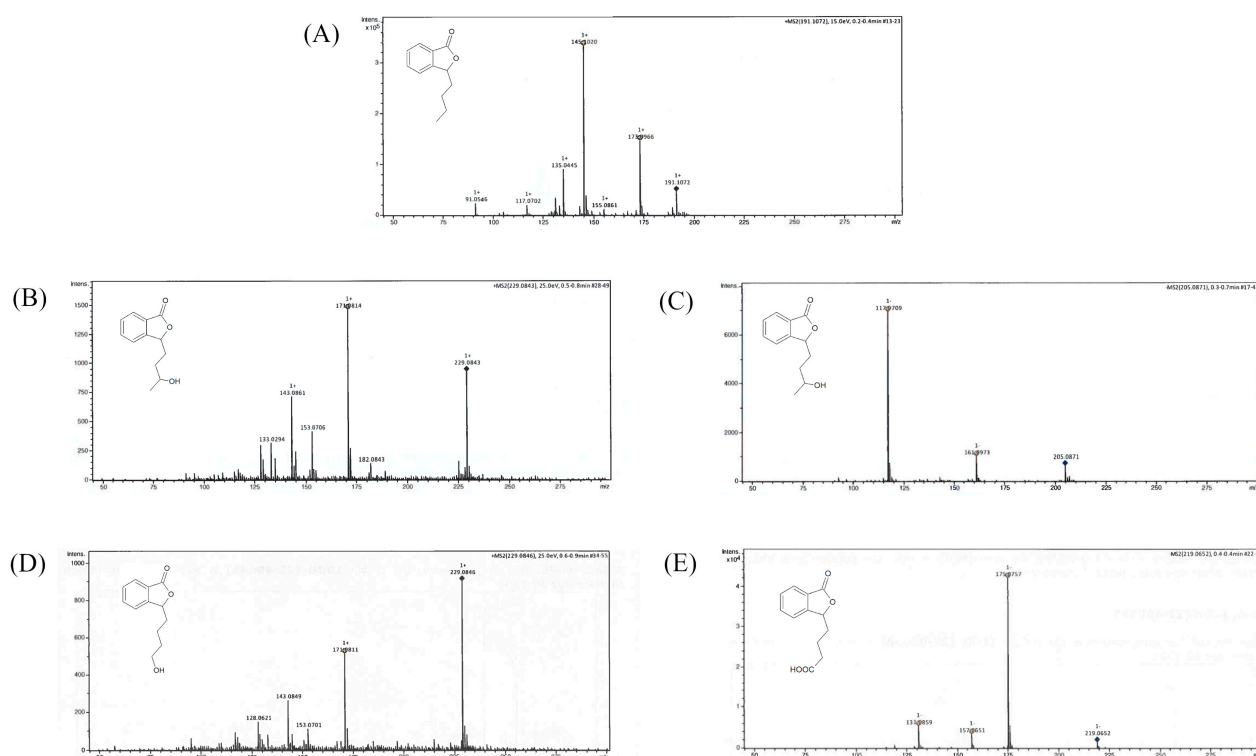


Figure 3. LC/ESI-MS/MS chromatograms of (A) 3-*n*-butylphthalide (1)—positive ion mode, (B) 3-*n*-butyl-10-hydroxy-phthalide (2)—positive ion mode, (C) 3-*n*-butyl-10-hydroxy-phthalide (2)—negative ion mode, (D) 3-*n*-butyl-11-hydroxy-phthalide (3)—positive ion mode, and (E) 3-*n*-butylphthalide-11-oic acid (4)—negative ion mode.

Table 1. Pseudo-molecular ions and fragment ions in ESI-HR-MS analysis of compounds 1–4.

Compound	[M + H] ⁺	[M + Na] ⁺	[M + H] [−]	Formula	Fragment Ions (ESI+) Exp.	Fragment Ions (ESI+) Lit.	Fragment Ions (ESI-) Exp. *	Fragment Ions (ESI-) Lit. *
1	191.1065	213.0891	-	C ₁₂ H ₁₅ O ₂ C ₁₂ H ₁₄ NaO ₂	145.1012 173.0961	173.0962, 145.1011, 135.0440, 117.0701, 131.0493, 105.0703, 91.0547 [24]; 173.098, 145.103, 135.047, 131.052, 117.072, 105.074, 103.057, 91.057 [21]	-	-
2	-	229.0844	205.0863	C ₁₂ H ₁₄ NaO ₃ C ₁₂ H ₁₃ O ₃	171.0804	189.0908, 171.0805, 153.0700, 145.1011, 143.0855, 133.0285, 117.0700 [24]; 189.091, 171.079, 153.071, 145.102, 143.086, 133.031, 128.064, 117.072 [21]	117.0710 161.0972	161.092
3	-	229.0844	-	C ₁₂ H ₁₄ NaO ₃	171.0804	-	-	-
4	-	-	219.0650	C ₁₂ H ₁₁ O ₄	-	203.0699, 185.0594, 175.0752, 159.0441, 157.0649, 143.0489, 131.0490 [24]; 203.081, 185.070, 175.080, 159.052, 157.075, 143.059, 131.058, 103.060 [21]	131.0866 157.0659 175.0765	175.0755, 157.0652, 131.0853 [24]; 175.078, 157.068, 131.089 [21]

* exp—experimental, lit.—literature source.

Compound 2 ionized in negative and positive modes, resulting in the formation of [M + H][−] 205.0863 and the adduct [M + Na]⁺ 229.0844, respectively. Fragment ion 171.0804 was formed after the loss of two water molecules. Product 2 was confirmed as 3-*n*-butyl-10-hydroxyphthalide (2).

The characteristic of the ¹H NMR spectrum of compound 3 is the presence of a triplet at δ = 3.64 ppm of the integration, indicating the presence of two protons. The ¹³C NMR

spectrum of **3** is similar to that of the 10-hydroxylated derivative (**2**), with a slight shift upfield of the signals $\delta = 21.36$, 32.39 , and 62.58 ppm. Compound **3** ionized in positive mode, and the 229.0844 $[M + Na]^+$ adduct was formed with a similar fragment ion 171.0804 as that for product **2**. Product **3** was confirmed as 3-*n*-butyl-11-hydroxyphthalide.

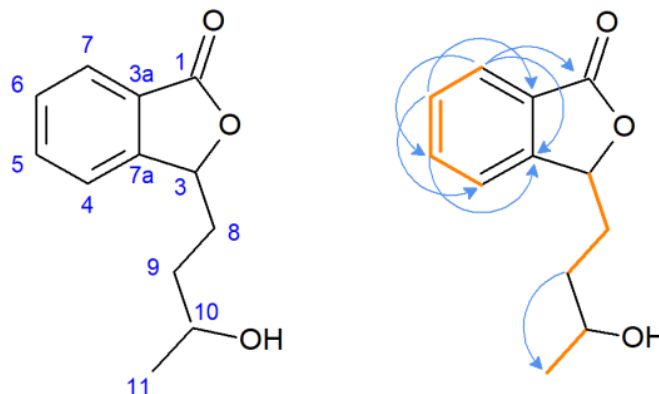


Figure 4. Pivotal couplings for compound **2**—correlation spectroscopy (orange) and nuclear multiple bond coherence (blue arrows).

In the ^1H NMR spectrum of compound **4**, we observed the shift of the proton signals concerning the side chain of lactone towards the lower field compared to that of the substrate (**1**) and the product with a hydroxyl group at the C-10 position. The total integration of multiplets in the areas 1.74–1.88, 2.10–2.20, and 2.37–2.50 ppm indicated the presence of six protons. In the carbon spectrum, there were only three signals in the area characteristic for the side chain (14–30 ppm), with a lack of signal characteristic for C-11 in the substrate **1** spectrum (at $\delta = 14.0$ ppm). However, we observed a new strongly de-shielded signal at $\delta = 179.8$ ppm. The product ionized in the negative mode, leading to the formation of $[M + H]^-$ 219.0650. The main fragment ions included 175.0765, formed after the loss of $-\text{CO}_2$, 157.0659 (after the loss of $-\text{CO}_2$ and $-\text{H}_2\text{O}$), and 131.0866. Product **4** was identified as 3-*n*-butylphthalide-11-oic acid.

During the purification of the crude mixture after biotransformation, we isolated pure fractions of products **2–4** and mixtures of these compounds enriched with metabolites. As we had doubts concerning the assessment of the process efficiency, we conducted additional experiments to assess the percentage of substrate and products in the mixtures. For this purpose, biotransformations were performed with 3-*n*-butylphthalide (**1**) at a concentration of 260 mg per 1000 mL of culture. The cultures were extracted with ethyl acetate after 12 days for *Penicillium* sp. AM91, *B. cinerea* AM235, and *Botrytis* sp. KKP3292, and after 6 days for *Penicillium dierckxii* AM32. We prolonged the extraction time using new portions of solvent until no substrate or product remained in the extract. After the extraction, the amounts of the remaining substrate and the individual products **2–4** were assessed using gas chromatography coupled with a flame-ionization detector (GC-FID) using calibration curves from previously purified products. The obtained yields in relation to the biocatalyst are presented in Table 2.

Similar to the screening scale biotransformations, compound **2** was the most dominant metabolite for strains *B. cinerea* AM235 and *Botrytis* sp. KKP3292. *Botrytis* sp. KKP3292 led to an almost total conversion of substrate **1**. However, *Penicillium* sp. AM91, applied as a biocatalyst, led to the obtaining of, predominantly, compound **3**. AM32 led to the obtaining of mainly products **3** and **4**, and their relative ratio changed with the prolonged biotransformation time in favor of **4** (from 2:1 to 18:1 in biotransformation after 6 and 12 days, respectively).

Table 2. Yields (g per g of the substrate; determined by GC) of compounds 2–4 in the biotransformation extracts in relation to the strains used.

Microorganism Strain	Compound 2 [g/g]	Compound 3 [g/g]	Compound 4 [g/g]	Yield of Compounds 2–4 [g/g]
AM32 (6 days)	0.04	0.25	0.53	0.82
AM32 (12 days)	0.01	0.04	0.73	0.77
AM91	0.08	0.27	0.02	0.38
AM235	0.57	0.07	0.02	0.66
KKP3292	0.78	0.02	0	0.80

2.2. Inhibition of MAO-A Activity

Protein-ligand interaction analysis was performed using isothermal titration calorimetry (ITC). During the analysis, the heat of uptake or release, due to the interaction of MAO-A with the tested compounds, was recorded. In this way, raw data were obtained in the form of exothermic heat versus time graphs. Additionally, the ligand was injected into 1% DMSO with methanol to subtract the energetic effects of the dilution of the ligand solution. The obtained thermodynamic parameters are presented in Table 3. The highest negative change in enthalpy was characterized by the interaction of the enzyme with compounds 3 (−19.19 kJ/mol) and 4 (−13.37 kJ/mol), and the lowest value of ΔH was recorded during interactions with compound 1 (−4.51 kJ/mol). The paired compounds caused a decrease in enthalpy while maintaining the exothermic effect of the reaction; the enthalpy ranged from −3.80 kJ/mol (1 with 2) to −8.28 kJ/mol (3 with 4). Affinity (ΔG) values were more evenly distributed between compound 1, compounds 1 with 4, 2 with 4, and 2 with 3. The lowest affinities were characterized by 1 with 3 and 1 with 2, amounting to −20.69 and 22.69 kJ/mol, respectively, and the highest one was compounds 4, amounting to −28.42 kJ/mol. The ability of the ligands to inhibit BChE activity was described on the basis of the IC_{50} parameter. The lowest IC_{50} value was shown by compound 3 (1.29 $\mu\text{mol/L}$), and the highest by compound 1 with 2 (45.00 $\mu\text{mol/L}$).

Table 3. Thermodynamic parameters of interactions between MAO-A and compounds 1–4.

Compound	K_D ($\mu\text{mol/L}$)	$K_A \times 10^3$ (L/mol)	ΔH (kJ/mol)	ΔG (kJ/mol)	ΔS (J/mol * K)	IC_{50} (1 $\mu\text{mol/L}$ Inhibitor:1 $\mu\text{mol/L}$ MAO-A)	K_i ($\mu\text{mol/L}$) K_M 5-HT 0.35 mmol
1	24.30 ± 1.39 ^a	41.15 ± 0.36 ^d	−4.51 ± 0.02 ^e	−27.33 ± 1.14	73.85 ± 1.05 ^d	6.51 ± 2.29 ^l	241.00 ± 3.55 ^{c,d}
2	29.90 ± 1.09 ^a	33.44 ± 0.15 ^a	−7.77 ± 0.01 ^e	−26.79 ± 1.55 ^j	61.55 ± 1.84 ^d	9.66 ± 0.64 ^l	994.00 ± 3.18 ^e
3	239.00 ± 4.25 ^c	4.18 ± 0.35 ^e	−19.19 ± 0.01 ^f	−23.49 ± 1.42 ⁱ	13.92 ± 0.92 ^a	1.29 ± 0.59 ^k	<0.001 ^a
4	67.40 ± 3.15 ^d	14.83 ± 0.25 ^e	−13.37 ± 0.02 ^f	−28.42 ± 1.43 ^j	48.71 ± 1.05 ^a	5.45 ± 0.10 ^l	128.00 ± 1.25 ^c
1, 2	147.00 ± 3.18 ^b	6.80 ± 0.15 ^e	−3.80 ± 0.02 ^e	−22.69 ± 1.91 ⁱ	61.13 ± 1.91 ^d	45.00 ± 4.44 ⁿ	0.08 ± 0.00 ^b
1, 3	320.00 ± 5.55 ^c	3.12 ± 0.25 ^e	−4.63 ± 0.02 ^e	−20.69 ± 1.52 ⁱ	51.97 ± 1.64 ^a	35.61 ± 3.45 ⁿ	200.00 ± 1.18 ^{c,d}
1, 4	24.60 ± 1.18 ^a	40.65 ± 0.33 ^d	−5.02 ± 0.02 ^{e,g}	−27.29 ± 1.33 ^j	72.07 ± 1.25 ^d	14.03 ± 1.25 ^m	716.00 ± 3.95 ^e
2, 4	20.00 ± 1.45 ^a	50.00 ± 0.49 ^d	−5.60 ± 0.01 ^{e,g}	−27.84 ± 1.45 ^j	71.97 ± 1.85 ^d	5.63 ± 2.45 ^l	<0.001 ^a
2, 3	21.70 ± 1.49 ^a	46.08 ± 0.19 ^d	−5.27 ± 0.01 ^{e,g}	−27.62 ± 1.54 ^j	72.33 ± 1.08 ^d	15.02 ± 1.15 ^m	0.94 ± 0.01 ^b
3, 4	109.00 ± 2.55 ^b	9.17 ± 0.52 ^e	−8.28 ± 0.01 ^e	−23.74 ± 1.59 ⁱ	50.03 ± 1.19 ^a	2.02 ± 1.19 ^k	0.92 ± 0.01 ^b

* Values are expressed as mean value ± SD; n = 3; different letters in one column or no index correspond to significant differences ($p < 0.05$).

2.3. Absorption, Distribution, Metabolism, Excretion, and Toxicity (ADMET) Profiling

Substrate 1 and products 2–4 were tested for their pharmacokinetic properties, using the bioinformatic SWISS ADME tool reported by Daina et al. [25], including lipophilicity, solubility, and inhibition of the selected isoenzymes and drug-likeness. Toxicity to rat

cells after oral administration was determined using the Way2Drug platform described by Druzhilovskiy et al. [26] (Table 4).

Table 4. In silico profiling, including lipophilicity (Log $P_{o/w}$), solubility (Log S), and inhibition of the isoenzymes CYP1A2, CYP2C19, CYP2C9, CYP2D6, and CYP3A4 toxicity to rat cells, expressed as LD₅₀ [mg/kg], and compliance with the objectives of Lipinski, Ghose, Webber, Egan, Muegge.

Compound	Log $P_{o/w}$	Log S	Inhibition of CYP Isoenzymes	LD ₅₀ [mg/kg]	Drug-like Properties
1	2.81	−2.90	CYP1A2	4872	Lipinski, Ghose, Webber, Egan
2	1.92	−2.14	-	4582	Lipinski, Ghose, Webber, Egan, Muegge
3	1.94	−2.03	-	3896	Lipinski, Ghose, Webber, Egan, Muegge
4	1.60	−1.99	-	2065	Lipinski, Ghose, Webber, Egan, Muegge

Lipophilicity is the distribution of the drug between the organic and water phases [27]. Biotransformation led to the obtaining of more polar and less lipophilic metabolites 2–4 compared to their precursor 1. Among these, the most soluble metabolite in water was 3-*n*-butylphthalide-11-oic acid (4).

There are several selection criteria for predicting the potential drug properties, including Lipinski, Ghose, Veber, Egan and Muegge [28–32], describing the optimal number of carbon atoms, heteroatoms, rings, hydrogen bond donors and acceptors, rotatable bonds, the range for lipophilicity, molar refractivity, total polar surface, and molecular weight [33]. According to the predictions, compounds 2–4 match the objectives described by these researchers [28–32]; however, their precursor, 3-*n*-butylphthalide (1) does not meet the criterion of Muegge.

Interestingly, metabolism led to an increase in toxicity as the half-lethal dose of compounds 2–4 declined. The half-lethal dose for precursor (1) was 4872 mg/kg. The least toxic of the metabolites was 3-*n*-butyl-10-hydroxyphthalide (2), while 3-*n*-butylphthalide-11-oic acid (4) was twice as toxic to rat cells than 3-*n*-butylphthalide (1).

The inhibition of CYP isoenzymes leads to drug interactions, causing side effects [34,35]. In silico tests were performed for the five isoforms, accounting for almost 90% of the metabolic reactions [35]. They revealed no inhibition of lactones 1–4 against CYP2C19, CYP2C9, CYP2D6, and CYP3A4. CYP1A2 was inhibited only by the precursor, 3-*n*-butylphthalide (1). This isoform is crucial for the inhibition of many drugs, including Alzheimer’s and Parkinson’s disease medications and analgesics [36].

2.4. Molecular Species Identification

The PROTAX-fungi tool results of the ITS fragment for the analyzed samples are shown in Figure S9. For the AM32 strain, the results indicate that the analyzed sample belongs to *P. dierckxii* (Figure S9, part A). The ITS results for the AM91 strain did not identify the systematic affiliation, as the results showed an 18% probability for unknown species and a 14% probability for *P. spinulosum* and *P. thomii* (Figure S10, part B). The AM235 strain was identified as *Botrytis cinerea* (Figure S9, part B). The ITS sequences for AM32 and AM235 were deposited in the National Center for Biotechnology Information (NCBI) database under accession number OQ875855 for AM32 and OQ875856 for AM235.

The genome sequence obtained for strain AM91 (after base-calling) had 1.64e + 09 bases with N50 = 1.23 kbp and median PHRED = 10.931. The Flye assembly results were 35,547,927 bp of total genome length with 91 fragments (N50 = 3,603,452 bp and longest fragment 7,742,766 bp) and a mean coverage of 28. Medaka analyses did not improve genome assembly in terms of length. Finally, the assembled genome was deposited in the NCBI database under accession number SAMN34128561.

3. Discussion

Based on the results of chromatographic analysis, we selected four fungal strains that allowed high substrate (**1**) conversion, including *Penicillium dierckxii* AM32, *Penicillium* sp. AM91, *Botrytis cinerea* AM235, and *Botrytis* sp. KKP3292, and we observed three main products. Notably, several *Penicillium* spp. have been used previously to convert one of the phthalides, mycophenolic acid, to the corresponding hydroxyderivative [11]. The hydroxylation of piperitone occurred in *Botrytis* AM235 [37]. The structures of the obtained main products depending on the biocatalyst are presented in Figure 5.

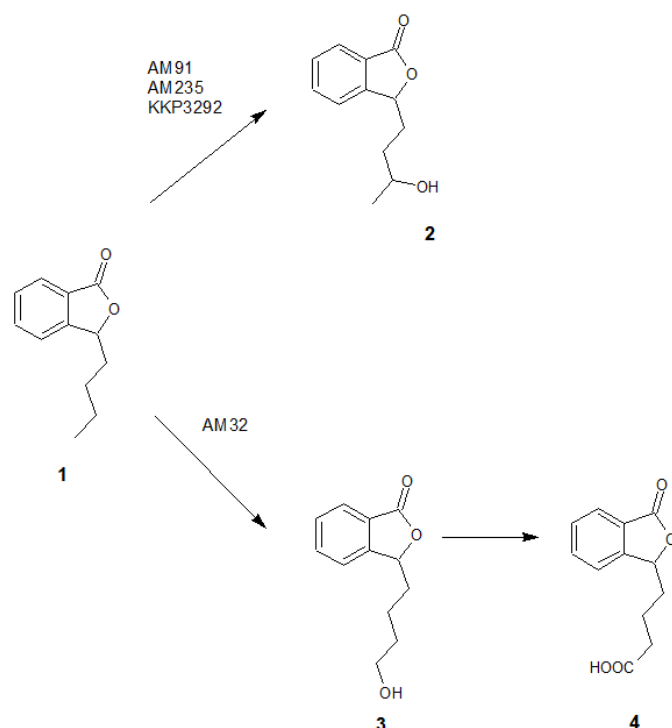


Figure 5. The structures of the main products formed during fungal-mediated biotransformations of 3-*n*-butylphthalide (**1**)—3-*n*-butyl-10-hydroxyphthalide (**2**), 3-*n*-butyl-11-hydroxyphthalide (**3**) and 3-*n*-butylphthalide-11-oic acid (**4**).

Diao et al. reported that the main direction of 3-*n*-butylphthalide (**1**) metabolism using human liver microsomes was the hydroxylation of the side chain. In vivo studies showed that 3-*n*-butyl-10-hydroxyphthalide (**2**) was the dominant circulating human metabolite, followed by the carboxylic acid derivative **4**, the hydroxylation product in the C-3 position, and the keto derivative. The biocatalysis of 3-*n*-butylphthalide (**1**) by whole cells of the *Cunninghamella blakesleana* ATCC9244 strain led to the formation of the products mentioned above; however, their ratio was not stated [21]. Moreover, the research conducted by Lin et al. confirmed that 3-*n*-butyl-10-hydroxyphthalide (**2**) was the main metabolite in the rat plasma and liver microsomes [38].

In our research, whole-cell biotransformations, similar to the in vivo tests, resulted in the obtaining of, primarily, the derivative in the C-10 position. Interestingly, there are no articles on the formation of two diastereoisomers of compound **2** during biotransformation; however, their presence was confirmed in the extract of *Ligusticum chuanxiong* [12]. Based on the decreasing content of C-11 hydroxyderivative (**3**) in favor of the 3-*n*-butylphthalide-11-oic acid (**4**) and the research conducted by Diao et al. [21], it can be confirmed that 3-*n*-butyl-11-hydroxyphthalide (**3**) is the mediatory product and is further oxidized to compound **4**.

Compounds **1–4** were tested for their inhibition of MAO-A activity by the ITC method. In the first stage, we assumed interactions between compounds **1–4** and the MAO-A enzyme to be potential ligands protecting against 5-HT degradation. Considering that a mixture of

compounds may act differently than a single substance, with possible synergistic, additive, and antagonistic effects, we also tested compounds 1–4 in combinations [39,40]. The interactions between 1–4 and the MAO-A enzyme showed an exothermic effect, evidenced by negative enthalpy changes. An analysis of the stoichiometry of the resulting complexes showed a single 1:1 reaction-binding model [41]. During the analysis, there was a decrease in heat emitted after subsequent injections, which reflects the observed negatively charged compounds or mixtures in compounds, while interactions 1 and 2 with MAO-A were so weak that ITC could detect them. The change in the free enthalpy (affinity ΔG) indicated negative values, which characterizes the spontaneous nature of interactions. The values of individual compounds ranged from -28.42 to -23.49 kJ/mol for 4 and 3 associated with MAO-A complexation and blocking. The pairing of the compounds resulted in the stabilization of affinity at approximately -27 kJ/mol for pairs 1 with 4, 2 with 3, and 2 with 4. However, for the remaining pairs, the affinity decreased, which may be related to the change in the energetic effect resulting from the rearrangement of the protein structure.

The compounds with the most significant exothermic effects were 3 and 4, suggesting the most significant conformational changes of MAO-A. In addition to complexation with active sites, exothermic changes were observed; therefore, injections of these compounds may limit the ability to deviate 5-HT. According to Prah, the calculated 5-HT degradation barrier is 62 kJ/mol, while the reaction catalyzed by the enzyme is reduced to -35.42 kJ/mol at pH 7.5. However, the same reaction in an aquatic environment shows a lower free energy of -22.06 kJ/mol, which means that the compounds are less stable in the aquatic environment than in pH 7.5 [42]. Our research confirms that the most stable bonds with the enzyme are characterized by compound 4 and the pairs of compounds 2 with 4, 1 with 4, and 2 with 3. The values of the binding constant of the resulting complexes ranged from 3.12×10^3 to 50×10^3 L/mol. The significant differences in the height of K_A may be because some of the compounds have deprotonated, and the resulting electrostatic interaction affects the binding constant of these compounds with the enzyme. The highest MAO-A bond constant was characterized by the pair of compounds 2 and 4, amounting to 50×10^3 L/mol. In all cases, the values of free enthalpy and enthalpy of interactions were negative, and the entropy values were positive, indicating the formation of a ligand–protein complex through non-covalent hydrophobic interactions [43].

The tested compounds demonstrated the ability to reduce the rate of 5-HT deamination by the MAO-A enzyme. The IC_{50} was lowest for compound 3, and the pair of compounds 3 and 4, at $1.29 \mu\text{mol}/\mu\text{mol}$ of enzyme and $2.02 \mu\text{mol}/\mu\text{mol}$ of enzyme, respectively. Compounds 4 and 4 combined with 2 were at a similar level of about $5 \mu\text{mol}/\mu\text{mol}$ of the enzyme. Substrate 1, tested with lactones 2 and 3, turned out to be the least beneficial compounds, with a high concentration inhibiting the activity of the enzyme by 50%, and had the least favorable affinity. This effect can be explained by the binding of several compounds in the mixture to different MAO-A residues at the active site and in other regions. Molecular docking can be used in future research to confirm this assumption [44,45].

The K_i of the tested compounds indicates that they bound to MAO-A as competitive inhibitors and were characterized by a fairly similar and low K_i value for compounds 3 and 4 combined with 2, amounting to $<0.001 \mu\text{mol}/\text{L}$. Various phthalide analogs have been tested regarding their MAO-inhibiting activity. According to Strydom et al., the K_i values for 6-phenyl-propoxyphthalide and CF_3 -substituted benzyloxyphthalide, the most active phthalide derivatives regarding MAO-A and MAO-B inhibition, were $0.062 \mu\text{M}$ and $0.0007 \mu\text{M}$, respectively [46]. Qiang et al. tested the 3-*n*-butylphthalide–Edaravone complexes, that showed an inhibitory effect at IC_{50} , in the ranges of 4.40 – $19.32 \mu\text{M}$ [47].

Absorption, distribution, metabolism, excretion, and toxicity are key in drug development [48]. The increase in lipophilicity is related to higher permeability through membranes and low solubility [49]. The values of this parameter for both butylphthalide and its metabolite were within the optimal range of $\log P$, described as $\log P$ 1–3, ensuring their sufficient permeability and solubility [50]. The drug-likeness prediction for metabolites 2–4 revealed their obedience to the most common set of guidelines described by Lipinski, Ghose, Web-

ber, Egan, and Muegge. However, 3-n-butylphthalide (**1**) showed incompatibility with the drug-likeness concept, according to Muegge, for the molecular weight, which is under 200.

The predictions indicated the increased toxicity of the metabolites **2–4** compared to that of their precursor **1**. According to the research of Xue et al., the compounds phthalide **1** and their metabolites **2–4** were not toxic for primary rat hepatocytes and primary human hepatocytes tested at a concentration of 0–500 μM . However, the repetitive administration of **1** caused a reduction in cell viability [51]. Considering that toxicity is the second cause for clinical failures of drug development, it is crucial to conduct further preclinical studies on the metabolites **2–4** [52].

4. Materials and Methods

4.1. General

The content of the products was monitored using an HPLC—Dionex UltiMate 3000 instrument with a diode array detector (Thermo Fisher Scientific, Waltham, MA, USA) with a column Agilent Zorbax Bonus-RP 3.5 μm 150 \times 3 mm. The mobile phase was composed of water acidified with 0.5% formic acid (A) and acetonitrile (B) using gradient elution conditions: 0–3 min, 65% A/35% B; 3–12 min, 35% A/65% B, 12–13 min, 10% A/90% B; 13–14 min, 0% A/100% B; 14–16 min 0% A/100% B; 16–19 min, 65% A/35% B; and 19–23 min, 65% A/35% B. The following parameters were selected: flow rate, 0.4 mL/min; column incubation temperature, 30 $^{\circ}\text{C}$; and detection wavelength, 275 nm. The compounds were purified by column chromatography using silica gel Kieselgel 60, 230–400 mesh, 40–63 μm (Merck, Darmstadt, Germany). The purity of the substrate and the yield of the products were assessed by GC using Agilent Technologies 8860 (GC System, Santa Clara, USA) with a flame-ionization detector and carrier gas H_2 using HP-5 column 30 m \times 0.32 mm \times 0.25 μm (Agilent, Santa Clara, CA, USA) with the following temperature program: 80 $^{\circ}\text{C}$ (1 min), 320 $^{\circ}$ (30 $^{\circ}\text{C}/\text{min}$) (1 min).

The structures of the compounds were evaluated by NMR techniques. ^1H NMR, ^{13}C NMR, COSY, HSQC, and HMBC spectra were recorded in CDCl_3 on a Bruker Avance 500 (500 MHz, Billerica, MA, USA) spectrometer.

HR-ESI-MS/MS analyses of the compounds were performed with RSLC UltiMate 3000 (Dionex, Sunnyvale, CA, USA) coupled with the ESI-Q-TOF, maXis impact mass spectrometer (Bruker Daltonics, MA, USA), and the operating parameters were: flow rate of the sample of 180 $\mu\text{L}/\text{min}$, nebulizer pressure 0.4 bar, the heating gas flow of 3.0 L/min, heating gas temperature of 180/200 $^{\circ}\text{C}$, data acquisition range of m/z 50–1300/1400 m/z , ionization mode: positive and negative, and ion source energy of 5 eV.

4.2. Microorganisms

The strains used in this study were obtained from the Department of Food Chemistry and Biocatalysis collection at the Wrocław University of Environmental and Life Sciences and from the Institute of Agricultural and Food Biotechnology Collection of Industrial Microbial Cultures (full list available in the Supplementary Materials). The strains were stored on Sabouraud or Czapek agar slants at 4 $^{\circ}\text{C}$.

Molecular Species Identification

We performed DNA analyses for strains with high substrate conversion to confirm proper species identification (based on morphology). Strain KKP3292 was not included in this step, as it was obtained from commercial culture collections and was already identified. DNA from samples AM32, AM91, and AM235 was isolated with a Bead-Beat Micro AX Gravity isolation kit from A&A Biotechnology (Poland, Gdańsk) according to the manufacturer's instructions. Next, isolated cellular DNA was assessed for its quality (with agarose gel electrophoresis) and quantity (with Qubit 4 fluorometer). An internal transcribed spacer (ITS) fragment was used as a genetic marker in fungal species identification. PCR conditions and sequencing procedures were similar to those described by Hernik et al. [53]. ITS

sequences from all analyzed samples were input into the online PROTAX-fungi tool [54] to identify the species.

As we could not determine the identification of the species level for strain AM32 with ITS, we sequenced the whole genome of the strain to aid in additional identification in the future. We used the Oxford Nanopore MinION platform with SQK-LSK110 chemistry and R10.3.1 flow cells and obtained approximately 2 Gb of data for the sample. After sequencing, we used Guppy 6.4.2 (<https://community.nanoporetech.com/> (accessed on 4 April 2023)) and dna_r10.3_450bps_sup model for base-calling. Basecalled fastq files were then screened for quality with PycoQC [55]. To assemble the genome, we first used Canu v2.2 [56] and then Flye [57,58] and polished assembly with Medaka (<https://github.com/nanoporetech/medaka> (accessed on 4 April 2023)) to enhance assembly length. Finally, before submission to the NCBI, the obtained data were screened for contaminants using the Foreign Contamination Screen (FCS) tool (<https://github.com/ncbi/fcs> (accessed on 4 April 2023)) and submitted to the NCBI genome database.

4.3. Chemical Synthesis

For this step, 4.3 g (0.023 M) of 3-*n*-butylidene-phthalide (Sigma–Aldrich; Saint Louis, MO, USA) and 110 mL of 0.5 M KOH solution in methanol were added to a two-neck round-bottom flask mounted under a reflux condenser. The reaction mixture turned orange. The hydrolysis reaction was carried out at boiling point for 1.5 h. The mixture was cooled, and 10% hydrochloric acid was added until a yellow color appeared. Then, methanol and water were evaporated; 100 mL of THF, 5 mL of 0.1 M KOH aqueous solution, and 0.95 g (0.025 M) of sodium borohydride (Sigma–Aldrich) were added to the residue. The solution again turned orange. The reaction was stirred at 22 °C for 12 h. An aqueous solution of 10% hydrochloric acid was added until a yellow color appeared, and stirring was continued for another 4 h. The solvents were evaporated, ethyl acetate was added, and the reaction mixture was filtered through a 30 cm layer of silica gel placed in a 3 cm diameter column. After complete elution of the product and evaporation of the solvents, 4.0 g of product was obtained (84% yield) with 92% purity according to GC. Compound **1** was purified on silica gel using a mixture of petroleum ether: acetone: ethyl acetate: isopropanol 150:5:5:15 *v/v* as the eluent.

4.4. Biotransformations

4.4.1. Screening Scale Biotransformations

The screening scale biotransformations were performed in 300 mL Erlenmeyer flasks with sterile Sabouraud medium [23], acidified by HCl to pH 5.6. After inoculation, the cultures were incubated for eight days at 25 °C on a rotary shaker. Next, 20 mg of 3-*n*-butylphthalide (**1**) dissolved in 0.5 mL of acetone was added. The samples were collected after 4, 8, and 12 days, extracted using ethyl acetate, and dried with MgSO₄. After evaporation, they were dissolved in acetonitrile, filtered through a 0.45 µm PTFE filter, and subjected to HPLC analysis.

4.4.2. Preparative Scale Biotransformations

- Method I

Biotransformations with AM91 and AM235 were carried out in the bioreactor–3 L New Brunswick Scientific BioFlo III (Brunswick, Ramsey, MN, USA). The bioreactor with Sabouraud medium was sterilized at 121 °C for 25 min. After sterilization, the temperature was maintained at 20–22 °C, and agitation was set to 75 rpm. A Broadley James D100 Series Oxyprobe was used to measure the level of dissolved oxygen. The air was passed through a sterile 0.2 µm PTFE filter at a 1 L/min flow rate. The previously pre-cultured inoculum (10% *v/v*) was placed into the bioreactor, resulting in a final volume of 1500 mL; 0.4 g of 3-*n*-butylphthalide (**1**) diluted in 5 mL of acetone was added during the exponential phase of growth. The 8-day biotransformation progress was monitored by HPLC. The reaction mixture was divided into three portions (3 × 500 mL), acidified by 0.1 M HCl, washed

with brine, and extracted overnight with ethyl acetate (3×500 mL) on a laboratory shaker. After extraction, the mixture was centrifuged and evaporated. The crude product was purified by column chromatography using gradient elution—a mixture of petroleum ether: acetone: ethyl acetate: isopropanol 150:5:5:15 *v/v* was initially used and, after substrate **1** was washed, their proportion was changed to 50:5:5:15 *v/v*.

- Method II

In the second method for the preparative scale biotransformation, we used AM32, AM91, AM235, and KKP3292 as the biocatalysts. The microorganisms were grown in 2 L flasks with 500 mL of a sterile Sabouraud medium containing 10% pre-cultured inoculum. After five days of incubation at 25 °C on a rotary shaker, 130 mg of lactone **1** in 0.5 mL was added to the cultures.

The biotransformations were extracted by ethyl acetate after 12 days for *Penicillium* sp. AM91, *B. cinerea* AM235, and *Botrytis* sp. KKP3292 and, additionally, after 6 days for *Penicillium dierckxii* AM32. The prolonged extraction of the biotransformation mixtures on the laboratory shaker lasted 96 h. After the extraction, the isolation of the products proceeded as described above.

4.5. MAO-A Activity

A MicroCal PEAQ-ITC200 calorimeter (Malvern, Worcestershire, UK) was used to study the interactions of MAO-A with the compounds. The enzyme and compounds were prepared in 1% DMSO with methanol. The measurements were performed at 36.6 °C. The stirring speed was set to 307 rpm, and a total of 19 injections were performed within 50 min, with the reference power set to 10.00 $\mu\text{cal/s}$. All sample solutions were thoroughly degassed before use. The calorimetric cell was filled with a 20 μM (350 μL) MAO-A sample, and the syringe (2 μL of injection volume) was loaded with a 1 mM/L solution or /and 5-HT (1 mM/L). The ITC data were processed using MicroCal PEAQ-ITC analysis software with calorimetric routines. The following parameters were determined: the standard interaction Gibbs energy (ΔG), standard interaction enthalpy (ΔH), entropy (ΔS), equilibrium constant (K_D), and stoichiometry of reaction (N) [59].

4.6. ADMET Profiling

The pharmacokinetic parameters involving lipophilicity, solubility, and inhibition of CYP isoenzymes CYP1A2, CYP2C9, CYP2C19, CYP2D6, and CYP3A4 were predicted using the Swiss Institute of Bioinformatics tool at the University of Lausanne (<http://www.swissadme.ch/index.php> (accessed on 25 March 2023)). Toxicity to rat cells was assessed using the Way2Drug platform (<http://www.way2drug.com/gusar/acutoxpredict.html> (accessed on 25 March 2023)).

5. Conclusions

Biotransformations catalyzed by fungi are a useful method to obtain derivatives of 3-*n*-butylphthalide (**1**). Two strains of *Botrytis* and two isolates of *Penicillium* were the most effective in terms of substrate transformation. Both 3-*n*-butylphthalide (**1**) and its metabolites **2–4**, obtained via fungal biotransformation, acted as MAO-A inhibitors. Two metabolites, **3** and **4**, were more active than substrate **1**. The lipophilicity for all products, assessed by *in silico* tests, was in the optimal range, correlating with good permeability and solubility. Contrary to its precursor **1**, the most active 3-*n*-butyl-11-hydroxyphthalide (**3**) had no inhibitory activity on the CYP1A2 isoform; therefore, the possibility of interference with drugs metabolized by this isoform is lower. However, further evaluation of the toxicity of compound **3** is required, as the *in silico* prediction of this parameter revealed higher toxicity to rat cells than 3-*n*-butylphthalide (**1**).

Further research may involve tests regarding the reversibility of the process to determine if the usage of phthalide **1** analogs leads to tyramine accumulation, like most commercially available drugs, or has similar actions with moclobemide, a reversible inhibitor of MAO-A.

Supplementary Materials: The following supporting information can be downloaded at: <https://www.mdpi.com/article/10.3390/ijms241310605/s1>.

Author Contributions: Conceptualization, T.O. and J.G. (Joanna Gach); methodology, T.O. and F.B.; software, J.G. (Joanna Gach); formal analysis, J.G. (Joanna Gach), T.O. and F.B.; investigation, J.G. (Joanna Gach), T.O., J.G. (Joanna Grzelczyk) and T.S.; resources, J.G. (Joanna Gach), T.O. and F.B.; writing—original draft preparation, J.G. (Joanna Gach), J.G. (Joanna Grzelczyk) and T.S.; writing—review and editing, T.O. and F.B.; visualization, J.G. (Joanna Gach), J.G. (Joanna Grzelczyk) and T.S.; supervision, T.O. and F.B.; funding acquisition, J.G. (Joanna Gach). All authors have read and agreed to the published version of the manuscript.

Funding: This research was funded by the project “UPWR 2.0: international and interdisciplinary program of development of Wrocław University of Environmental and Life Sciences” and co-financed by the European Social Fund under the Operational Program Knowledge Education Development, under contract No. POWR.03.05.00-00-Z062/18 of 4 June 2019.

Institutional Review Board Statement: Not applicable.

Informed Consent Statement: Not applicable.

Data Availability Statement: The data presented in this study are available on request from the corresponding author.

Conflicts of Interest: The authors declare no conflict of interest.

References

1. Moncrieff, J.; Cooper, R.E.; Stockmann, T.; Amendola, S.; Hengartner, M.P.; Horowitz, M.A. The Serotonin Theory of Depression: A Systematic Umbrella Review of the Evidence. *Mol. Psychiatry* **2022**. [CrossRef] [PubMed]
2. Bhatt, S.; Devadoss, T.; Jha, N.K.; Baidya, M.; Gupta, G.; Chellappan, D.K.; Singh, S.K.; Dua, K. Targeting Inflammation: A Potential Approach for the Treatment of Depression. *Metab. Brain Dis.* **2023**, *38*, 45–59. [CrossRef] [PubMed]
3. Roets, M.; Brand, L.; Steyn, S.F. Increased Depressive-like Behaviour of Postpartum Flinders Sensitive and Resistant Line Rats Is Reversed by a Predictable Postpartum Stressor. *Behav. Brain Res.* **2023**, *442*, 114321. [CrossRef]
4. Greener, M. New Antidepressants: Monoamines and Beyond. *Prescriber* **2023**, *34*, 17–20. [CrossRef]
5. Kim, T.T.; Amsterdam, J.D. Effectiveness and Safety of Monoamine Oxidase Inhibitor Treatment for Bipolar Depression versus Unipolar Depression: An Exploratory Case Cohort Study. *Acta Psychiatr. Scand.* **2023**, *147*, 198–204. [CrossRef] [PubMed]
6. Merce, A.P.; Ionică, L.N.; Bîna, A.M.; Popescu, S.; Lighezan, R.; Petrescu, L.; Borza, C.; Sturza, A.; Muntean, D.M.; Crețu, O.M. Monoamine Oxidase Is a Source of Cardiac Oxidative Stress in Obese Rats: The Beneficial Role of Metformin. *Mol. Cell. Biochem.* **2023**, *478*, 59–67. [CrossRef]
7. Finberg, J.P.M.; Rabey, J.M. Inhibitors of MAO-A and MAO-B in Psychiatry and Neurology. *Front. Pharmacol.* **2016**, *7*, 340. [CrossRef]
8. Muellers, S.N.; Tararina, M.A.; Kuzmanovic, U.; Galagan, J.E.; Allen, K.N. Structural Insights into the Substrate Range of a Bacterial Monoamine Oxidase. *Biochemistry* **2023**, *62*, 851–862. [CrossRef]
9. Syu, G.-D.; Sutandy, F.X.R.; Chen, K.; Cheng, Y.; Chen, C.-S.; Shih, J.C. Autoantibody Profiling of Monoamine Oxidase A Knockout Mice, an Autism Spectrum Disorder Model. *Brain Behav. Immun.* **2023**, *107*, 193–200. [CrossRef]
10. Barrowman, J.; Wilson, M. Antidepressants and Antipsychotics. *Anaesth. Intensive Care Med.* **2023**, *24*, 228–234. [CrossRef]
11. León, A.; Del-Ángel, M.; Ávila, J.L.; Delgado, G. Phthalides: Distribution in Nature, Chemical Reactivity, Synthesis, and Biological Activity. In *Progress in the Chemistry of Organic Natural Products*; Kinghorn, A.D., Falk, H., Gibbons, S., Kobayashi, J., Eds.; Springer International Publishing: Cham, Switzerland, 2017; Volume 104, pp. 127–246. [CrossRef]
12. Zhang, X.; Feng, Z.; Yang, Y.; Jiang, J.; Zhang, P. Bioactive Butylphthalide Derivatives from *Ligusticum Chuanxiong*. *Bioorganic Chem.* **2019**, *84*, 505–510. [CrossRef]
13. Bi, M.; Zhang, M.; Guo, D.; Bi, W.; Liu, B.; Zou, Y.; Li, Q. N-Butylphthalide Alleviates Blood–Brain Barrier Impairment in Rats Exposed to Carbon Monoxide. *Front. Pharmacol.* **2016**, *7*, 394. [CrossRef] [PubMed]
14. Wang, M.; Zhang, Q.; Hua, W.; Huang, M.; Zhou, W.; Lou, K.; Peng, Y. Pharmacokinetics, Safety and Tolerability of L-3-n-Butylphthalide Tablet after Single and Multiple Oral Administrations in Healthy Chinese Volunteers. *Braz. J. Pharm. Sci.* **2015**, *51*, 525–531. [CrossRef]
15. Xiong, Y.; Liu, J.; Xu, Y.; Xie, S.; Zhou, X.; Cheng, S. Butylphthalide Combined With Conventional Treatment Attenuates MMP-9 Levels and Increases VEGF Levels in Patients With Stroke: A Prospective Cohort Study. *Front. Neurol.* **2021**, *12*, 686199. [CrossRef]
16. Lv, J.; Zhao, D.; Zhao, G.; Xie, Z. Efficacy and Safety of Butylphthalide in Secondary Prevention of Stroke: Study Protocol for a Multicenter, Real World Trial Based on Internet. *BMC Neurol.* **2022**, *22*, 305. [CrossRef] [PubMed]
17. Wang, M.; Feng, Y.; Yuan, Y.; Gui, L.; Wang, J.; Gao, P.; Qin, B.; Sima, D.; Wang, Q.; Pan, W. Use of L-3-n-Butylphthalide within 24 h after Intravenous Thrombolysis for Acute Cerebral Infarction. *Complement. Ther. Med.* **2020**, *52*, 102442. [CrossRef] [PubMed]

18. Chen, C.; Ma, H.; Fu, Z. Antidepressant-like Effect of 3-*n*-Butylphthalide in Rats Exposed to Chronic Unpredictable Mild Stress: Modulation of Brain-Derived Neurotrophic Factor Level and MTOR Activation in Cortex. *Neurochem. Res.* **2021**, *46*, 3075–3084. [[CrossRef](#)] [[PubMed](#)]
19. Geng, C.; Hao, G.; Yi, Q.; Guo, Y.; Chen, D.; Han, W.; Zhang, J.; Yang, M.; Jiang, P. The Impact of DI-3-*n*-Butylphthalide on the Lipidomics of the Hippocampus in a Rat Model of Lipopolysaccharide-Induced Depression. *Prostaglandins Other Lipid Mediat.* **2020**, *150*, 106464. [[CrossRef](#)]
20. Shen, J.; Yang, L.; Wei, W. DI-3-*n*-butylphthalide prevents chronic restraint stress-induced depression-like behaviors and cognitive impairment via regulating CaMKII/CREB/BDNF signaling pathway in hippocampus. *Neuroreport* **2022**, *33*, 597–603. [[CrossRef](#)]
21. Diao, X.; Deng, P.; Xie, C.; Li, X.; Zhong, D.; Zhang, Y.; Chen, X. Metabolism and Pharmacokinetics of 3-*n*-Butylphthalide (NBP) in Humans: The Role of Cytochrome P450s and Alcohol Dehydrogenase in Biotransformation. *Drug Metab. Dispos.* **2013**, *41*, 430–444. [[CrossRef](#)]
22. Shanu-Wilson, J.; Evans, L.; Wrigley, S.; Steele, J.; Atherton, J.; Boer, J. Biotransformation: Impact and Application of Metabolism in Drug Discovery. *ACS Med. Chem. Lett.* **2020**, *11*, 2087–2107. [[CrossRef](#)]
23. Gach, J.; Olejniczak, T.; Krężel, P.; Boratyński, F. Microbial Synthesis and Evaluation of Fungistatic Activity of 3-Butyl-3-Hydroxyphthalide, the Mammalian Metabolite of 3-*n*-Butylideneophthalide. *Int. J. Mol. Sci.* **2021**, *22*, 7600. [[CrossRef](#)]
24. Tian, J.; Lei, P.; He, Y.; Zhang, N.; Ge, X.; Luo, L.; Yan, S.; Diao, X. Absorption, Distribution, Metabolism, and Excretion of [¹⁴C]NBP (3-*n*-Butylphthalide) in Rats. *J. Chromatogr. B* **2021**, *1181*, 122915. [[CrossRef](#)] [[PubMed](#)]
25. Daina, A.; Michielin, O.; Zoete, V. SwissADME: A Free Web Tool to Evaluate Pharmacokinetics, Drug-Likeness and Medicinal Chemistry Friendliness of Small Molecules. *Sci. Rep.* **2017**, *7*, 42717. [[CrossRef](#)] [[PubMed](#)]
26. Druzhilovskiy, D.S.; Rudik, A.V.; Filimonov, D.A.; Glorizova, T.A.; Lagunin, A.A.; Dmitriev, A.V.; Pogodin, P.V.; Dubovskaya, V.I.; Ivanov, S.M.; Tarasova, O.A.; et al. Computational Platform Way2Drug: From the Prediction of Biological Activity to Drug Repurposing. *Russ. Chem. Bull.* **2017**, *66*, 1832–1841. [[CrossRef](#)]
27. Tafreshi, N.K.; Kil, H.; Pandya, D.N.; Tichacek, C.J.; Doligalski, M.L.; Budzevich, M.M.; Delva, N.C.; Langsen, M.L.; Vallas, J.A.; Boulware, D.C.; et al. Lipophilicity Determines Routes of Uptake and Clearance, and Toxicity of an Alpha-Particle-Emitting Peptide Receptor Radiotherapy. *ACS Pharmacol. Transl. Sci.* **2021**, *4*, 953–965. [[CrossRef](#)]
28. Egan, W.J.; Merz, K.M.; Baldwin, J.J. Prediction of Drug Absorption Using Multivariate Statistics. *J. Med. Chem.* **2000**, *43*, 3867–3877. [[CrossRef](#)]
29. Ghose, A.K.; Viswanadhan, V.N.; Wendoloski, J.J. A Knowledge-Based Approach in Designing Combinatorial or Medicinal Chemistry Libraries for Drug Discovery. 1. A Qualitative and Quantitative Characterization of Known Drug Databases. *J. Comb. Chem.* **1999**, *1*, 55–68. [[CrossRef](#)] [[PubMed](#)]
30. Lipinski, C.A. Drug-like Properties and the Causes of Poor Solubility and Poor Permeability. *J. Pharmacol. Toxicol. Methods* **2000**, *44*, 235–249. [[CrossRef](#)]
31. Muegge, I.; Heald, S.L.; Brittelli, D. Simple Selection Criteria for Drug-like Chemical Matter. *J. Med. Chem.* **2001**, *44*, 1841–1846. [[CrossRef](#)]
32. Veber, D.F.; Johnson, S.R.; Cheng, H.-Y.; Smith, B.R.; Ward, K.W.; Kopple, K.D. Molecular Properties That Influence the Oral Bioavailability of Drug Candidates. *J. Med. Chem.* **2002**, *45*, 2615–2623. [[CrossRef](#)] [[PubMed](#)]
33. Pathania, S.; Singh, P.K. Analyzing FDA-Approved Drugs for Compliance of Pharmacokinetic Principles: Should There Be a Critical Screening Parameter in Drug Designing Protocols? *Expert Opin. Drug Metab. Toxicol.* **2021**, *17*, 351–354. [[CrossRef](#)] [[PubMed](#)]
34. Sychev, D.; Ashraf, G.M.; Svistunov, A.; Maksimov, M.; Tarasov, V.; Chubarev, V.N.; Otdelenov, V.A.; Denisenko, N.P.; Barreto, G.E.; Aliev, G. The Cytochrome P450 Isoenzyme and Some New Opportunities for the Prediction of Negative Drug Interaction in Vivo. *DDDT* **2018**, *12*, 1147–1156. [[CrossRef](#)]
35. Yim, S.-K.; Kim, K.; Chun, S.; Oh, T.; Jung, W.; Jung, K.; Yun, C.-H. Screening of Human CYP1A2 and CYP3A4 Inhibitors from Seaweed In Silico and In Vitro. *Mar. Drugs* **2020**, *18*, 603. [[CrossRef](#)] [[PubMed](#)]
36. Bhatt, S.; Dhiman, S.; Kumar, V.; Gour, A.; Manhas, D.; Sharma, K.; Ojha, P.K.; Nandi, U. Assessment of the CYP1A2 Inhibition-Mediated Drug Interaction Potential for Pinocembrin Using *In Silico*, *In Vitro*, and *In Vivo* Approaches. *ACS Omega* **2022**, *7*, 20321–20331. [[CrossRef](#)]
37. Grudniewska, A.; Gniłka, R.; Wawrzęńczyk, C. Enantioselectivity of Hydroxylation of Racemic Piperitone by Fungi. *Chirality* **2010**, *22*, 929–935. [[CrossRef](#)]
38. Lin, L.; Lin, L.; Lin, T.; Wu, Y. Simultaneous Determination of 3-*n*-butylphthalide and Its Metabolite 10-hydroxy-butylphthalide in Rat Plasma Using Liquid Chromatography–Tandem Mass Spectrometry and Application to a Pharmacokinetic Study. *Biomed. Chromatogr.* **2021**, *35*, e5184. [[CrossRef](#)]
39. Roell, K.R.; Reif, D.M.; Motsinger-Reif, A.A. An Introduction to Terminology and Methodology of Chemical Synergy—Perspectives from Across Disciplines. *Front. Pharmacol.* **2017**, *8*, 158. [[CrossRef](#)]
40. Tallarida, R.J. Quantitative Methods for Assessing Drug Synergism. *Genes Cancer* **2011**, *2*, 1003–1008. [[CrossRef](#)]
41. Du, X.; Li, Y.; Xia, Y.-L.; Ai, S.-M.; Liang, J.; Sang, P.; Ji, X.-L.; Liu, S.-Q. Insights into Protein–Ligand Interactions: Mechanisms, Models, and Methods. *Int. J. Mol. Sci.* **2016**, *17*, 144. [[CrossRef](#)]
42. Prah, A.; Purg, M.; Stare, J.; Vianello, R.; Mavri, J. How Monoamine Oxidase A Decomposes Serotonin: An Empirical Valence Bond Simulation of the Reactive Step. *J. Phys. Chem. B* **2020**, *124*, 8259–8265. [[CrossRef](#)] [[PubMed](#)]

43. López-Nicolás, J.M.; Escorial Camps, M.; Pérez-Sánchez, H.; García-Carmona, F. Physicochemical and Thermodynamic Characterization of the Encapsulation of Methyl Jasmonate by Natural and Modified Cyclodextrins Using Reversed-Phase High-Pressure Liquid Chromatography. *J. Agric. Food Chem.* **2013**, *61*, 11347–11354. [[CrossRef](#)]
44. Konc, J.; Lešnik, S.; Janežič, D. Modeling Enzyme-Ligand Binding in Drug Discovery. *J. Cheminform.* **2015**, *7*, 48. [[CrossRef](#)] [[PubMed](#)]
45. Meng, X.-Y.; Zhang, H.-X.; Mezei, M.; Cui, M. Molecular Docking: A Powerful Approach for Structure-Based Drug Discovery. *CAD* **2011**, *7*, 146–157. [[CrossRef](#)]
46. Strydom, B.; Bergh, J.J.; Petzer, J.P. Inhibition of Monoamine Oxidase by Phthalide Analogues. *Bioorganic Med. Chem. Lett.* **2013**, *23*, 1269–1273. [[CrossRef](#)]
47. Qiang, X.; Li, Y.; Yang, X.; Luo, L.; Xu, R.; Zheng, Y.; Cao, Z.; Tan, Z.; Deng, Y. DL-3-n-Butylphthalide-Edaravone Hybrids as Novel Dual Inhibitors of Amyloid- β Aggregation and Monoamine Oxidases with High Antioxidant Potency for Alzheimer's Therapy. *Bioorganic Med. Chem. Lett.* **2017**, *27*, 718–722. [[CrossRef](#)]
48. Guan, L.; Yang, H.; Cai, Y.; Sun, L.; Di, P.; Li, W.; Liu, G.; Tang, Y. ADMET-score-a comprehensive scoring function for evaluation of chemical drug-likeness. *MedChemComm* **2018**, *10*, 148–157. [[CrossRef](#)]
49. Miller, R.R.; Madeira, M.; Wood, H.B.; Geissler, W.M.; Raab, C.E.; Martin, I.J. Integrating the Impact of Lipophilicity on Potency and Pharmacokinetic Parameters Enables the Use of Diverse Chemical Space during Small Molecule Drug Optimization. *J. Med. Chem.* **2020**, *63*, 12156–12170. [[CrossRef](#)]
50. Chmiel, T.; Mieszkowska, A.; Kempnińska-Kupczyk, D.; Kot-Wasik, A.; Namieśnik, J.; Mazerska, Z. The Impact of Lipophilicity on Environmental Processes, Drug Delivery and Bioavailability of Food Components. *Microchem. J.* **2019**, *146*, 393–406. [[CrossRef](#)]
51. Xue, Y.; Ren, X.; Zhu, Z.; Lei, P.; Liu, M.; Wan, M.; Zhong, D.; Huang, H.; Diao, X. Site-Specific Protein Modification by 3-n-Butylphthalide in Primary Hepatocytes: Covalent Protein Adducts Diminished by Glutathione and N-Acetylcysteine. *Life Sci.* **2021**, *287*, 120125. [[CrossRef](#)]
52. Sun, D.; Gao, W.; Hu, H.; Zhou, S. Why 90% of Clinical Drug Development Fails and How to Improve It? *Acta Pharm. Sin. B* **2022**, *12*, 3049–3062. [[CrossRef](#)] [[PubMed](#)]
53. Hernik, D.; Szczepańska, E.; Brenna, E.; Patejuk, K.; Olejniczak, T.; Strzała, T.; Boratyński, F. *Trametes hirsuta* as an Attractive Biocatalyst for the Preparative Scale Biotransformation of Isosafrole into Piperonal. *Molecules* **2023**, *28*, 3643. [[CrossRef](#)]
54. Abarenkov, K.; Somervuo, P.; Nilsson, R.H.; Kirk, P.M.; Huotari, T.; Abrego, N.; Ovaskainen, O. Protax-fungi: A web-based tool for probabilistic taxonomic placement of fungal internal transcribed spacer sequences. *New Phytol.* **2018**, *220*, 517–525. [[CrossRef](#)]
55. Leger, A.; Leonardi, T. pycoQC, interactive quality control for Oxford Nanopore Sequencing. *J. Open Source Softw.* **2019**, *4*, 1236. [[CrossRef](#)]
56. Koren, S.; Walenz, B.P.; Berlin, K.; Miller, J.R.; Bergman, N.H.; Phillippy, A.M. Canu: Scalable and accurate long-read assembly via adaptive κ -mer weighting and repeat separation. *Genome Res.* **2017**, *27*, 722–736. [[CrossRef](#)]
57. Kolmogorov, M.; Yuan, J.; Lin, Y.; Pevzner, P.A. Assembly of long, error-prone reads using repeat graphs. *Nat. Biotechnol.* **2019**, *37*, 540–546. [[CrossRef](#)] [[PubMed](#)]
58. Lin, Y.; Yuan, J.; Kolmogorov, M.; Shen, M.W.; Chaisson, M.; Pevzner, P.A. Assembly of long error-prone reads using de Bruijn graphs. *Proc. Natl. Acad. Sci. USA* **2016**, *113*, E8396–E8405. [[CrossRef](#)]
59. Grzelczyk, J.; Budryn, G.; Peña-García, J.; Sz wajgier, D.; Gałazka-Czarnecka, I.; Oracz, J.; Pérez-Sánchez, H. Evaluation of the Inhibition of Monoamine Oxidase A by Bioactive Coffee Compounds Protecting Serotonin Degradation. *Food Chem.* **2021**, *348*, 129108. [[CrossRef](#)] [[PubMed](#)]

Disclaimer/Publisher's Note: The statements, opinions and data contained in all publications are solely those of the individual author(s) and contributor(s) and not of MDPI and/or the editor(s). MDPI and/or the editor(s) disclaim responsibility for any injury to people or property resulting from any ideas, methods, instructions or products referred to in the content.

Supplementary Materials

Microbial Metabolites of 3-*n*-butylphthalide as Monoamine Oxidase A Inhibitors

Joanna Gach ^{1,*}, Joanna Grzelczyk ², Tomasz Strzała ³, Filip Boratynski ¹ and Teresa Olejniczak ^{1,*}

- ¹ Department of Food Chemistry and Biocatalysis, Wrocław University of Environmental and Life Sciences, Norwida 25, 50-375 Wrocław, Poland; filip.boratynski@upwr.edu.pl (F.B.)
 - ² Institute of Food Technology and Analysis, Faculty of Biotechnology and Food Sciences, Lodz University of Technology, Stefanowskiego 2/22, 90-924 Łódź, Poland; joanna.grzelczyk@p.lodz.pl
 - ³ Department of Genetics, Wrocław University of Environmental and Life Sciences, Koźuchowska 7, 51-631 Wrocław, Poland; tomasz.strzala@upwr.edu.pl
- * Correspondence: joanna.gach@upwr.edu.pl (J.G.); teresa.olejniczak@upwr.edu.pl (T.O.)

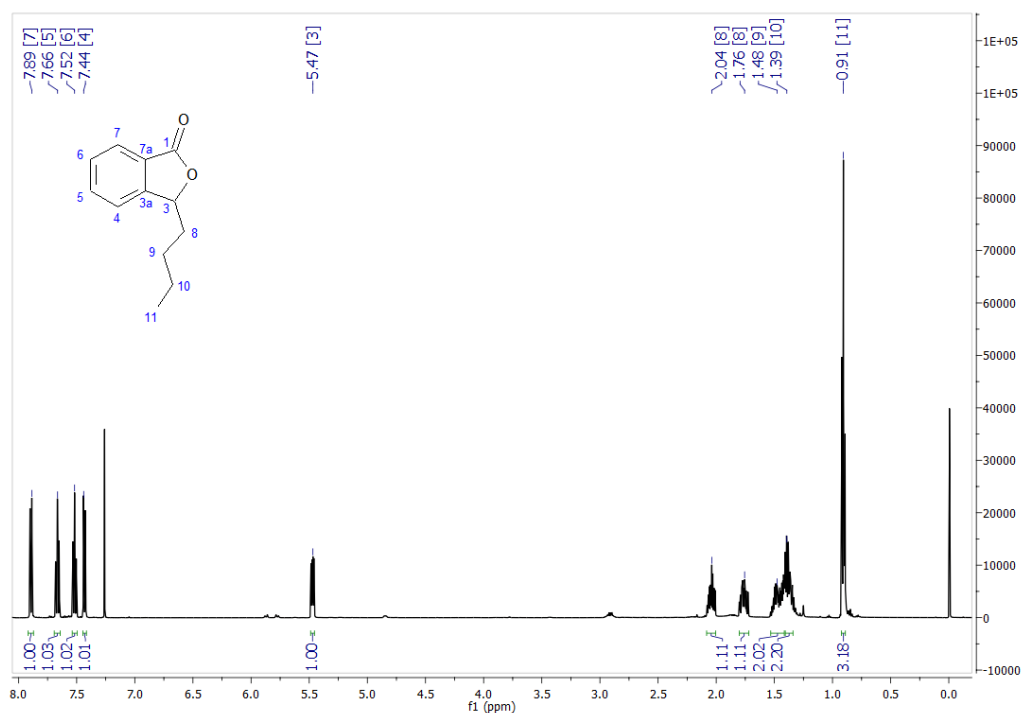


Figure S1. ¹H NMR of 3-*n*-butylphthalide (1).

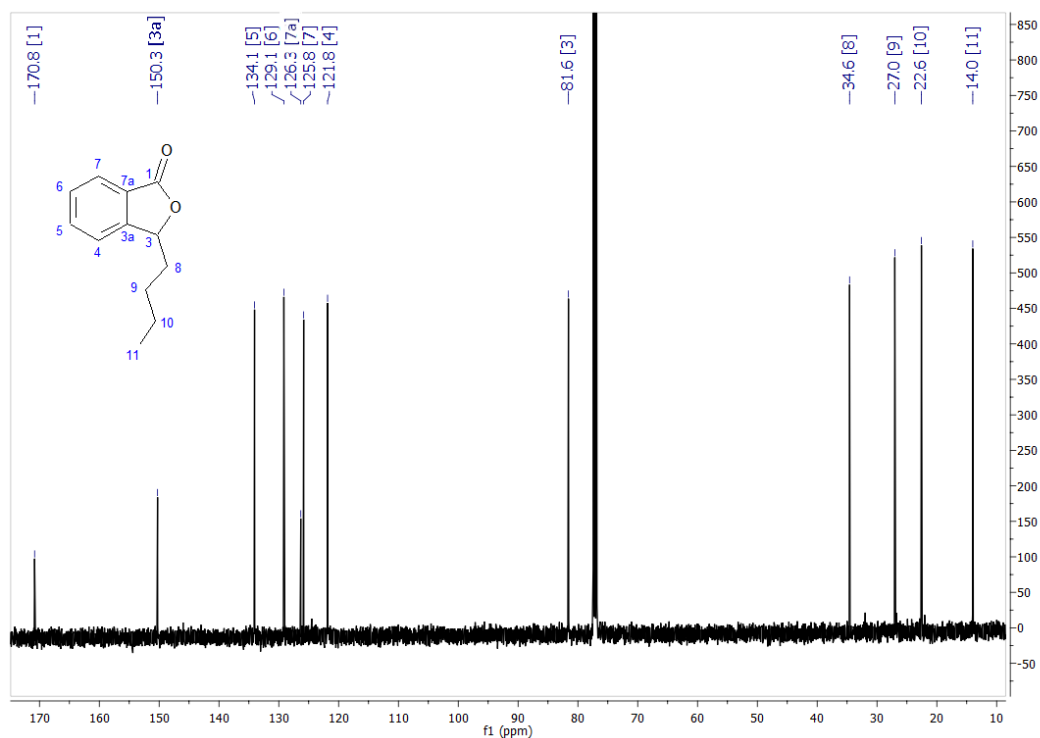


Figure S2. ¹³C NMR of 3-*n*-butylphthalide (**1**).

3-*n*-butylphthalide (**1**).

Spectroscopic data: ¹H NMR (500 MHz, CDCl₃), δ (ppm): 0.91 (t, 3, *J* = 7.2 Hz, CH₃-11), 1.31–1.44 (m, 2, CH₂-10), 1.44–1.54 (m, 2, CH₂-9), 1.65–1.80 (m, 1, one of CH₂-8), 1.99–2.12 (m, 1, one of CH₂-8), 5.47 (dd, 1, *J* = 7.9, 3.7 Hz, CH-3), 7.44 (d, 1, *J* = 7.7 Hz, CH-4), 7.52 (t, 1, *J* = 7.5 Hz, CH-6), 7.66 (t, 1, *J* = 7.5 Hz, CH-5), 7.89 (d, 1, *J* = 7.7 Hz, CH-7).

¹³C NMR (151 MHz), δ (ppm): 14.0 (C-11), 22.6 (C-10), 27.0 (C-9), 34.6 (C-8), 81.6 (CH-3), 121.8 (CH-4), 125.8 (CH-7), 126.3 (C-7a) 129.1 (CH-6), 134.1 (CH-5), 150.3 (C-3a), 170.8 (C-1).

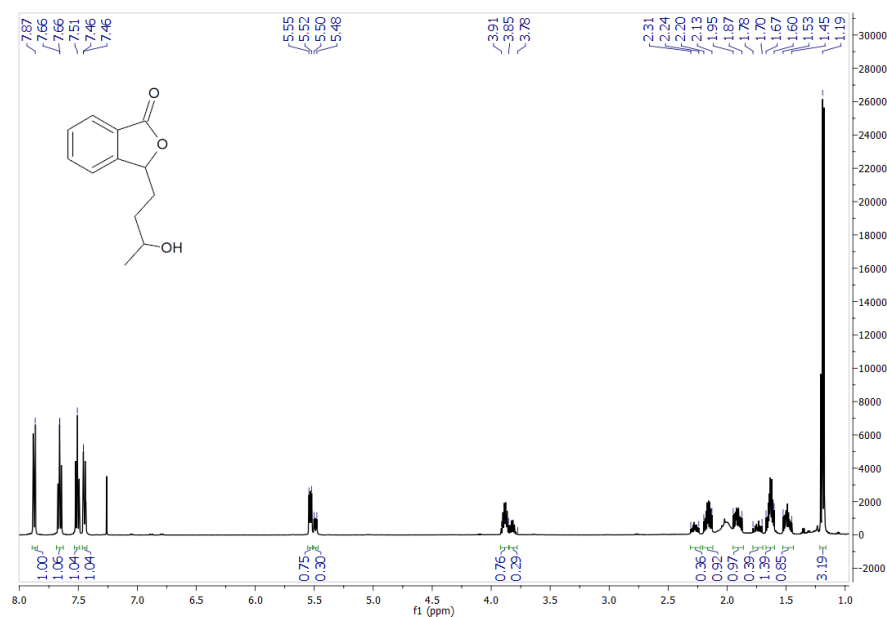


Figure S3. ^1H NMR of 3-*n*-Butyl-10-hydroxy-phthalide (**2**)

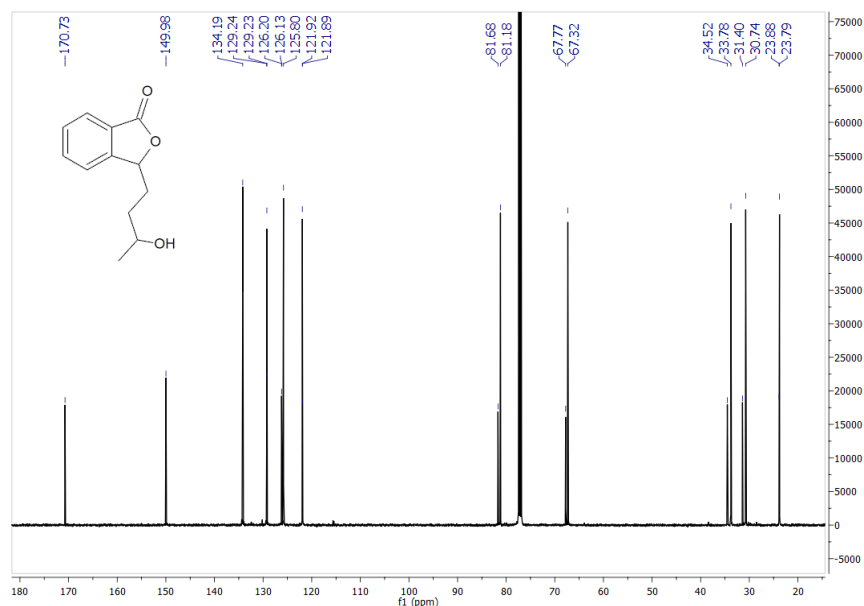


Figure S4. ^{13}C NMR of 3-*n*-Butyl-10-hydroxy-phthalide (**2**)

3-*n*-Butyl-10-hydroxyphthalide (**2**)

Spectroscopic data: ^1H NMR (500 MHz, CDCl_3), δ (ppm): 1.19 (dd, 3H, $J = 8.2, 6.2$ Hz, CH_3 -11), 1.44-1.53 (m, 1H, one of CH_2 -9), 1.60-1.67 (m, 1H, one of CH_2 -9), 1.87-1.95 (m, 1H, one of CH_2 -8), 2.13-2.20 (m, 1H, one of CH_2 -8), 3.78-3.85 (m, 1H, CH-10-minor isomer), 3.85-3.91 (m, 1H, CH-10-major isomer), 5.48-5.50 (dd, 1H, $J = 7.8, 4.0$ Hz, CH-3-minor isomer), 5.52-5.55 (dd, 1H, $J = 8.3, 3.8$ Hz, CH-3-major isomer), 7.45 (ddd, 1H, $J = 7.6, 2.8, 0.6$ Hz, CH-4), 7.51 (t, 1H, $J = 7.5$ Hz, CH-6), 7.66 (td, 1H, $J = 7.5, 1.0$ Hz, CH-5), 7.87 (d, 1H, $J = 7.7$ Hz, CH-7).

^{13}C NMR (151 MHz), δ (ppm): 23.79 (C-11-major isomer), 23.88 (C-11-minor isomer), 30.74 (C-8-major isomer), 31.40 (C-8-minor isomer), 33.78 (C-9-major isomer), 34.58 (C-9-minor isomer), 67.32 (C-10-major isomer), 67.77 (C-10-minor isomer), 81.18 (C-3-major isomer), 81.68 (C-3-minor isomer), 121.89 (C-4-minor isomer), 121.92 (C-4-major isomer), 125.80 (C-7), 126.12 (C-7a-minor isomer), 126.20 (C-7a-major isomer), 129.23 (C-6-major isomer), 129.24 (C-6-minor isomer), 134.19 (C-5), 149.98 (C-3a), 170.73 (C-1).

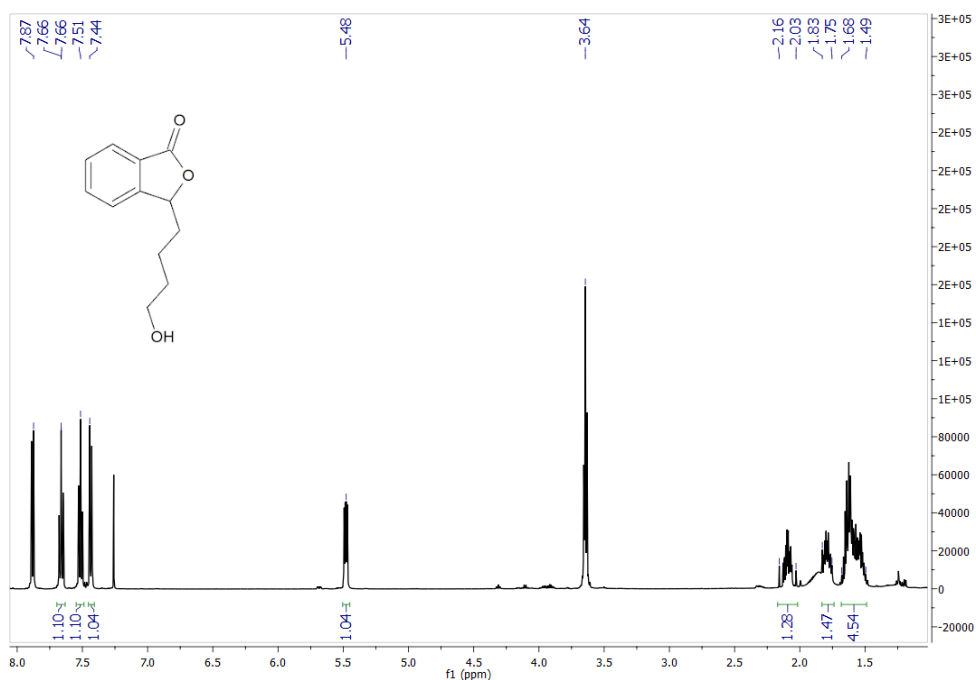


Figure S5. ¹H NMR of 3-*n*-Butyl-11-hydroxy-phthalide (3)

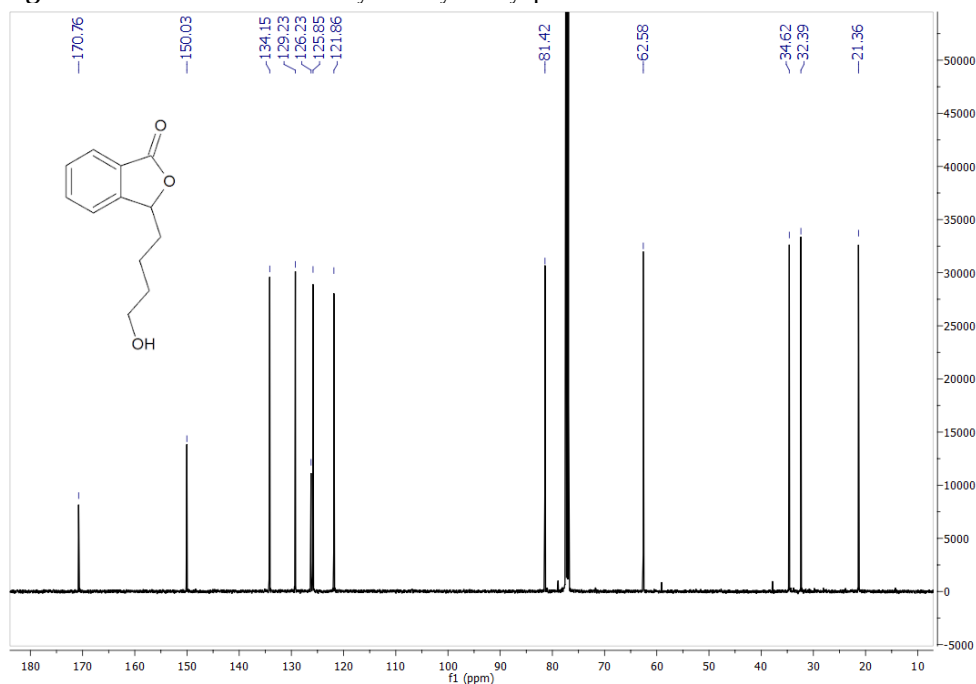


Figure S6. ¹³C NMR of 3-*n*-Butyl-11-hydroxy-phthalide (3)

3-*n*-Butyl-11-hydroxyphthalide (3)

Spectroscopic data: ¹H NMR (500 MHz, CDCl₃), δ (ppm): 1.49-1.68 (m, 4H, CH₂-10, CH₂-9), 1.75-1.83 (m, 1H, one of CH₂-8), 2.03-2.16 (m, 1H, one of CH₂-8), 3.64 (t, 2H, *J* = 6.2 Hz, CH₂), 5.48 (dd, 1H, *J* = 7.9, 4.0 Hz, CH-3), 7.44 (d, 1H, *J* = 7.7 Hz, CH-7), 7.51 (t, 1H, *J* = 7.5 Hz, CH-6), 7.66 (td, 1H, *J* = 7.6, 0.8 Hz, CH-5), 7.87 (d, 1H, *J* = 7.6 Hz, CH-7).

¹³C NMR (151 MHz), δ (ppm): 21.36 (C-9), 32.39 (C-10), 34.62 (C-8), 62.58 (C-11), 81.42 (C-3), 121.86 (C-4), 125.85 (C-7), 126.23 (C-7a), 129.23 (C-6), 134.15 (C-5), 150.03 (C-3a), 170.76 (C-1).

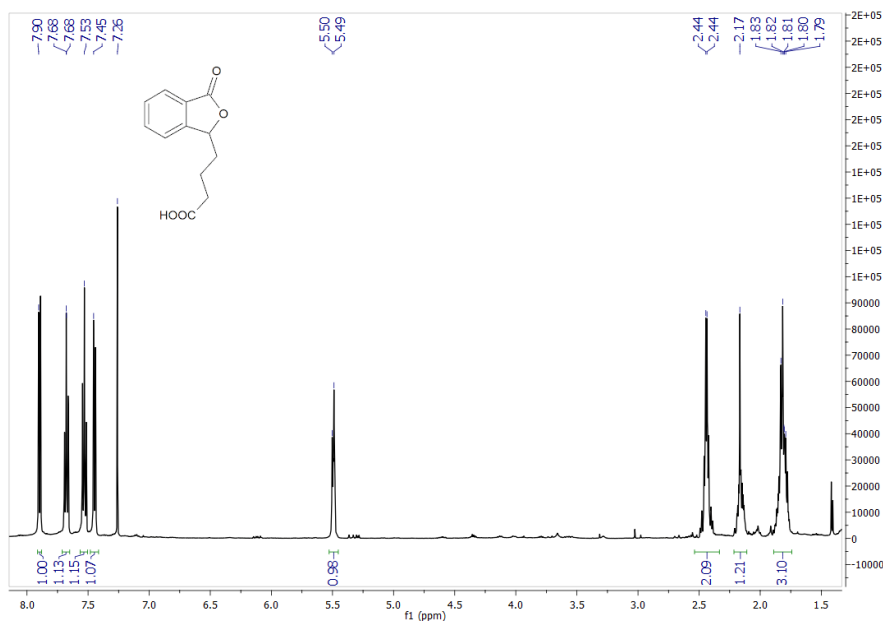


Figure S7. ¹H NMR of 3-*n*-butylphthalide-11-oic acid (**4**)

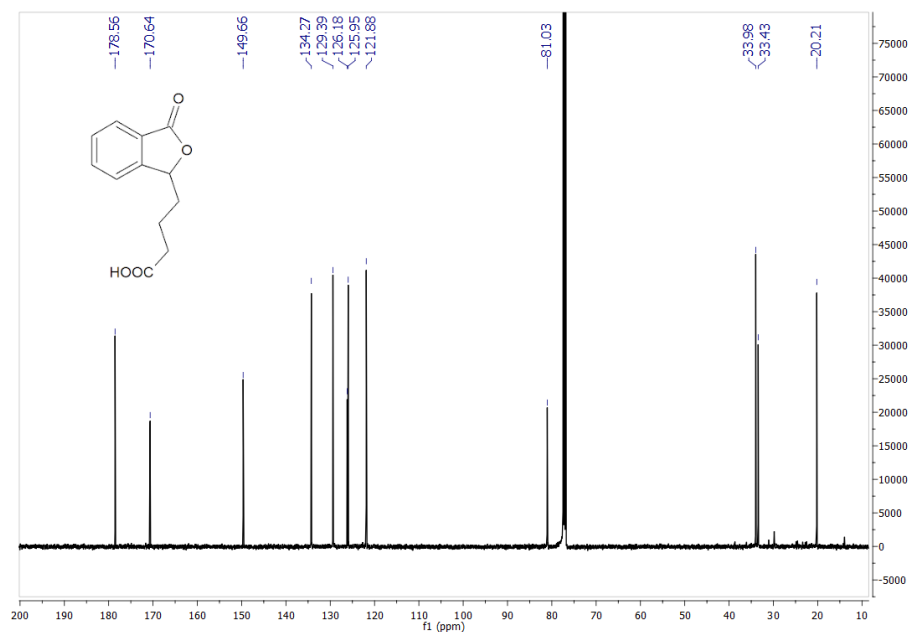


Figure S8. ¹³C NMR of 3-*n*-butylphthalide-11-oic acid (**4**)

3-*n*-butylphthalide-11-oic acid (**4**)

Spectroscopic data: ¹H NMR (500 MHz, CDCl₃), δ (ppm): 1.74-1.88 (m, 3H, CH₂-9, one of CH₂-8), 2.10-2.20 (m, 1H, one of CH₂-8), 2.37-2.50 (m, 2H, CH₂-10), 5.49 (dd, 1H, *J* = 7.0, 3.5 Hz, CH-3), 7.45 (d, 1H, *J* = 7.6 Hz, CH-4), 7.53 (t, 1H, *J* = 7.5 Hz, CH-6) 7.67 (td, 1H, *J* = 7.6, 0.9 Hz, CH-5), 7.90 (d, 1H, *J* = 7.7 Hz, CH-7).

¹³C NMR (151 MHz), δ (ppm): 20.21 (C-9), 33.43 (C-8), 33.98 (C-10), 81.03 (C-3), 121.88 (C-4), 125.87 (C-7), 126.18 (C-7a), 129.39 (C-6), 134.27 (C-5), 149.66 (C-3a), 170.64 (C-1), 178.56 (C-11).

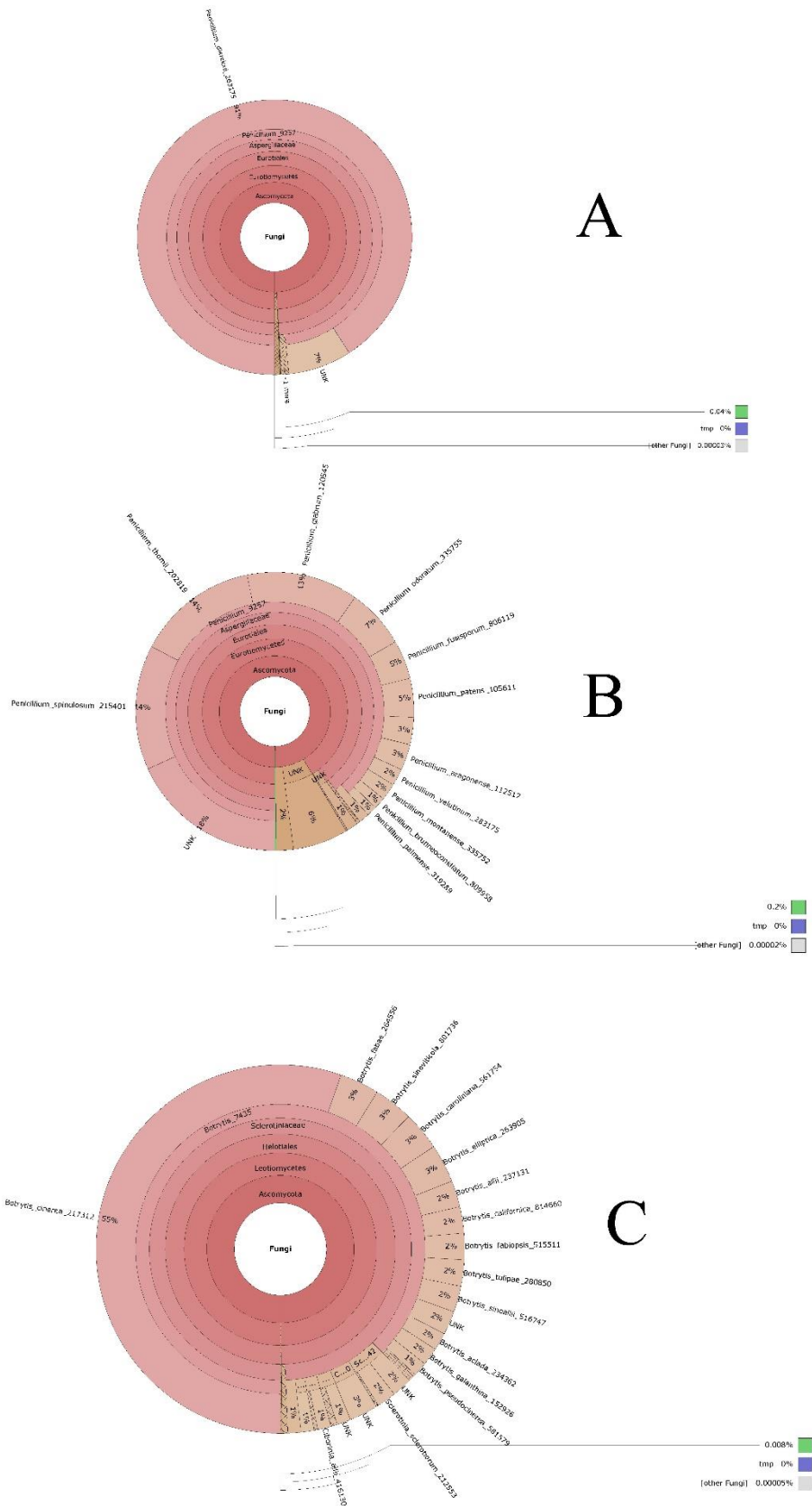


Figure S9. Species identification results of PROTAX-fungi online tool. A is for strain AM32, B is for strain AM91 and C is for strain AM235.

Table S1. Titer (g per liter of culture volume; determined by GC) of compounds 1–4 in the biotransformation extracts in relation to the strains used

Microorganism strain	Compound 2 [g/L]	Compound 3 [g/L]	Compound 4 [g/L]	Compounds 2-4 [g/L]
AM32 (6 days)	0.01	0.06	0.14	0.24
AM32 (12 days)	0.00	0.01	0.19	0.20
AM91	0.02	0.07	0.00	0.11
AM235	0.15	0.02	0.00	0.19
KKP3292	0.20	0.01	0.00	0.21

Table S2. Productivity (g of product per liter of culture volume per hour; determined by GC) of compounds 2–4 in the biotransformation extracts in relation to the strains used

Microorganism strain	Compound 2 [g/L/h]	Compound 3 [g/L/h]	Compound 4 [g/L/h]	Compound 2-4 [g/L/h]
AM32 (6 days)	0.69×10^{-4}	4.1×10^{-4}	9.7×10^{-4}	16.7×10^{-4}
AM32 (12 days)	0.0	0.3×10^{-4}	6.6×10^{-4}	6.9×10^{-4}
AM91	0.7×10^{-4}	2.4×10^{-4}	0.0	3.8×10^{-4}
AM235	5.2×10^{-4}	0.7×10^{-4}	0.0	6.5×10^{-4}
KKP3292	6.9×10^{-4}	0.3×10^{-4}	0.0	7.3×10^{-4}

Full microbial strains list used for the study:

1. Department of Food Chemistry and Biocatalysis collection at the Wrocław University of Environmental and Life Sciences:
 - *Fusarium culmorum* AM 7,
 - *F. culmorum* AM 9,
 - *Papularia rosea* AM 17,
 - *Acremoniella atra* AM 29,
 - *Penicillium dierckxii* AM 32,
 - *Poria placenta* AM 38,
 - *Sclerophoma pythiopila* AM 55,
 - *Piptoporus betulinus* AM 57,
 - *Penicillium* sp. AM 91,
 - *Spicaria fusispora* AM 136,
 - *Chaetomium indicum* AM 158,
 - *Mortierella isabellina* AM 212,
 - *Botrytis cinerea* AM 235,
 - *Fusicoccum amygdali* AM 258,
 - *Beauveria bassiana* AM 278,
 - *Armillaria mellea* AM 296,
 - *Absidia cylindrospora* AM 336,
 - *Aphanocladium album* AM 417,
 - *Verticillium* sp. AM 424,
 - *Mucor hiemalis* AM 450,
 - *Armillaria mellea* AM 461,
 - *Cunninghamella japonica* AM 472,
 - *Pleurotus ostreatus* AM 482,
 - *Marasmius scorodoni* AM 497,
 - *Laetiporus sulphurens* AM 498,
 - *Pholiota aurivella* AM 522,
 - *Laetiporus sulphurens* AM 524,
 - *Trametes versicolor* AM 536,
 - *Biscognausia marginiata* AM 562
2. Collection of Industrial Microbial Cultures at the Institute of Agricultural and Food Biotechnology:
 - *Aspergillus niger* KKP 45,
 - *A. niger* KKP 423,
 - *A. niger* KKP 424,
 - *A. flavus* KKP 686,
 - *A. flavus* KKP 689,
 - *Phanerochaete chrysosporium* KKP 784,
 - *Trichoderma lignorum* KKP 786,
 - *Botrytis* sp. KKP 3292

Article

Fungistatic Effect of Phthalide Lactones on *Rhodotorula mucilaginosa*

Joanna Gach ^{*}, Teresa Olejniczak ^{*}, Jakub Pannek  and Filip Boratyński 

Department of Food Chemistry and Biocatalysis, Wrocław University of Environmental and Life Sciences, Norwida 25, 50-375 Wrocław, Poland; jpannek@gmail.com (J.P.); filip.boratynski@upwr.edu.pl (F.B.)

^{*} Correspondence: joanna.gach@upwr.edu.pl (J.G.); teresa.olejniczak@upwr.edu.pl (T.O.)

Abstract: Currently, there is an increasing number of cases of fungal infections caused by opportunistic strains of the yeast *Rhodotorula mucilaginosa*, mainly in immunocompromised patients during hospitalization. The excessive use of antibiotics and azole compounds increases the risk of resistance to microorganisms. A new alternative to these drugs may be synthetic phthalide lactones with a structure identical to or similar to the natural ones found in celery plants, which show low toxicity and relatively high fungistatic activity. In the present study, the fungistatic activity of seven phthalide lactones was determined against *R. mucilaginosa* IHEM 18459. We showed that 3-*n*-butylidene-phthalide, the most potent compound selected in the microdilution test, caused a dose-dependent decrease in dry yeast biomass. Phthalide accumulated in yeast cells and contributed to an increase in reactive oxygen species content. The synergistic effect of fluconazole resulted in a reduction in the azole concentration required for yeast inhibition. We observed changes in the color of the yeast cultures; thus, we conducted experiments to prove that the carotenoid profile was altered. The addition of lactones also triggered a decline in fatty acid methyl esters.

Keywords: broth microdilution; biomass determination; synergistic effect; fatty acid methyl esters; carotenoids



Citation: Gach, J.; Olejniczak, T.; Pannek, J.; Boratyński, F. Fungistatic Effect of Phthalide Lactones on *Rhodotorula mucilaginosa*. *Molecules* **2023**, *28*, 5423. <https://doi.org/10.3390/molecules28145423>

Academic Editors: Robert Musiol and Carlos L. Cespedes Acuña

Received: 2 June 2023

Revised: 6 July 2023

Accepted: 12 July 2023

Published: 15 July 2023



Copyright: © 2023 by the authors. Licensee MDPI, Basel, Switzerland. This article is an open access article distributed under the terms and conditions of the Creative Commons Attribution (CC BY) license (<https://creativecommons.org/licenses/by/4.0/>).

1. Introduction

Rhodotorula mucilaginosa is a saprophytic eukaryote ubiquitous in the ecological environment. Numerous strains of *R. mucilaginosa* are being tested for their biotechnological importance in the production of carotenoids, lipids, enzymes, and other functional bio-products, using cheap agricultural waste [1,2]. *R. mucilaginosa* can be isolated from food, mainly cheese, dairy products, sausages, and fruit juices [3,4]. There is a growing concern that food may be an underestimated source of environmental pathogens [5]. Moreover, for many years, we have observed some pathogenic strains that cause local mycosis of the skin in critically ill patients and those taking immunosuppressive medications [6]. There is a slow but alarming increase in the number of bloodstream infections associated with the use of central venous catheters. *Rhodotorula* infections of the eyes, meninges, prosthetic joints, and peritoneum occur less frequently. Many have no documented relationship with central venous catheter use or immunosuppression. These infections occur mainly in patients receiving corticosteroids, cytotoxic drugs, and broad-spectrum antibiotics [7–10].

R. mucilaginosa infections are treated similarly to other pathogenic yeast infections with drugs from the azole group (fluconazole, itraconazole, and ketoconazole), 5-fluorocytosine, and amphotericin. Several studies reported on the resistance of microorganisms to commonly used antibiotics. The so-called multidrug-resistant microorganisms include some *Candida*, *Aspergillus*, and *Cryptococcus* strains resistant to azole drugs, and methicillin-resistant *Staphylococcus aureus* [11,12].

In addition to the search for new drugs, one of the methods to tackle the problem of resistance is to use the synergistic effect. This phenomenon has been studied in various

strains of *Candida*, including drug-resistant strains. In the case of *C. albicans*, a synergistic effect with fluconazole and 3-*n*-butylphthalide allowed for a 5–20-fold reduction in the doses [13–15]. The aforementioned 3-*n*-butylphthalide belongs to the group of phthalide lactones and is found in various celery plants: *Angelica archangelica* (angelica), *A. sinensis* (Chinese angelica), *Apium graveolens* (celery), *Cnidium officinale*, and *Levisticum officinale* (lovage) [16].

Phthalides have been studied for their antimicrobial properties against phytopathogens and species pathogenic to animals and humans [17]. For example, 3-*n*-butylidenephthalide is active against *Bacillus cereus*, *Escherichia coli*, *Listeria monocytogenes*, *Shigella flexneri*, *S. sonnei*, *Staphylococcus aureus*, *Vibrio harvei*, *V. parahaemolyticus*, and *V. vulnificus*. Some phthalides are active against *Mycobacterium bovis* and *M. tuberculosis*, which are the bacilli that cause tuberculosis in animals and humans, respectively [16–18].

Gong et al. showed that the fungistatic 3-*n*-butylphthalide inhibited genes responsible for the biosynthesis of CDR1 and CDR2 transport pumps in *Candida albicans* strains isolated from patients, contributing to the accumulation of both lactones and azole compounds inside the cell [13]. The presence of the phthalide in the cytosol led to increased production of reactive oxygen species (ROS) by the mitochondria as demonstrated by measuring the mitochondrial membrane potential ($\Delta\psi_m$). The accumulation of ROS resulted in the direct destruction of the mitochondrial cell membrane and the release of large amounts of ROS into the cytosol. The damaging effects of ROS include structural changes in DNA and RNA, peroxidation of membrane phospholipids (consisting of polyunsaturated fatty acids), and oxidation of proteins that perform numerous functions inside the cell. Figure 1 shows the mechanism of synergistic interactions between 3-*n*-butylphthalide and fluconazole. In our latest publication, we confirmed that this effect was shown not only by 3-*n*-butylphthalide but also by 3-*n*-butylidenephthalide and 3-*n*-butyl-4,5,6,7-tetrahydrophthalide [15].

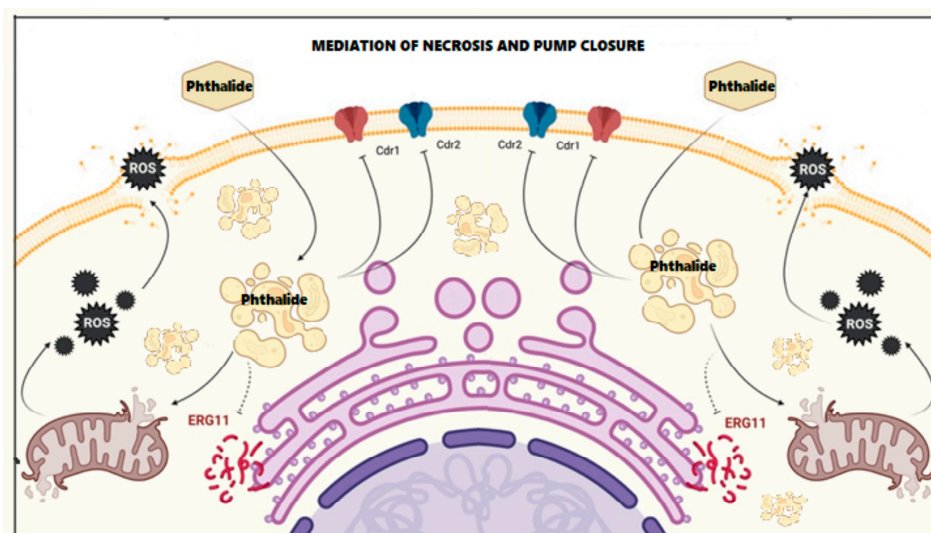


Figure 1. Mechanism of action of 3-*n*-butylphthalide on *C. albicans* (figure created in BioRender <https://www.biorender.com/>, accessed on 14 February 2023).

To the best of our knowledge, no studies have described the effect of phthalide lactones on *Rhodotorula* strains. The main goal of our work was to deepen our knowledge of the action of this synthetic phthalide lactone with structures identical to or similar to natural compounds on yeast cells. In this study, we selected a strain of *R. mucilaginosa* that can colonize food products and constitutes a potential opportunistic strain. We were interested in the fact that the cultures of this microorganism lost their characteristic orange-red color in the presence of phthalide. We tested seven lactones against this strain. Owing to their low toxicity and, for most of them, natural occurrence, they can be used as yeast growth-

inhibitory agents. We analyzed the effect of 3-*n*-butylidenephthalide on synergism with fluconazole, ROS content, carotenoids, fatty acid composition, and ergosterol production.

2. Results and Discussion

In the first stage of this study, we synthesized and determined the fungistatic activities of seven lactones against *R. mucilaginosa* IHEM 18459. However, the main goal of this study was to explain the fungistatic effect of phthalide lactones. Figure 2 shows a diagram of the experiments conducted in this study.

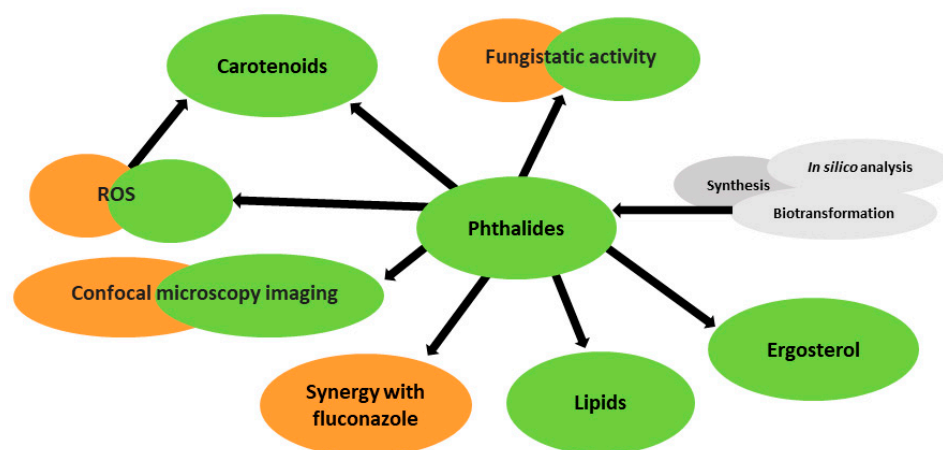


Figure 2. Schematic of the experiments.

In the next part of the study, we referred to the work of Gong et al. [13] and Krężel et al. [15] describing the effect of phthalide lactone on fluconazole-resistant *C. albicans* cells and compared it with the effect on *R. mucilaginosa* IHEM 18459 cells (Figure 2, orange).

Finally, we determined how 3-*n*-butylidenephthalide (1) affects the quantity and quality of carotenoids, fatty acid methyl ester (FAME), and ergosterol. We also visualized the cells using confocal microscopy (Figure 2, green). Other experiments, such as synthesis, biotransformations, and in silico analysis, unrelated to the elucidation of the fungistatic effect of phthalide lactones, are highlighted in gray (Figure 2, gray).

2.1. Synthesis of Phthalide Lactones

The following compounds were used to test fungistatic activity: 3-*n*-butylidenephthalide (1), 3-*n*-butylphthalide (2), 3-*n*-propylidenephthalide (3), 3-*n*-propylphthalide (4), 3-*n*-butyl-4,5,6,7-tetrahydrophthalide (5), 3-*n*-butyl-hexahydrophthalide (6), and 3-*n*-butyl-3a,4,7,7a-tetrahydrophthalide (7) (Figure 3). Lactones, except lactone 3, which was purchased, were obtained in two-stage syntheses with a yield of 40–60%, in which the intermediate product 3-butyl-3-hydroxylactone or 3-propyl-3-hydroxylactone formed from dialkylcadmium and the appropriate anhydride was subjected to reduction with NaBH₄ or dehydration with *p*-toluenesulfonic acid (Figure 4) [16]. The structures of the compounds were confirmed using ¹H NMR, ¹³C NMR, and HR-ESI-MS/MS analyses performed using an ESI-Q-TOF mass spectrometer.

2.2. Fungistatic Activity against *R. mucilaginosa* IHEM 18459 and Correlation with Structure and In Silico Data

IC₅₀ values for phthalide lactones 1–7 and fluconazole (8) against *R. mucilaginosa* IHEM 18459 were determined using the broth microdilution method (Table 1). As *Rhodotorula* spp. may grow in a broad range of temperatures from 5 to 35 °C, and the optimal value is species-dependent [19], microdilution tests were conducted in temperatures of both 25 °C and 30 °C.

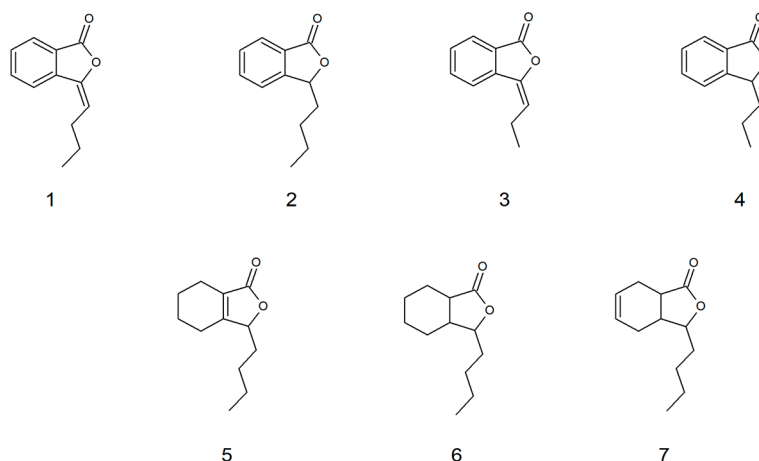


Figure 3. Structures of lactones 1–7 used to test fungistatic activity.

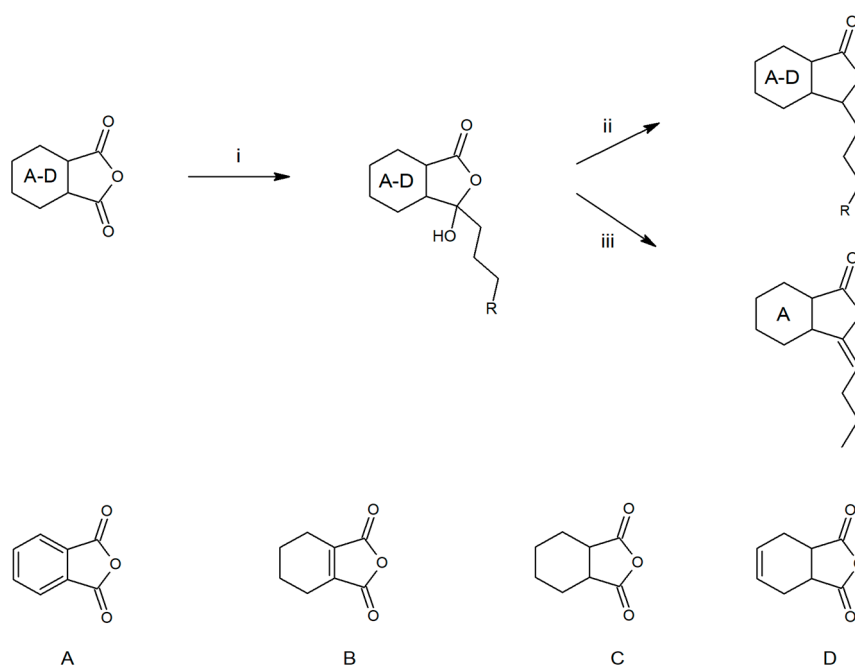


Figure 4. Synthetic route for the obtainment of phthalide lactones. R = H or Me; i-Et₂O, Mg, *n*-C₄H₉Br or C₃H₇Br, CdCl₂; ii-THF, NaBH₄; iii-toluene, TsOH.

Table 1. Fungistatic activity (IC₅₀) using microdilution method, *in silico* prediction of lipophilicity (Log P), solubility (log S), and oral toxicity to rat cells (LC₅₀). Prediction of CYP isoenzymes inhibition: CYP1A2, CYP2C19, CYP2C9, CYP2D6, and CYP3A4, based on chemical structures of compounds 1–8.

Compound	IC ₅₀ at 25 °C [μg/mL]	IC ₅₀ at 30 °C [μg/mL]	Log P	Log S	LC ₅₀ [mg/kg]	Inhibition of:
1	13	13	2.93	−3.30	1865	CYP1A2
2	20	23	2.81	−3.01	4872	CYP1A2 CYP2C9
3	38	32	2.78	−2.43	1895	CYP1A2
4	130	109	2.44	−2.45	4061	CYP1A2
5	65	66	2.93	−3.20	5184	-
6	42	43	2.96	−3.79	4702	CYP2C9
7	54	57	2.93	−3.20	4186	CYP2C9
8	199	207	0.88	−1.63	584	CYP2C19

Six of the seven lactones inhibited the mycelial growth of *R. mucilaginosa* IHEM 18459 at concentrations ranging from 13 to 66 µg/mL. In contrast, fluconazole (**8**), most commonly used for yeast infections, reduced mycelial growth at a concentration of 199–207 µg/mL.

Data on absorption, distribution, metabolism, and excretion (ADME) parameters are crucial for drug development [20]. Therefore, *in silico* ADME analysis was included in the study (Table 1). Among these parameters, lipophilicity, solubility, toxicity to rat cells, and inhibition of isoenzymes of P450 cytochrome, which are responsible for the biotransformation and detoxification of drugs, are frequently tested [20–23].

In addition to the analysis of the differences in the structure of compounds, we analyzed the influence of structure on biological activity. Lactones **1–4** are flat aromatic compounds, and cis lactones **5–7** with a cyclohexane or cyclohexene ring form conformations intermediate between the chair and boat forms, depending on the environment. With such minor differences in biological activity, it should be noted that lactones **1** and **3**, with an aromatic ring and a double bond at the three-carbon atom, were the most active and three times less toxic than fluconazole (**8**). In contrast, lactones **2** and **4–7** were seven to nine times less toxic than fluconazole (**8**). Considering the experimental data, the studies on the toxicity of 3-*n*-butylphthalide (**2**) were conducted by Xue et al., 2011—the IC₅₀ values for both primary rat and human hepatocytes were described as above 500 µM, which was the highest concentration tested. This phthalide has been accepted as the treatment of the brain ischemia after clinical studies [24,25].

Aromatic lactones **1–4** inhibited the enzyme CYP1A2, which means that they might prolong the metabolism of some classes of drugs, including analgesic, antipsychotic, anti-Parkinson, anti-Alzheimer, and anticancer drugs. In contrast, CYP1A2 inhibitors prevent the bioactivation of procarcinogens [26]. Lactones **2**, **6**, and **7** reduced the activity of CYP2C9 and therefore may influence the metabolism of proton pump inhibitors, antiepileptic agents, and antiplatelet agents [27]. In contrast to fluconazole (**8**), the lactones did not reduce CYP2C19 activity. CYP2D6 and CYP3A4 were not inhibited by any of the compounds tested.

The lowest fungistatic activity was observed for 3-*n*-propylphthalide (**4**). This compound has a low lipophilicity (LogP = 2.44) compared to the rest of the lactones (log P = 2.78–2.96), which is less soluble in fat than other lactones. All lactones **1–7** are poorly soluble in water, although lactones **3–4** with a three-carbon side chain differ slightly in this matter.

2.3. Determination of Fungistatic Activity for 3-*n*-Butylidenephthalide (**1**) against *R. mucilaginosa* IHEM 18459 *In Vitro* and in Food Matrices

The IC₅₀ values of compounds **1–7** against *R. mucilaginosa* IHEM 18459 were determined using the broth microdilution method. The main advantages of this method include the low amount of compounds required for testing and the low cost; nevertheless, some drawbacks related to inoculum viability and solvent-inhibiting properties occur [28]. Moreover, it has been stated that the incubation temperature, inoculum size, and culture medium may influence the inhibitory concentrations using the microdilution method [29,30].

In connection with the discussion on the advantages and limitations of the broth microdilution method for the most active compound, 3-*n*-butylidenephthalide (**1**), we determined the fungistatic activity based on the weight of the mycelia cultured in various lactone **1** concentrations. Moreover, we discussed the contribution of phthalide **1** to the inhibition of *R. mucilaginosa* using the plate count method and determined yeast growth in dairy food matrices.

2.3.1. Determination of Dry Yeast Biomass

To evaluate the effect of the addition of different concentrations of 3-*n*-butylidenephthalide (**1**) on the dry yeast biomass, we performed two experiments in 0.3 and 2 L flasks with 50 mL and 500 mL Sabouraud medium with inoculum 0.5% vol. and 10% vol., respectively.

The total dry biomass of the control samples were 0.238 and 3.254 g, respectively (Figure 5). In both experiments, a marked decrease in yeast biomass by almost half of the control value was noted for the lowest concentration of 3-*n*-butylidenephthalide (1)—25 µg/mL. The use of higher concentrations resulted in subsequent but smaller decreases in dry matter values. Fluconazole (8) at a concentration of 50 µg/mL caused only a slight inhibition compared with the control—the amount of reduction of dry biomass was 0.031 and 0.025 g, depending on the inoculum volume (0.5% and 10% volume of the medium, correspondingly).

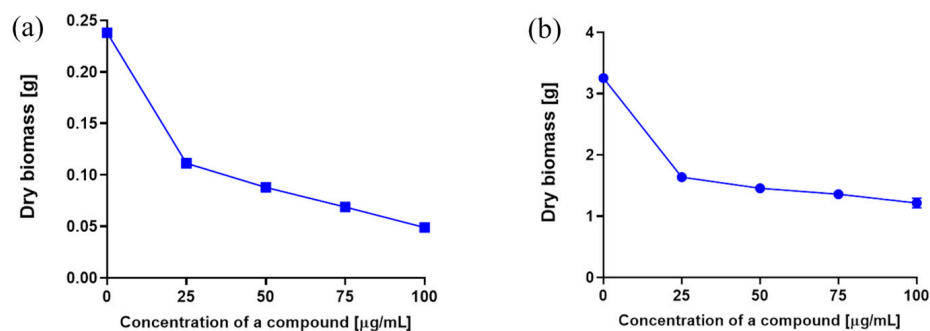


Figure 5. Biomass weight depending on the concentration of compound 1 used, cultivation of *R. mucilaginosa* using different inoculum (% volume medium): (a) 0.5% and (b) 10%.

2.3.2. Plate Count Method In Vitro and in Food Matrices

The total number of yeasts (CFU/mL) depending on the concentration of compound 1 used for the two assays is shown in Figure 6.

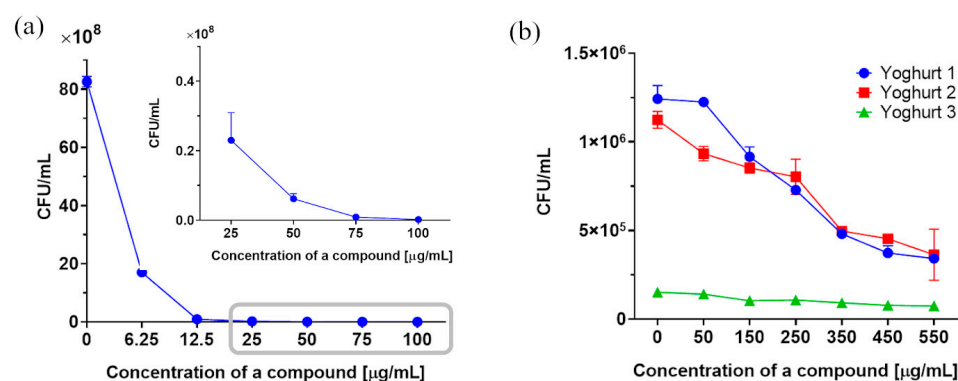


Figure 6. Total yeast cell counts (CFU/mL) depending on the concentration of compound 1 using plate count method (a) in vitro and (b) in three types of yogurts. The corresponding data represent the mean ± standard deviation.

The number of colonies in the control sample was 8.26×10^9 CFU/mL. We showed that 3-*n*-butylidenephthalide (1) caused a notable reduction in this value at the lowest tested concentration of 6.25 µg/mL to the amount of 1.70×10^9 CFU/mL, which means that the 50% inhibition of CFU/mL is below this dose. Fluconazole (8), tested at a dose of 50 µg/mL, reduced the number of colonies up to 5.87×10^9 CFU/mL, i.e., by 20% (Figure 6a).

The antimicrobial activity of 3-*n*-butylidenephthalide (1) against *R. mucilaginosa* IHM 18459 was evaluated in food matrices (Figure 6b). Following the promising results of 3-*n*-butylidenephthalide (1) in vitro tests, we decided to evaluate the functional antifungal properties of three commercially available yogurt types (1 and 2 are thick yogurts and 3 is a drinking yogurt). Because dairy-derived *Lactobacillus* spp. can affect yeast growth, the results were compared with those of the control [31]. No inhibition was observed using

compound **1** at concentrations below 50 µg/mL in preliminary tests. Therefore, phthalide was tested at higher concentrations of 50–550 µg/mL.

The food matrices allowed *Rhodotorula* to grow from 1.12×10^6 CFU/mL for thick yogurt 2 to 1.51×10^5 CFU/mL for drinking yogurt 3. Lactone **1** at concentrations above 50 µg/mL caused a considerable decrease in yeast colonies compared with the control. Inhibition of CFU/mL by half occurred at a concentration of 220–250 µg/mL (1.2–1.3 mM) for thick yogurt. Lactone may serve as a promising alternative to sodium chloride, potassium sorbate, sodium acetate, sodium benzoate, and other preservatives used in dairy products [32].

The differences in activity between the in vitro assay and the assay that mimics the target conditions may be due to the uneven distribution of the antifungal agent in the food matrix. This corresponds to the relatively high lipophilicity of 3-*n*-butylidenephthalide (**1**) associated with its poor solubility in water [33]. Blanco-Padilla pointed out that a potential problem with natural antimicrobials could also be their stability and drew attention to nanocarriers to improve cell delivery [34]. However, the amount of 3-*n*-butylidenephthalide (**1**) used is still low, and considering its low toxicity, it can be recommended for use.

2.4. Microbial Transformation 3-*n*-Butylidenephthalide (**1**) by *R. mucilaginosa*

We examined whether the yeast *R. mucilaginosa* IHEM 18459 transformed 3-*n*-butylidenephthalide (**1**). Biotransformations were carried out for eight days. The cultures to which lactone **1** was added were centrifuged and separated from the mycelium and supernatant using ethyl acetate. We found that 90% of the lactone was accumulated in the yeast mycelium. A slight loss of substrate over time was observed. The above results indirectly indicate that 3-*n*-butylidenephthalide (**1**) with log P 2.93 and log S −3.3, which is highly soluble in lipids, was accumulated in the cytosol.

2.5. The Influence of the 3-*n*-Butylidenephthalide (**1**) on ROS Level

Physiological ROS are necessary for proper cell functioning, including signaling pathways [35]. However, according to the research conducted by Gong et al., 3-*n*-butylphthalide (**2**) antifungal activity is likely associated with intracellular ROS overproduction, which leads to mitochondrial dysfunction [13]. The damaging effects of ROS inside cells and mitochondria include structural changes in DNA and RNA, peroxidation of membrane phospholipids (consisting of polyunsaturated fatty acids), and oxidation of cellular proteins that perform numerous functions inside the cell [36]. ROS values result from the xenobiotic effect and the well-known antioxidative properties exhibited by carotenoids, including α- and β-carotene and lycopene [37]. It has been stated that supplementation with some antioxidants, e.g., ascorbic acid, may reduce fluconazole-induced inhibition [38]. The 4 h treatment of *R. mucilaginosa* IHEM 18459 cells with 3-*n*-butylidenephthalide (**1**) or fluconazole (**8**) increased the level of intracellular ROS up to 53% compared with the control at a concentration of 75 µg/mL (Figure 7). Fluconazole (**8**) at 50 µg/mL also caused elevated levels of oxidative stress. An increase in ROS under the influence of fluconazole was observed in experiments using *Candida tropicalis*, *C. albicans*, and *Cryptococcus neoformans* [39].

We evaluated whether the effect of 3-*n*-butylidenephthalide (**1**) on yeast cells can be visualized using confocal microscopy with Calcofluor White staining. This dye was used previously by Dagher et al. [40] and Suchodolski et al. [41] for staining yeast cell walls as it binds with chitin. However, we did not observe a change in the fluorescence intensity between the control and tested samples (Figure 8).

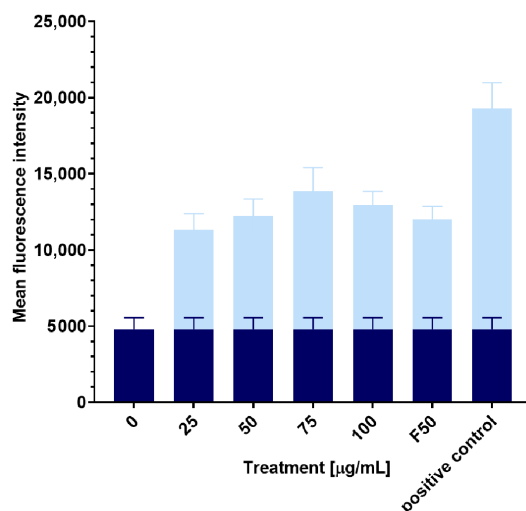


Figure 7. Reactive oxygen species (ROS) levels with different concentrations of added compounds. Control levels of ROS are marked by the dark blue color. F means fluconazole. Data represent the mean \pm standard deviation.

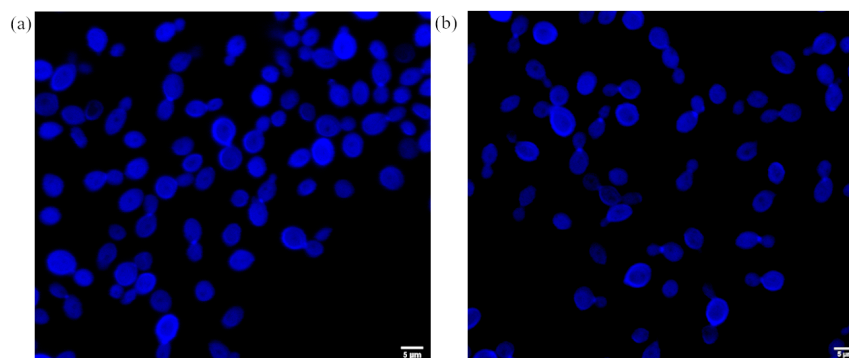


Figure 8. Calcofluor staining of the *R. mucilaginosa* cells: (a) the control, and (b) sample with the addition of 100 µg/mL 3-*n*-butylidene-phthalide (1).

2.6. Synergistic Effect of 3-*n*-Butylidene-phthalide (1) and Fluconazole (8)

The checkerboard protocol previously described in the literature was used to determine the effects of 3-*n*-butylidene-phthalide (1) and fluconazole (8) in combination [15,42].

Fractional inhibitory concentration values less than 0.5 indicated that phthalide 1 and fluconazole (8) showed a synergistic effect. The compounds inhibited the growth of *R. mucilaginosa* IHEM 18459 by 90% when tested in combination at lower concentrations, e.g., 4 µg/mL of lactone 1 and 32 µg/mL of fluconazole (8), instead of doses of 32 µg/mL and 256 µg/mL for the compounds administered separately (Figure 9). This action greatly reduces drugs from the azole group, causing drug resistance [13,15].

2.7. The Influence of the 3-*n*-Butylidene-phthalide (1) on the Production of Carotenoids

R. mucilaginosa is known to produce carotenoids [43]. As we observed changes in the color of the cultures depending on the compound 1 concentration used, we investigated the β -carotene content and overall carotenoid composition in those samples. The connection between carotenoid profiles and factors triggering oxidative stress has been reported in the literature [44].

Kot et al. noted that the pigments are deposited in lipid bodies; therefore, an appropriate cell disruption method is required before extraction [45]. Indeed, direct extraction of biomass using dimethyl sulfoxide with incubation at 50 °C and subsequent extraction using acetone was not sufficient, as some pigments remained in the cells. Therefore, we implemented ultrasonic disintegration of yeast cells, followed by centrifugation and vortexing

The differences in particular pigments between the samples were visualized using quantitative comparative analysis (Table 2). The relative quantity of the compounds was defined as 1 for the control sample, and the remaining samples were multiples of this number within each row.

Table 2. *R. mucilaginosa* IHEM 18459 pigments detected using APCI-LC-HR-MS and their relative composition depending on the different concentrations of the 3-*n*-butylidenephthalide (**1**) and fluconazole (**8**) [$\mu\text{g}/\text{mL}$].

Carotenoid	APCI-LC-HR-MS [M + H] ⁺	0	25	50	75	100	F50
Phytoene	545.5081	1	50.92	70.61	95.83	35.33	3.52
Neurosporene	539.4611	n.d.	n.d.	n.d.	d.	n.d.	n.d.
β -carotene + lycopene	537.4445	1	4.45 ^a	1.10 ^a	1.72 ^a	0.20	2.30 ^a
Torulene	535.4280	1	0.88	0.21	0.35	0.07	1.66
Torularhodin	565.4063	1	0.41	0.01	0.05	n.d.	1.63

F means fluconazole; ^a the identification of these pigments was confirmed by the compounds' standards using HPLC-DAD; n.d.—not detected; and d.—detected.

Our results confirmed a change in pigment formation in cultures supplemented with 3-*n*-butylidenephthalide (**1**). Similarly, Moç et al. showed that antifungal naftifine caused dose-dependent depigmentation of cells. A possible mechanism of action involves compound-induced ROS formation, triggering the carotenoid defense response [47]. Another known inhibitor of carotenogenesis is diphenylamine, which inhibits the desaturation processes affecting phytoene synthase, leading to the accumulation of phytoene [46]. Additionally, the content of the carotenoid precursor in samples with the addition of 3-*n*-butylidenephthalide (**1**) increased up to 96 times when the inhibitor was tested at a concentration of 75 $\mu\text{g}/\text{mL}$. This result may indicate the same mechanism of action as for diphenylamine. The next carotenoid in the pathway, neurosporene, was detected in only one sample, in which the highest content of its precursor was also detected. The production of β -carotene and lycopene was over fourfold increased when a lower concentration of compound **1** was applied; however, it decreased along with the addition of a higher concentration of the inhibitor, leading to even five times less β -carotene production than the control sample. Torulene and torularhodin were formed in reduced quantities at all the 3-*n*-butylidenephthalide (**1**) concentrations tested. At 100 $\mu\text{g}/\text{mL}$, only trace amounts of torulene were noted, whereas torularhodin was not detected.

According to the literature, ketoconazole at doses of 20–50 mg/L significantly increased the content of pigments, interpreted as overexpression of the HMG1 gene increasing the activity of HMG-CoA reductase, which results in enhancement of the pigment precursor [48]. We observed that the addition of fluconazole (**8**) also led to increased amounts of colored β -carotene and lycopene, torulene, and torularhodin by up to 2.30, 1.60, and 1.63 times, respectively, as compared with the control. Fluconazole (**8**) did not induce phytoene accumulation to the same extent as phthalide **1**, causing only a threefold increase.

By analyzing the data on β -carotene content in the samples determined using HPLC-DAD, it can be concluded that, similar to the previous experiment, the smallest dose of 3-*n*-butylidenephthalide (**1**) caused an increase in β -carotene content in comparison with the control (Table 3). In addition, fluconazole (**8**) greatly increased pigment production. This enhancement of β -carotene production using a medium containing compound **8** is consistent with the findings of Li et al. [49]. Interestingly, the application of phthalide **1** at a higher concentration of 75 $\mu\text{g}/\text{mL}$ caused a twofold decline, whereas, at a dose of 100 $\mu\text{g}/\text{mL}$, carotenoids were not detected using the HPLC-DAD method.

Table 3. β -Carotene content in the *R. mucilaginosa* IHEM 18459 biomass depending on the different concentrations of the 3-*n*-butylidenephthalide (1) and fluconazole (8); data represent the mean \pm standard deviation.

Concentration of Compounds [$\mu\text{g/mL}$]	β -Carotene Content [mg/g d.m.]
0	0.2108 ± 0.0055
25	0.4433 ± 0.0282
50	0.2305 ± 0.0108
75	0.0262 ± 0.0042
100	n.d.
F50	0.4792 ± 0.0055

F means fluconazole.

2.8. The Influence of the 3-*n*-Butylidenephthalide (1) on the Production of FAME

Lipid biosynthesis occurs in the cytoplasm of yeast cells through enzyme-derived sequences that form biosynthetic substrates of saccharides, glycerol, or acetyl-CoA to long-chain fatty acids. This process is closely related to glycolysis and the Krebs cycle [50,51].

R. mucilaginosa and other members of this genus are considered oleaginous yeasts [52]. Lipids, with special emphasis on sterols, amphipathic phospholipids, and fatty acids (FAs) as their components, are essential for membrane creation [53]. *Rhodotorula* strains store up to 40% of lipids in dry matter, of which triglycerides constitute 65–90% of their content [2].

The efficiency and effectiveness of lipid biosynthesis in *R. mucilaginosa* are determined by several factors. First, a high molar C/N ratio in the culture medium is a key factor in the development of lipid-accumulating yeasts. *R. mucilaginosa* LP-2 has been observed to produce 46.7% lipid levels at a C/N ratio of 65 and 35.7% at a ratio of 25 [54]. In this study, we used a C/N ratio of 23, which was constant in all experiments. In addition, carbon sources play an important role [55]. The third important parameter influencing the fatty acid profile was the yeast incubation temperature. In Adel et al. [56], a study conducted at three temperatures of 7 °C, 15 °C, and 26 °C, it was shown that the most unsaturated acids 63.4% are obtained at 15 °C, compared with 57.4% at 7 °C and 43.5% at 26 °C. All our experiments regarding FAME analyses were carried out at the temperature of 25 °C.

The key parameter that affects lipid biosynthesis is pH. Karatay and Donmez [57] conducted various experiments at pH values ranging from 4 to 7. The maximum content of lipids in *Rhodotorula* biomass was obtained at pH = 5, equaling 69.5%, while the pH 4, 6, and 7 resulted in the obtainment of 50.8%, 51.7%, and 64.5%, respectively. In this study, the pH of the control sample was 4.75 and changed with increasing concentrations of 3-*n*-butylidenephthalide (1) up to 25 $\mu\text{g/mL}$. In the concentration range of 25–100 $\mu\text{g/mL}$, the pH remained relatively stable near the value of 5.5 ± 0.1 (Figure 11a).

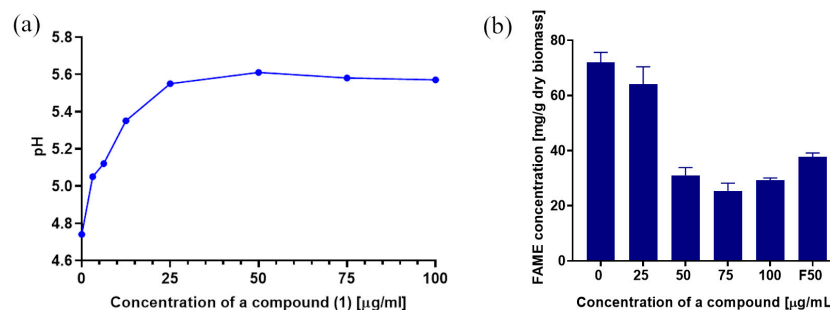


Figure 11. (a) The change in pH values of *R. mucilaginosa* cultures with different concentrations of 3-*n*-butylidenephthalide (1), and (b) FAME content depending on different doses of the compounds (F means fluconazole). The data are shown as the mean \pm standard deviation.

Another crucial factor is the increase in ROS inside the cell and mitochondria under the influence of 3-*n*-butylidenephthalide (1). ROS are responsible for lipid peroxidation, chang-

ing the quantitative and qualitative composition and contributing to the disintegration of cell membranes [36].

The addition of azoles may cause a shift in the desaturation and elongation of FAs, impacting membrane function and growth [58]. To determine the concentration and change in the FA profile between the tested samples, the dry biomass of *R. mucilaginosa* was subjected to alkaline hydrolysis and methylation to obtain FAMES. The use of glucose-rich Sabouraud medium resulted in a total FAME yield of 75.65 mg/g dry biomass in the control sample (Figure 11b). Khot [52] reported maximum FAMES content in *R. mucilaginosa* IIPL32 at 97.23 mg/g dry biomass; however, it has been stated that lipid composition varies depending on aeration, medium composition, and incubation time [59]. During the experiment, no considerable difference was noted for 3-*n*-butylidenephthalide (1) dosed at 25 µg/mL in the medium as compared with the control. Nevertheless, there was a decline in FAME content by nearly 57% with compound 1 addition in the concentration of 50 µg/mL. The reference antimycotic fluconazole (8) at this dose caused a smaller decrease. The concentrations of 75 and 100 µg/mL of 3-*n*-butylidenephthalide (1) caused a similar effect in FAME reduction, up to 66% in relation to the control (Figure 11b).

The vast majority (79.49%) of the control sample consisted of monounsaturated fatty acid esters, while the polyunsaturated accounted only for 1.49%. The predominant FAME detected included oleic acid (*cis* C18:1) ester with a concentration of 77.15; next, in descending order of proportion, were palmitic (C16:0), lignocerate (C24:0), stearic (C18:0), and linoleic (C18:2 *n*-6) methyl esters (Figure 12).

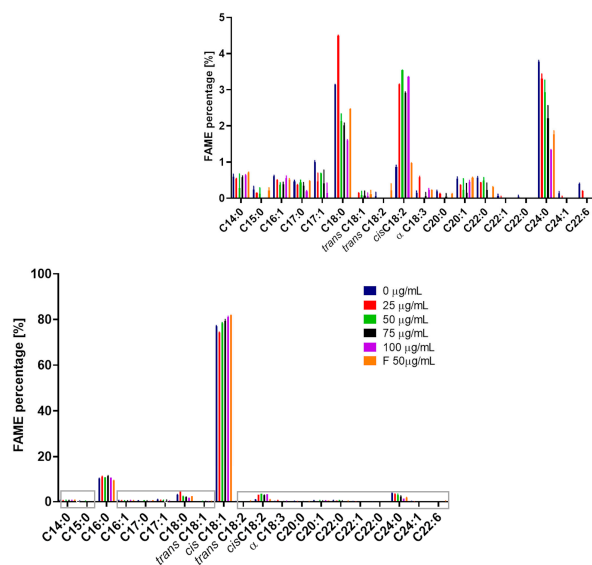


Figure 12. FAME percentage depending on the addition of compounds to the culture (F means fluconazole).

Other detected FAMES did not exceed 1% separately. Among these, only negligible amounts of the odd-chain fatty acids C15:0, C17:0, and C17:1 were formed. Their microbial production is very limited; nevertheless, attempts to increase their yield have been made through propionate addition or genetic engineering [60].

Similarly, Ayadi et al. [61] noted that *cis* C18:1 and C16:0 were dominant in *R. mucilaginosa* Y-MG1 biomass with 58.30% and 15.20%, respectively, of overall FAMES content, using a synthetic medium with glucose as the carbon source. Other FAMES previously reported in the literature in various *R. mucilaginosa* strains included palmitoleic (C16:1), linoleic (C18:2), and other C10-18 esters present in a minority [52,59,61].

As the distribution of saturated and unsaturated lipids is crucial for membrane fluidity, we examined the proportions of these components [62]. Considering the impact of the dose of the compounds on the profile of FAMES, the control sample contained 19.02% of saturated FAs, but the highest percentage of saturated fatty acids (20.31%) was recorded

for the addition of compound **1** at a concentration of 25 $\mu\text{g}/\text{mL}$. The proportion further decreased with increasing levels of 3-*n*-butylidenephthalide (**1**), except 75 $\mu\text{g}/\text{mL}$, which showed no considerable difference compared with 50 $\mu\text{g}/\text{mL}$. A reduction in the saturated FAs content was noted at a dose of 100 $\mu\text{g}/\text{mL}$, resulting in a content of 14.12%. The addition of fluconazole (**8**) also notably declined their share to 15.27%. As unsaturation increased, the proportion of polyunsaturated FAs increased when using compound **1** compared with the control, although there was no straightforward dose dependency. Fluconazole (**8**) did not cause notable shifts in the polyunsaturated FAs content between the control and tested groups (Table 4).

Table 4. The impact of the dose of the compounds on the profile of all detected FAMES; the data are shown as the mean \pm standard deviation.

Concentration of a Compound [$\mu\text{g}/\text{mL}$]	Saturated [%]	Unsaturated [%]	Unsaturated Including:	
			Monounsaturated (MUFA) [%]	Polyunsaturated (PUFA) [%]
0	19.02 \pm 0.08	80.98 \pm 0.08	98.16 \pm 0.14	1.84 \pm 0.14
25	20.31 \pm 0.05	79.69 \pm 0.05	95.06 \pm 0.02	4.94 \pm 0.02
50	16.77 \pm 0.01	83.23 \pm 0.01	95.74 \pm 0.02	4.26 \pm 0.02
75	16.54 \pm 0.04	83.46 \pm 0.04	96.43 \pm 0.09	3.57 \pm 0.09
100	14.12 \pm 0.18	85.88 \pm 0.18	95.82 \pm 0.05	4.18 \pm 0.05
F50	15.27 \pm 0.14	84.73 \pm 0.14	98.00 \pm 0.12	2.00 \pm 0.12

F means fluconazole.

The rising proportion of unsaturated FAs suggests an increase in membrane fluidity, as phospholipids with these FAs have relatively lower melting points [63]. An explanation for the increased share of unsaturated FAs with increasing concentration of added compound **1** may be the influence on the expression of genes encoding fatty acid desaturases. These enzymes catalyze the formation of unsaturated acids from their saturated analogues, and their expression in the OLE pathway may be affected by nutrient and environmental factors [64]. For instance, Δ^9 -fatty acid desaturase is responsible for the formation of palmitoleic acid (C16:1) and oleic acid (*cis* C18:1) [65]. The increase in the percentage of *cis* C18:1 acid with the simultaneous decline of saturated analogue C18:0 (Figure 12) suggests the involvement of 3-*n*-butylidenephthalide (**1**) in the OLE pathway.

2.9. The Influence of the 3-*n*-Butylidenephthalide (**1**) on the Ergosterol Content

The main antifungal mechanism of action of azoles includes blocking the sterol pathway by lowering lanosterol 14 α -demethylase activity (Erg11p). Consequently, another toxic sterol is created by other enzymes in this pathway, which leads to the inhibition of cell growth or death [66,67].

However, 3-*n*-butylidenephthalide (**1**) did not notably change ergosterol content (Figure 13). This indicates that the observed fungistatic activity of lactones **1**–**7** is not related to the disintegration of the cell membrane associated with the lack of ergosterol.

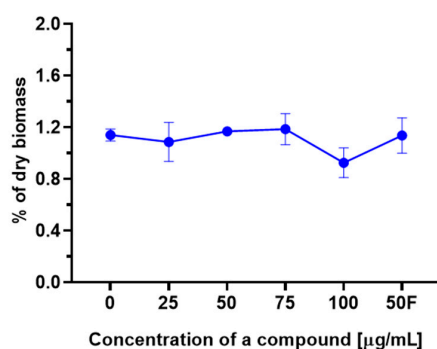


Figure 13. Ergosterol content [% of dry biomass] depending on the concentration of the added compound. The data are shown as the mean \pm standard deviation.

3. Materials and Methods

3.1. General

Solvents used in this study were purchased from Merck (Darmstadt, Germany). 3-*n*-Propylidene-phthalide (**3**) was purchased from Sigma-Aldrich (St. Louis, MO, USA). Fluconazole (**8**) was purchased from TCI (Tokyo, Japan). Supelco 37 Component FAME Mix, β -carotene (European Pharmacopoeia (EP) Reference Standard), Calcofluor White, 2',7'-dichlorofluorescein diacetate (H₂DCFDA), phosphate-buffered saline (PBS) pH 7.2, and boron trifluoride in diethyl ether (48%) were purchased from Merck (Darmstadt, Germany). Preparative column chromatography of the lactones after synthesis was performed using Silica Gel (Kieselgel 60, 230–400 mesh, 40–63 μ m, Merck).

The following microbiological media were used: RPMI 1640 medium buffered with 3-(*N*-morpholino)propanesulfonic acid (MOPS): 10.4 g RPMI 1640 with L-glutamine, without sodium bicarbonate (Sigma-Aldrich, St. Louis, MO, USA), 34.53 g MOPS (Pol-Aura, Dywity, Poland), 1 L distilled water; pH adjusted to 7.0, medium was sterile-filtered; Sabouraud medium: 30 g glucose (Chempur, Piekary Śląskie, Poland), 10 g peptone and 2 g bacteriological LAB-AGAR™ (Biomaxima, Lublin, Poland), and 1 L of distilled water; pH was adjusted to 5.6.

The strain used for the study was *R. mucilaginosa* IHEM 18459 derived from Belgian Coordinated Collections of Microorganisms (BCCM).

Centrifugation of samples was carried out using an Eppendorf centrifuge 5810 R (Hamburg, Germany). The yeast biomass was lyophilized using a LYO SRK GT2 Basic (Riedstadt, Germany). Incubation of microtiter plates for the broth microdilution test took place in a Biosan PST-60 HL ThermoShaker (Riga, Latvia), while their analysis was performed using a BioTek TS-800 microplate reader (Riga, Latvia). Carotenoids were extracted from the biomass using a Vortex Mixer (VELP SCIENTIFICA, Usmate Velate, Italy). Fluorometric measure for the ROS determination was taken using a Synergy H1 microplate reader (BioTek Instruments, Winooski, VT, USA).

Gas chromatography analyses (GC, FID, carrier gas H₂) were performed on an Agilent Technologies 8860 (GC System, Santa Clara, CA, USA). For the FAME determination, column Zebron ZB-FAME, 60 m \times 0.25 mm \times 0.2 μ m (Phenomenex, Torrance, CA, USA), while for tests of the purity of compounds **1–7**, HP-5 column, 30 m \times 0.32 mm \times 0.25 μ m (Agilent, Santa Clara, CA, USA) were used.

β -carotene content and microbial transformations of 3-*n*-butylidene-phthalide (**1**) were analyzed using a Dionex UltiMate 3000 instrument with a diode array detector (Thermo Fisher Scientific, Waltham, MA, USA) with column Agilent Zorbax Bonus-RP 3.5 μ m 150 \times 3 mm.

HR-APCI-MS/MS analyses of the carotenoids were performed with RSLC UltiMate 3000 (Dionex, Sunnyvale, CA, USA) coupled with mass spectrometer APCI-Q-TOF, maXis impact (Bruker, Billerica, MA, USA). Luna Omega 1.6 μ m C18, 50 mm \times 2.1 (Phenomenex, Torrance, CA, USA) was the column used for the pigments determination and quantitative comparative analysis.

The staining of the yeast cells was performed in Millicell® EZ SLIDE (Merck, Darmstadt, Germany), assembled with the microscope Epredia X1000 Coverslip 24 \times 50 mm #1.5 (0.16–0.19 mm) slides (Epredia, Kalamazoo, MI, USA). The confocal microscopy imaging was performed using a STEDyCON superconfocal microscope (Abberior Instruments, Göttingen, Germany) installed on a Nikon Ti2E microscope body with a 100 \times objective lens (Nikon, Tokyo, Japan).

A Cintra 101 spectrophotometer (GBC Scientific, Braeside, Australia) was used to analyze the ergosterol content of the samples.

¹H NMR and ¹³C NMR spectra were recorded in CDCl₃ on a Bruker Avance 500 (500 MHz, Billerica, MA, USA) spectrometer.

3.2. Synthesis of Phthalide Lactones

Compounds **1–2** and **4–7** were synthesized using the method described below:

Step 1: We used the method we described in a previous article [68]. Briefly, synthesis was carried out in a multinecked flask equipped with a dropping funnel, magnetic stirrer core, and reflux condenser. Diethyl ether or THF, freshly distilled from LiAlH_4 , was used as the solvent. Magnesium chips (0.05 M) were activated by heating with a few iodine crystals, and 0.055 mM of the appropriate alkyl bromide was added dropwise. Anhydrous cadmium chloride (0.025 M) was added to the obtained Grignard compound, and the mixture was heated for 1 h. After cooling, 0.05 M of an appropriate anhydride was added dropwise. The reaction mixture was heated for 6 h. A 10% HCl solution was added to the cooled reaction mixture for acidification. The solvents were evaporated on a rotary evaporator, and the reaction residue was extracted using a separatory funnel with methylene chloride. The collected organic layer was dried over anhydrous MgSO_4 , filtered through a filter paper, and evaporated.

Step 2a (compounds 2; 4–7): The concentrated mixture was dissolved in 100 mL of THF, followed by the addition of 6 mM NaBH_4 . The mixture was stirred under reflux for 8 h. The mixture was acidified with 10% HCl and stirring was continued. The solvent was then evaporated and the residue was extracted using a separatory funnel with methylene chloride. The residue was purified using liquid column chromatography.

Step 2b (compound 1): The mixture was dissolved in 300 mL of toluene in a round-bottomed flask equipped with an azeotropic cap, after which 1 mM *p*-toluenesulfonic acid was added and heated with a heating mantle until the substrate has completely reacted, that is, until the water stopped evaporating.

The obtained compounds were purified via liquid column chromatography using hexane/isopropanol/acetone/ethyl acetate (60:3:1:1) as the eluent.

For the HR-ESI-MS/MS analyses of lactones 1–7, the major operating parameters were as follows: flow rate of the sample: 180 $\mu\text{L}/\text{min}$; nebulizer pressure: 0.4 bar, heating gas flow: 3.0 L/min, heating gas temperature: 180/200 $^\circ\text{C}$; data acquisition range: m/z 50–1300/1400 m/z ; ionization mode: positive and negative; and ion source energy: 5 eV.

The additional spectral data are presented in the attached Supplementary Materials.

3-*n*-butylidene-phthalide (1) was prepared according to the procedure (steps 1 and 2b), and $\text{C}_4\text{H}_9\text{Br}$ and phthalic anhydride (7.5 g, 0.05 mole) were used as the substrate. An amount of 3.57 g (yield 38%) of phthalide was obtained as a mixture of two diastereoisomers. Bioactivity of compound 1 was tested for the mixture of isomers *E* and *Z*, of percentage composition 8 and 92%, correspondingly.

Spectroscopic data: ^1H NMR (500 MHz, CDCl_3), δ (ppm): 0.98 (t, 3, $J = 7.4$, CH_3 -11), 1.54 (m, 2, CH_2 -10), 2.45 (q, 2, $J = 15.0$, 7.5, CH_2 -9), 5.63 (t, 1, $J = 7.8$, CH-8), 7.49 (t, 1, $J = 7.3$, CH-5), 7.62–7.69 (m, 2, CH-4), 7.62–7.69 (m, 2, CH-6), 7.88 (d, 1, $J = 7.7$, CH-7). ^{13}C NMR (151 MHz), δ (ppm): 13.9 (C-11), 22.6 (C-10), 28.0 (C-9), 109.6 (CH-8), 119.8 (CH-4), 124.6 (C-7a), 125.4 (C-7), 129.5 (CH-6), 134.3 (CH-5), 139.7 (C-3a), 145.9 (C-3), 167.3 (C-1). HRMS (m/z): $[\text{M} + \text{H}]^+$ 189.0908 (experimental), 189.0910 (calculated); formula: $\text{C}_{12}\text{H}_{12}\text{O}_2$.

3-*n*-butylphthalide (2) was prepared according to the procedure (steps 1 and 2a), and $\text{C}_4\text{H}_9\text{Br}$ and phthalic anhydride (7.5 g, 0.05 mole) were used as the substrate. An amount of 4.65 g (yield 48.8%) of phthalide was obtained. Spectroscopic data: ^1H NMR (500 MHz, CDCl_3), δ (ppm): 0.91 (t, 3, $J = 7.2$, CH_3 -11), 1.31–1.44 (m, 2, CH_2 -10), 1.44–1.54 (m, 2, CH_2 -9), 1.65–1.80 (m, 1, one of CH_2 -8), 1.99–2.12 (m, 1, one of CH_2 -8), 5.47 (dd, 1, $J = 7.9$, 3.7, CH-3), 7.44 (d, 1, $J = 7.7$, CH-4), 7.52 (t, 1, $J = 7.5$, CH-6), 7.66 (t, 1, $J = 7.5$, CH-5), 7.89 (d, 1, $J = 7.7$, CH-7). ^{13}C NMR (151 MHz), δ (ppm): 14.0 (C-11), 22.6 (C-10), 27.0 (C-9), 34.6 (C-8), 81.6 (CH-3), 121.8 (CH-4), 125.8 (CH-7), 126.3 (C-7a), 129.1 (CH-6), 134.1 (CH-5), 150.3 (C-3a), 170.8 (C-1). HRMS (m/z): $[\text{M} + \text{H}]^+$ 191.1065 (exp.), 191.1067 (calc.); formula: $\text{C}_{12}\text{H}_{14}\text{O}_2$.

3-*n*-propylphthalide (4) was prepared according to the procedure (steps 1 and 2a), and $\text{C}_3\text{H}_7\text{Br}$ and phthalic anhydride (7.5 g, 0.05 mole) were used as the substrate. An amount of 3.61 g (yield 42%) of phthalide was obtained. Spectroscopic data: ^1H NMR (500 MHz, CDCl_3), δ (ppm): 0.98 (t, 3, $J = 7.4$, CH_3 -10), 1.46–1.58 (m, 2, CH_2 -9), 1.72–1.78 (m, 1, one of CH_2 -8), 1.98–2.04 (m, 1, one of CH_2 -8), 5.48 (dd, 1, $J = 8.0$, 4.0, CH-3), 7.44 (d, 1, $J = 7.7$, CH-4), 7.52 (t, 1, $J = 7.5$, CH-6), 7.66 (t, 1, $J = 7.5$, CH-5), 7.89 (d, 1, $J = 7.7$, CH-7). ^{13}C NMR

(151 MHz), δ (ppm): 13.97 (CH₃-10), 18.41 (CH₂-9), 36.99 (CH₂-8), 81.42 (CH-3), 121.87 (CH-4), 125.88 (CH-7), 126.32 (C-7a), 129.18 (CH-6), 134.08 (CH-5), 150.31 (C-3a), 170.86 (C-1). HRMS (m/z): [M + H]⁺ 177.0908 (exp.), 177.0910 (calc.); formula: C₁₁H₁₂O₂.

3-*n*-butyl-4,5,6,7-tetrahydrophthalide (5) was prepared according to the procedure (steps 1 and 2a), and C₄H₉Br and 3,4,5,6-tetrahydrophthalic anhydride (7.7 g, 0.05 mole) were used as the substrate. An amount of 4.37 g (yield 45.1%) of phthalide was obtained. Spectroscopic data: ¹H NMR (500 MHz, CDCl₃), δ (ppm): 0.88 (t, 3, J = 7.1, CH₃-11), 1.22–1.40 (m, 4, CH₂-10, CH₂-9), 1.41–1.50 (m, 1, one of CH₂-8), 1.59–1.77 (m, 4, CH₂-5, CH₂-6), 1.79–1.87 (m, 1, one of CH₂-8), 2.13–2.24 (m, 4, CH₂-4, CH₂-7), 4.74–4.79 (m, 1, CH-3). ¹³C NMR (151 MHz), δ (ppm): 13.77 (CH₃-11), 19.77 (CH₂-7), 21.66 (CH₂-5), 21.69 (CH₂-6), 22.52 (CH₂-10), 23.25 (CH₂-4), 26.66 (CH-9), 32.08 (CH-8), 83.01 (C-3), 126.49 (C-7a), 163.84 (C-3a), 173.85 (C-1). HRMS (m/z): [M + H]⁺ 195.1376 (exp.), 195.1380 (calc.); formula: C₁₂H₁₈O₂.

3-*n*-butyl-hexahydrophthalide (6) was prepared according to the procedure (steps 1 and 2a), and C₄H₉Br and hexahydrophthalic anhydride (7.8 g, 0.05 mole) were used as the substrates. An amount of 4.70 g (yield 48%) of phthalide was obtained. Spectroscopic data: ¹H NMR (500 MHz, CDCl₃) δ (ppm): 0.90 (t, 3, J = 7.1 Hz, CH₃-11), 1.07–1.10 (m, 2, CH₂-10), 1.29–1.36 (m, 2, CH₂-7), 1.37–1.65 (m, 8, CH₂-4, CH₂-5, CH₂-6, CH₂-9), 1.70–1.77 (m, 1, one of CH₂-8), 2.15–2.18 (m, 1, one of CH₂-8), 2.29–2.31 (m, 1, CH-3a), 2.72 (t, 1, J = 6.2, CH-7a), 4.20–4.26 (m, 1, CH-3). ¹³C NMR (151 MHz) δ (ppm): 13.91. (CH₃-11), 22.48 (CH₂-10, CH₂-9), 22.55 (CH₂-5), 22.88 (CH₂-8), 23.58 (CH₂-6, CH₂-4), 27.96 (CH₂-7), 38.95 (CH-3a), 42.08 (CH-7a), 82.03 (C-3), 178.10 (C-1). HRMS (m/z): [M + Na]⁺ 219.1367 (exp.), 219.1434 (cal.); formula: C₁₂H₂₀O₂.

3-*n*-butyl-3a,4,7,7a-tetrahydrophthalide (7) was prepared according to the procedure (steps 1 and 2a), and C₄H₉Br and 1,2,5,6-tetrahydrophthalic anhydride (7.7 g, 0.05 mole) were used as the substrate. An amount of 4.85 g (yield 50%) of phthalide was obtained. Spectroscopic data: ¹H NMR (500 MHz, CDCl₃) δ (ppm): 0.91 (t, 3, J = 7.1 Hz, CH₃-11), 1.30–1.40 (m, 3, one of CH₂-9, CH₂-10), 1.42–1.50 (m, 1, one of CH₂-9), 1.52–1.61 (m, 2, one of CH₂-9, one of CH₂-8), 1.72–1.79 (m, 1, one of CH₂-8), 1.80–1.88 (m, 1, one of CH₂-4), 2.01 (dt, 1, J = 17.3, 5.8, one of CH₂-4), 2.30–2.38 (m, 1, one of CH₂-7), 2.38–2.46 (m, 1, one of CH₂-7), 2.49–2.59 (m, 1, CH-3a), 2.79–2.87 (m, 1, CH-7a), 4.32–4.38 (m, 1, CH-3), 5.63–5.75 (m, 2, CH-5, CH-6). ¹³C NMR (151 MHz) δ (ppm): 14.0 (CH₃-11), 19.72 (CH₂-10), 22.07 (CH₂-4), 22.65 (CH₂-7), 28.09 (CH-7a), 29.00 (CH₂-9), 35.40 (CH₂-8), 40.03 (CH-3a), 82.69 (CH-3), 124.45 (CH-5), 125.30 (CH-6), 178.74 (C-1). HRMS (m/z): [M + Na]⁺ 217.1202 (exp.), 217.1277 (cal.); formula: C₁₂H₁₈O₂.

3.3. Fungistatic Activity against *R. mucilaginosa* IHEM 18459 and Correlation with Structure and In Silico Data

3.3.1. Broth Microdilution Method

The compounds 1–8 were screened for their antimicrobial activity using the microdilution method with modified CLSI guidelines [69]. The broth used for the tests included RPMI 1640 medium buffered with MOPS.

Different concentrations of compounds 1–8 were prepared in DMSO and then diluted 50 times in the medium. An amount of 100 microliters of each concentration was placed into the wells of 96-well microplates. *R. mucilaginosa* IHEM 18459 was cultivated on Sabouraud agar. The inoculum was made from a 24 h culture by a dilution to 0.5 McFarland and then further diluted to obtain a density of 1×10^3 – 5×10^3 CFU/mL. The inoculum volume pipetted into the previously placed antifungals was 100 μ L. All the compounds were tested in triplicate. The plates were then incubated separately at 25 °C and 30 °C for 48 h using 1200 RPM. The activity was determined spectrophotometrically at a wavelength of 595 nm and determined as the half-maximal inhibitory concentration (IC₅₀).

3.3.2. In Silico ADME Studies

The prediction of lipophilicity (Log P), solubility (log S), and CYP isoenzyme inhibition for compounds 1–8 was performed using the tool designed by the Swiss Institute of Bioinformatics at the University of Lausanne (<http://www.swissadme.ch/index.php> (accessed on 25 February 2023)), reported by Daina et al. [23].

The toxicity of rat cells was tested using the computational tool GUSAR (General Unrestricted Structure-Activity Relationships: <http://www.way2drug.com/gusar/index.html> (accessed on 25 February 2023)) as part of the Way2Drug platform, as reported by Druzhilovskiy et al. [22].

3.4. Determination of Fungistatic Activity for 3-*n*-Butylidenephthalide (1) against *R. mucilaginosa* IHEM 18459 In Vitro and Food Matrices

3.4.1. Dry Biomass Determination

Compound 1 dissolved in DMSO (0.5 mL) was added to four 2 L Erlenmeyer flasks containing Sabouraud medium, resulting in final concentrations of 25, 50, 75, and 100 µg/mL. Fluconazole (8) was tested in the flask at a concentration of 50 µg/mL. The positive control contained medium with the addition of DMSO (0.5 mL) without antifungals. The inoculum of *R. mucilaginosa* IHEM 18459 with an OD₆₀₀ = 0.180 and an amount equal to 10% was added to the Sabouraud medium, resulting in a total volume of 500 mL. After 7 days of incubation at 25 °C, the biomass was washed three times with distilled water to remove the medium and centrifuged at 3220 RCF for 15 min at 8 °C. The biomass was then frozen and lyophilized to a constant weight.

3.4.2. Plate Count Method

The fungicidal activity of 3-*n*-butylphthalide (1) was visualized using the plate count method. Preincubation cultures of *R. mucilaginosa* IHEM 18459 were prepared in flasks with Sabouraud medium. First, various concentrations of 3-*n*-butylidenephthalide (1) were added to DMSO (0.5 mL) in each flask. Fluconazole (8) was administered as a single dose. Subsequently, 1 mL of the inoculum at a density of 1×10^3 – 5×10^3 CFU/mL was added to the samples. Flasks were incubated on a rotary shaker at 30 °C for 48 h. Serial dilutions of each sample were then prepared, and 100 µL of cultures were transferred to agar plates and spread on the surface. After further incubation for 48 h at 30 °C, the yeast colonies were counted.

Antimicrobial activity assessed in food matrices: 25 g of commercially available yogurt was placed in sterile Nasco Whirl-Pak bags. 3-*n*-butylidenephthalide (1) was tested at the final concentrations of 50, 150, 250, 350, 450, and 550 µg/mL in DMSO (0.5 mL). The control involved only solvent addition. Subsequently, 1 mL of inoculum of *R. mucilaginosa* at a density of 1×10^3 – 5×10^3 CFU/mL was added to each bag. After their incubation at 30 °C for 48 h, serial dilutions of each sample were performed. Selected dilutions (100 µL) were spread onto the surface of Sabouraud agar using a cell spreader. The tests were performed in triplicate. After 48 h incubation at 30 °C, the yeast colonies were counted.

3.5. Microbial Transformation of 3-*n*-Butylidenephthalide (1) by *R. mucilaginosa* IHEM 18459

First, 1 mL of 0.5 McFarland inoculum of *R. mucilaginosa* IHEM 18459 was added to the Sabouraud medium, resulting in a total volume of 75 mL. After eight days of incubation on a rotary shaker at 25 °C, 20 mg of 3-*n*-butylidenephthalide (1) in 0.5 mL of acetone was added. Transformations were continued for an additional 8 days. The culture was then centrifuged at 3220 RCF for 15 min, and the yeast cells were separated from the supernatant. Mycelia and supernatants were extracted separately using 25 mL of ethyl acetate. The extracts were subjected to analysis using HPLC-DAD. The mobile phase was 0.5% formic acid (A) and acetonitrile (B). Gradient elution conditions were as follows: 0–3 min, 65% A/35% B; 3–12 min, 35% A/65% B; 12–13 min, 10% A/90% B; 13–14 min, 0% A/100% B; 14–16 min 0% A/100% B; 16–19 min, 65% A/35% B; and 19–23 min, 65% A/35% B. The following parameters were selected: flow rate, 0.4 mL/min; column incubation temperature, 30 °C; and detection wavelength, 275 nm.

3.6. The Influence of 3-*n*-Butylidenephthalide (1) on the ROS Level

The level of oxidative stress was assessed using the adherent cell microplate assay. Briefly, 100 μ L of *R. mucilaginosa* inoculum ($OD_{600} = 0.1$) in PBS was added to the wells of a 96-well microtiter plate. After overnight incubation at 25 °C and adhesion of the cells, PBS was collected from above the cell sediment. Then, 100 μ L of 40 μ M H₂DCFDA was added to each well of the first four rows, and 100 μ L of PB buffer was added to the next four rows (unstained background control). After incubation of the plate at 37 °C for 45 min, the dye and PBS were removed from the wells. The cells were washed with 10 \times diluted PBS, followed by the addition of 100 μ L of the same buffer. Next, 100 μ L of compound 1 at 25, 50, 75, and 100 μ g/mL and fluconazole (8) at a concentration of 50 μ g/mL were loaded into wells and mixed. The positive control contained 3% H₂O₂, whereas the negative control did not contain the inhibitor. After 4 h of incubation at 25 °C, fluorometric measure was taken at excitation and emission wavelengths of 485 nm and 385 nm, respectively.

3.7. Confocal Microscopy

The 24 h yeast inoculum was standardized in Sabouraud medium to obtain a density of 0.5 McFarland and transferred to a sterile tube. After centrifugation, the medium was discarded, and the precipitate was suspended in PBS. The sample was then transferred to a Millicell[®] EZ SLIDE chamber and assembled on a microscope slide. Next, 20 μ L of 3-*n*-butylidenephthalide (1), at a final concentration of 100 μ g/mL, was added to the wells and mixed. After 20 min, the slide was dismounted, and the cells were stained with Calcofluor White, according to the manufacturer's recommendations.

3.8. Synergistic Effect—Determination of Fractional Inhibitory Concentration (FIC)

To test the synergistic effect of the compounds, a checkerboard method was performed based on the methods described by Pillai et al. [42] and Krežel et al. [15]. Sabouraud medium was used for all tests. First, 3-*n*-butylidenephthalide (1) and fluconazole (8) were prepared in a DMSO solution and then diluted directly in the medium in a 96-well microtiter plate to obtain final concentrations of 1–528 μ g/mL for fluconazole (8) and 0.5–32 μ g/mL for 3-*n*-butylidenephthalide (1). The reference sample was diluted in DMSO with Sabouraud medium without the inoculum. Samples containing only one of the tested compounds served as controls. All the samples were tested in triplicate. The plates were then incubated separately in a thermoshaker at 25 °C, using 1000 RPM agitation. The absorbance was read at a wavelength of 595 nm to determine the antifungal activity. A synergistic effect was recorded when the inhibition caused by the mixture of both compounds was higher than that of the separately tested agents. FIC was calculated as follows:

$$\sum FIC = \frac{MIC \text{ of agent A in combination}}{MIC \text{ of agent A tested separately}} + \frac{MIC \text{ of agent B in combination}}{MIC \text{ of agent B tested separately}}$$

3.9. The Determination of Carotenoids in Biomass

3.9.1. Samples Preparation

Because of carotenoid instability, the subsequent cultures were grown to obtain fresh samples. The growth conditions were analogous to those of the previous experiment with the determination of dry biomass; however, at a low scale, the total volume was 50 mL. After seven days of incubation at 25 °C, the biomass was washed three times with distilled water and frozen.

Subsequently, washed yeast cells (0.5 g) were defrosted, dissolved in 3 mL PBS, pH 7.2, and disintegrated using an ultrasonic homogenizer for 1200 s (using an 80 s:20 s work-rest cycle). The lysates were centrifuged for 3 min and the supernatants were discarded. Samples were extracted three times (two times with DMSO and once with Folch solution) using the following procedure: vortexing for 5 min at 1600 RPM with 2 mL of the solvent and centrifugation for 3 min. The fractions were collected, and the Folch solution was evaporated using a rotary evaporator. Subsequently, 1 mL of the remaining mixture was

evaporated under a stream of nitrogen. The residue was dissolved in gradient-grade acetonitrile and subjected to HPLC and HR-APCI-MS/MS analyses.

3.9.2. HR-APCI-MS/MS Analyses

Pigments determination and quantitative comparative analysis: The pigments were eluted with A-water with 0.1% formic acid, B-acetonitrile with 0.1% formic acid, and C-isopropanol with 0.1% formic acid in gradient mode: 0 min, 25% A/25% B/50% C; 0–45 min, 2.5% A/2.5% B/95% C; 45–50 min, 2.5% A/2.5% B/95% C; and 51–60 min, 25% A/25% B/50% C.

The flow rate was 200 $\mu\text{L}/\text{min}$. The operating parameters were as follows: nebulizer pressure: 0.3 bar, heating gas flow: 3.0 L/min, heating gas temperature, 250 $^{\circ}\text{C}$; data acquisition range, m/z 50–2000 m/z ; ionization mode, positive; and ion source energy, 10 eV.

3.9.3. HPLC-DAD Analyses of β -Carotene Content

To determine the β -carotene calibration curve, the results were calculated according to the dry mass. The mobile phase comprised water (A) and acetonitrile (B). Gradient elution conditions were as follows: 0–2 min, 10% A/0% B; 2–10 min, 0% A/100% B; 10–20 min, 0% A/100% B; 20–22 min, 10% A/90% B; and 22–27 min, 10% A/90% B. The following parameters were selected: flow rate, 0.9 mL/min; column incubation temperature, 30 $^{\circ}\text{C}$; and detection wavelength, 450 nm.

3.10. FAME Content

FAME content was determined using 50 mg of dry yeast biomass. The biomass was heated under reflux using 5 mL of 0.5 M KOH in methanol for 15 min. Next, 2 mL of boron trifluoride in diethyl ether was added, and the mixture was heated for 5 min. After cooling, the mixture was extracted with hexane (1 mL). Samples were analyzed using the following temperature program: 100 $^{\circ}\text{C}$ (hold for 3 min), 240 $^{\circ}\text{C}$ (2.5 $^{\circ}\text{C}/\text{min}$; hold for 4 min), 260 $^{\circ}\text{C}$ (15 $^{\circ}\text{C}/\text{min}$; hold for 1 min). FAMES were detected by comparing their retention times with those of the standard.

3.11. Ergosterol Content

Ergosterol was determined using the method described by Arthington-Skaggs et al. [70] with minor modifications, using wet biomass previously obtained for carotenoid determination. Briefly, wet biomass samples were weighted and subjected to saponification with 25% potassium hydroxide in ethanol. After 1 h incubation at 85 $^{\circ}\text{C}$ and cooling, samples were extracted with hexane using a vortex, and the upper layer was collected, diluted 5 \times in ethanol, and measured using a spectrophotometer scanning between 200 and 300 nm. The ergosterol content was calculated as the percentage of the dry biomass.

4. Conclusions

Synthetic phthalide lactones limit the growth of *R. mucilaginosa* IHEM 18459 cells. Lactone **1** demonstrated a synergistic effect with fluconazole (**8**), which reduced the amount of this drug required for yeast inhibition.

In this study, we performed various experiments to determine the effects of phthalide lactone on *R. mucilaginosa* IHEM 18459 cells. We have shown that 3-*n*-butylidenephthalide (**1**) is not metabolized to other compounds and accumulates in yeast cells, which contributes to an increase in ROS. The effect of 3-*n*-butylidenephthalide (**1**) on *R. mucilaginosa* IHEM 18459 cells was similar to that of *C. albicans* ATCC 10231, *C. albicans* ATCC 2091, and *C. guilliermondii* KKP 3390 cells, confirming the mechanism proposed in the literature.

The data show the strong influence of phthalide **1** on the quantitative composition of FAME, where, for example, at a concentration of 75 mg/mL, it decreased three times. The increasing proportion of unsaturated fatty acids suggested that the fluidity of the cell membrane increased. This effect may be related to the expression of the genes encoding

fatty acid desaturases. 3-*n*-Butylidenephthalide (1) did not notably change the amount of ergosterol. This means that the observed fungistatic activity of lactones 1–7 and fluconazole (8) is not related to cell membrane damage associated with the lack of ergosterol.

Cultures of *R. mucilaginosa* IHEM 18459 grown in the presence of 3-*n*-butylidenephthalide (1) changed color from orange/red to light yellow, which was related to the inhibition of torulene and torularhodin.

In some experiments, we observed a surprising effect of fluconazole (8): an increase in the production of β -carotene, torulene, and torularhodin, or an increase in ROS. The high value of IC₅₀ and IC₉₀ and the lack of substantial effect on ergosterol content may be related to the fluconazole resistance of *R. mucilaginosa* IHEM 18459.

Supplementary Materials: The following supporting information can be downloaded at: <https://www.mdpi.com/article/10.3390/molecules28145423/s1>, Figure S1a: ¹H NMR of 3-*n*-butylidenephthalide (1); Figure S1b: ¹³C NMR of 3-*n*-butylidenephthalide (1); Figure S1c: HR-ESI-MS/MS of 3-*n*-butylidenephthalide (1); Figure S2a: ¹H NMR of 3-*n*-butylphthalide (2); Figure S2b: ¹³C NMR of 3-*n*-butylphthalide (2); Figure S2c: HR-ESI-MS/MS of 3-*n*-butylphthalide (2); Figure S3: HR-ESI-MS/MS of 3-*n*-propylidenephthalide (3); Figure S4a: ¹H NMR of 3-*n*-propylphthalide (4); Figure S4b: ¹³C NMR of 3-*n*-propylphthalide (4); Figure S4c: HR-ESI-MS/MS of 3-*n*-propylphthalide (4); Figure S5a: ¹H NMR of 3-butyl-4,5,6,7-tetrahydrophthalide (5); Figure S5b: ¹³C NMR of 3-butyl-4,5,6,7-tetrahydrophthalide (5); Figure S5c: HR-ESI-MS/MS of 3-butyl-4,5,6,7-tetrahydrophthalide (5); Figure S6a: ¹H NMR of 3-*n*-butyl-hexahydrophthalide (6); Figure S6b: ¹³C NMR of 3-*n*-butyl-hexahydrophthalide (6); Figure S6c: HR-ESI-MS/MS of 3-*n*-butyl-hexahydrophthalide (6); Figure S7a: ¹H NMR of 3-*n*-butyl-1,2,6,7-tetrahydrophthalide (7); Figure S7b: ¹³C NMR of 3-*n*-butyl-1,2,6,7-tetrahydrophthalide (7); Figure S7c: HR-ESI-MS/MS of 3-*n*-butyl-1,2,6,7-tetrahydrophthalide (7).

Author Contributions: Conceptualization, J.G. and T.O.; methodology, J.G., T.O., J.P. and F.B.; formal analysis, J.G., T.O. and F.B.; investigation, J.G. and J.P.; resources, J.G., T.O. and F.B.; writing—original draft preparation, J.G. and T.O.; writing—review and editing, F.B. and J.P.; supervision, T.O. and F.B.; funding acquisition, J.G. All authors have read and agreed to the published version of the manuscript.

Funding: This research was financed by the project “UPWR 2.0: international and interdisciplinary program of development of Wrocław University of Environmental and Life Sciences”, cofinanced by the European Social Fund under the Operational Program Knowledge Education Development, under contract No. POWR.03.05.00-00-Z062/18 of June 4, 2019 and project “Innowacyjny Doktorat” N070/0013/20. The APC was financed by POWR.03.05.00-00-Z062/18 of 4 June 2019.

Institutional Review Board Statement: Not applicable.

Informed Consent Statement: Not applicable.

Data Availability Statement: The data presented in this study are available on request from the corresponding author.

Acknowledgments: The analytical part of this work was conducted under POWR.03.05.00-00-Z062. The research tasks regarding fungistatic activity were financed by the project “Innowacyjny Doktorat” N070/0013/20.

Conflicts of Interest: The authors declare no conflict of interest.

Sample Availability: Samples of the compounds are available from the authors upon request.

References

1. Lyman, M.; Urbin, S.; Strout, C.; Rubinfeld, B. The Oleaginous Red Yeast *Rhodotorula/Rhodospiridium*: A Factory for Industrial Bioproducts. In *Yeasts in Biotechnology*; Peixoto Basso, T., Ed.; IntechOpen: London, UK, 2019; pp. 1–18.
2. Li, Z.; Li, C.; Cheng, P.; Yu, G. *Rhodotorula mucilaginosa*—Alternative Sources of Natural Carotenoids, Lipids, and Enzymes for Industrial Use. *Heliyon* **2022**, *8*, e11505. [CrossRef] [PubMed]
3. Geronikou, A.; Larsen, N.; Lillevang, S.K.; Jespersen, L. Occurrence and Identification of Yeasts in Production of White-Brined Cheese. *Microorganisms* **2022**, *10*, 1079. [CrossRef] [PubMed]
4. Fleet, G.H. Yeasts in fruit and fruit products. In *Yeasts in Food. Beneficial and Detrimental Aspects*; Boekhout, T., Robert, V., Eds.; CRC Press Woodhead Publishing: Cambridge, UK, 2003; Volume 28, pp. 219–316.

5. Koutsoumanis, K.P.; Lianou, A.; Sofos, J.N. Food Safety: Emerging Pathogens. In *Encyclopedia of Agriculture and Food Systems*; Elsevier: Amsterdam, The Netherlands, 2014; pp. 250–272.
6. Tomsíková, A. Risk of fungal infection from foods, particularly in immunocompromised patients. *Epidemiol. Mikrobiol. Imunol. Cas. Spol. Epidemiol. Mikrobiol. Ceske Lek. Spol. JE Purkyne* **2002**, *51*, 78–81.
7. Sanna, C.; Marras, L.; Desogus, A.; Marras, B.; Montero, N.; Bertolino, G.; Schintu, M.; Coroneo, V. Evaluation of *Rhodotorula* spp. Contamination in Hospital Environments. *Environ. Monit. Assess* **2021**, *193*, 152. [[CrossRef](#)]
8. Wirth, F.; Goldani, L.Z. Epidemiology of *Rhodotorula*: An Emerging Pathogen. *Interdiscip. Perspect. Infect. Dis.* **2012**, *2012*, 465717. [[CrossRef](#)]
9. Spiliopoulou, A.; Anastassiou, E.D.; Christofidou, M. *Rhodotorula* Fungemia of an Intensive Care Unit Patient and Review of Published Cases. *Mycopathologia* **2012**, *174*, 301–309. [[CrossRef](#)]
10. Neofytos, D.; Horn, D.; De Simone, J.A. *Rhodotorula mucilaginosa* catheter-related fungemia in a patient with sickle cell disease: Case presentation and literature review. *South. Med. J.* **2007**, *100*, 198–200. [[CrossRef](#)]
11. Low, C.-Y.; Rotstein, C. Emerging Fungal Infections in Immunocompromised Patients. *F1000 Med. Rep.* **2011**, *3*, 14. [[CrossRef](#)]
12. Catalano, A.; Iacopetta, D.; Ceramella, J.; Scumaci, D.; Giuzio, F.; Saturnino, C.; Aquaro, S.; Rosano, C.; Sinicropi, M.S. Multidrug Resistance (MDR): A Widespread Phenomenon in Pharmacological Therapies. *Molecules* **2022**, *27*, 616. [[CrossRef](#)]
13. Gong, Y.; Liu, W.; Huang, X.; Hao, L.; Li, Y.; Sun, S. Antifungal Activity and Potential Mechanism of N-Butylphthalide Alone and in Combination with Fluconazole Against *Candida albicans*. *Front. Microbiol.* **2019**, *10*, 1461. [[CrossRef](#)]
14. Singh, D.K.; Tóth, R.; Gácsér, A. Mechanisms of Pathogenic *Candida* Species to Evade the Host Complement Attack. *Front. Cell. Infect. Microbiol.* **2020**, *10*, 94. [[CrossRef](#)]
15. Krężel, P.; Olejniczak, T.; Tołoczko, A.; Gach, J.; Weselski, M.; Bronisz, R. Synergic Effect of Phthalide Lactones and Fluconazole and Its New Analogues as a Factor Limiting the Use of Azole Drugs against Candidiasis. *Antibiotics* **2022**, *11*, 1500. [[CrossRef](#)]
16. León, A.; Del-Ángel, M.; Ávila, J.L.; Delgado, G. Phthalides: Distribution in Nature, Chemical Reactivity, Synthesis, and Biological Activity. In *Progress in the Chemistry of Organic Natural Products*; Kinghorn, A.D., Falk, H., Gibbons, S., Kobayashi, J., Eds.; Springer International Publishing: Cham, Switzerland, 2017; Volume 104, pp. 127–246.
17. Pannek, J.; Gach, J.; Boratyński, F.; Olejniczak, T. Antimicrobial Activity of Extracts and Phthalides Occurring in Apiaceae Plants: Antimicrobial Activity of Phthalides. *Phytother. Res.* **2018**, *32*, 1459–1487. [[CrossRef](#)]
18. Miran, M.; Monsef Esfahani, H.R.; Jung, J.H.; Aliahmadi, A.; Skropeta, D.; Abbas-Mohammadi, M.; Ebrahimi, S.; Moridi Farimani, M. Characterization and Antibacterial Activity of Phthalides from the Roots of the Medicinal Herb *Levisticum officinale* WDJ Koch. *IJPR* **2020**, *19*, 182. [[CrossRef](#)]
19. Dya, A.; Soliman, H.; Abdelrazak, A.; Samra, B.N.; Khojah, E.; Ahmed, A.F.; El-Esawi, M.A.; Elsayed, A. Optimization of Carotenoids Production from *Rhodotorula* Sp. Strain ATL72 for Enhancing Its Biotechnological Applications. *J. Fungi* **2022**, *8*, 160. [[CrossRef](#)]
20. Zadorozhnyi, P.V.; Kiselev, V.V.; Kharchenko, A.V. *In Silico* ADME Profiling of Salubrinal and Its Analogues. *Future Pharmacol.* **2022**, *2*, 160–197. [[CrossRef](#)]
21. Chmiel, T.; Mieszkowska, A.; Kempieńska-Kupczyk, D.; Kot-Wasik, A.; Namieśnik, J.; Mazerska, Z. The Impact of Lipophilicity on Environmental Processes, Drug Delivery and Bioavailability of Food Components. *Microchem. J.* **2019**, *146*, 393–406. [[CrossRef](#)]
22. Druzhilovskiy, D.S.; Rudik, A.V.; Filimonov, D.A.; Glorizova, T.A.; Lagunin, A.A.; Dmitriev, A.V.; Pogodin, P.V.; Dubovskaya, V.I.; Ivanov, S.M.; Tarasova, O.A.; et al. Computational Platform Way2Drug: From the Prediction of Biological Activity to Drug Repurposing. *Russ. Chem. Bull.* **2017**, *66*, 1832–1841. [[CrossRef](#)]
23. Daina, A.; Michielin, O.; Zoete, V. SwissADME: A Free Web Tool to Evaluate Pharmacokinetics, Drug-Likeness and Medicinal Chemistry Friendliness of Small Molecules. *Sci. Rep.* **2017**, *7*, 42717. [[CrossRef](#)]
24. Wang, M.; Feng, Y.; Yuan, Y.; Gui, L.; Wang, J.; Gao, P.; Qin, B.; Sima, D.; Wang, Q.; Pan, W. Use of L-3-n-Butylphthalide within 24 h after Intravenous Thrombolysis for Acute Cerebral Infarction. *Complement. Ther. Med.* **2020**, *52*, 102442. [[CrossRef](#)]
25. Zhang, C.; Zhao, S.; Zang, Y.; Gu, F.; Mao, S.; Feng, S.; Hu, L.; Zhang, C. The Efficacy and Safety of DL-3n-Butylphthalide on Progressive Cerebral Infarction: A Randomized Controlled STROBE Study. *Medicine* **2017**, *96*, e7257. [[CrossRef](#)] [[PubMed](#)]
26. Bhatt, S.; Dhiman, S.; Kumar, V.; Gour, A.; Manhas, D.; Sharma, K.; Ojha, P.K.; Nandi, U. Assessment of the CYP1A2 Inhibition-Mediated Drug Interaction Potential for Pinocembrin Using *In Silico*, *In Vitro*, and *In Vivo* Approaches. *ACS Omega* **2022**, *7*, 20321–20331. [[CrossRef](#)] [[PubMed](#)]
27. Lee, S.-J. Clinical Application of CYP2C19 Pharmacogenetics toward More Personalized Medicine. *Front. Gene* **2013**, *3*, 318. [[CrossRef](#)] [[PubMed](#)]
28. Benkova, M.; Soukup, O.; Marek, J. Antimicrobial Susceptibility Testing: Currently Used Methods and Devices and the near Future in Clinical Practice. *J. Appl. Microbiol.* **2020**, *129*, 806–822. [[CrossRef](#)]
29. Cruz, R.C.; Werneck, S.M.C.; Oliveira, C.S.; Santos, P.C.; Soares, B.M.; Santos, D.A.; Cisalpino, P.S. Influence of Different Media, Incubation Times, and Temperatures for Determining the MICs of Seven Antifungal Agents against *Paracoccidioides Brasiliensis* by Microdilution. *J. Clin. Microbiol.* **2013**, *51*, 436–443. [[CrossRef](#)]
30. Smith, K.P.; Kirby, J.E. The Inoculum Effect in the Era of Multidrug Resistance: Minor Differences in Inoculum Have Dramatic Effect on MIC Determination. *Antimicrob. Agents Chemother.* **2018**, *62*, e00433-18. [[CrossRef](#)]

31. Afzali, S.; Edalatian Dovom, M.R.; Habibi Najafi, M.B.; Mazaheri Tehrani, M. Determination of the Anti-Yeast Activity of *Lactobacillus* Spp. Isolated from Traditional Iranian Cheeses in Vitro and in Yogurt Drink (Doogh). *Sci. Rep.* **2020**, *10*, 6291. [[CrossRef](#)]
32. Lima, R.C.; de Carvalho, A.P.A.; Vieira, C.P.; Moreira, R.V.; Conte-Junior, C.A. Green and Healthier Alternatives to Chemical Additives as Cheese Preservative: Natural Antimicrobials in Active Nanopackaging/Coatings. *Polymers* **2021**, *13*, 2675. [[CrossRef](#)]
33. Gach, J.; Olejniczak, T.; Krężel, P.; Boratyński, F. Microbial Synthesis and Evaluation of Fungistatic Activity of 3-Butyl-3-Hydroxyphthalide, the Mammalian Metabolite of 3-*n*-Butylidenephthalide. *Int. J. Mol. Sci.* **2021**, *22*, 7600. [[CrossRef](#)]
34. Blanco-Padilla, A.; Soto, K.M.; Hernández Iturriaga, M.; Mendoza, S. Food Antimicrobials Nanocarriers. *Sci. World J.* **2014**, *2014*, 837215. [[CrossRef](#)]
35. Sena, L.A.; Chandel, N.S. Physiological Roles of Mitochondrial Reactive Oxygen Species. *Mol. Cell* **2012**, *48*, 158–167. [[CrossRef](#)]
36. Yadav, D.K.; Kumar, S.; Choi, E.-H.; Chaudhary, S.; Kim, M.-H. Molecular Dynamic Simulations of Oxidized Skin Lipid Bilayer and Permeability of Reactive Oxygen Species. *Sci. Rep.* **2019**, *9*, 4496. [[CrossRef](#)]
37. Kumar, S.; Saxena, J.; Srivastava, V.K.; Kaushik, S.; Singh, H.; Abo-EL-Sooud, K.; Abdel-Daim, M.M.; Jyoti, A.; Saluja, R. The Interplay of Oxidative Stress and ROS Scavenging: Antioxidants as a Therapeutic Potential in Sepsis. *Vaccines* **2022**, *10*, 1575. [[CrossRef](#)]
38. Dbouk, N.H.; Covington, M.B.; Nguyen, K.; Chandrasekaran, S. Increase of Reactive Oxygen Species Contributes to Growth Inhibition by Fluconazole in *Cryptococcus neoformans*. *BMC Microbiol.* **2019**, *19*, 243. [[CrossRef](#)]
39. Peng, C.A.; Gaertner, A.A.E.; Henriquez, S.A.; Fang, D.; Colon-Reyes, R.J.; Brumaghim, J.L.; Kozubowski, L. Fluconazole Induces ROS in *Cryptococcus neoformans* and Contributes to DNA Damage in Vitro. *PLoS ONE* **2018**, *13*, e0208471. [[CrossRef](#)]
40. Dagher, Z.; Xu, S.; Negoro, P.E.; Khan, N.S.; Feldman, M.B.; Reedy, J.L.; Tam, J.M.; Sykes, D.B.; Mansour, M.K. Fluorescent Tracking of Yeast Division Clarifies the Essential Role of Spleen Tyrosine Kinase in the Intracellular Control of *Candida glabrata* in Macrophages. *Front. Immunol.* **2018**, *9*, 1058. [[CrossRef](#)]
41. Suchodolski, J.; Feder-Kubis, J.; Krasowska, A. Antiadhesive Properties of Imidazolium Ionic Liquids Based on (–)-Menthol Against *Candida* spp. *Int. J. Mol. Sci.* **2021**, *22*, 7543. [[CrossRef](#)]
42. Pillai, S.K.; Moellering, R.C.; Eliopoulos, G.M. Antimicrobial Combinations. In *Antibiotics in Laboratory Medicine*; Lorian, V., Ed.; Lippincott Williams & Wilkins: Philadelphia, PA, USA, 2005; pp. 365–440.
43. Sharma, R.; Ghoshal, G. Optimization of Carotenoids Production by *Rhodotorula mucilaginosa* (MTCC-1403) Using Agro-Industrial Waste in Bioreactor: A Statistical Approach. *Biotechnol. Rep.* **2020**, *25*, e00407. [[CrossRef](#)]
44. Irazusta, V.; Nieto-Peñalver, C.G.; Cabral, M.E.; Amoroso, M.J.; de Figueroa, L.I.C. Relationship among Carotenoid Production, Copper Bioremediation and Oxidative Stress in *Rhodotorula mucilaginosa* RCL-11. *Process Biochem.* **2013**, *48*, 803–809. [[CrossRef](#)]
45. Kot, A.M.; Błazejak, S.; Kurcz, A.; Gientka, I.; Kieliszek, M. *Rhodotorula Glutinis*—Potential Source of Lipids, Carotenoids, and Enzymes for Use in Industries. *Appl. Microbiol. Biotechnol.* **2016**, *100*, 6103–6117. [[CrossRef](#)]
46. Moliné, M.; Libkind, D.; van Broock, M. Production of Torularhodin, Torulene, and β -Carotene by *Rhodotorula* Yeasts. In *Microbial Carotenoids from Fungi*; Barredo, J.-L., Ed.; Methods in Molecular Biology; Humana Press: Totowa, NJ, USA, 2012; Volume 898, pp. 275–283. ISBN 9781617799174.
47. Moř, A.C.; Părvu, M.; Părvu, A.E.; Roșca-Casian, O.; Dina, N.E.; Leopold, N.; Silaghi-Dumitrescu, R.; Mircea, C. Reversible Naftifine-Induced Carotenoid Depigmentation in *Rhodotorula mucilaginosa* (A. Jörg.) F.C. Harrison Causing Onychomycosis. *Sci. Rep.* **2017**, *7*, 11125. [[CrossRef](#)] [[PubMed](#)]
48. Wang, Q.; Liu, D.; Yang, Q.; Wang, P. Enhancing Carotenoid Production in *Rhodotorula mucilaginosa* KC8 by Combining Mutation and Metabolic Engineering. *Ann. Microbiol.* **2017**, *67*, 425–431. [[CrossRef](#)]
49. Li, J.; Zhou, H.; Pan, X.; Li, Z.; Lu, Y.; He, N.; Meng, T.; Yao, C.; Chen, C.; Ling, X. The Role of Fluconazole in the Regulation of Fatty Acid and Unsaponifiable Matter Biosynthesis in *Schizochytrium* sp. MYA 1381. *BMC Microbiol.* **2019**, *19*, 256. [[CrossRef](#)] [[PubMed](#)]
50. Beopoulos, A.; Nicaud, J.-M.; Gaillardin, C. An Overview of Lipid Metabolism in Yeasts and Its Impact on Biotechnological Processes. *Appl. Microbiol. Biotechnol.* **2011**, *90*, 1193–1206. [[CrossRef](#)]
51. Dourou, M.; Aggeli, D.; Papanikolaou, S.; Aggelis, G. Critical Steps in Carbon Metabolism Affecting Lipid Accumulation and Their Regulation in Oleaginous Microorganisms. *Appl. Microbiol. Biotechnol.* **2018**, *102*, 2509–2523. [[CrossRef](#)]
52. Khot, M.; Ghosh, D. Lipids of *Rhodotorula mucilaginosa* IIP132 with Biodiesel Potential: Oil Yield, Fatty Acid Profile, Fuel Properties. *J. Basic Microbiol.* **2017**, *57*, 345–352. [[CrossRef](#)]
53. Klug, L.; Daum, G. Yeast Lipid Metabolism at a Glance. *FEMS Yeast Res.* **2014**, *14*, 369–388. [[CrossRef](#)]
54. Liang, C.-M.; Yang, C.-F.; Du, J.-S. Lipid Production and Waste Reutilization Combination Using Yeast Isolate *Rhodotorula mucilaginosa* LP-2. *Bioenerg. Res.* **2021**, *14*, 1184–1195. [[CrossRef](#)]
55. Chaturvedi, S.; Bhattacharya, A.; Nain, L.; Prasanna, R.; Khare, S.K. Valorization of Agro-Starchy Wastes as Substrates for Oleaginous Microbes. *Biomass Bioenergy* **2019**, *127*, 105294. [[CrossRef](#)]
56. Adel, A.; El-Baz, A.; Shetaia, Y.; Sorour, N.M. Biosynthesis of Polyunsaturated Fatty Acids by Two Newly Cold-Adapted Egyptian Marine Yeast. *3 Biotech* **2021**, *11*, 461. [[CrossRef](#)]
57. Karatay, S.E.; Dönmez, G. Improving the Lipid Accumulation Properties of the Yeast Cells for Biodiesel Production Using Molasses. *Bioresour. Technol.* **2010**, *101*, 7988–7990. [[CrossRef](#)]

58. Sorgo, A.G.; Heilmann, C.J.; Dekker, H.L.; Bekker, M.; Brul, S.; de Koster, C.G.; de Koning, L.J.; Klis, F.M. Effects of Fluconazole on the Secretome, the Wall Proteome, and Wall Integrity of the Clinical Fungus *Candida albicans*. *Eukaryot. Cell* **2011**, *10*, 1071–1081. [[CrossRef](#)]
59. Dasgupta, D.; Sharma, T.; Bhatt, A.; Bandhu, S.; Ghosh, D. Cultivation of Oleaginous Yeast *Rhodotorula mucilaginosa* IIP32 in Split Column Airlift Reactor and Its Influence on Fuel Properties. *Biocatal. Agric. Biotechnol.* **2017**, *10*, 308–316. [[CrossRef](#)]
60. Park, Y.; Ledesma-Amaro, R.; Nicaud, J.-M. De Novo Biosynthesis of Odd-Chain Fatty Acids in *Yarrowia lipolytica* Enabled by Modular Pathway Engineering. *Front. Bioeng. Biotechnol.* **2020**, *7*, 484. [[CrossRef](#)]
61. Ayadi, I.; Belghith, H.; Gargouri, A.; Guerfali, M. Utilization of Wheat Bran Acid Hydrolysate by *Rhodotorula mucilaginosa* Y-MG1 for Microbial Lipid Production as Feedstock for Biodiesel Synthesis. *BioMed Res. Int.* **2019**, *2019*, 3213521. [[CrossRef](#)]
62. Ballweg, S.; Ernst, R. Control of Membrane Fluidity: The OLE Pathway in Focus. *Biol. Chem.* **2017**, *398*, 215–228. [[CrossRef](#)]
63. Rodríguez-Vargas, S.; Sánchez-García, A.; Martínez-Rivas, J.M.; Prieto, J.A.; Rande-Gil, F. Fluidization of Membrane Lipids Enhances the Tolerance of *Saccharomyces cerevisiae* to Freezing and Salt Stress. *Appl. Environ. Microbiol.* **2007**, *73*, 110–116. [[CrossRef](#)]
64. Liu, Y.; Koh, C.M.J.; Yap, S.A.; Cai, L.; Ji, L. Understanding and Exploiting the Fatty Acid Desaturation System in *Rhodotorula toruloides*. *Biotechnol. Biofuels* **2021**, *14*, 73. [[CrossRef](#)]
65. Tsai, Y.-Y.; Ohashi, T.; Wu, C.-C.; Bataa, D.; Misaki, R.; Limtong, S.; Fujiyama, K. Delta-9 Fatty Acid Desaturase Overexpression Enhanced Lipid Production and Oleic Acid Content in *Rhodospiridium toruloides* for Preferable Yeast Lipid Production. *J. Biosci. Bioeng.* **2019**, *127*, 430–440. [[CrossRef](#)]
66. Bhattacharya, S.; Sae-Tia, S.; Fries, B.C. Candidiasis and Mechanisms of Antifungal Resistance. *Antibiotics* **2020**, *9*, 312. [[CrossRef](#)]
67. Delattin, N.; Cammue, B.P.; Thevissen, K. Reactive Oxygen Species-Inducing Antifungal Agents and Their Activity against Fungal Biofilms. *Future Med. Chem.* **2014**, *6*, 77–90. [[CrossRef](#)] [[PubMed](#)]
68. Walczak, P.; Pannek, J.; Boratyński, F.; Janik-Polanowicz, A.; Olejniczak, T. Synthesis and Fungistatic Activity of Bicyclic Lactones and Lactams against *Botrytis Cinerea*, *Penicillium Citrinum*, and *Aspergillus glaucus*. *J. Agric. Food Chem.* **2014**, *62*, 8571–8578. [[CrossRef](#)] [[PubMed](#)]
69. National Committee for Clinical Laboratory Standards. *Reference Method for Broth Dilution Antifungal Susceptibility Testing of Yeasts*; Approved Standard—Second Edition; NCCLS Document M27-A2; National Committee for Clinical Laboratory Standards: Pittsburgh, PA, USA, 2002.
70. Arthington-Skaggs, B.A.; Lee-Yang, W.; Ciblak, M.A.; Frade, J.P.; Brandt, M.E.; Hajjeh, R.A.; Harrison, L.H.; Sofair, A.N.; Warnock, D.W. Comparison of Visual and Spectrophotometric Methods of Broth Microdilution MIC End Point Determination and Evaluation of a Sterol Quantitation Method for In Vitro Susceptibility Testing of Fluconazole and Itraconazole against Trailing and Nontrailing *Candida* Isolates. *Antimicrob. Agents Chemother.* **2002**, *46*, 2477–2481. [[CrossRef](#)] [[PubMed](#)]

Disclaimer/Publisher’s Note: The statements, opinions and data contained in all publications are solely those of the individual author(s) and contributor(s) and not of MDPI and/or the editor(s). MDPI and/or the editor(s) disclaim responsibility for any injury to people or property resulting from any ideas, methods, instructions or products referred to in the content.

Fungistatic effect of phthalide lactones on *Rhodotorula mucilaginosa*

Joanna Gach^{1*}, Teresa Olejniczak^{1*}, Jakub Pannek¹ and Filip Boratyński¹

¹ Department of Food Chemistry and Biocatalysis, Wrocław University of Environmental and Life Sciences, Norwida 25, 50-375 Wrocław, Poland; jpannek@gmail.com (J.P.), filip.boratyński@upwr.edu.pl (F.B.)

* Correspondence: joanna.gach@upwr.edu.pl (J.G.), teresa.olejniczak@upwr.edu.pl (T.O.)

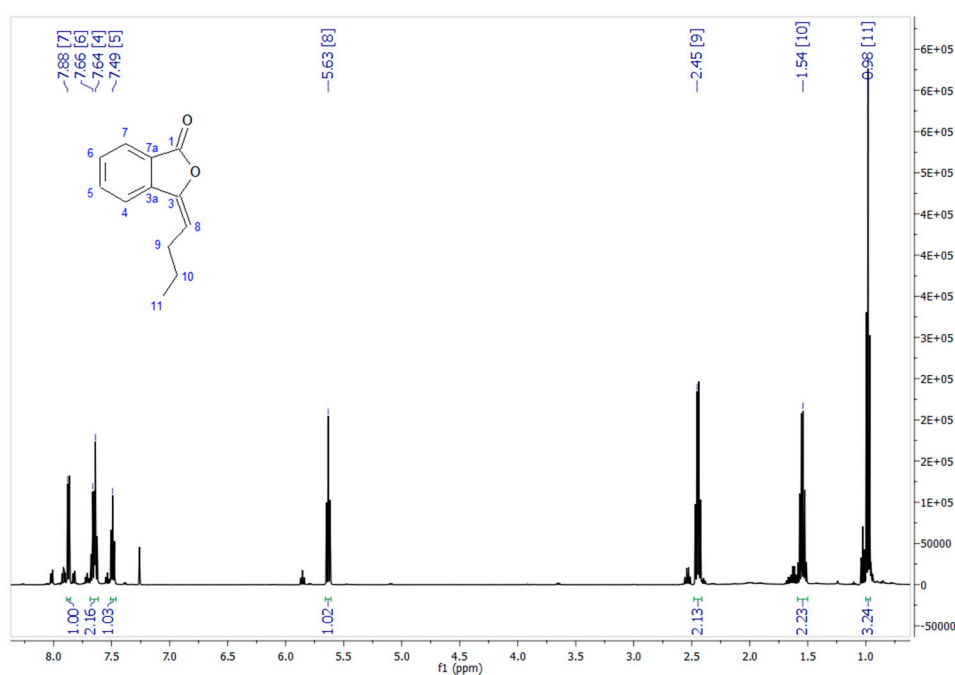


Figure S1a. ¹H NMR of 3-*n*-butylidene-phthalide (1).

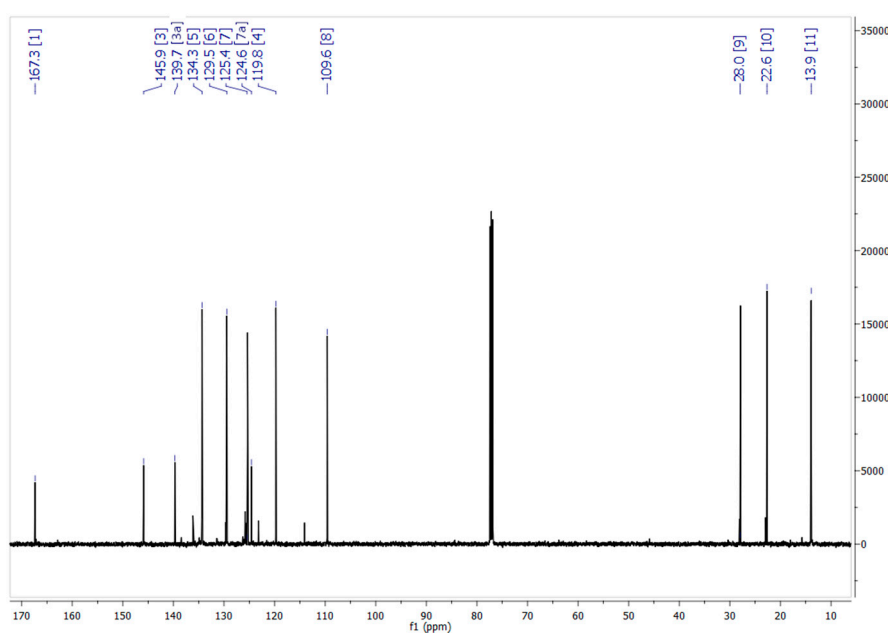
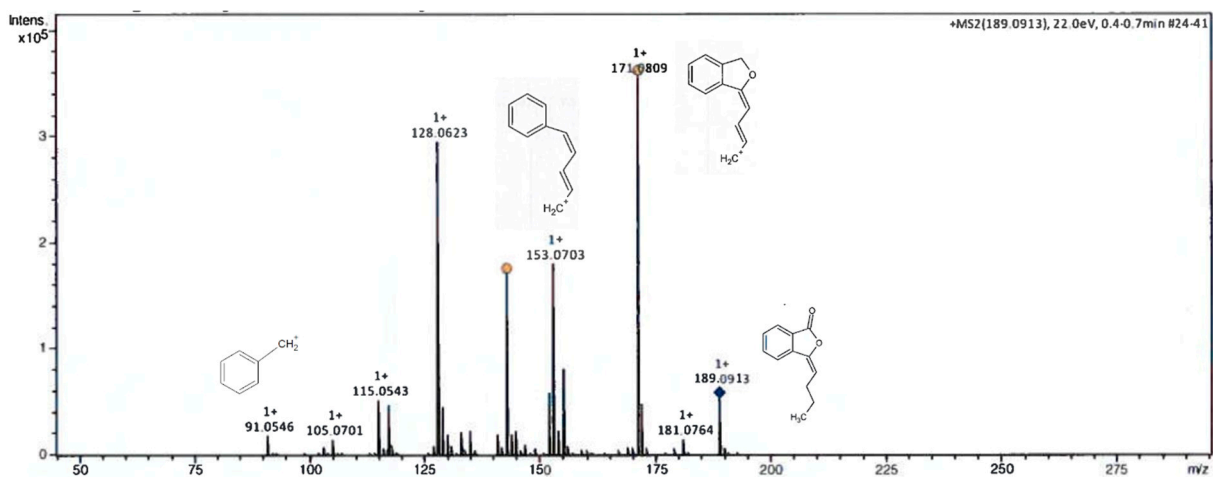
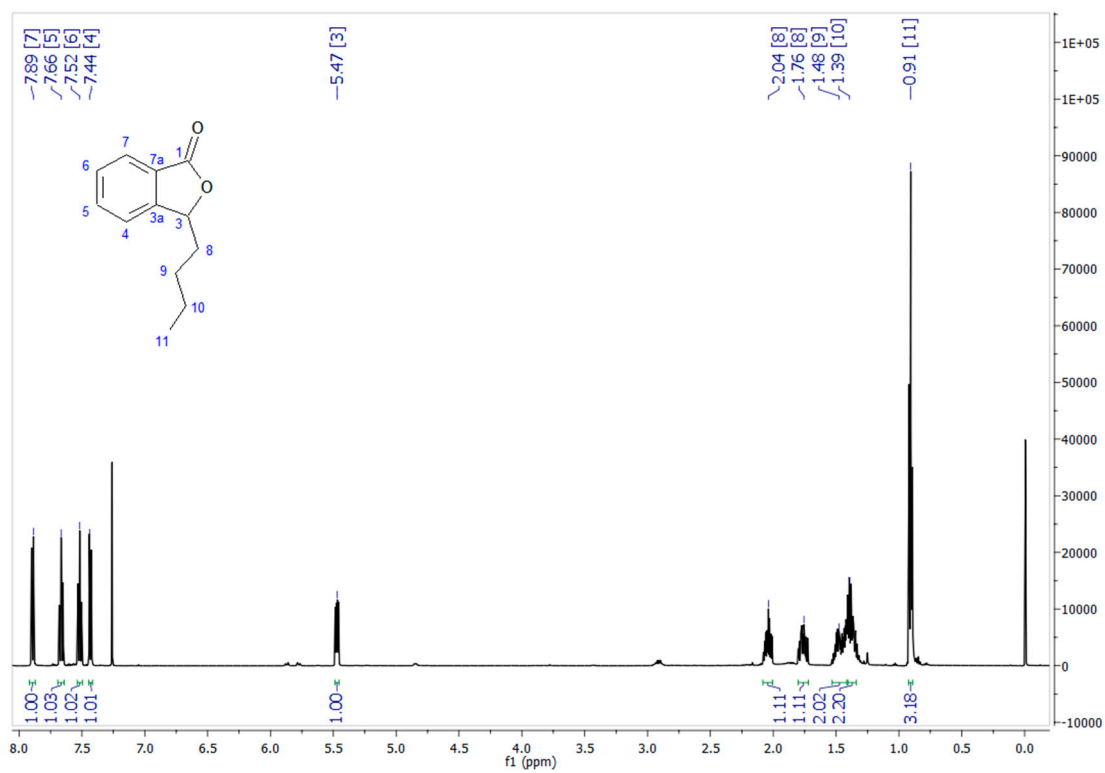
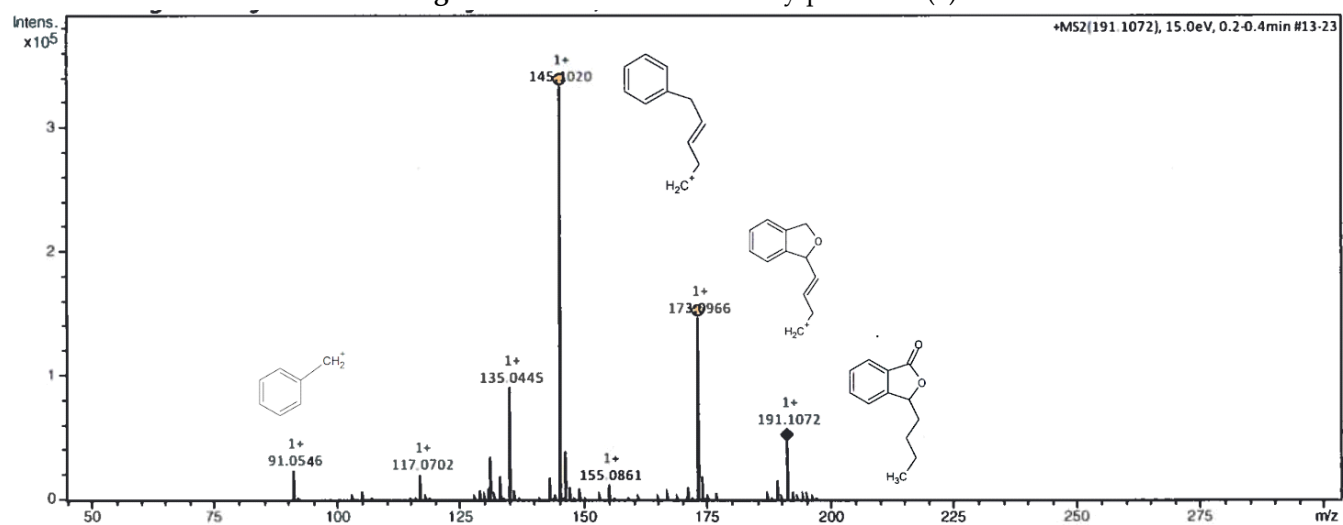
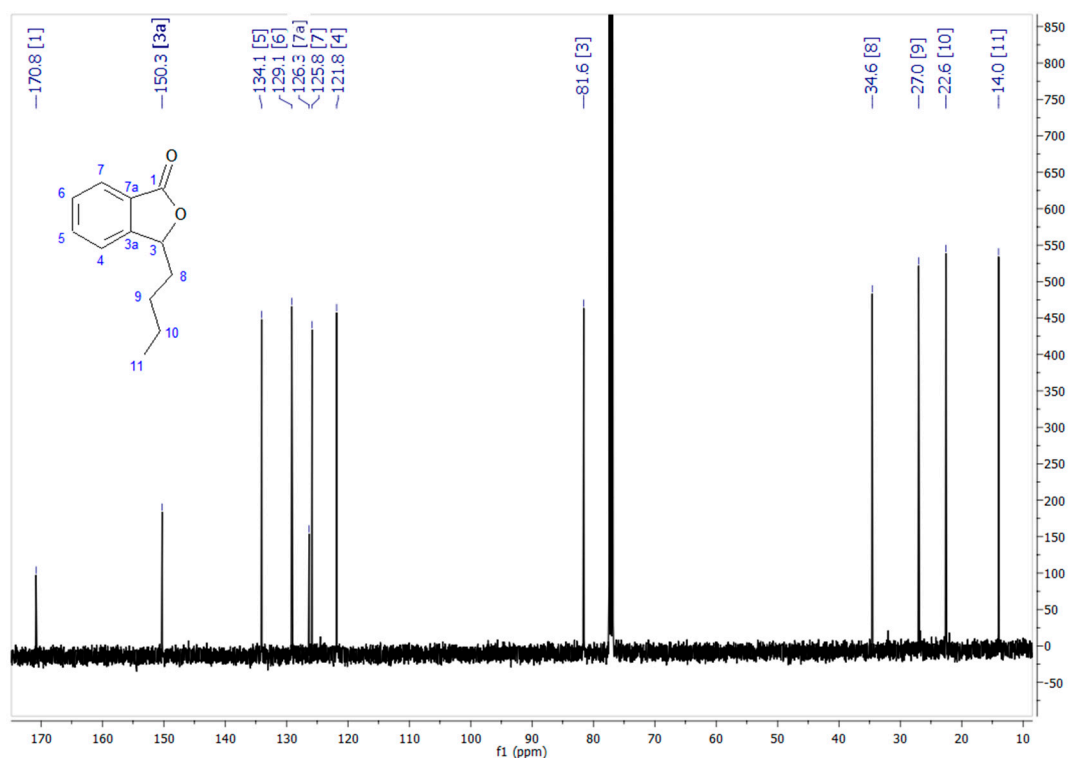


Figure S1b. ¹³C NMR of 3-*n*-butylidene-phthalide (1).

Figure S1c. HR-ESI-MS/MS of 3-*n*-butylidene-phthalide (1).Figure S2a. ¹H NMR of 3-*n*-butylphthalide (2).



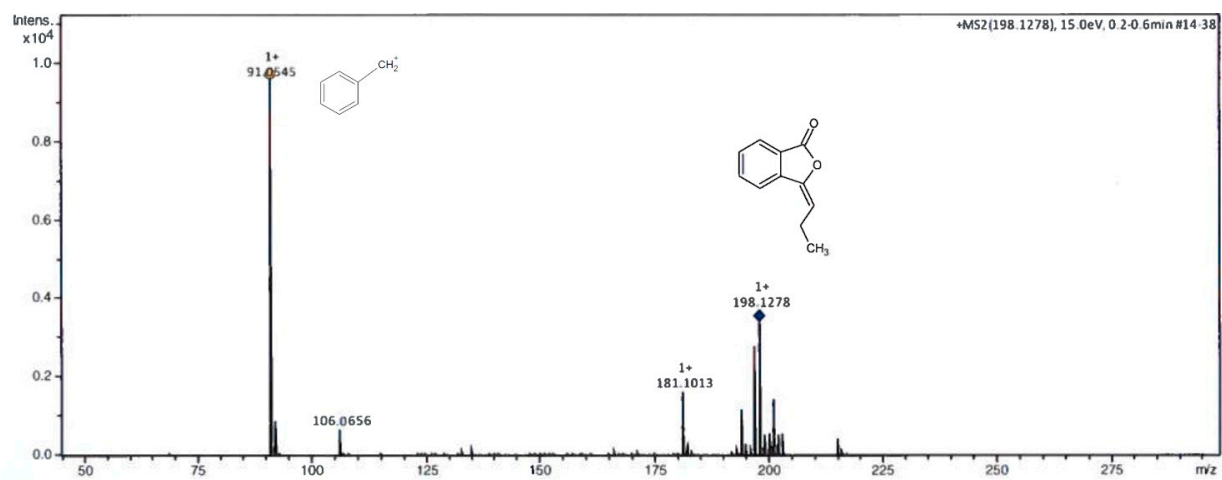


Figure S3 HR-ESI-MS/MS of 3-*n*-propyldenephthalide (3).

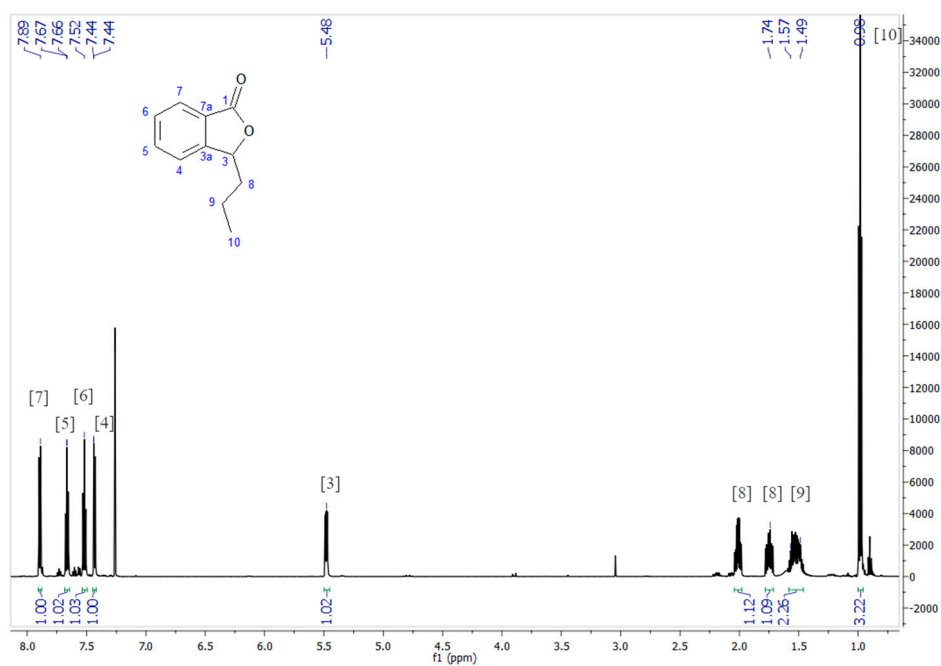


Figure S4a ^1H NMR of 3-*n*-propylphthalide (**4**).

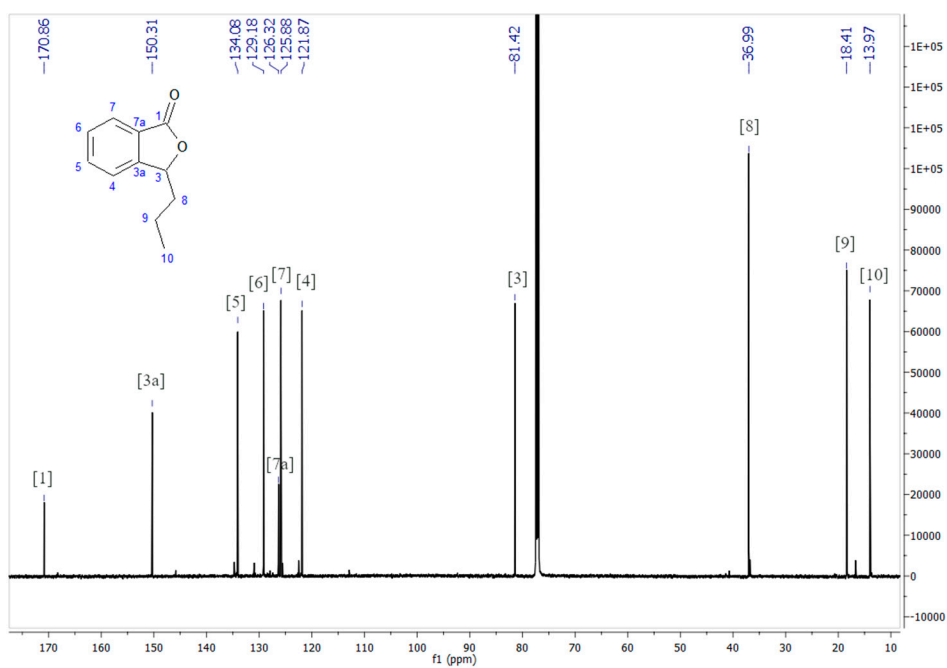


Figure S4b ^{13}C NMR of 3-*n*-propylphthalide (**4**).

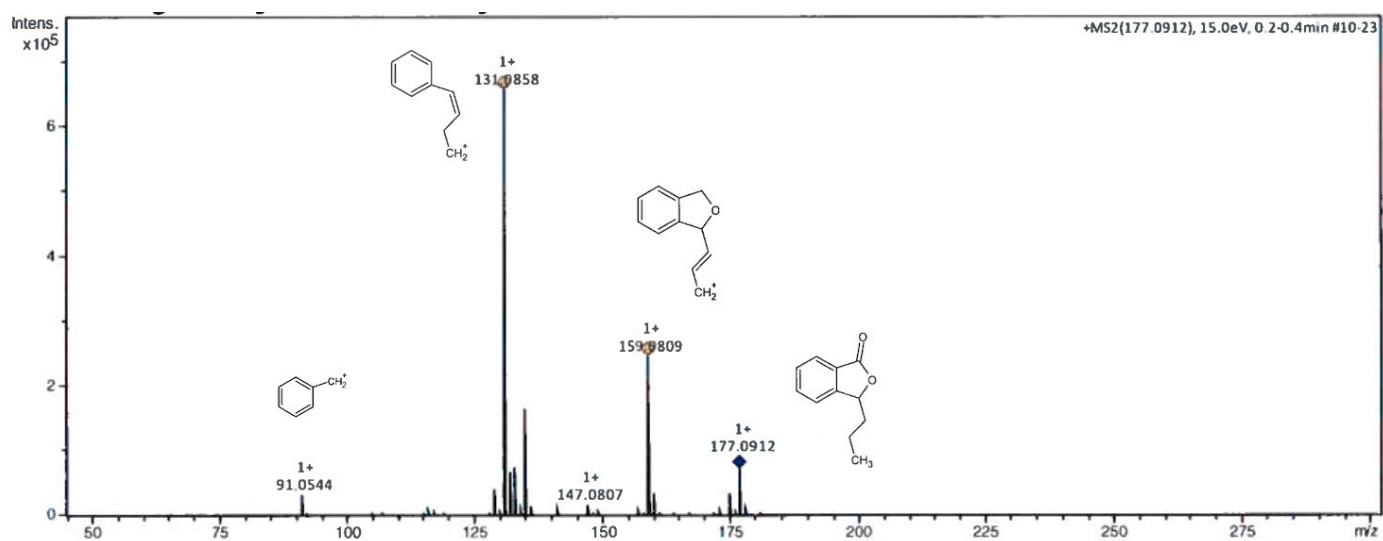


Figure S4c HR-ESI-MS/MS of 3-*n*-propylphthalide (4).

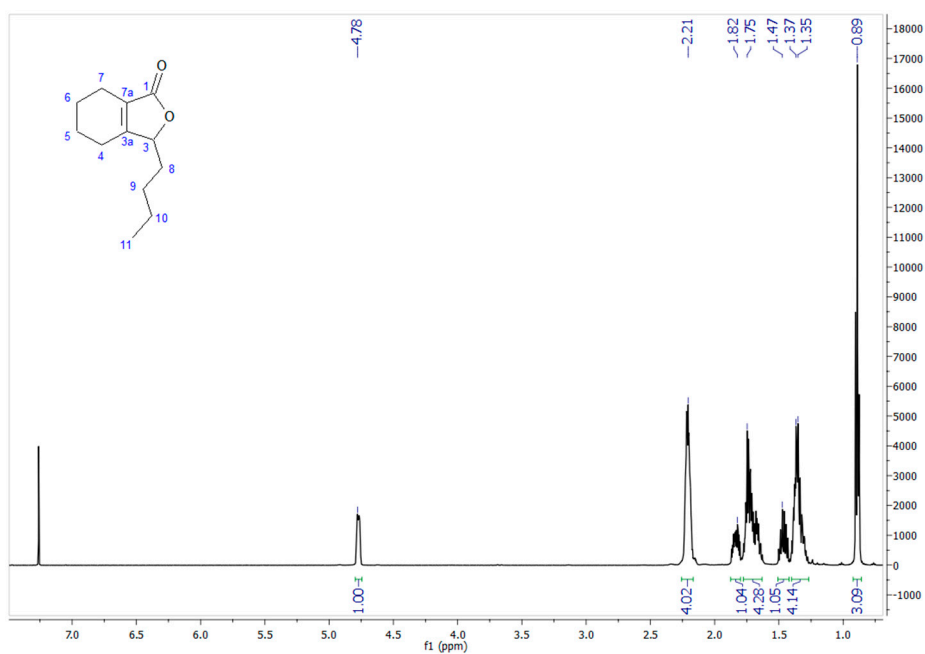
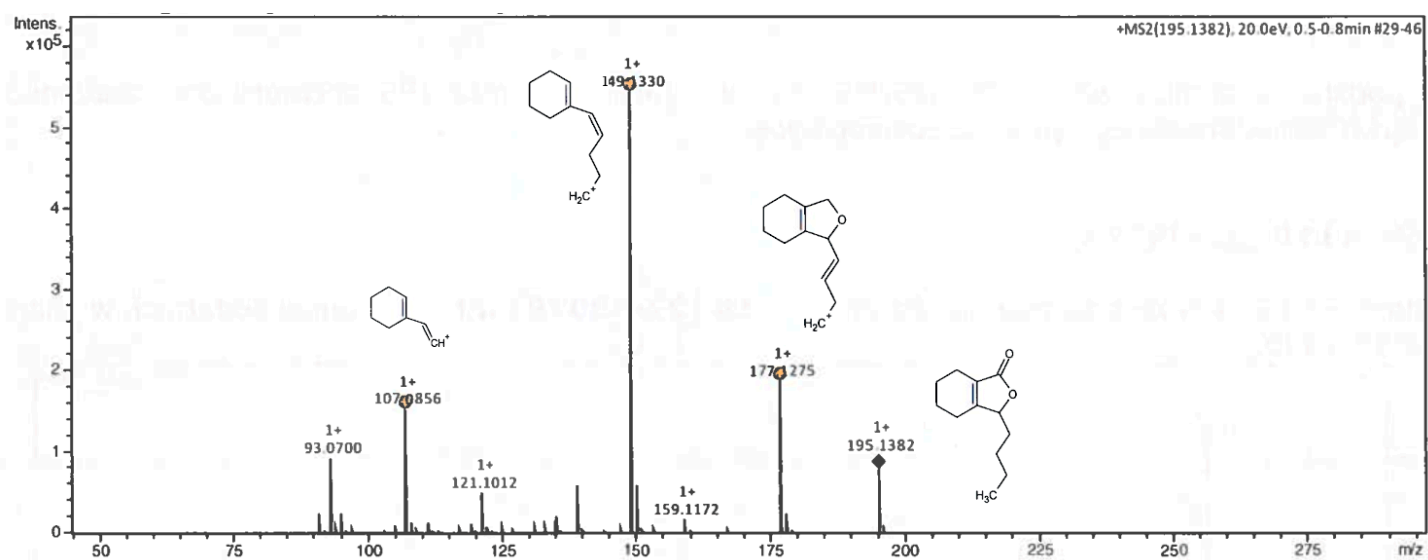
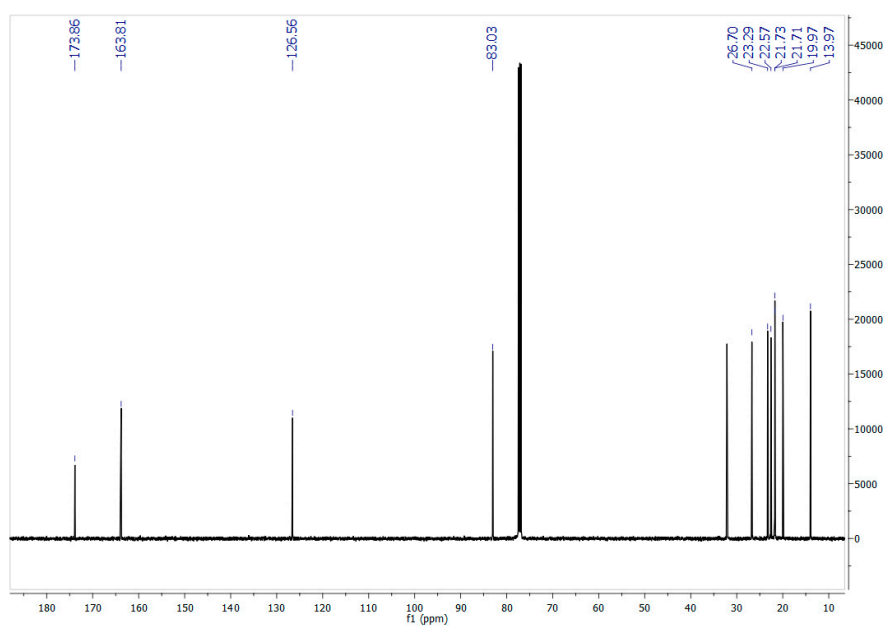


Figure S5a. ^1H NMR of 3-butyl-4,5,6,7-tetrahydrophthalide (5).



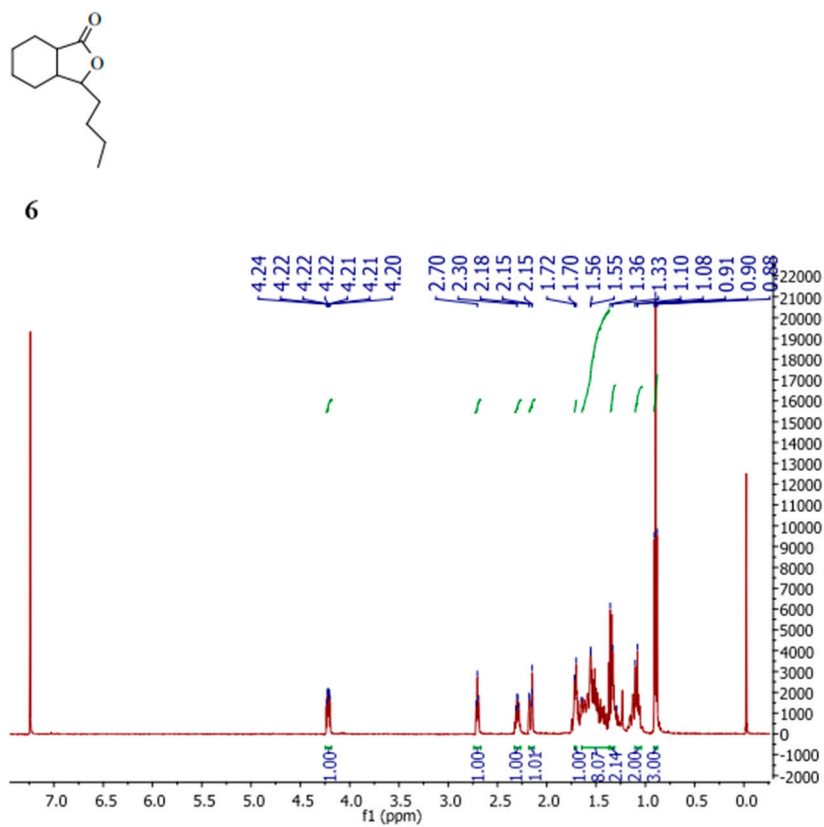


Figure S6a. ¹H NMR of 3-*n*-butyl-hexahydrophthalide (6).

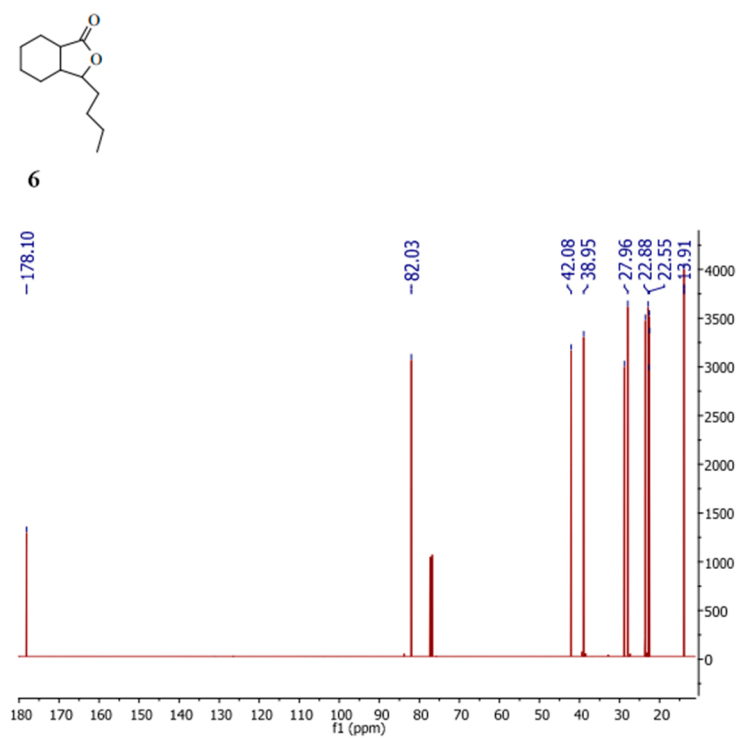


Figure S6b. b ¹³C NMR of 3-*n*-butyl-hexahydrophthalide (6).

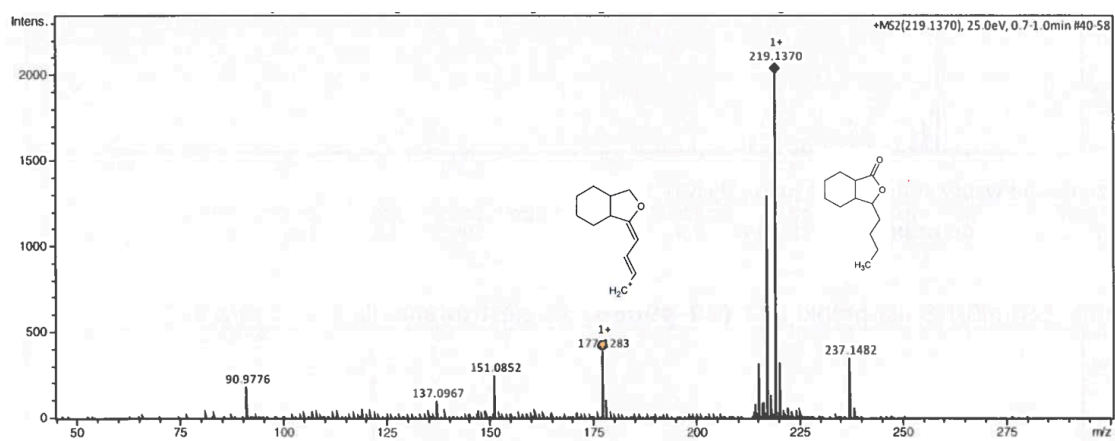


Figure S6c. HR-ESI-MS/MS of 3-*n*-butyl-hexahydrophthalide (6).

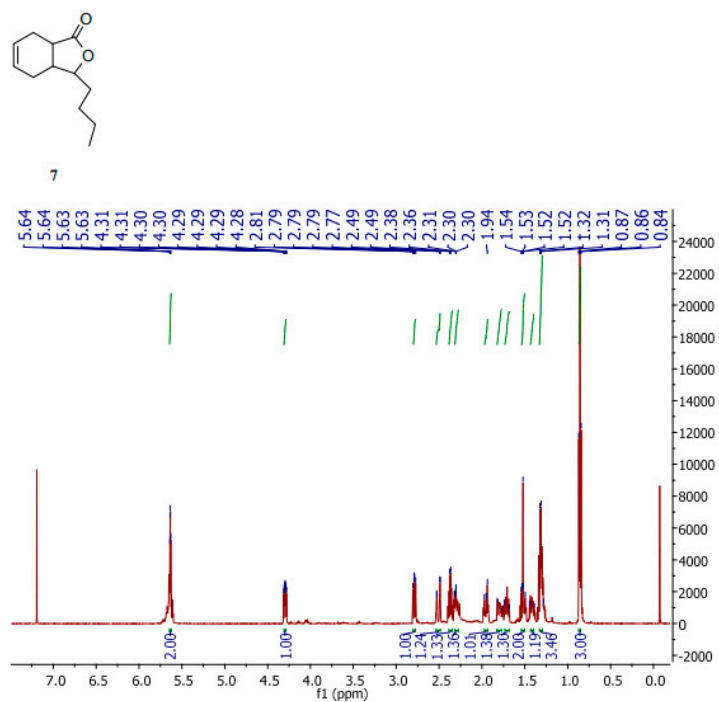


Figure S7a. ¹H NMR of 3-*n*-butyl-1,2,6,7-tetrahydrophthalide (7).

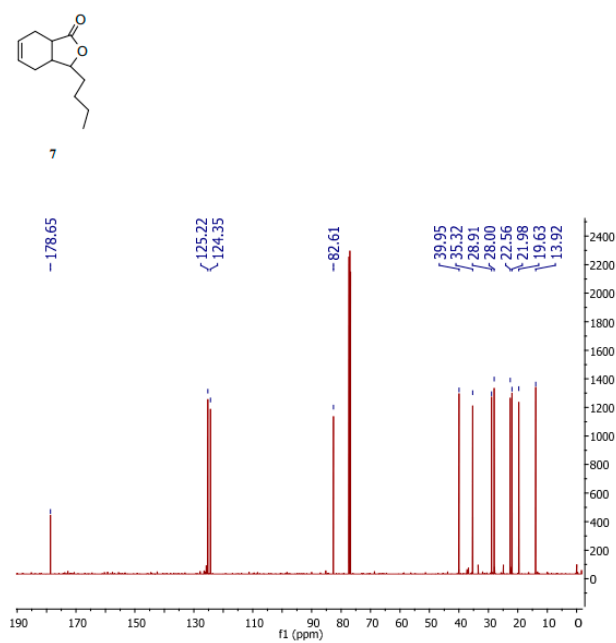


Figure S7b. ¹³C NMR of 3-*n*-butyl-1,2,6,7-tetrahydrophthalide (7).

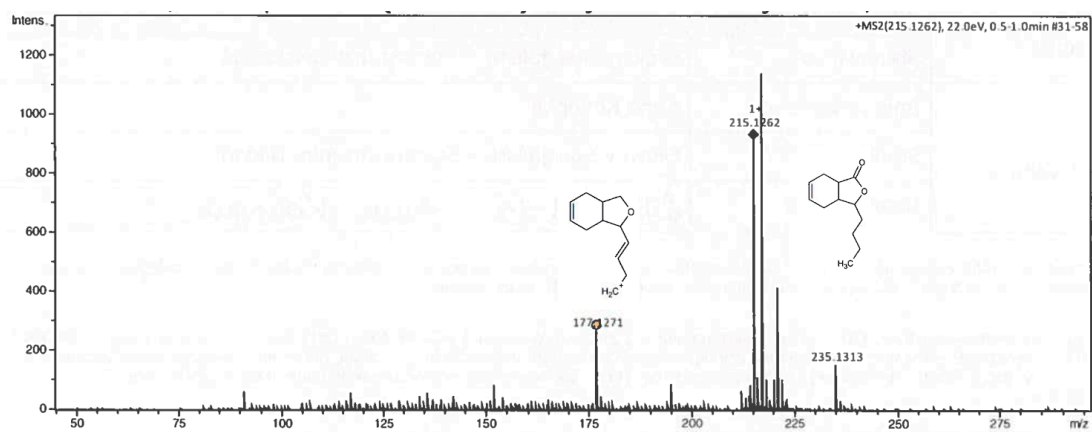


Figure S7c. HR-ESI-MS/MS of 3-*n*-Butyl-1,2,6,7-tetrahydrophthalide (7).

DOROBEK NAUKOWY

Publikacje

1. **Gach, J.**; Grzelczyk, J.; Strzała, T.; Boratyński, F.; Olejniczak, T. Microbial Metabolites of 3-*n*-Butylphthalide as Monoamine Oxidase A Inhibitors. *IJMS* **2023**, *24*, 10605.
2. **Gach, J.**; Olejniczak, T.; Pannek, J.; Boratyński, F. Fungistatic Effect of Phthalide Lactones on *Rhodotorula mucilaginosa*. *Molecules* **2023**, *28*, 5423.
3. Krężel, P.; Olejniczak, T.; Tołoczko, A.; **Gach, J.**; Weselski, M.; Bronisz, R. Synergic Effect of Phthalide Lactones and Fluconazole and Its New Analogues as a Factor Limiting the Use of Azole Drugs against Candidiasis. *Antibiotics* **2022**, *11*, 1500.
4. El-Sayed, E.-S.R.; **Gach, J.**; Olejniczak, T.; Boratyński, F. A New Endophyte *Monascus Ruber* SRZ112 as an Efficient Production Platform of Natural Pigments Using Agro-Industrial Wastes. *Sci Rep* **2022**, *12*, 12611.
5. **Gach, J.**; Olejniczak, T.; Krężel, P.; Boratyński, F. Microbial Synthesis and Evaluation of Fungistatic Activity of 3-Butyl-3-Hydroxyphthalide, the Mammalian Metabolite of 3-*n*-Butylidene-phthalide. *IJMS* **2021**, *22*, 7600.
6. Pannek, J.; **Gach, J.**; Boratyński, F.; Olejniczak, T. Antimicrobial Activity of Extracts and Phthalides Occurring in *Apiaceae* Plants. *Phytotherapy Research* **2018**, *32*, 1459–1487.

Patenty

1. Sposób wytwarzania (-)-izomeru 3-hydroksy-3-butyloftalidu
Pat.242602; 27-04-2021/04-01-2023
2. Sposób wytwarzania (-)-izomeru 3-hydroksy-3-butyloftalidu
Pat.242601; 27-04-2021/04-01-2023
3. Sposób wytwarzania (-) izomeru-(S)-1-hydroksymetylo-2-(1-hydroksubutylo)benzenu
Pat.242600; 12-11-2019/21-12-2022
4. Sposób wytwarzania (+) izomeru-(3R)-3-*n*-propyloftalidu
Pat.242414; 12-11-2019/25-11-2022
5. Sposób wytwarzania (-) izomeru-(3S)-3-*n*-butyloftalidu
Pat.431762; 12-11-2019/18-05-2023

6. Sposób wytwarzania (+) izomeru-(3R)-3-*n*-butyloftalidu
Pat.238970; 14-08-2019/22-07-2021

Zgłoszenia patentowe

1. Sposób wytwarzania 1-hydroksymetylo-2-(1-hydroksybutylo)benzenu **P.431765**
2. Sposób wytwarzania 1-hydroksymetylo-2-(1-hydroksy-3-metylobutylo)benzenu **P.431766**
3. Sposób wytwarzania kwasu-2-pentylobenzoowego **P.431767**
4. Sposób wytwarzania (-)-izomeru 3-hydroksy-3-butyloftalidu **P.437712**

Monografie

1. Durys K., **Gach J.**, Pannek J. Otrzymywanie, aktywność biologiczna i występowanie *Z* i *E*-ligustylidu. *Badania i Rozwój Młodych Naukowców w Polsce – Chemia, część III*, 2016 Poznań ISBN (całość) 978-83-65362-13-1.
2. **Gach J.**, Pannek J. Otrzymywanie, aktywność biologiczna i występowanie 3-*n*-butyloftalidu. *Badania i Rozwój Młodych Naukowców w Polsce – Chemia, część III*, 2016 Poznań ISBN (całość) 978-83-65362-13-1.

Wystąpienia konferencyjne

1. **Gach J.**, Serra S., Marzorati S., Olejniczak T. Application of linoleate 13-hydratase in stereoselective hydration of 18-carbon unsaturated fatty acids, BIOTRANS 2023, La Rochelle.
2. **Gach J.**, Olejniczak T. Efekt fungistyczny laktonów z rodziny *Apiaceae* i ich pochodnych. VIII Ogólnopolska Konferencja Doktorantów Nauk o Życiu BioOpen, 2023, on-line (wyróżnienie).
3. **Gach J.**, Olejniczak T. Fungistatic potential of *Apiaceae* lactones and their derivatives. Biotech France, 2022 Paryż (komunikat ustny).
4. **Gach J.**, Boratyński F. Krężel P., Olejniczak T., Biotransformation of 3-*n*-butylidenephthalide to 3-hydroxy-3-butylphthalide. The fungistatic activity against *Candida* strains. BIOTRANS 2021, Graz, on-line.
5. **Gach J.**, Olejniczak T. Biotransformacje 3-*n*-butylidenoftalidu. e-Zjazd Wiosenny Sekcji Studenckiej Polskiego Towarzystwa Chemicznego, 2021, on-line (komunikat ustny).
6. **Gach J.**, Pannek J., Olejniczak T. Wpływ podłoża na enancjoselektywne utlenienie diolu do 3-*n*-butyloftalidu, Zjazd Wiosenny SSPTChem, 2018 Skorzęcin.

7. **Gach J.**, Pannek J., Olejniczak T. Biomedyczne zastosowanie porfiryn. XXII Międzynarodowa Konferencja Studenckich Kół Naukowych i XXXIV Sejmik SKN, 2017 Wrocław.
8. **Gach J.**, Pannek J., Olejniczak T. Bioaktywność ftalidów pochodzenia naturalnego. VI Wroclawska Konferencja Studentów Nauk Technicznych i Ścisłych, 2017 Wrocław (I miejsce w sesji posterowej).
9. **Gach J.**, Durys K., Skarbek M., Pannek J. Otrzymywanie, aktywność biologiczna i występowanie Z i E-butyliidenoftalidu oraz butyloftalidu. III Ogólnokrajowa Konferencja Naukowa Młodzi Naukowcy w Polsce – Badania i Rozwój, 2016 Wrocław.
10. Durys K., **Gach J.**, Skarbek M., Pannek J. Otrzymywanie, aktywność biologiczna i występowanie Z, E-ligustylidu oraz neocnidilidu. III Ogólnokrajowa Konferencja Naukowa Młodzi Naukowcy w Polsce – Badania i Rozwój, 2016 Wrocław.
11. Skarbek M., **Gach J.**, Durys K., Pannek J. Występowanie, aktywność biologiczna oraz otrzymywanie izobutyloftalidu i jego nienasyconej pochodnej. III Ogólnokrajowa Konferencja Naukowa Młodzi Naukowcy w Polsce – Badania i Rozwój, 2016 Wrocław.
12. **Gach J.**, Skarbek M., Durys K., Pannek J. Olejniczak T. Otrzymywanie i aktywność biologiczna butyliidenoftalidu i butyloftalidu wobec *Rhodotorula mucilaginosa*. V Wroclawska Konferencja Studentów Nauk Technicznych i Ścisłych Puzzel 2016, 2016 Wrocław.
13. Skarbek M., **Gach J.**, Durys K., Pannek J. Otrzymywanie i aktywność biologiczna izobutyloftalidu i jego nienasyconej pochodnej wobec *Rhodotorula mucilaginosa*. V Wroclawska Konferencja Studentów Nauk Technicznych i Ścisłych Puzzel 2016, 2016 Wrocław.
14. **Gach J.**, Durys K., Skarbek M., Pannek J., Olejniczak T. Synteza bicyklicznych laktonów oraz ich aktywność fungistatyczna wobec *Rhodotorula mucilaginosa*. XXI Międzynarodowa Konferencja Studenckich Kół Naukowych i XXXIII Sejmik SKN, 2016 Wrocław (I miejsce w sesji posterowej).
15. Pannek J., **Gach J.**, Durys K., Walczak P., Janik-Polanowicz A., Olejniczak T. Synteza, biotransformacje oraz aktywność biologiczna nienasyconych bicyklicznych laktonów o strukturze bicyklo[4.3.0]nonanu. Zjazd Wiosenny Sekcji Studenckiej Polskiego Towarzystwa Chemicznego, 2015 Dobieszków (nagroda publiczności).
16. Durys K., **Gach J.**, Pannek J., Olejniczak T. Aktywność biologiczna wobec *Candida albicans* oraz przekształcenia mikrobiologiczne n-butyloftalidu i jego nienasyconej

pochodnej. XX Międzynarodowa Konferencja Studenckich Kół Naukowych i XXXII Sejmik SKN, 2015 Wrocław (II miejsce w sesji posterowej).

17. **Gach J.**, Durys K., Pannek J., Olejniczak T. Otrzymywanie, przekształcenia mikrobiologiczne oraz aktywność wobec *Candida albicans* 4-butylo-3-oksabicyklo[4.3.0]non-7-en-2-onu i 4-butylieno-3-oksabicyklo[4.3.0]non-7-en-2-onu. XX Międzynarodowa Konferencja Studenckich Kół Naukowych i XXXII Sejmik SKN, 2015 Wrocław.

Udział w projektach badawczych

1. „UPWR 2.0: międzynarodowy i interdyscyplinarny program rozwoju Uniwersytetu Przyrodniczego we Wrocławiu”, współfinansowanego ze środków Europejskiego Funduszu Społecznego w ramach Działania 3.5. Kompleksowe programy szkół wyższych Osi III Szkolnictwo wyższe dla gospodarki i rozwoju Programu Operacyjnego Wiedza Edukacja Rozwój oraz budżetu państwa na podstawie umowy o dofinansowanie nr POWR.03.05.00-00-Z062/18 z dnia 4 czerwca 2019 r. – wykonawca projektu.
2. Grant wewnętrzny – „Innowacyjny doktorat” N070/0013/20 – „Badanie potencjału laktonów jako nowych naturalnych środków przedłużających trwałość żywności” – kierownik i wykonawca projektu.

Staże zagraniczne

Staż na Politecnico di Milano, Włochy (01.09.2022-14.08.2023). Udział w badaniach nad redukcją wiązania podwójnego nienasyconych laktonów, a także hydratami kwasów tłuszczowych we współpracy z dr. Stefano Serrą z CNR SCITEC.